UNIVERSITAT DE BARCELONA

Tornadic events in the Iberian Peninsula and Balearic Islands: characteristics and environmental conditions

Oriol Rodríguez i Ballester

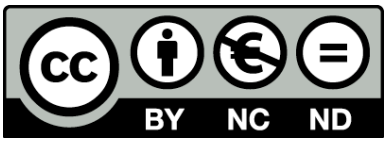

Tesi doctoral

Tornadic events in the Iberian Peninsula and Balearic Islands: characteristics and environmental conditions

Oriol Rodríguez i Ballester

UNIVERSITAT DE BARCELONA

Universitat de Barcelona

Departament de Física Aplicada

Tornadic events in the Iberian Peninsula and Balearic Islands: characteristics and environmental conditions

Memòria presentada per optar al grau de doctor per la Universitat de Barcelona

Programa de doctorat en Física

Autor: Oriol Rodríguez i Ballester

Director: Joan Bech i Rustullet

Tutor: Alberto Manrique Oliva

Barcelona, desembre de 2020

Agraïments

Voldria començar agraint a en Joan Bech, el director d'aquesta tesi, l'acompanyament i el suport d'aquests darrers anys. Vam contactar per primera vegada a mitjans de desembre de 2013, aleshores per començar a preparar el treball de final de grau de Física, titulat "Sounding-derived parameters associated to tornadic storms in Catalonia" (el tema ja apuntava maneres). Des de llavors, sempre m'ha animat a seguir endavant amb l'estudi dels fiblons, alhora que m'ha obert les portes al món de la investigació que, realment, m'ha deixat meravellat. L'empenta, les ganes i el rigor científic amb què treballa l'han fet ser un magnífic director.

M'agradaria donar les gràcies a en Salvador Castán i a en Joan Arús per tots els treballs de camp que, juntament amb en Joan Bech, hem compartit. Les hores de cotxe, de discussions sobre si calia anar a veure la perifèria de la zona afectada o si analitzar els danys d'un bosc, o sobre si l'origen de les destrosses havia estat un tornado o un esclafit han estat dels moments més divertits del doctorat, i també dels més intensos. Només cal posar d'exemple aquella tarda de gener que vam quedar-nos amb el cotxe encallat en una pista forestal de Darnius fins ben entrada la nit, i tot per fer unes fotografies a unes branques trencades.

També vull agrair a en Miquel Gayà la gran tasca que ha fet durant anys per a recollir, estudiar i analitzar amb detall els tornados, les mànegues marines i els esclafits a les Illes Balears i al conjunt de la Península Ibèrica. Sense cap mena de dubte, ha estat un referent per a mi. El seu magnífic treball ha estat cabdal, tant en l'àmbit mediterrani com europeu, i ha fet possible alguns dels avenços d'aquest segle. També la seva predisposició a atendre consultes i dubtes que, al llarg del procés d'elaboració de la tesi, han anat sorgint.

Gràcies al conjunt dels professors de meteorologia de la Universitat de Barcelona. Sense l'entusiasme que desprenen a les classes, tant del grau de Física com del màster de Meteorologia, de ben segur que no m'hagués endinsat en un projecte com el de fer un doctorat.

Als companys del Servei Meteorològic de Catalunya, especialment els de l'Equip de Predicció i Vigilància i els de Teledetecció, moltes gràcies. Santi, Montse, Aleix, Clara, Manuel, Pere, Carme, Francesc, Xavi, Sergio, Jordi Via, Dolors, Jordi Mateo, Jordi Toda, Abel, Estel, Ester, Jordi Cruz, Roc, Bel, Anna, Lola, Nico, Patri, Helen, Oriol, Pau, a tots vosaltres us estic molt agraït per com m'heu acollit a la cinquena planta durant el temps que hi he estat i per haver sigut uns autèntics mestres. Menció a banda es mereix en Tomeu Rigo, a qui sovint li he omplert la safata de correu electrònic de peticions d'imatges de radar, de dubtes i demanant consell. Sempre que ha calgut hi ha estat, amb rapidesa i sobretot bon humor.

Aquests gairebé cinc anys de doctorat no haurien estat el mateix sense la Yolanda, la Mireia Udina, l'Àngela, la Montse, en Joan Gilabert, la Isa, en Javi, la Froila, la Chloé, en Jordi, en Gaby, en Joan Puigdueta, en Carrasco, la Marina, en Sergi, la Mireia Mateu, en Raül, la Míriam, l'Àlex, en Francesc i en Richard, amb qui hem compartit llargs esmorzars, cafès, dinars i moments de desconnexió a la minúscula saleta de la setena planta de la Facultat de Física. I per descomptat, moltes gràcies a l'Anna, la Maria i l'Enric, per no dir mai que no a anar a prendre una cervesa, pels congressos i seminaris als quals hem assistit plegats i per tots els moments (de vegades surrealistes) que hem viscut. A banda, també vull donar les gràcies a en Miquel Bernis pels més de sis anys que fa que treballem plegats i per posar sempre les coses molt fàcils, sobretot durant la recta final del doctorat.

Vull agrair als amics i als socis de l'ACOM, al conjunt dels observadors meteorològics, als presentadors de la informació del temps dels diversos mitjans de comunicació, especialment de la CCMA, del Grup Godó i de BTV, als ajuntaments, als consells comarcals, als Bombers de la Generalitat de Catalunya, a Emergències de Catalunya i a totes aquelles persones que han observat tornados i mànegues marines per facilitar-me la informació sempre que ha calgut. Sense la seva col·laboració aquesta tesi no hauria estat possible.

Fora de l'àmbit del doctorat, vull fer esment dels amics de Badalona, en Joan, la Laia, l'Adrià, l'Anaïs, en Pol i en Sergi, i dels del Vendrell, l'Ignacio, la Roser, en Marcel, l'Angèlica, la Sandra Cantero, en Joan, en Xesc, la Meri, la Sandra Ramírez, en Toni, en Guillem, la Xènia, la Roser Graell, l'Anna, l'Oriol, l'Aleix, la Cristina i la Laia, per tots els sopars, les calçotades, les excursions, els dies de platja i els bons moments que, sempre que ens veiem, passem plegats. També a la Isa, en Manel, l'Ana, en Marc, la Laia, la Laura, en Dani i l'Albert, la colla d'amics de Física amb qui anys després d'haver compartit hores d'estudi a la biblioteca, festes i viatges, gairebé no hi ha dia que no parlem.

M'agradaria fer un especial agraïment als meus pares, en Guillem i la Dolors. No podria estar més agraït per tot el que heu fet per mi. Heu estat el pal de paller de la meva vida, un exemple a seguir per com encareu tot allò que us ofereix la vida. M'ho heu donat tot i heu estat allà on calia sempre que us he necessitat. Per tot això, gràcies.

A la Marta, la meva germana, per l'alegria i l'empenta que tant et caracteritza, per tots els bons moments que hem passat junts, per tot el que m'has ensenyat des que vas néixer, per fer-me feliç. Moltíssimes gràcies per ser-hi sempre.

Gràcies als avis, la Dolors, en Vicenç, l'Eloísa i en Guillermo; als tiets, en especial a la Marta, en Joan, l'Ignacio, la Cati, en Jorge i la Montse; als cosins, l'Helena, la Laura, en Pau i la Marina, així com a l'Agnès, l'Òscar i l'Adrià, i també a la Neus, en Joan, la Neus, en Lluís i la Ivet. Sou la millor família que hauria pogut tenir.

Vull acabar els agraïments donant les gràcies a una persona molt especial per a mi, la meva parella, la Marta. Fa molts anys que compartim el camí i sempre, en tot moment, m'has ensenyat que cal viure amb un somriure d'orella a orella, que la positivitat i el bon humor no han de faltar mai. Gràcies per la paciència que tens i pel suport incondicional que m'has brindat durant tot aquest temps. Gràcies per tot i, especialment, per fer que cada dia sigui una aventura.

Resum

Els tornados són el fenomen meteorològic que pot donar lloc als vents més forts en superfície a la Terra. La seva longitud i temps característics tan petits fan que avui en dia no sigui possible pronosticar quan i on hi haurà un tornado amb dies o hores d'antelació. Si bé a les Grans Planes dels Estats Units és on es registren fiblons amb més freqüència, a Europa també se n'observen, fins i tot amb danys milionaris, ferits i víctimes mortals. Diversos estudis apunten que la inestabilitat termodinàmica podria augmentar a causa de l'escalfament global, principalment degut a l'increment de la humitat específica a nivells baixos. Com a conseqüència, i juntament amb una tendència poc clara respecte al cisallament vertical del vent, tot apunta que augmentaria la freqüència d'ocurrència d'entorns favorables per a tempestes violentes, especialment durant la segona meitat de segle. Davant d'aquest escenari, és necessari aprofundir en el coneixement dels fiblons.

L'objectiu d'aquesta tesi és estudiar els tornados a la Península Ibèrica i a les Illes Balears, tant pel que fa a la caracterització dels episodis com pel que fa a les condicions favorables per a la seva formació. Per a estructurar el treball, es defineixen els sis objectius específics següents:

- OE1. Proposar una metodologia per a dur a terme treballs de camp.
- OE2. Utilitzar ortofotografies per a analitzar episodis de ventades fortes d'origen convectiu.
- OE3. Desenvolupar una base de dades de tornados i trombes marines a Catalunya i analitzar les característiques dels episodis.
- OE4. Estudiar paràmetres termodinàmics i cinemàtics per a diversos tipus de temps.
- OE5. Analitzar el comportament de paràmetres específics per a detectar entorns favorables per a la formació de tornados.
- OE6. Validar la detecció d'entorns favorables per a la formació de mànegues marines mitjançant el nomograma de Szilagyi.

La tesi, que consisteix en un compendi de cinc publicacions, es divideix en tres blocs principals. A la primera part s'estudien alguns recursos que afavoreixen l'homogeneïtzació de les bases de dades de ventades fortes d'origen convectiu. L'objectiu és que siguin robustes i que diferenciïn entre tornados, esclafits i altres fenòmens. A la segona part es construeix una base de dades de tornados i mànegues marines a Catalunya i es fa una anàlisi de la distribució espacial i temporal dels casos i de les característiques dels episodis. Finalment, a la tercera part, es caracteritzen els entorns típics per a diversos tipus de temps, estudiant amb especial atenció els dies de tornado i, sobretot, els episodis més intensos.

Per començar el primer bloc, es presenta una metodologia per a dur a terme treballs de camp, basada en l'adquisició *in situ* de les dades d'interès (p. ex. coordenades dels elements afectats, direcció de caiguda dels arbres o estat de conservació de les estructures malmeses) i la posterior anàlisi de les destrosses. A partir de la disposició i l'orientació dels danys sovint

és possible conèixer-ne l'origen (i.e. tornado o esclafit). A més, també es pot caracteritzar la zona afectada (amplada i llargada) i estimar la intensitat del fenomen mitjançant l'ús d'escales com la de Fujita (F) o la de Fujita millorada (EF). Els resultats mostren que la metodologia proposada és d'utilitat per a analitzar episodis de vent fort d'origen convectiu, malgrat les limitacions que presenta.

Posteriorment, s'utilitzen ortofotografies per a detectar les zones afectades per ventades fortes, mitjançant la comparativa d'imatges anteriors i posteriors als casos d'estudi. L'alta resolució de les ortofotografies permet identificar individualment els arbres i la direcció amb què han caigut. Per tant, a partir del patró de danys observat en zones forestals és possible conèixer quin fenomen meteorològic ha tingut lloc. A més, es pot estimar la intensitat de l'esdeveniment tenint en compte la relació que existeix entre l'amplada i la llargada de la traça de danys amb l'escala F, i la de la ràtio d'arbres afectats i l'escala EF. Malgrat que els danys causats pels casos més febles són difícilment observables mitjançant aquesta tècnica, aquest tipus d'anàlisi demostra ser una eina idònia per a completar els treballs de camp, sobretot a l'hora d'estudiar episodis extensos.

El segon bloc se centra en l'elaboració d'una base de dades de tornados i mànegues marines a Catalunya per al període 2000-2019. S'utilitzen les observacions obtingudes a través de diverses fonts d'informació, on destaquen els mitjans de comunicació, les bases de dades anteriors i les xarxes socials. A més, es fan servir ortofotografies i els resultats de treballs de camp per a estudiar les traces de danys. El recull conté un total de 434 casos (105 tornados i 329 trombes marines). Les dades obtingudes s'empren per a fer una anàlisi de la distribució espacial i temporal dels episodis, dels *outbreaks* i dels episodis múltiples, de les característiques de les franges de danys i de l'impacte socioeconòmic. D'aquesta manera s'aconsegueix disposar d'una descripció completa d'aquests tipus de fenòmens i de les seves conseqüències.

A continuació, i per encetar el tercer bloc, s'analitzen 333 radiosondatges associats a diversos tipus de temps a Catalunya entre els anys 2000 i 2016: dies sense precipitació, dies de tempesta sense tornado, dies de tornado d'intensitat EF0, dies de tornado d'intensitat EF1 o superior i dies de mànega marina. S'estudien un total de dotze paràmetres termodinàmics, cinemàtics i compostos per a caracteritzar cadascuna de les categories amb què s'han classificat els perfils verticals. Els resultats mostren que l'energia potencial convectiva disponible no és un bon indicador per a diferenciar entre els diversos tipus de temps. Per altra banda, s'observa que hi ha una correlació directa entre el cisallament vertical del vent i la intensitat dels fiblons, sobretot per a l'estrat 0-3 km. L'*universal tornadic index* demostra ser d'utilitat per a discriminar entre els dies de tempesta sense tornado i els dies de tornado. Per contra, el *significant tornado parameter* presenta diferències més modestes. A més, es proposen nous llindars per als paràmetres que discerneixen millor els entorns de tempesta sense tornado respecte als dies de tornado d'intensitat EF1 o superior.

Finalment, s'estudien els episodis de tornados i mànegues marines registrats a la Península Ibèrica i les Illes Balears entre 1980 i 2018 amb dades de la darrera reanàlisi de l'ECMWF, l'ERA5. En total s'analitzen 907 perfils verticals de temperatura, vent i humitat i se'n calculen diversos paràmetres termodinàmics, cinemàtics i compostos. A més, també s'utilitza el nomograma de Szilagyi per a estudiar com identifica els entorns favorables per a la formació de mànegues marines a la regió d'interès. A conseqüència de la diferent distribució mensual dels episodis entre el nord-est de la Península i les Illes (més freqüents a l'època càlida) i el sud-oest de la Península (més usuals a l'època freda), els resultats s'analitzen per separat per a ambdues regions. S'identifiquen dos casos particulars d'entorns favorables per a la tornadogènesi, descrits prèviament per diversos autors: el de cisallament del vent elevat i energia potencial convectiva disponible baixa (més típic de l'època freda), i el d'helicitat baixa i nivell de condensació per elevació elevat (més habitual durant l'època càlida). A banda, s'observa que hi ha una relació inversa entre l'energia potencial convectiva disponible i el cisallament vertical del vent, sobretot

per a l'estrat 0-3 km. Això motiva la redefinició del paràmetre WMAXSHEAR (el producte de l'arrel quadrada de dues vegades l'energia potencial convectiva disponible pel cisallament vertical del vent) fent ús del cisallament per a l'estrat 0-3 km, en comptes del 0-6 km. Aquest nou paràmetre demostra discriminar amb eficàcia els entorns associats als episodis d'intensitat (E)F2 o superior, els quals solen superar els 500 m^2 s^{-2}, de la resta. Independentment, s'observa que el nomograma de Szilagyi identifica correctament els entorns relacionats amb trombes marines per a una àmplia majoria dels casos.

Els resultats d'aquesta tesi contribueixen a millorar la detecció i l'anàlisi de les zones afectades per ventades fortes d'origen convectiu a la Península Ibèrica i les Illes Balears. Les eines que es presenten poden ajudar a elaborar bases de dades robustes i homogènies, que discriminin entre tornados i esclafits. Precisament, aquestes dades han de poder servir com a base per a futurs estudis i per a tenir un major coneixement de la distribució i característiques dels fiblons. Per altra banda, l'anàlisi de les condicions favorables per a la tornadogènesi duta a terme pot ser d'ajut per a la predicció i la vigilància d'aquest tipus de fenòmens de temps violent. La millora en la detecció dels entorns típics d'episodis de tornados és d'especial interès, tenint en compte que l'àrea d'estudi engloba algunes de les regions on més se'n registren del sud d'Europa.

Abstract

Tornadoes are the meteorological phenomenon which can produce the strongest surface wind on Earth. Nowadays, it is not possible to forecast when and where a tornado can occur due to their small characteristic length and time. Although Great Plains from the United States is where tornadoes are the most frequent, in Europe they are also observed, even causing multimillion-worth losses, injuries and fatalities. Several studies point out that thermodynamic instability might increase in the future on account of global warming, mainly due to the low-level specific humidity increase. As a consequence, and together with an unclear vertical wind-shear tendency, favourable severe storm environments could be more frequent, especially during the second half of this century. Thus, it is necessary to deep on tornado knowledge.

The main aim of this thesis is to study tornadic events in the Iberian Peninsula and Balearic Islands both for characterise them and describe favourable conditions for tornadogenesis. Six specific goals have been defined to structure the work:

- OE1. To propose a methodology to carry out damage surveys.
- OE2. To use orthophotographs to analyse strong-convective wind events.
- OE3. To build up a tornado and waterspout database for Catalonia and analyse events characteristics.
- OE4. To study thermodynamic and kinematic parameters for different weather-type days.
- OE5. To analyse the behaviour of specific parameters related to the detection of favourable tornadic environments.
- OE6. To validate the detection of environments favourable to waterspout formation through the Szilagyi nomogram.

The thesis, which is based on five publications, is divided into three parts. In the first one, some resources that help to the homogenisation of strong-convective wind events databases are studied, making them more robust and allowing to discriminate between tornadoes, downbursts and other phenomena. In the second one, a tornado and waterspout database for Catalonia is built up and an analysis of spatiotemporal distribution and characteristics of the events is carried out. Finally, in the third one, several weather-type environments are characterised, focusing on tornado days and, especially, on the most intense events.

To start the first block, it has been developed a methodology to carry out fieldworks, which is based on *in situ* data acquirement (e.g. affected element coordinates, fall direction of trees or previous weaknesses on damaged structures) and the subsequent damage analysis. Then, it is usually possible to know which meteorological phenomenon took place (i.e. tornado or downburst) through the damage pattern study. Moreover, the affected area can be characterised (length and width) and the intensity of the event can be estimated using the Fujita (F) scale or the Enhanced Fujita (EF) scale. Results show that the proposed methodology is useful to analyse strong-convective wind events, despite the limitations that presents.

After that, orthophotographs have been used to detect areas affected by damaging winds, through the comparison of images taken before and after the case studies. The high resolution of orthophotographs even allows to identify trees individually and their fallen direction. Then, it is possible to know which phenomenon occurred analysing the observed damage pattern in forest areas. Moreover, the event intensity can be estimated using the relation exhibited between the length and width with the F-scale, and between the ratio of affected trees and the EF-scale. Although damage caused by weak cases is hardly observable using this technique, this kind of analysis is a suitable complement for fieldworks, especially when studying widespread events.

The second block is centred into the elaboration of a tornado and waterspout database for Catalonia for the period 2000-2019. Several sources of information are used, standing out mass media, previous databases and social networks. Furthermore, fieldwork results and orthophotographs are used to study the damage paths. The dataset consists of 434 events (105 tornadoes and 329 waterspouts). The data gathered is used to carry out an analysis of spatiotemporal distribution, outbreaks and multiple events, damage swath characteristics and socioeconomic impact. Therefore, it is possible to achieve a complete depiction of this kind of severe weather events and its consequences.

In the third part, 333 soundings associated with several weather-types in Catalonia between 2000 and 2016 have been analysed, considering non-precipitation days, non-tornadic thunderstorms days, EF0 tornado days, EF1 or stronger tornado days and waterspout days. Twelve thermodynamic, kinematic and composite parameters have been tested to characterise each sounding category. Results show that convective available potential energy is not a good indicator to differentiate between weather-types. On the other hand, it exists a direct correlation between vertical wind-shear and tornado intensity, especially for 0-3 km layer. The universal tornadic index proves to be useful to discriminate between non-tornadic thunderstorm days and days with tornado. By contrast, significant tornado parameter presents more modest differences. Furthermore, new thresholds are presented for the parameters that better discriminate non-tornadic thunderstorm from EF1 or stronger tornadic environments.

Finally, tornado and waterspout events registered in the Iberian Peninsula and Balearic Islands between 1980 and 2018 have been studied, using the latest ECMWF reanalysis, ERA5. Several thermodynamic, kinematic and composite parameters have been calculated for the 907 temperature, humidity and wind vertical profiles analysed. In addition, the Szilagyi nomogram has been used to study how identifies environments favourable to waterspout formation in the region of interest. As a consequence of the different monthly distribution of tornadic events between the north-east of the Peninsula and the Islands (more frequent during the warm season) and the south-west of the Peninsula (more usual during the cool-season), these two subregions have been analysed separately. Two particular cases of environments favourable to tornadogenesis, described previously by several authors, have been identified: high-shear, low-convective available potential energy (more typical from cool-season), and low-helicity, high-lifting condensation level (more usual from warm-season). Moreover, it has been observed an inverse correlation between convective available potential energy and vertical wind-shear, especially at 0-3 km layer. This has motivated the redefinition of WMAXSHEAR parameter (the product of the square root of two times convective available potential energy and vertical wind-shear), using the 0-3 km layer for wind-shear, instead of 0-6 km layer. The new parameter has demonstrated to discriminate effectively those environments associated with (E)F2 or stronger events, which usually surpass 500 m^2 s^{-2}, from the rest. Furthermore, it has been observed that Szilagyi nomogram identify correctly waterspout-related environments in the vast majority of cases.

Results may contribute to enhance the detection and analysis of damaged areas due to strong-convective winds in the Iberian Peninsula and Balearic Islands. The tools presented

here may help to build up robust and homogeneous databases which discriminate between tornadoes and downburst. Indeed, these data should be able to be used as the base for future works and to enhance the knowledge of tornadic events distribution and characteristics. On the other hand, the analysis of favourable conditions for tornadogenesis carried out may be useful for forecasting and surveillance tasks of this kind of severe weather phenomena. The improvement of typical tornadic environments detection is especially interesting for the area of study, as contains some of the regions where tornadoes are the most frequent in southern Europe.

Índex

Acrònims

AEMET Agencia Estatal de Meteorología.

B Escala de Beaufort.

BRNSHR Bulk Richardson number shear.

CAPE Energia potencial convectiva disponible / Convective available potential energy.

CCS Consorcio de Compensación de Seguros.

CIN Inhibició convectiva / Convective inhibition.

DI Indicador de dany / Damage indicator.

DoD Grau de dany / Degree of damage.

ECMWF European Centre for Medium-Range Weather Forecasts.

EF Escala de Fujita millorada / Enhanced Fujita scale.

EHI Energy helicity index.

EL Nivell d'equilibri / Equilibrium level.

EMA Estació meteorològica automàtica.

ESSL European Severe Storms Laboratory.

ESWD European Severe Weather Database.

F Escala de Fujita.

HSLC Cisallament del vent elevat i CAPE baixa / High-shear, low-CAPE.

ICGC Institut Cartogràfic i Geològic de Catalunya.

IF Escala internacional de Fujita.

LCL Nivell de condensació per elevació / Lifting condensation level.

LFC Nivell de convecció lliure / Level of free convection.

LHHLCL Helicitat baixa i LCL elevat / Low-helicity, high-LCL.

LMI Radar de Tivissa-Llaberia, del SMC.

ML Parcel·la d'aire de la capa de mescla / Mixed-layer parcel.

MU Parcel·la d'aire més inestable / Most-unstable parcel.

NWS National Weather Service.

SB Parcel·la d'aire de superfície / Surface-based parcel.

SCP Supercell composite parameter.

SINOBAS Sistema de Notificación de Observaciones Atmosféricas Singulares.

SMC Servei Meteorològic de Catalunya.

SRH Helicitat relativa a la cèl·lula convectiva / Storm-relative helicity.

STP Significant tornado parameter.

T Escala de TORRO.

TORRO Tornado and Storm Research Organisation.

UTI Universal tornadic index.

VGP Vorticity generation parameter.

WMAXSHEAR producte del cisallament vertical del vent i l'arrel quadrada de dues vegades la CAPE.

WS Cisallament vertical del vent / Wind-shear.

XOM Xarxa d'Observadors Meteorològics.

XRAD Xarxa de Radars, del SMC.

Capítol 1

Introducció

1.1 Tornados i mànegues marines

L'*American Meteorological Society Glossary* (AMS, 2020), defineix tornado i mànega marina com (traduït de l'anglès):

- **Tornado**: columna d'aire en rotació, en contacte amb la superfície, que penja d'un núvol cumuliforme, i sovint visible en forma de tuba (núvol d'embut) i/o pols/restes en rotació a prop del terra (Figura 1.1a).
- **Mànega marina (o tromba marina)**: en general, un tornado sobre la superfície marítima (Figura 1.1b).

Unes definicions amb les quals ens hem basat a l'hora d'escriure aquest treball i que, de manera semblant, també queden recollides al glossari meteorològic d'Eduard Fontserè (Fontserè, 1948). Cal afegir que el terme *tuba* o *núvol d'embut* també s'utilitza per a referir-se a aquells casos en què és visible el complement de núvol en forma d'embut que penja d'un núvol cumuliforme malgrat que el vòrtex no arriba a estar en contacte amb la superfície terrestre o marítima (Figura 1.1c). A banda, els termes *fibló* i *cap de fibló* es fan servir indistintament tant per a referir-se a tornados situats terra endins com a mànegues marines (Gayà, 2018).

Els tornados són el fenomen meteorològic que pot donar lloc als vents més forts en superfície a la Terra. En els casos més intensos, el vent pot arribar a superar àmpliament els 100 m s^{-1} (Fujita, 1971; Wakimoto et al., 2015). És per aquest motiu que poden provocar danys materials molt greus en tota mena d'edificacions, amb el consegüent impacte socioeconòmic, i fins i tot danys personals. Segons la classificació proposada per Orlanski (1975), formen part de l'escala micro-α o micro-β, amb un temps i una longitud característics d'1 min a 1 h i de 20 m a 2 km, respectivament. En canvi, seguint la classificació de Fujita (1981), els tornados se situen entre l'escala miso-α i la miso-β, amb una longitud característica de 40 m a 4 km.

Qualsevol estructura convectiva, si es donen les condicions adequades, pot donar lloc a un tornado, des d'una cèl·lula aïllada fins a un sistema convectiu de mesoescala, de vegades sense necessitat que hi hagi precipitació intensa ni descàrregues elèctriques (Wakimoto i Wilson, 1989). Ara bé, els més intensos i que tenen una major durada solen estar lligats a un mesocicló, que és el corrent d'aire ascendent en rotació que caracteritza les supercèl·lules. És per aquest motiu que sovint es diferencia entre els tornados mesociclònics i els no mesociclònics (Markowski i Richardson, 2009).

A causa de les seves escales de temps i de longitud característiques tan petites, avui en dia no és possible pronosticar on i quan es pot formar un tornado amb dies o hores d'antelació. En canvi, sí que es pot conèixer quan hi pot haver un entorn favorable per a la seva formació, que sol estar caracteritzat per unes condicions d'inestabilitat i cisallament vertical del vent elevades

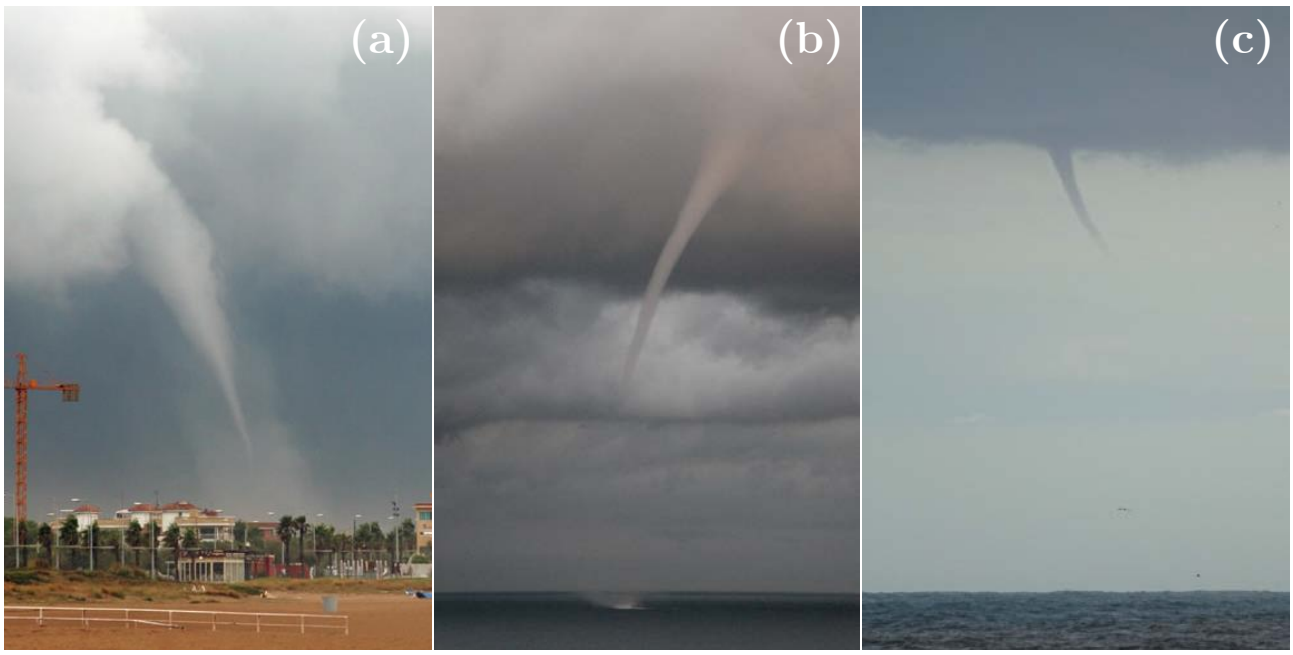

Figura 1.1: (a) Fotografia d'un tornado al Baix Llobregat el 7 de setembre de 2005 (autor: Manuel M. Conde), (b) d'una mànega marina a Badalona el 27 d'octubre de 2012 (autor: Oriol Rodríguez) i (c) d'una tuba a Malgrat de Mar el 15 d'octubre de 2018 (autor: Oriol Rodríguez).

(Rasmussen i Blanchard, 1998). A partir d'aquí, la vigilància meteorològica és un factor clau per a poder identificar les cèl·lules o estructures convectives que poden acabar donant lloc a un tornado mitjançant eines de teledetecció i els productes que se'n deriven (Zrnić et al., 1985; Elizaga et al., 2007; Stensrud et al., 2009; Farnell et al., 2017). D'aquesta manera és possible anticipar-se uns minuts a la seva formació, un temps que pot ser clau per a alertar a la població (Durage et al., 2013).

Els tornados poden formar-se a qualsevol indret del planeta, si bé se solen concentrar entre els 20° i 60° de latitud (Goliger i Milford, 1998). La seva distribució no és gens homogènia. Hi ha algunes regions on les condicions favorables per a la seva formació es presenten amb una major freqüència i són més extremes, de manera que hi ha més tornados i aquests són més intensos. És el cas dels Estats Units, on cada any de mitjana s'observen 1217 fiblons (NOAA/SPC, 2019). A la zona de les Grans Planes, sobretot durant la primavera, se superposa l'aire càlid i humit advectat des del Golf de Mèxic, i l'aire sec i sobreelevat per les muntanyes Rocalloses situades a l'oest amb el pas de solcs i baixes que porten associat aire fred en altura (Taszarek et al., 2020b). D'aquesta manera s'aconsegueixen els tres ingredients necessaris per a la convecció profunda (inestabilitat, humitat a nivells baixos i algun mecanisme que dispari la convecció) i un cisallament vertical del vent marcat, que afavoreix l'organització de la convecció (Markowski i Richardson, 2010). El sud-est de l'Amèrica del Sud i l'extrem est de l'Àsia són altres dues zones on els entorns favorables per a la formació de tornados són freqüents (Brooks et al., 2003).

En el cas d'Europa, de mitjana hi ha 242 tornados cada any i, des de 1950, els fiblons han arribat a causar 4462 ferits i 316 morts, amb danys per valor de, com a mínim, 1 bilió d'euros (Antonescu et al., 2017). A l'hora d'interpretar aquestes xifres, cal tenir en compte que a Europa no existeix un sistema de seguiment i rastreig dels tornados tan exhaustiu com als Estats Units, de manera que molt probablement la proporció de casos no comptabilitzats és superior que a l'Amèrica del Nord. Tot i que la majoria de tornados al continent europeu són febles (Antonescu et al., 2016), com també passa a la resta del planeta, ocasionalment es produeixen alguns episodis violents (Wesolek i Mahieu, 2011; Zanini et al., 2017). Els països europeus on els tornados són més habituals són Alemanya, els Països Baixos, Bèlgica i el Regne Unit, segons Antonescu et al. (2017). Nogensmenys, a la Mediterrània hi ha alguns dels indrets

on l'orografia juga un paper clau a l'hora de fer-los molt més freqüents que en zones properes. Destaquen Xipre, la costa sud de Turquia, la vall del riu Po (Itàlia) i la zona compresa entre Catalunya i les Illes Balears (Gayà, 2011; Riesco et al., 2015).

La distribució espacial dels tornados al conjunt de Catalunya tampoc és homogènia. El tram del litoral i prelitoral comprès entre els rius Tordera i Llastres és on se n'observen més habitualment, coincidint amb la zona amb una major densitat de població (Gayà, 2018). D'aquesta manera, les dues àrees metropolitanes més importants, la de Barcelona i la de Tarragona, es troben dins la zona més afectada pels tornados, alguns dels quals s'han descrit en diversos casos d'estudi (Bech et al., 2007, 2011, 2016, 2018; Mateo et al., 2009; Pineda et al., 2011).

Si es posa el focus en els tornados significatius, és a dir, aquells que han estat catalogats amb una intensitat igual o superior a F2 o EF2, segons l'escala de Fujita (F; Fujita, 1971) o l'escala de Fujita millorada (EF; WSEC, 2006), respectivament, es pot observar que la major incidència és a l'àmbit del Camp de Tarragona (Figura 1.2). En aquesta regió de 2700 km^2 (8,4 % de la superfície de Catalunya) hi ha hagut 7 dels 24 (E)F2+ registrats (el 29,2 %) entre els anys 1850 i 2019.

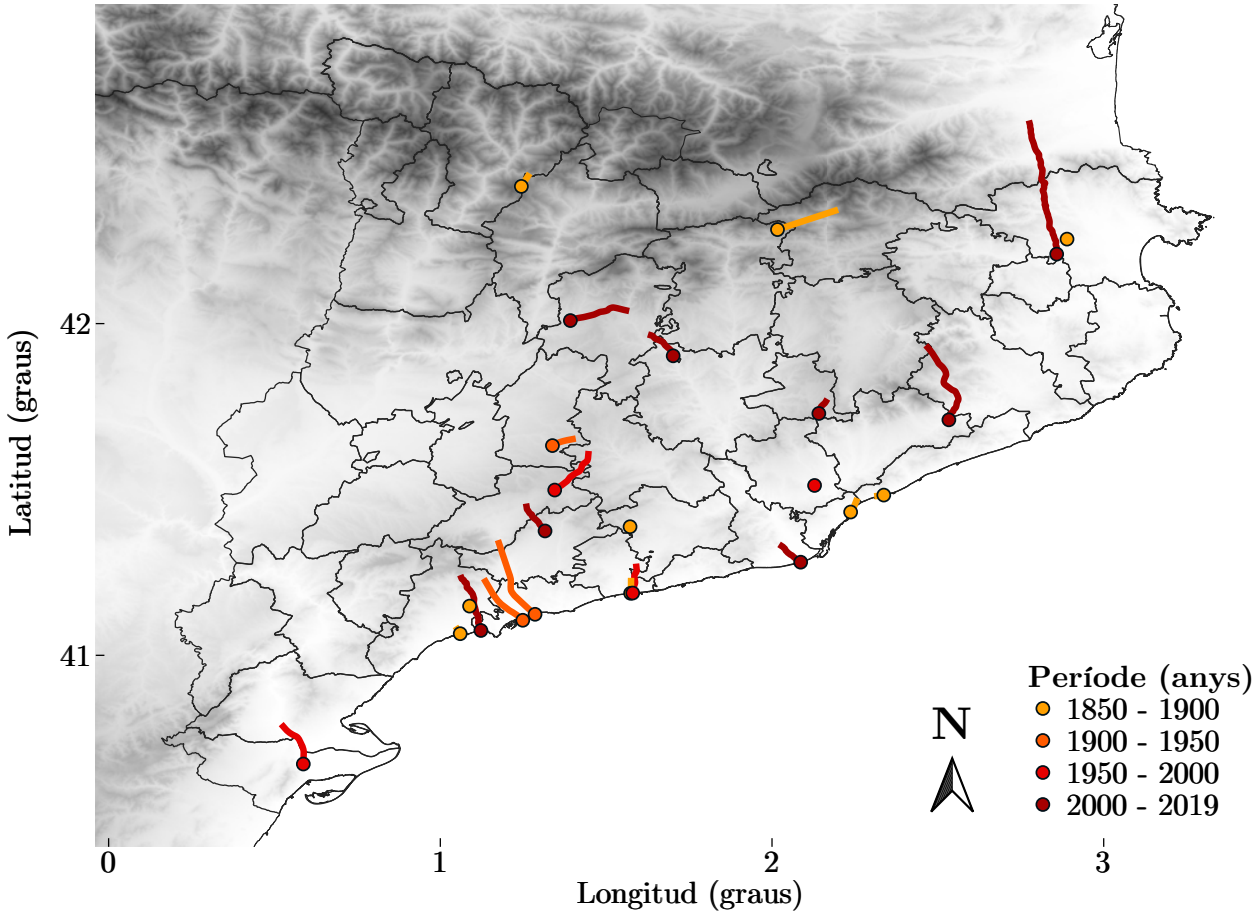

Figura 1.2: Punt d'inici i recorregut dels tornados d'intensitat (E)F2+ registrats a Catalunya entre 1850 i 2019. Dades de Gayà (2018), Rodríguez i Bech (2018, 2020a) i de l'hemeroteca de diversos mitjans de comunicació.

No és cap novetat que hi hagi tornados i trombes marines a Catalunya. Hi ha referències històriques sobre l'observació d'aquest fenomen al territori (Gayà, 2018) i, fins i tot, apareixen en algunes obres d'art (Hoinka i de Castro, 2005) i en obres literàries d'autors reconeguts com Jacint Verdaguer (Verdaguer, 1887), Joaquim Ruyra (Ruyra, 1920) o Josep Pla (Pla, 1966). De fet, a "Excursions i viatges" Verdaguer descriu l'estat amb què va trobar una avetosa del Pirineu, a cavall de les comarques de l'Alt Urgell i el Pallars Sobirà, fruit del pas d'un possible fibló a la segona meitat del segle XIX (vegeu el requadre; Gasull, 2015).

«Tot aquell vessant immens fa vint-i-cinc anys estava cobert d'avets, com un cap jove de cabells, que abrigaven la muntanya. Era l'avetar més gran de Catalunya per sa extensió i el més notable per l'altura i gruixudària de sos avets descomunals, anomenats en tota nostra muntanya: gairebé com en la Palestina los cedres del Líbano. Doncs, una 'torbera', com diuen allà, o un terbolí infernal, que hi passà de deu a onze hores de la nit, ne trencà la gran part, los arrancà, transportant-los ab son gran pa d'arrels a llargues distàncies, llançant-los a dreta i a esquerra, torçuts, malmesos i eixonats. Més avall los avets eren més alts i espessos, i no podent-los la ventada arrancar tots, los trencava arran de terra, o un tros amunt, i els llançava còrrecs avall a feixos, com si fossen cames de blat de moro.» (Verdaguer, 1887)

Al conjunt de Catalunya, les indemnitzacions pagades pel *Consorcio de Compensación de Seguros* (CCS) entre els anys 2005 i 2019 per danys per tornado a béns assegurats corresponen a 17,0 M€. Es tracta del 6,7 % dels 252,6 M€ de danys per vent. Ara bé, cal tenir en compte que 192,5 M€ del total són fruit del temporal de vent causat pel cicló Klaus dels dies 23 i 24 de gener de 2009 (Liberato et al., 2011; Bertotti et al., 2012). Per tant, excloent aquest episodi excepcional, el percentatge de danys per tornado sobre el total ascendeix fins al 28,3 %. Les indemnitzacions per a la resta de fenòmens que porten associat vent fort d'origen convectiu (esclafits i fronts de ratxa) corresponen a 5,3 M€.

Durant les darreres dècades s'ha detectat un augment en el nombre d'observacions de tornados a bona part del planeta. En bona part, l'increment ha estat degut a les noves tecnologies, com per exemple els telèfons mòbils amb càmera i internet, i les xarxes socials (Hyvärinen i Saltikoff, 2010). Aquestes eines han afavorit que fenòmens locals i de curta durada com els fiblons puguin ser fàcilment fotografiats i que aquesta informació pugui arribar de manera ràpida a un públic molt més ampli (Gayà et al., 2011; Rauhala et al., 2012).

Ara bé, en el context actual de canvi climàtic, l'escalfament global ha tingut algun efecte sobre la tendència creixent del nombre d'observacions de tornados? Segons consta a l'informe "*Managing the Risks of Extreme Events and Disasters to Advance Climate Change Adaptation*" de l'*Intergovernmental Panel on Climate Change* (IPCC, Seneviratne et al., 2012) el nivell de confiança és baix en relació amb la tendència creixent observada en fenòmens de petita escala com els tornados, a causa de la inhomogeneïtat de les dades i la manca d'adequació dels sistemes de control. Alguns articles recents basats en l'anàlisi de l'evolució de paràmetres convectius mitjançant dades de reanàlisi mostren que durant les darreres dècades no hi ha hagut una tendència clara i amb significança estadística pel que fa a la freqüència amb què hi ha entorns favorables per a tempestes violentes i per a tornados a la Mediterrània occidental (Taszarek et al., 2020a).

Tot i això, diversos estudis apunten que al llarg d'aquest segle la inestabilitat termodinàmica podria augmentar, principalment a causa de l'augment de la humitat específica a nivells baixos fruit de l'escalfament planetari, mentre que la tendència del cisallament vertical del vent és poc clara. Això podria conduir a un augment de la freqüència en l'ocurrència d'entorns favorables per a tempestes violentes, incloent-hi els tornados (Viceto et al., 2017; Martins et al., 2020). Segons Púčik et al. (2017), aquest increment s'accentuaria a finals de segle, i seria més destacable en els escenaris amb un forçament radiatiu major (RCP8.5).

A partir del que s'ha exposat prèviament, es poden identificar diversos punts que motiven aquest treball:

- La Península Ibèrica i les Illes Balears concentren algunes de les zones on els tornados es presenten amb més freqüència al sud d'Europa
- La regió de Catalunya més afectada pels tornados inclou les dues àrees metropolitanes més importants del país

- De cara al futur és probable que augmenti la freqüència amb què es presenten els entorns favorables per a les tempestes violentes
- El coneixement dels entorns favorables per a la formació de tornados pot ajudar a millorar la predicció i la vigilància meteorològica

Per tant, és necessari un major coneixement dels fiblons al sud-oest d'Europa, tant pel que fa a la seva distribució espacial i temporal i les seves característiques, com pels entorns que n'afavoreixen la formació. Així, l'exposició anterior motiva les següents qüestions generals, per a les quals s'ha treballat per a donar-hi resposta:

- Quines eines es poden utilitzar per a construir una base de dades robusta i tan homogènia com sigui possible d'episodis de tornados?
- Com són els entorns favorables per a la tornadogènesi a la Península Ibèrica i a les Illes Balears?
- Quines diferències hi ha entre els entorns favorables per a la formació de tornados significatius i per a tornados febles?

1.2 Estat de l'art

1.2.1 Escales d'intensitat

Una de les característiques més rellevants d'un tornado que se sol incloure a les bases de dades és la intensitat de l'episodi, és a dir, la velocitat màxima del vent en superfície. Ara bé, és molt poc habitual aconseguir-ne mesures directes. En ser fenòmens molt locals, és estrany que un tornado afecti una estació meteorològica (Fox-Hughes et al., 2018) i, en cas de fer-ho, és molt probable que no coincideixi amb el moment en el qual ha estat més intens. Per exemple, en el cas de Catalunya, tan sols en 6 dels 105 tornados registrats entre els anys 2000 i 2019 s'ha pogut obtenir dades de vent d'alguna estació meteorològica automàtica (EMA) situada dins la traça de danys (Taula 1.1).

Taula 1.1: Data, municipi, localització (latitud, longitud i distància respecte al centre de la traça de danys) i font de les EMA que han mesurat el vent associat a un tornado a Catalunya entre els anys 2000 i 2019. Els valors positius de la distància de l'EMA respecte al centre de la traça indiquen que se situa a la dreta d'aquest segons el sentit de moviment del tornado, mentre que els negatius indica que se situa a l'esquerra. Les dades provenen d'AEMET, de la Xarxa General d'Alarmes i Comunicacions (XAC) de la Direcció General de Protecció Civil i de diversos observadors meteorològics (OBS). Només s'han llistat els registres de les EMA que s'han situat dins la traça de danys.

Data	**Municipi**	**Lat.**	**Lon.**	**Distància al centre (m)**	**Ratxa màx.** ($m\ s^{-1}$)	**Font**
07/09/2005	el Prat de Ll.	41,3045°	2,1029°	70	34,5	AEMET
08/09/2005	Mollet del V.	41,5398°	2,2180°	-40	24,2	OBS
02/11/2008	Reus	41,1563°	1,1009°	10	31,4	OBS
21/03/2012	Ivars d'Urgell	41,6781°	0,9907°	15	26,4	OBS
14/10/2018	els Pallaresos	41,1768°	1,2585°	25	36,7	XAC
15/10/2018	Tordera	41,7176°	2,6895°	-30	30,3	OBS

Precisament, durant les darreres dècades als Estats Units s'han dut a terme diverses campanyes, com per exemple VORTEX (Rasmussen et al., 1994), VORTEX2 (Wurman et al., 2012)

i VORTEX-Southeast (NSSL/NOAA, 2020), que entre altres objectius perseguien aconseguir mesures *in situ* del vent associat als tornados. Una de les pràctiques que se segueix en aquest tipus d'estudis de camp consisteix a col·locar estacions meteorològiques portàtils a la trajectòria del tornado (Karstens et al., 2010b).

Una altra manera de mesurar la velocitat del vent és mitjançant dades radar (Wurman et al., 2013; Kosiba et al., 2013). Amb les dades de les xarxes de radars del Servei Meteorològic de Catalunya (SMC) o de l'*Agencia Estatal de Meteorología* (AEMET), que treballen amb banda C (longitud d'ona entorn els 5,35 cm), en els episodis mesociclònics sovint es pot observar la rotació del mesocicló, però en general no tenen prou resolució per a resoldre el vòrtex associat al tornado. Per a fer-ho possible, és necessari l'ús de radars portàtils que típicament treballen amb una longitud d'ona nominal curta, com és el cas de la banda X (4 - 2,5 cm) (Toth et al., 2013). Ara bé, com menor és la longitud d'ona, més petit és l'abast del radar, de manera que per a poder prendre mesures d'un tornado cal que aquest afecti una zona propera.

Finalment, en cas de disposar d'imatges de vídeo, també es pot estimar la velocitat del vent mitjançant tècniques de fotogrametria (Golden i Purcell, 1977; Gayà i Redaño, 1999). Tot i això, aquesta tècnica d'anàlisi tan sols és possible quan hi ha imatges de vídeo referenciades correctament en l'espai i el temps, amb una bona resolució, obtingudes a una distància no gaire allunyada del vòrtex i en condicions de bona visibilitat.

Amb cap dels mètodes exposats prèviament és possible aconseguir dades de manera habitual per a la majoria dels tornados observats, sinó tan sols per a alguns casos concrets. Davant la necessitat de conèixer la intensitat d'aquests fenòmens, T. T. Fujita va proposar durant la dècada dels anys setanta del segle passat una escala que relacionava els danys causats per un tornado amb la velocitat del vent, coneguda com a escala de Fujita (F; Fujita, 1971, 1981).

Per definició, l'escala de Fujita uneix l'extrem superior de l'escala de Beaufort (B; força 12) amb el número 1 de Mach en 12 graus, fent coincidir el llindar inferior de B12 amb l'inferior de F1. Segueix l'equació següent:

$$v_F = 6,30(F+2)^{3/2} \tag{1.1}$$

essent v_F el llindar inferior de la velocitat del vent (en m s^{-1}) corresponent al grau F de l'escala de Fujita. Malgrat que tal com s'ha comentat aquesta escala té 12 graus, el seu ús habitual per a estimar la intensitat dels fiblons queda restringida en els primers 6 (de F0 a F5, vegeu la Taula 1.2). Segons la definició de Fujita (1971), es considera que la durada de la ràfega de vent responsable d'uns danys determinats hauria de durar el temps que trigaria a recórrer 1/4 de milla (p. ex., per a 100 m s^{-1}, serien 4 s).

Aquesta escala fou adoptada pel *National Weather Service* (NWS, EEUU) durant la dècada dels anys setanta i el seu ús es va estendre per bona part de la comunitat científica d'arreu. Posteriorment, a Fujita (1992) es va introduir una ponderació de l'escala F original en funció del tipus d'element malmès i de la solidesa de les estructures afectades.

Independentment, i també durant la dècada dels anys setanta, des de la *Tornado and Storm Research Organisation* (TORRO, Regne Unit) es va proposar una altra escala que tenia la mateixa funció que l'escala F (Meaden, 1976). Amb el nom d'escala de TORRO (T), es va concebre com una extensió de l'escala Beaufort, prenent com a llindar inferior del primer grau el valor corresponent a l'extrem inferior de B8, seguint l'equació següent:

$$v_T = 2,367(T+4)^{3/2} \tag{1.2}$$

essent v_T el llindar inferior de la velocitat del vent (en m s^{-1}), en mitjana de 3 s, corresponent al grau T de l'escala de TORRO.

La resolució que proporciona aquesta escala és major que l'escala F, ja que el rang que s'acostuma a utilitzar té 12 graus, en lloc de 6. Precisament, això facilita l'estimació de la

Taula 1.2: Llindars inferior i superior (en m s^{-1}) dels diversos graus de les escales T, F i EF i classificació dels tornados en funció de la intensitat.

T0 17-24 m s^{-1}	F0 18-32 m s^{-1}	Feble		
T1 25-32 m s^{-1}	EF0 29-38 m s^{-1}			
T2 33-41 m s^{-1}	F1 33-49 m s^{-1}			
T3 42-51 m s^{-1}	EF1 39-49 m s^{-1}			
T4 52-61 m s^{-1}	F2 50-69 m s^{-1}	Fort	Significatiu	
T5 62-72 m s^{-1}	EF2 50-60 m s^{-1}			
T6 73-83 m s^{-1}	F3 70-92 m s^{-1}			Intens
T7 84-95 m s^{-1}	EF3 61-73 m s^{-1}			
T8 96-107 m s^{-1}	F4 93-116 m s^{-1}	Violent		
T9 108-120 m s^{-1}	EF4 74-89 m s^{-1}			
T10 121-134 m s^{-1}	F5 117-142 m s^{-1}			
T11 $>$ 134 m s^{-1}	EF5 $>$ 89 m s^{-1}			

velocitat màxima del vent en els episodis més febles, els quals són els més habituals al conjunt del planeta (Meaden et al., 2007). Malgrat tot, l'ús de l'escala T no està tan estès.

Després de més de 30 anys emprant l'escala F, des de l'NWS es va iniciar una revisió d'aquesta a causa de les importants limitacions que presentava a l'hora de determinar la intensitat dels tornados. Per una banda, la descripció dels danys era massa general, sense indicadors de danys concrets. A més, tampoc es tenia en compte la variabilitat dels tipus de construcció, i no hi havia una correlació clarament definida entre els danys i la velocitat del vent, segons s'apunta a WSEC (2006). Per aquest motiu, a principis dels 2000 el *Wind Science and Engineering Research Center* de la *Texas Tech University* va desenvolupar l'escala de Fujita millorada (EF), amb la participació de 23 experts en l'estimació de la velocitat del vent en tornados.

La nova escala es divideix en sis categories, d'EF0 a EF5 (semblant a l'original), malgrat que els rangs de velocitat del vent per a cadascun dels nivells és diferent respecte als graus F0 a F5 de l'escala F (vegeu la Taula 1.2). Nogensmenys, existeix una relació entre les dues escales, la qual ve descrita per l'equació:

$$v_{EF} = 0,6246 v_{F'} + 16,269 \tag{1.3}$$

essent v_{EF} la velocitat del vent (en m s^{-1}) en mitjana de 3 s segons l'escala EF i $v_{F'}$ la velocitat del vent (en m s^{-1}) en mitjana de 3 s segons l'escala F havent-la ajustat amb la corba de Durst (Durst, 1960).

L'escala EF consisteix en 28 indicadors de dany (DI; tipus de construcció o d'element), que

són des de cases mòbils o hospitals fins a arbres de fusta tova (com els pins) o fanals. A banda, per a cadascun d'aquests DI hi ha entre 3 i 12 graus de dany (DoD). De la combinació d'ambdós paràmetres s'obté un rang de velocitat del vent compatible amb el dany observat (WSEC, 2006) i, amb aquest, és possible associar un grau de l'escala EF al tornado que ha causat aquelles destrosses. A partir de l'any 2007 l'NWS deixà de fer servir l'escala F i començà a utilitzar l'escala EF.

Malgrat la sensible millora a l'hora de classificar els fiblons en funció de la seva intensitat, l'escala EF també presenta limitacions en fer-ne ús fora dels Estats Units. La majoria dels indicadors de dany corresponen a edificacions típiques d'aquell país, les quals són prou diferents de les que hi ha, per exemple, a Europa (Feuerstein et al., 2011). Així, des de diversos països s'ha fet la tasca d'adaptar l'escala EF a les realitats de cada territori (Environment Canada, 2013; JMA, 2015) o d'ampliar-la afegint nous indicadors de dany (Mahieu i Wesolek, 2016), fins i tot incloent-hi els danys en vehicles (Paulikas et al., 2016). Tot i això, per a resoldre aquestes problemàtiques de manera homogènia, des de l'*European Severe Storms Laboratory* (ESSL) i en col·laboració amb diversos centres meteorològics i de recerca s'està treballant en la proposta d'una nova escala que sigui fàcilment aplicable a qualsevol país, l'escala internacional de Fujita (IF; Groenemeijer et al., 2019a).

Seguint les escales esmentades, els tornados es classifiquen en diversos grups (Taula 1.2). Per una banda, es consideren tornados febles la intensitat dels quals és (E)F0 o (E)F1, o bé entre T0 i T3; els forts són aquells taxats com a (E)F2 o (E)F3, o entre T4 i T7, i els violents, els classificats com a (E)F4 o (E)F5, o entre T8 i T11. Sovint també s'anomenen tornados significatius els que són d'intensitat (E)F2 - T4 o superior, i tornados intensos els d'intensitat (E)F3 - T6 o superior.

1.2.2 Camp de vent d'un tornado en superfície

La dinàmica d'un tornado és altament complexa (Honerkamp et al., 2020). Cal tenir en compte que en el si del fibló es poden formar subvòrtexs o vòrtexs de succió, descrits per Fujita (1981) com a vòrtexs de mosoescala (longitud característica de 40 cm a 40 m). Aquests, que tant poden ser estacionaris com orbitar al voltant del centre del tornado, produeixen una acceleració local de la força del vent.

Tot i això, com a aproximació simple per a descriure el camp de vent d'un fibló en superfície es pot utilitzar el model del vòrtex de Rankine (p. ex. Bech et al., 2009; Sánchez-Laulhé et al., 2017). Està caracteritzat per una regió central on l'aire rota com un sòlid rígid (velocitat angular constant) i una regió externa on la velocitat de rotació decau seguint una relació inversament proporcional a la distància respecte al centre del vòrtex. El camp de vent associat ve definit, en coordenades polars, per:

$$v(r) = \begin{cases} \frac{v_{max} r}{R} & \text{if } r \leq R \\ \frac{v_{max} R}{r} & \text{if } r > R \end{cases} \tag{1.4}$$

essent $v(r)$ la velocitat del vent en funció de la distància al centre del vòrtex r, v_{max} la velocitat màxima del vent i R el radi en el qual $v(r) = v_{max}$.

Ara bé, el vòrtex en superfície no és purament tangencial, sinó que també hi apareix una component radial que, en funció de l'instant del cicle de vida del fibló, és més o menys important (Peterson, 1992). Per aquest motiu, en aquest model se superposen dos camps, un de tangencial i un de radial, ambdós descrits per l'equació 1.4 i amb el mateix radi de velocitat màxima R. A més, com que els tornados se solen moure solidàriament amb la cèl·lula convectiva que els ha format, cal sumar-hi la velocitat de translació v_{trans} per a obtenir el camp de vent final.

Johannes Letzmann (Peterson, 1992), un pioner en l'estudi dels tornados de principis del segle passat, va proposar caracteritzar aquest model mitjançant dos paràmetres adimensionals:

G i α. G correspon al quocient entre els mòduls de la velocitat tangencial màxima del vòrtex i la velocitat de translació, mentre que α és l'angle que forma el vector resultant de la suma dels vectors vent radial i vent tangencial respecte a l'eix radial, essent $\alpha = 0°$ per a un *inflow* pur, $\alpha = 90°$ per a un flux purament tangencial en el sentit contrari de les agulles del rellotge i $\alpha = 180°$ per a un *outflow* pur.

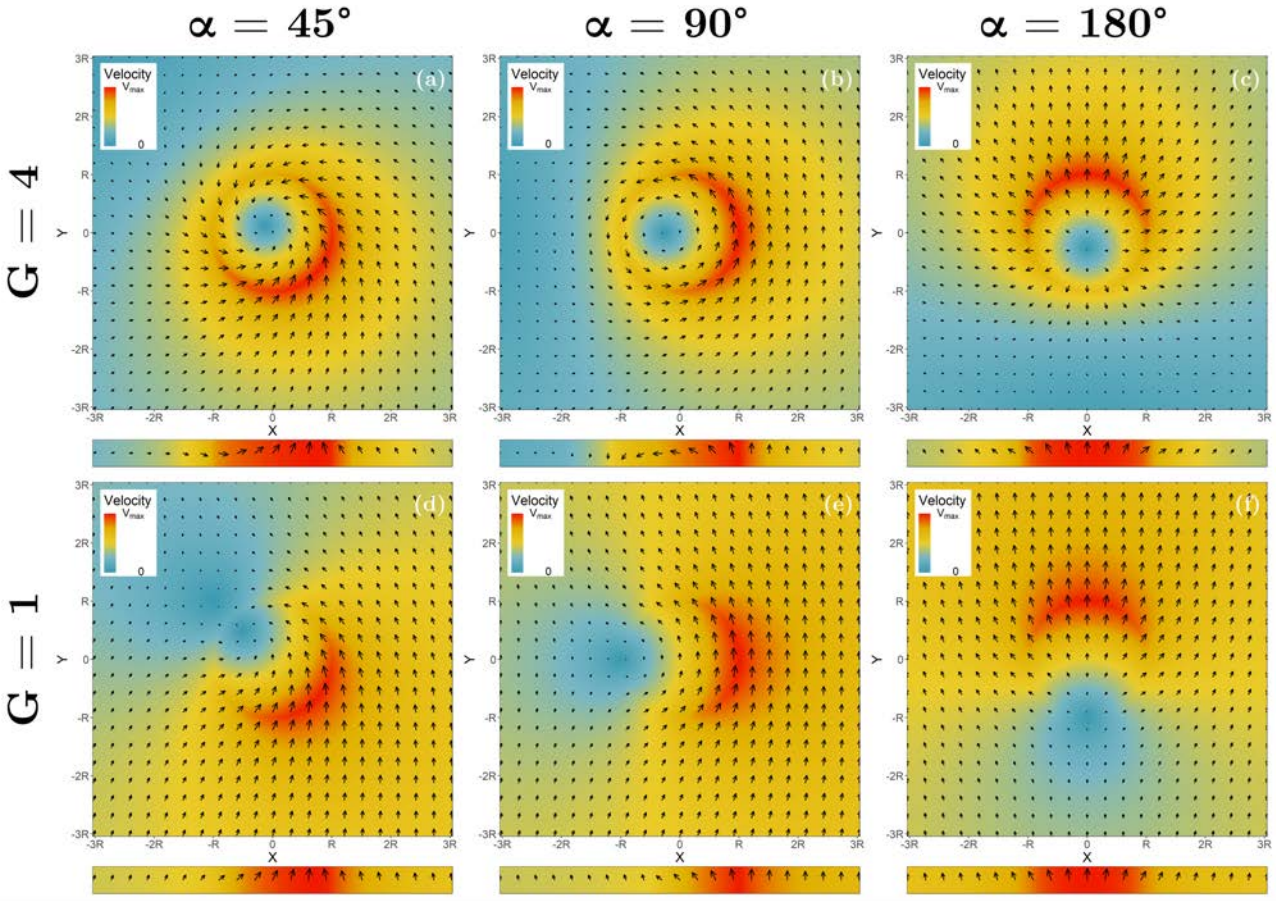

Figura 1.3: Camp de vent i franja de dany corresponent als casos particulars de $G = 4$ i (a) $\alpha = 45°$, (b) $\alpha = 90°$ i (c) $\alpha = 180°$, i $G = 1$ i (d) $\alpha = 45°$, (e) $\alpha = 90°$ i (f) $\alpha = 180°$. Figura extreta de Rodríguez et al. (2020), adaptada de (Bech et al., 2009).

A la Figura 1.3 es presenten sis casos particulars de combinacions de G i α: els panells (a), (b), (d) i (e) corresponen a un vòrtex en translació (tornado) i els panells (c) i (f), a un *outflow* pur en translació (esclafit). A banda del camp de vent, també s'hi mostra el patró de la franja de danys associat als diversos exemples (en el rectangle situat a sota de cadascun dels panells). Aquest es troba en calcular el vector màxim de vent al llarg de l'eix y, assumint que el vòrtex es desplaça de la part inferior a la part superior de la figura. Es pot observar com en el cas d'un fibló, el patró de danys és convergent o amb indicis de rotació, mentre que en el cas d'un esclafit, és divergent (Fujita, 1981; Wakimoto et al., 2020; Bolgiani et al., 2020).

Assumint que els arbres cauen seguint la direcció del vent, tal com es discuteix a Holland et al. (2006), es pot concloure que a partir de l'estudi del patró de danys sovint és possible estimar el camp de vent i, per tant, es pot conèixer quin fenomen meteorològic (tornado, esclafit o vent lineal, segons s'explica a la secció 1.2.3) ha tingut lloc. Aquesta és una tasca que té un especial interès per a aquells casos en els quals no existeix cap observació directa de l'esdeveniment.

L'ús d'aquest model ha donat resultats positius a l'hora de comparar-ho amb els danys reals causats per un tornado (Holland et al., 2006; Bech et al., 2009; Beck i Dotzek, 2010). Tot i això, hi ha altres models com el vòrtex de Burgers-Rott que, essent més complex, és també

més realista que el vòrtex de Rankine a l'hora de descriure el camp de vent d'un tornado en superfície (Tanamachi et al., 2007). Es tracta d'una solució exacta de les equacions de Navier-Stokes que presenta una transició més suau entre els sectors interior i exterior del màxim de vent.

1.2.3 Treballs de camp

Els treballs de camp són una de les fonts d'informació més importants en l'estudi dels fenòmens de vent intens d'origen convectiu. Es tracta de l'anàlisi *in situ* de les destrosses i de la recollida de tota aquella informació rellevant que pot ser d'utilitat per a reconstruir l'episodi, com per exemple el relat de testimonis directes de l'esdeveniment o la recopilació de vídeos de càmeres de seguretat i de dades d'estacions meteorològiques de particulars.

L'objectiu principal és geolocalitzar els elements afectats per a poder caracteritzar la traça de danys (amplada i longitud) i per a estimar la intensitat del vent fent ús d'alguna de les escales presentades a la secció 1.2.1 (Figura 1.4; Marshall, 2002). A banda, l'anàlisi del patró de danys, sobretot a partir de la direcció de caiguda dels arbres i d'altres elements, sovint permet estimar el camp de vent en superfície, tal com s'ha comentat a la secció 1.2.2. Això fa possible conèixer si les destrosses han estat causades per un tornado, un esclafit o per vents lineals, ja que la traça de danys presenta unes característiques concretes en funció del fenomen (Fujita, 1981; Bunting i Smith, 1993):

- Tornado: el patró de danys és convergent o presenta clars signes de rotació, la zona afectada sol ser estreta i allargada, i el gradient d'intensitat dels danys és elevat.
- Esclafit: el patró de danys és divergent, la zona afectada sol ser ampla i més aviat curta i tant pot ser rectilínia com corbada; el gradient d'intensitat dels danys és petit.
- Vent lineal (p. ex. front de ratxa): el patró de danys és lineal.

Precisament, a la Figura 1.4 es mostra el mapa resultant del treball de camp dut a terme al voltant del càmping Aqua Alba de Gualba (el Vallès Oriental) posterior al pas d'un tornado la nit del 22 al 23 d'octubre de 2019. Es pot observar com els arbres dels quals es va obtenir informació de la direcció de caiguda dibuixaven un patró convergent entorn de l'eix sud-nord (al centreesquerra del mapa), fruit del pas del fibló. Tot i això, cal tenir en compte que els patrons de danys no són sempre tan clars com el presentat en aquest exemple (Figura 1.3d, e, f) i, fins i tot, de vegades no és possible esclarir quin fenomen ha tingut lloc.

Aquest tipus d'anàlisi se sol fer mitjançant un estudi en superfície, recorrent l'àrea amb danys, per part d'un equip de persones sovint multidisciplinari (meteoròlegs, pèrits, enginyers). Ara bé, ocasionalment també s'utilitzen recursos com els vols d'helicòpter o d'avioneta (Bech et al., 2009) o, més recentment, els drons (Bai et al., 2017). Amb les imatges aèries es pot obtenir una visió general del conjunt de l'episodi i, a més, es pot aconseguir informació de zones de difícil accés. Tot i això, l'estudi a peu permet un major detall en l'anàlisi dels danys i en l'estimació de la intensitat del vent, especialment per als episodis més febles en els quals és difícil observar les destrosses menors (branques trencades o teules arrancades) des de l'aire.

Amb la informació obtinguda amb els treballs de camp es poden completar bases de dades de fenòmens de temps violent tal com es fa, per exemple, als EEUU (Verbout et al., 2006). Ara bé, per tal que la base de dades sigui homogènia, és convenient dur a terme aquests estudis per al nombre més gran possible d'episodis registrats. A banda, de les dades recollides *in situ* també se'n poden derivar informes i certificats d'utilitat per a l'administració i per a les asseguradores (SMC, 2018a, 2018b).

Les primeres guies sobre com procedir en l'anàlisi dels danys causats per un tornado en el lloc mateix dels fets foren McDonald i Marshall (1984) i Bunting i Smith (1993). Posteriorment,

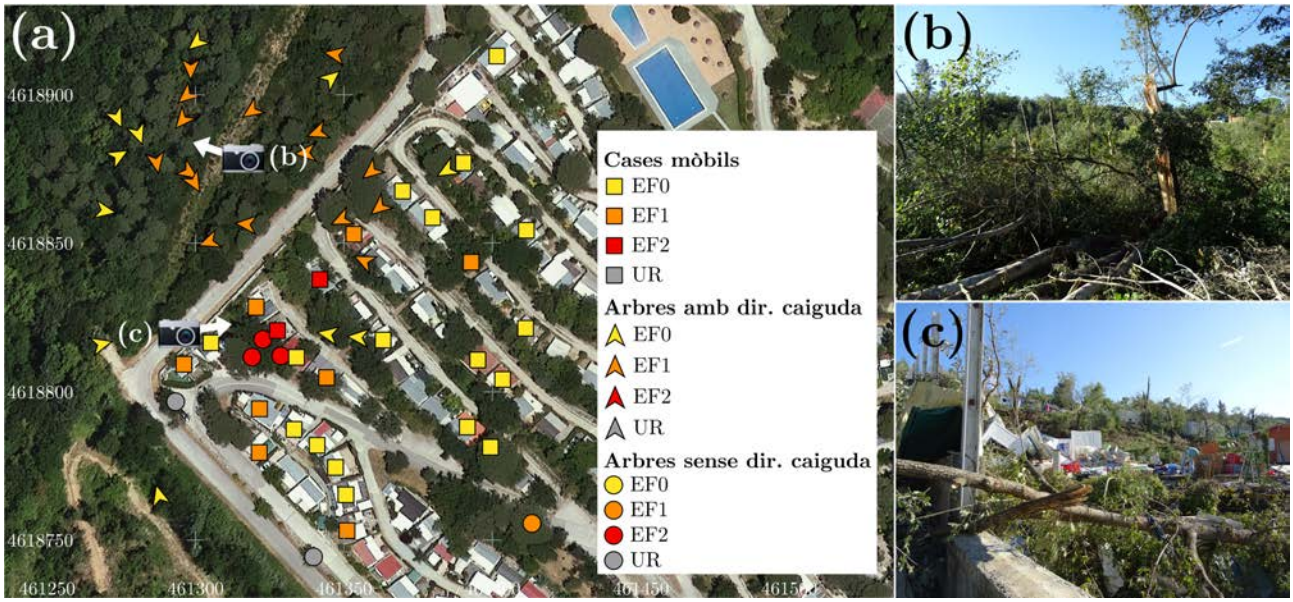

Figura 1.4: (a) Localització dels danys analitzats durant el treball de camp dut a terme el dia 25/10/2019 al càmping Aqua Alba de Gualba (el Vallès Oriental). S'hi mostren tres tipus de marcacions: els quadrats corresponen a cases mòbils, les sagetes a arbres amb direcció de caiguda coneguda, i els cercles a arbres sense direcció de caiguda coneguda. El color de les marcacions indica el grau de l'escala EF assignat als elements analitzats, essent el groc per a EF0, el carabassa per a EF1, el vermell per a EF2 i el gris per a indeterminat. A banda, al mapa s'hi mostra l'orientació i la localització des d'on es van prendre les fotografies (b) bosc afectat i (c) cases mòbils del càmping greument malmeses.

durant la primera dècada dels 2000 es va incorporar a l'operativa dels treballs de camp les càmeres de fotografiar digitals i l'ús del GPS, que va facilitar la feina de geolocalitzar de manera precisa els elements afectats (Edwards et al., 2013).

1.2.4 Identificació de traces de danys mitjançant imatges aèries d'alta resolució

Les imatges aèries d'alta resolució són una eina que sovint s'utilitza per a analitzar els canvis en el territori. Amb les dades de satèl·lits com el LANDSAT (30 m de resolució, Irons et al., 2012) i les ortofotografies que proporcionen entitats com l'Institut Cartogràfic i Geològic de Catalunya (ICGC, 25-35 cm de resolució, ICGC, 2019) es poden observar i estudiar les conseqüències d'esllavissades (Deijns et al., 2020), inundacions (Lucía et al., 2015) o incendis forestals (Shikhov et al., 2019).

La identificació de les traces de danys produïdes per tornados o esclafits també es pot dur a terme mitjançant l'anàlisi d'aquests tipus d'imatges (Molthan et al., 2014, 2020; Womble et al., 2018). L'estudi i comparativa d'imatges anteriors i posteriors a un episodi permet identificar canvis en la cobertura vegetal, ja sigui mitjançant una inspecció visual (Fig. 1.5) o amb el càlcul d'índexs de vegetació (p. ex. NDVI, Tucker, 1978; NDII, Wang et al., 2010). D'aquesta manera, s'aconsegueix delimitar les zones forestals afectades.

Per altra banda, quan les imatges tenen una resolució molt alta (inferior a 1 m) és possible observar canvis en les cobertes d'edificacions fruit de la substitució o reparació de les parts malmeses. També es poden identificar individualment els arbres afectats (Fig. 1.5b, c, d). Aquest fet permet l'estudi del patró de danys i conèixer quin fenomen en fou el causant (és a dir, un tornado o un esclafit), de manera semblant a com es fa en els treballs de camp.

Aquests tipus d'anàlisi complementen els treballs de camp, ja que permeten tenir una visió general de l'episodi estudiat i proporcionen informació de zones de difícil accés. Això fa possible

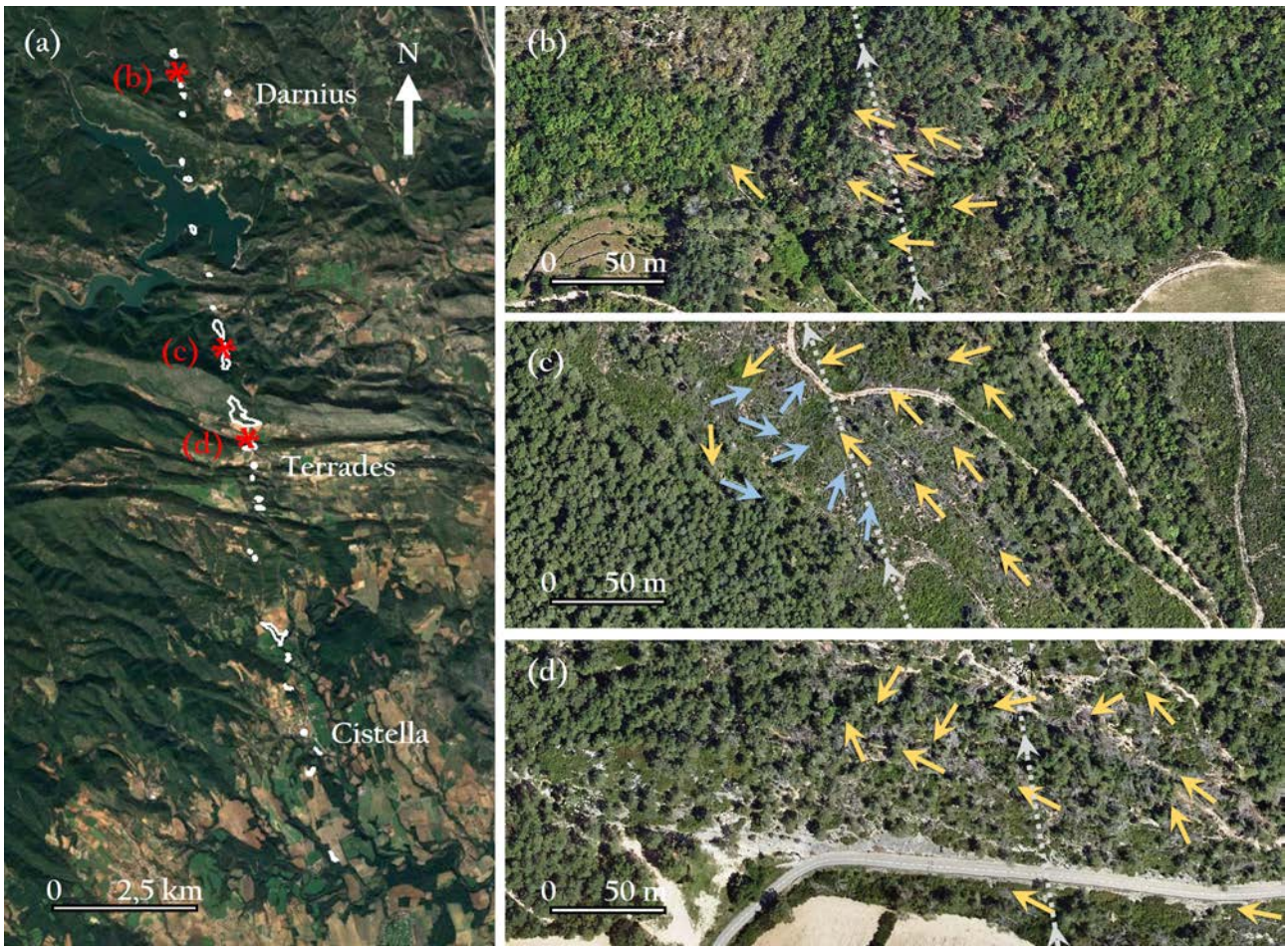

Figura 1.5: (a) Zones de bosc situades entre Cistella i Darnius afectades pel tornado que hi va haver el 7 de gener de 2018 entre Navata (l'Alt Empordà) i Terrats (el Vallespir), delimitades amb contorns blancs. Amb asteriscs vermells hi ha marcades les franges que es mostren amb més detall a (b), (c) i (d), on hi ha indicat el recorregut del tornado (línia puntejada grisa) i la direcció de caiguda dels arbres per a un angle de 0 a 179° respecte a la direcció del moviment del vòrtex (fletxes blaves) i per a un angle de 180 a 359° (fletxes grogues).

la construcció de bases de dades robustes i més homogènies, ja que l'observació de danys és independent de la densitat de població (Shikhov i Chernokulsky, 2018). Ara bé, cal tenir en compte que les destrosses ocasionades per fenòmens molt febles (normalment d'intensitat EF0) no solen ser observables amb imatges aèries. A més, per a fer una estimació detallada de la intensitat de l'episodi és necessari analitzar l'estat de conservació de les estructures i els elements malmesos, una tasca que cal fer-la *in situ*.

1.2.5 Bases de dades de tornados i mànegues marines a la Península Ibèrica i les Illes Balears

La detecció de tornados i de trombes marines depèn de l'observació directa. És per aquest motiu que generar un recull de casos és una tasca que no es pot automatitzar i que, a més, requereix dedicació per tal de no introduir-hi altres tipus d'episodis de vent fort d'origen convectiu. Tot i això, es tracta d'una feina necessària per a poder conèixer la freqüència amb què els fiblons afecten una zona concreta i les característiques que presenten, a banda de ser la base per a poder dur a terme altres estudis.

Tal com passa amb les bases de dades d'inundacions (Barnolas i Llasat, 2007), les de tornados sovint s'han nodrit de la informació facilitada pels mitjans de comunicació. A banda, els

observadors meteorològics i els testimonis casuals també han aportat un elevat nombre de casos als reculls. Ara bé, més recentment s'ha vist com la presència de telèfons mòbils amb càmera ha afavorit la detecció de fiblons i, per la seva banda, internet i les xarxes socials han ajudat a fer-ne una major difusió (Hyvärinen i Saltikoff, 2010; Farnell i Rigo, 2020). Aquest fet ha motivat la posada en marxa de diverses plataformes col·laboratives de ciència ciutadana com la Xarxa d'Observadors Meteorològics (XOM) de l'SMC (Ripoll et al., 2016), el *Sistema de Notificación de Observaciones Atmosféricas Singulares* (SINOBAS) de l'AEMET (Gutiérrez et al., 2015) i l'*European Severe Weather Database* (ESWD) de l'ESSL (Dotzek et al., 2009).

Miquel Gayà va fer un seguiment exhaustiu dels tornados a Espanya entre principis de la dècada dels noranta i fins a l'any 2012, incloent-hi l'elaboració de treballs de camp (Homar et al., 2001). A banda, el recull de casos fou completat amb episodis d'anys anteriors fruit d'una anàlisi meticulosa d'escrits històrics d'arxius i biblioteques i de l'hemeroteca de diversos diaris (p. ex. Gayà, 2007), fet que va derivar en la primera base de dades completa i d'accés públic d'Espanya (Gayà, 2018). Aquest llistat, que consta de 692 tornados, 223 possibles tornados, 489 mànegues marines, 16 possibles mànegues marines, 195 tubes i 1 possible tuba, ha estat una contribució molt rellevant per a poder estudiar la distribució espacial dels tornados en l'àmbit Europeu (Figura 1.6a; Antonescu et al., 2017).

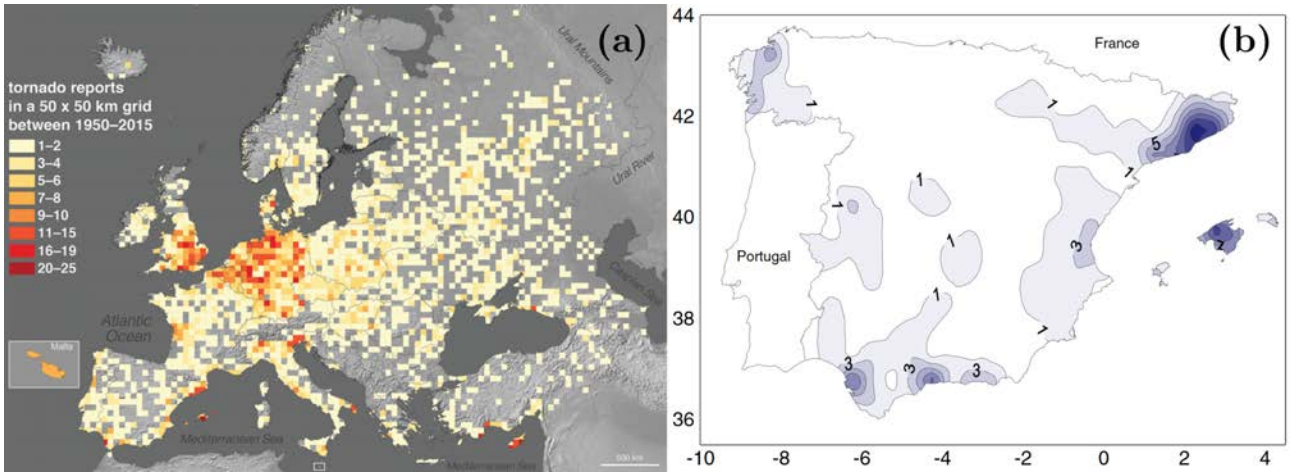

Figura 1.6: (a) Nombre de tornados observats a Europa entre 1950 i 2015 per a una malla de 50 km x 50 km (Figura 1a d'Antonescu et al. (2017)), i (b) densitat de tornados a l'Espanya peninsular i les Illes Balears (casos per 0.5° x 0.5°) per al període 1976-2009 (Figura 8 de Gayà (2011)).

L'anàlisi d'aquestes dades ha permès identificar les zones de la Península Ibèrica i les Illes Balears on els tornados són més freqüents (Figura 1.6b). D'acord amb Gayà (2011), el màxim se situa entre Catalunya i les Illes Balears. També destaca l'àrea del Golf de Cadis, la costa de Màlaga i, en menor mesura, l'oest de Galícia i la costa central del País Valencià. En estudis més recent s'han obtingut resultats semblants (Riesco et al., 2015; Grieser i Haines, 2020).

Estrictament en l'àmbit català, Joan Arús també desenvolupà una base de dades d'episodis de tornados. En aquest recull hi ha els casos observats des del setembre de 1992 i, a més, hi consten els esclafits (Arús, 2018). Les fonts d'informació utilitzades són similars a les de Gayà (2018), motiu pel qual a ambdós treballs hi ha referències creuades. En total, a la base de dades (1992-2017) hi consten 133 tornados, 280 mànegues marines i 77 esclafits.

La zona de Catalunya on es registren més tornados correspon al litoral i prelitoral central (Morales et al., 2009; Gayà, 2011; Arús, 2018). Coincideix amb l'àrea més poblada, on el nombre d'observadors potencials és clarament superior a altres sectors del territori. Tot i això, la proximitat al mar i la formació de convergències de vent en superfície en situacions de nord també ajuden a definir aquesta distribució. La majoria de tornados i mànegues marines s'observen entre els mesos d'agost i novembre. A banda, els tornados significatius només cor-

responen a una fracció petita del conjunt de fiblons, un fet que és comú amb altres zones (p. ex. Miglietta i Matsangouras, 2018; NOAA/SPC, 2019). També és destacable que una part important dels tornados que causen danys al litoral corresponen a trombes marines que toquen terra, malgrat que sovint se solen dissipar havent recorregut pocs centenars de metres (Figura 1.7).

Figura 1.7: Fotografies (ordenades cronològicament d'esquerra a dreta) del procés de dissipació d'una tromba marina en tocar terra, el 20 de novembre de 2002 al Masnou (el Maresme). Autor: Robert Flo.

1.2.6 Entorns favorables per a la tornadogènesi

Al llarg de les darreres dècades s'han dut a terme diversos estudis que tenien per objectiu caracteritzar els entorns favorables per a la formació de tornados (p. ex. Maddox, 1976; Thompson et al., 2003; Ingrosso et al., 2020).

Es basen en l'anàlisi de diversos paràmetres termodinàmics, com per exemple l'energia potencial convectiva disponible (CAPE), la inhibició convectiva (CIN), el nivell de condensació per elevació (LCL) o el nivell de convecció lliure (LFC); de cinemàtics, com el cisallament vertical del vent (WS), l'helicitat relativa a la cèl·lula convectiva (SRH) o el *bulk Richardson number shear* (BRNSHR), i de compostos a partir de la combinació dels anteriors, com ho són l'*energy helicity index* (EHI), el *vorticity generation parameter* (VGP), el *supercell composite parameter* (SCP), el *significant tornado parameter* (STP), l'*universal tornadic index* (UTI) i el producte del cisallament vertical del vent i l'arrel quadrada de dues vegades la CAPE (WMAXSHEAR). Tots aquests es calculen mitjançant el perfil vertical de temperatura, humitat i vent (les equacions es poden consultar a l'Apèndix A). En conèixer els valors que solen assolir durant episodis de tornados, és possible pronosticar quan hi pot haver entorns favorables per a la seva formació i, així, poder fer un seguiment acurat d'aquestes situacions mitjançant eines de teledetecció. Ara bé, tal com es discuteix a Doswell i Schultz (2006), aquests paràmetres resumeixen en un nombre algunes característiques de l'entorn, però a l'hora d'interpretar-los cal contemplar les limitacions que presenten i sempre s'ha de fer considerant el context sinòptic i mesoescalar.

Les dades utilitzades en aquest tipus d'estudis poden procedir de dues fonts d'informació: d'observacions o d'anàlisis/reanàlisis de model. Pel que fa a les observacions (radiosondatges), cal tenir en compte dos aspectes que condicionen la representativitat de les dades per a caracteritzar els episodis d'interès:

- **La freqüència de la realització de les observacions**. En general, se solen realitzar dos radiosondatges al dia (a les 00 i a les 12 UTC) a cadascuna de les estacions.

- **La distància entre les estacions**. Per exemple, a Europa la distància entre les estacions de radiosondatge oscil·la entre els 100 i els 500 km.

Per tant, cal establir uns criteris espacials i temporal per a seleccionar el radiosondatge més indicat per a estudiar cadascun dels esdeveniments. De criteris n'hi ha diversos, alguns de més restrictius, que fan minvar la mostra d'episodis, i d'altres de més laxes, que poden implicar una pèrdua de representativitat de les dades (vegeu la Taula 1.3). En aquest sentit, Potvin et al. (2010) mostrà que la utilització de criteris diferents dona lloc a diferències que poden ser estadísticament significatives en les distribucions dels valors dels paràmetres analitzats. Concretament, quan s'utilitzen radiosondatges més allunyats de l'esdeveniment, la CAPE i el cisallament vertical del vent tendeixen a ser més petits, malgrat que les diferències no tenen significança estadística, en aquest cas. En canvi, l'SRH que també és menor per a radiosondatges llunyans que per als propers, sí que presenta diferències estadísticament significatives.

Taula 1.3: Criteris de selecció de radiosondatges per a l'estudi d'episodis de tornados i mànegues marines.

Referència	**Distància màx. (km)**	**Finestra horària**
Novlan i Gray (1974)	185	± 3 h
Maddox (1976)	92,5	−2 h a +1 h
Brooks et al. (1994)	160	± 1 h
Kerr i Darkow (1996)	80	−105 min a +15 min
Rasmussen i Blanchard (1998)	400	−3 h a +6 h
Gayà et al. (2001)	150	± 3 h
Craven i Brooks (2004)	185	± 3 h
Groenemeijer i van Delden (2007)	100	± 4 h
Keul et al. (2009)	300	± 6 h
Taszarek i Kolendowicz (2013)	200	−3 h a +6 h
Renko et al. (2016)	400	−6 h a +3 h
Taszarek et al. (2017)	125	−2 h a +4 h

Per altra banda, també és habitual utilitzar dades d'anàlisi de models (p. ex. Rasmussen, 2003) o de reanàlisi (Romero et al., 2007; Chernokulsky et al., 2019) per al càlcul dels diveros paràmetres. Com que la densitat de punts amb dades és major (de fins a un ordre de magnitud en el cas de la reanàlisi ERA5 (C3S, 2017) de l'*European Centre for Medium-Range Weather Forecasts* (ECMWF) respecte a la xarxa de radiosondatges d'Europa) i la finestra horària és més petita (entre 1 i 6 hores), és possible obtenir dades d'un punt (x, y, t) molt més proper a l'esdeveniment d'interès. Tot i això, les dades de radiosondatge proporcionen una resolució vertical molt major i descriuen la capa límit de manera precisa. Justament, les diferències que hi ha en la descripció de la capa límit poden afectar en els resultats que es deriven del càlcul dels paràmetres que són sensibles al perfil vertical de temperatura, humitat i vent a nivells baixos (Taszarek et al., 2018).

Els resultats d'aquests estudis mostren que habitualment els tornados es formen en entorns caracteritzats per un rang ampli de CAPE, ja sigui calculada mitjançant les parcel·les de superfície (SB), la més inestable (MU) o la de la capa de mescla (ML), que pot oscil·lar entre els 100 i els més de 2000 J kg^{-1}, i un LCL inferior a 1000 m en la major part dels casos (Groenemeijer i van Delden, 2007; Thompson et al., 2012). Els paràmetres cinemàtics mostren una correlació positiva amb la intensitat dels tornados, que és més evident per als estrats més propers a la superfície. D'aquesta manera, mentre que per als tornados significatius (i.e. d'intensitat (E)F2 o superior, sovint d'origen mesociclònic) el WS per a l'estrat 0-6 km sol superar els 18 m s^{-1}, el WS 0-1 km els 10 m s^{-1} i l'SRH 0-1 km els 100 m^2 s^{-2}, els fiblons menys

intensos acostumen a formar-se en entorns amb un cisallament vertical del vent menor. Per la seva banda, les mànegues marines se solen formar en condicions menys restrictives, és a dir, en entorns amb una CAPE, un WS i un SRH més petits (Renko et al., 2016).

Ara bé, existeixen alguns casos particulars. Sobretot durant l'època freda de l'any, es poden formar tornados en entorns de cisallament del vent elevat i CAPE baixa (HSLC), que es caracteritzen per tenir una (SB)CAPE < 500 J kg^{-1}, una (MU)CAPE < 1000 J kg^{-1} i un WS 0-6 km > 18 m s^{-1} (Sherburn i Parker, 2014). En aquestes condicions, els tornados solen estar associats a mini-supercèl·lules (Markowski i Straka, 2000) i a sistemes convectius quasi lineals (Davis i Parker, 2014). Per altra banda, també s'han observat tornados en entorns de poca helicitat (SRH 0-1 km < 75 m^2 s^{-2}) i (ML)LCL elevat (> 1300 m), especialment durant l'època càlida (LHHLCL, Davies, 2006). En aquests casos és característic que el gradient vertical de temperatura sigui molt marcat (8-10 °C km^{-1} en els primers 2-3 km), alhora que l'(ML)CAPE 0-3 km presenti valors elevats (> 60 J kg^{-1}), l'(ML)CIN sigui petita (< 15 J kg^{-1}) i l'(ML)LFC, relativament baix (< 2000 m).

1.3 Objectius

1.3.1 Objectius generals

La predicció dels tornados avui en dia a Europa es basa principalment en la vigilància meteorològica i el *nowcasting*, és a dir, en l'observació i identificació de patrons característics en les cèl·lules convectives mitjançant dades de teledetecció (radar, satèl·lit i descàrregues elèctriques) i en la predicció a molt curt termini (Rauhala i Schultz, 2009). Per tant, és bàsic poder fer un seguiment detallat dels nuclis o sistemes convectius proclius a generar fiblons en dies en què hi ha condicions favorables per a la seva formació. Aquest fet posa de manifest que cal conèixer les característiques dels entorns favorables per tal de dur a terme una vigilància acurada, especialment en zones com Catalunya, les Illes Balears i el Golf de Cadis, on els tornados es presenten amb una certa freqüència (Antonescu et al., 2017).

Però per a fer possible aquesta anàlisi, abans cal disposar d'una base de dades que contingui tants casos com sigui possible i que aquests estiguin degudament validats i detallats. El catàleg dels tornados i trombes marines registrats a Espanya publicat recentment (Gayà, 2018) i les plataformes de ciència ciutadana com la XOM, SINOBAS i l'ESWD recullen un gran nombre d'esdeveniments. Nogensmenys, l'exploració d'altres eines, més enllà de les fonts citades, de les xarxes socials i dels mitjans de comunicació, podrien ajudar a aconseguir informació més detallada dels episodis ja coneguts i també podria afavorir la detecció de nous casos.

Així, s'han plantejat tres objectius generals al voltant dels quals s'ha desenvolupat aquesta tesi:

- **OG1. Explorar noves eines per a generar una base de dades de tornados i mànegues marines homogènia i robusta**. Cal disposar d'eines que facin possible l'anàlisi dels danys ocasionats per ventades fortes d'origen convectiu i, així poder discriminar si aquests han estat fruit d'un tornado, d'un esclafit o d'algun altre fenomen meteorològic. A més, és convenient trobar eines que permetin detectar les zones afectades pels fiblons sense necessitat que hagin estat prèviament observats, de manera que es pugui obtenir informació de qualsevol indret, independentment de la densitat de població.

- **OG2. Caracteritzar els entorns favorables per a la formació de tornados i mànegues marines al conjunt de la Península Ibèrica i les Illes Balears**. La descripció d'aquestes condicions se sol fer mitjançant l'anàlisi de diversos índexs termodinàmics, cinemàtics i amb la combinació d'aquests, els quals es calculen a partir del perfil vertical de temperatura, humitat i vent.

- **OG3. Identificar possibles factors relacionats amb els episodis més intensos**. Es tracta d'avaluar les diferències que hi pot haver en els valors dels diversos paràmetres calculats a partir del perfil termodinàmic en funció de la intensitat dels casos. També cal estudiar com aquests índexs poden ajudar a identificar els entorns favorables per a la formació de tornados significatius, els quals són prou forts per a causar danys materials i personals importants (Gayà, 2018).

1.3.2 Objectius específics

A partir dels objectius generals presentats en la subsecció anterior, s'han formulat sis objectius específics per als quals s'ha treballat per a donar resposta en aquest treball. S'exposen a continuació:

- **OE1. Proposar una metodologia per a dur a terme treballs de camp**. L'anàlisi dels danys *in situ* permet estimar la intensitat del fenomen que els ha causat i caracteritzar la zona afectada (i.e. amplada, llargada). A més, l'estudi del patró de danys sovint fa possible conèixer si les destrosses han estat causades per un tornado, un esclafit o algun altre fenomen, de manera que aporta informació molt valuosa i útil per a una base de dades. Cal que la metodologia proposada sigui fàcilment reproduïble i que optimitzi el temps i els recursos.

- **OE2. Utilitzar ortofotografies per a analitzar episodis de ventades fortes d'origen convectiu**. Les imatges aèries d'alta resolució han demostrat ser una eina de gran ajut a l'hora d'identificar i caracteritzar les traces de danys causades per tornados. Permeten tenir una visió general de l'episodi i fins i tot detectar zones afectades prèviament no conegudes. Per a dur a terme aquesta anàlisi es proposa fer ús de les ortofotografies de l'ICGC.

- **OE3. Desenvolupar una base de dades de tornados i trombes marines a Catalunya i analitzar les característiques dels episodis**. La combinació de diverses fonts d'informació d'episodis de temps violent, on destaquen les bases de dades anteriors i la contribució actual de les xarxes socials, permet generar un recull de casos de tornados i mànegues marines actualitzat. Amb aquestes dades és possible estudiar la distribució espacial i temporal dels episodis i analitzar algunes de les característiques més rellevants, com per exemple les dimensions de les traces de danys, la intensitat dels casos o l'impacte socioeconòmic.

- **OE4. Estudiar paràmetres termodinàmics i cinemàtics per a diversos tipus de temps**. Mitjançant l'ús de dades de radiosondatges observats es pretén analitzar els valors que solen adquirir paràmetres com la CAPE, l'SRH i el WS en diversos tipus de temps, incloent-hi dies sense precipitació, dies de tempesta sense tornado, dies de tornado i dies de mànega marina.

- **OE5. Analitzar el comportament de paràmetres específics per a detectar entorns favorables per a la formació de tornados**. En la predicció operativa de fenòmens de temps violent, a banda dels paràmetres termodinàmics i cinemàtics esmentats anteriorment sovint s'utilitzen índexs que els combinen. Així, es vol analitzar el comportament d'aquests paràmetres en dies en què hi ha hagut tornados, parant especial atenció als fiblons significatius. Es proposa fer-ho amb l'ús de dades d'observació (radiosondatge) i de reanàlisi (ERA5).

- **OE6. Validar la detecció d'entorns favorables per a la formació de mànegues marines mitjançant el nomograma de Szilagyi**. El nomograma de Szilagyi (Szilagyi, 2009) determina si hi ha condicions favorables per a la formació de trombes marines per mitjà de paràmetres termodinàmics, com són la diferència entre la temperatura de 850 hPa i la temperatura superficial de l'aigua del mar i la diferència entre el nivell d'equilibri (EL) i el nivell de condensació per elevació (LCL). Aquest mètode fou desenvolupat a la regió dels Grans Llacs de l'Amèrica del Nord, i es vol testejar per a les aigües marítimes de l'entorn de la Península Ibèrica i les Illes Balears mitjançant dades de reanàlisi (ERA5).

1.4 Estructura de la tesi

La tesi que teniu a les vostres mans, que és un compendi d'articles, està dividida en cinc capítols. Al **Capítol 1**, que és on es troba la present secció, hi ha la introducció, que inclou l'estat de l'art de les línies de treball que s'han desenvolupat a la tesi i els objectius. Al **Capítol 2**, sota el títol "Recursos per a la construcció d'una base de dades", es tracten dues eines que aporten informació rellevant a les bases de dades sobre els tornados registrats. Per una banda, es proposa una metodologia per a dur a terme treballs de camp, la qual és fàcilment reproduïble i optimitza el temps i els recursos. Per l'altra, es mostra la utilitat de les imatges aèries d'alta resolució, com les ortofotografies de l'ICGC, per a localitzar i caracteritzar traces de danys. En aquest bloc s'hi inclouen les següents publicacions:

- Rodríguez O., Bech J., Soriano J.D., Gutiérrez D. i Castán S. (2020): A methodology to conduct wind damage field surveys for high-impact weather events of convective origin. *Natural Hazards and Earth System Sciences*, **20(5)**: 1513–1531. doi:10.5194/nhess-20-1513-2020.

- Rodríguez O. i Bech J. (2020): Reanalysing strong-convective wind damage paths using high-resolution aerial images. *Natural Hazards*, **104(1)**: 1021–1038. doi:10.1007/s11069-020-04202-6.

Al **Capítol 3**, anomenat "Base de dades de tornados i mànegues marines a Catalunya", es presenta un recull d'episodis de tornados i trombes marines detectats a Catalunya entre els anys 2000 i 2019. Les observacions provenen de diverses fonts, entre les quals destaquen les xarxes socials i publicacions anteriors, com Gayà (2018). Aquestes dades han servit, en part, per a desenvolupar els treballs del quart capítol de la tesi. A més, també s'analitza i es discuteix la distribució temporal i espacial dels episodis, les característiques de les traces de danys i l'impacte socioeconòmic. Aquest capítol és constituït per l'article següent:

- Rodríguez O., Bech J., Arús J., Castán S., Figuerola F. i Rigo T. (2021): An overview of tornado and waterspout events in Catalonia (2000-2019). *Atmospheric Research*, **250**: 105415. doi:10.1016/j.atmosres.2020.105415.

Al **Capítol 4**, titulat "Entorns favorables per a la formació de tornados i mànegues marines", s'estudia el comportament de diversos paràmetres derivats de perfils termodinàmics per a diversos tipus de temps amb l'objectiu d'analitzar quines diferències presenten els dies de tornado i de mànega marina respecte als dies sense precipitació i als dies de tempesta sense tornado. A banda, s'estudia amb especial atenció les condicions característiques per a fiblons significatius i es valida el nomograma de Szilagyi per a la detecció d'entorns favorables per a la formació de mànegues marines a les costes properes a la Península Ibèrica i a les Illes Balears. Els articles que conformen aquesta part són:

- Rodríguez O. i Bech J. (2018): Sounding-derived parameters associated with tornadic storms in Catalonia. *International Journal of Climatology*, **38**: 2400–2414. doi:10.1002/joc.5343.

- Rodríguez O. i Bech J. (2020): Tornadic environments in the Iberian Peninsula and the Balearic Islands based on ERA5 reanalysis. *International Journal of Climatology*: 1–21. doi:10.1002/joc.6825.

A continuació, es presenten les conclusions obtingudes en aquesta tesi, al **Capítol 5**. Per a fer-ho, es recuperen els objectius formulats a la secció 1.3 i, de manera concisa i ordenada, s'hi dona resposta. A banda, també s'esbossen les línies de treball futur que poden sortir dels resultats de la investigació.

Finalment, hi ha quatre apèndixs. En el primer es mostren les equacions dels paràmetres termodinàmics, cinemàtics i compostos analitzats al Capítol 4 (**Apèndix A**). En segon lloc, es llisten les contribucions fetes durant el període predoctoral, incloent-hi les publicacions en revistes indexades, les presentacions orals i els pòsters en congressos i jornades i els informes (**Apèndix B**). Tot seguit, al tercer apèndix, es presenten els treballs de camp realitzats, també, al llarg del període predoctoral (**Apèndix C**). Per acabar, al quart, es mostra la utilitat de geolocalitzar les fotografies de tornados a l'hora d'analitzar un episodi i, com a exemple, es posa el cas del tornado del 21 de març de 2016 a Sant Llorenç d'Hortons (l'Alt Penedès) (**Apèndix D**).

Capítol 2

Recursos per a la construcció d'una base de dades

2.1 Metodologia per a dur a terme treballs de camp per a episodis de vent fort d'origen convectiu

2.1.1 Resum de l'article

En aquest article s'hi presenta una metodologia per a dur a terme treballs de camp en episodis de vent fort d'origen convectiu. El procediment proposat és fàcilment reproduïble i optimitza el temps i els recursos dedicats a l'estudi *in situ* dels episodis. D'aquesta manera és possible analitzar la gran majoria de casos registrats, en lloc de només fer-ho per a aquells esdeveniments més rellevants i afavorint, així, una homogeneïtzació de les bases de dades de fenòmens de temps violent.

L'objectiu principal de la metodologia és reproduir l'escenari de danys mitjançant la geolocalització dels elements malmesos. A banda, es proposa complementar aquesta informació amb la recollida d'altres dades d'interès, com per exemple el testimoni d'observadors directes i imatges del fenomen, registres d'estacions meteorològiques particulars i dades de teledetecció. Així, es pot dur a terme una anàlisi de l'episodi estudiat des del punt de vista meteorològic.

Per a sintetitzar i fer fàcilment interpretable tota la informació, es proposa la confecció de tres lliurables: (i) una fitxa estandarditzada amb el resum del treball de camp, (ii) una taula en la qual consti la informació geolocalitzada i (iii) un mapa o un arxiu KML (Keyhole Markup Language) que contingui la informació presentada a la taula. Per a il·lustrar-ho, s'adjunta com a material suplementari els lliurables resultants del treball de camp del tornado que hi va haver el 15 d'octubre de 2018 entre els municipis de Malgrat de Mar (el Maresme) i Massanes (la Selva), disponibles a:

- `https://doi.org/10.5194/nhess-20-1513-2020-supplement`

La metodologia proposada està basada en diverses publicacions prèvies, i també en l'experiència dels autors de l'article, que han participat en un total de 136 treballs de camp realitzats entre els anys 2004 i 2018 a Espanya. La majoria d'aquests s'han concentrat a Catalunya i a Andalusia, on hi ha zones densament poblades que són afectades per tornados amb freqüència.

Les dades obtingudes durant la inspecció de les destrosses al lloc dels fets són de gran utilitat. Per una banda, a partir de l'anàlisi de la distribució i la disposició dels danys sovint és possible conèixer quin fenomen meteorològic ha tingut lloc (tornado, esclafit, vent lineal), quelcom necessari a determinar quan no hi ha cap testimoni directe de l'episodi. A banda, també es pot caracteritzar la franja de danys amb el càlcul de l'amplada i la llargada de la zona

afectada i l'estimació de la intensitat màxima del vent. Tot plegat proporciona a les bases de dades d'aquest tipus de fenòmens informació rellevant que les fa robustes.

Aquest article dona resposta a l'objectiu general **OG1** i a l'objectiu específic **OE1**.

2.1.2 Article

Rodríguez O., Bech J., Soriano J.D., Gutiérrez D. i Castán S. (2020): A methodology to conduct wind damage field surveys for high-impact weather events of convective origin. *Natural Hazards and Earth System Sciences*, **20(5)**: 1513–1531. doi:10.5194/nhess-20-1513-2020.

Nat. Hazards Earth Syst. Sci., 20, 1513–1531, 2020
https://doi.org/10.5194/nhess-20-1513-2020

Natural Hazards and Earth System Sciences
Open Access
EGU

A methodology to conduct wind damage field surveys for high-impact weather events of convective origin

Oriol Rodríguez[1], Joan Bech[1], Juan de Dios Soriano[2], Delia Gutiérrez[2], and Salvador Castán[3]

[1]Department of Applied Physics – Meteorology, University of Barcelona, Barcelona, 08028, Spain
[2]Agencia Estatal de Meteorología, Seville, 41092, Spain
[3]Agencia Pericial, Cornellà de Llobregat, 08940, Spain

Correspondence: Oriol Rodríguez (orodriguez@meteo.ub.edu)

Received: 5 September 2019 – Discussion started: 17 September 2019
Revised: 18 April 2020 – Accepted: 2 May 2020 – Published: 29 May 2020

Abstract. Post-event damage assessments are of paramount importance to document the effects of high-impact weather-related events such as floods or strong wind events. Moreover, evaluating the damage and characterizing its extent and intensity can be essential for further analysis such as completing a diagnostic meteorological case study. This paper presents a methodology to perform field surveys of damage caused by strong winds of convective origin (i.e. tornado, downburst and straight-line winds). It is based on previous studies and also on 136 field studies performed by the authors in Spain between 2004 and 2018. The methodology includes the collection of pictures and records of damage to human-made structures and on vegetation during the in situ visit to the affected area, as well as of available automatic weather station data, witness reports and images of the phenomenon, such as funnel cloud pictures, taken by casual observers. To synthesize the gathered data, three final deliverables are proposed: (i) a standardized text report of the analysed event, (ii) a table consisting of detailed geolocated information about each damage point and other relevant data and (iii) a map or a KML (Keyhole Markup Language) file containing the previous information ready for graphical display and further analysis. This methodology has been applied by the authors in the past, sometimes only a few hours after the event occurrence and, on many occasions, when the type of convective phenomenon was uncertain. In those uncertain cases, the information resulting from this methodology contributed effectively to discern the phenomenon type thanks to the damage pattern analysis, particularly if no witness reports were available. The application of methodologies such as the one presented here is necessary in order to build homogeneous and robust databases of severe weather cases and high-impact weather events.

1 Introduction

Meteorological phenomena associated with strong surface wind of convective origin (i.e. tornadoes, downbursts, straight-line winds) can cause important disruption to socio-economic activity, including injuries or even fatalities, despite their local character compared to larger-scale mid-latitude synoptic windstorms or tropical storms. For example, from 1950 to 2015, tornadoes in Europe caused 4462 injuries, 316 fatalities and economic losses of at least EUR 1 billion (Antonescu et al., 2016, 2017). Due to their economic and social impact, a large number of works have been devoted to the study of these phenomena both from a meteorological point of view (e.g. Taszarek et al., 2017; Miller and Mote, 2018; Rodríguez and Bech, 2018) and from the point of view of their consequences (e.g. Rosencrants and Ashley, 2015; Strader et al., 2015).

The systematic elaboration of post-event forensic field surveys is still the standard way to evaluate the damage caused by a strong-convective-wind event (Marshall, 2002; Marshall et al., 2012; Zanini et al., 2017), despite the recent progress on assessing wind damage using remote-sensing data such as high-resolution radar observations (Wurman et al., 2013; Wakimoto et al., 2018). A detailed damage analysis from these meteorological phenomena allows us to estimate the wind intensity using a wind damage scale such as the Fujita scale (F scale; Fujita, 1981) or the Enhanced Fujita scale

Published by Copernicus Publications on behalf of the European Geosciences Union.

(EF scale; WSEC, 2006). Similarly to field surveys of hailstorms (Farnell et al., 2009) or floods (Molinari et al., 2014; Li et al., 2018), wind damage field studies contribute to a better characterization of the affected area, making it possible to estimate the length and width of the damage swath (e.g. Burgess et al., 2014; Meng and Yao, 2014; Bech et al., 2015). Moreover, in situ damage surveys are especially useful to determine which phenomenon took place when there is an absence of observations by analysing damage patterns on forest and how debris is spread (Hall and Brewer, 1959; Holland et al., 2006; Bech et al., 2009; Beck and Dotzek, 2010; Rhee and Lombardo, 2018). This information can be added to natural hazard databases such as the US Storm Prediction Center Severe Weather Database (Verbout et al., 2006) or the European Severe Weather Database (Dotzek et al., 2009), making it possible to build up robust and homogeneous datasets, improving the knowledge of spatial–temporal distribution and characteristics of tornadoes, downbursts and straight-line winds.

Currently, field studies are usually performed to assess damage of specific strong-convective-wind events (e.g. Lemon et al., 2003; Bech et al., 2011; Wesolek and Mahieu, 2011) but rarely to analyse in detail most of the reported cases. The timing and economical costs, especially when helicopter flights are used, prevent carrying out in situ damage analysis frequently (Edwards, 2020), particularly outside of the USA. Therefore, there is a need for a methodology to conduct wind damage field surveys for high-impact weather events of convective origin that is easily reproducible anywhere and should be efficient to optimize time and economic resources, allowing the study of as many reported events as possible.

The objective of this paper is to propose a methodology to conduct in situ damage surveys of strong wind events from convective origin. It can contribute to improve the detection, mapping and characterization of wind damage in a homogeneous way, which is important to better describe specific meteorological phenomena, with the particularities associated with damage from convective local storms. Therefore, the main goal of the proposed methodology is to gather as much geo-referenced information (pictures and records) as possible about relevant damaged elements (i.e. human-made structures and vegetation) to reproduce the damage scenario. This information should be complemented with other available data, such as witness enquiries, data from automatic weather stations (AWSs) located close to the affected area, remote-sensing data and images of the phenomenon together with their location and orientation to analyse strong-convective-wind phenomena from a meteorological point of view.

The methodology presented here is based on previous studies (McDonald and Marshall, 1984; Bunting and Smith, 1993; Gayà, 2018; Holzer et al., 2018) and also on 136 wind damage surveys performed between 2004 and 2018 by the authors. All the analysed events have been recorded in Spain (south-western Europe), which includes the vast majority of the Iberian Peninsula and also the Balearic and Canary islands. Nevertheless, most of these field studies have been carried out in the Catalonia and Andalusia regions (Fig. 1), where highly densely populated areas are frequently affected by tornadoes (Bech et al., 2007, 2011; Mateo et al., 2009; Sánchez-Laulhé, 2013; Gayà et al., 2011; Riesco et al., 2015). Three final deliverables are suggested to synthesize the data recorded: (i) a text report of the analysed event, (ii) a table consisting of detailed geolocated information, and (iii) a map or a KML (Keyhole Markup Language) file containing the previous information ready for graphical display and further analysis.

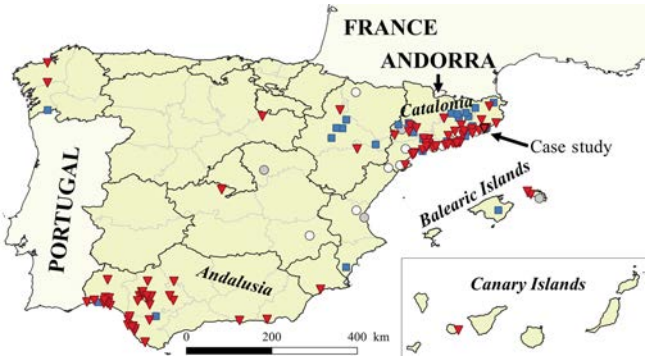

Figure 1. Location of 136 analysed events in Spain using the proposed methodology between 2004 and 2018, mostly concentrated in Andalusia and Catalonia. Symbols indicate locations of tornadoes (red triangles), downbursts (blue squares), undetermined phenomena (grey circles) and other phenomena such as gust fronts, funnel clouds which did not touch down or dust devils (white circles). The case study location for which final deliverables are attached as the Supplement is indicated on the map. Black contours delimitate regions and grey lines show provinces.

The rest of the article is organized as follows. Firstly, in Sect. 2 an overview of previous in situ fieldwork techniques is provided. Section 3 describes, in detail, the field survey methodology proposed. In Sect. 4 specific strengths and limitations of the methodology are discussed, as well as possible uses of fieldwork data. Finally, Sect. 5 presents a summary and final conclusions of the study. In the Supplement, an example of deliverables (text report, table and KML file) of a damage survey of a recent tornadic event is provided with the aim to better illustrate the methodology proposed and to facilitate its application.

2 Background

McDonald and Marshall (1984) and Bunting and Smith (1993) provided guidelines to carry out strong-convective-wind damage surveys. There, the process of mapping data by locating images taken during the fieldwork was challenging due to non-digital cameras and the absence of Global Navigation Satellite System on these devices. Both documents rec-

ommended complementing surface observations with aerial images if available, and, in the second one, it was also explained how to treat direct witnesses and ask them for specific information about the event and damage.

On the other hand, the analysis of historical events such as those of Gayà (2007) and Holzer et al. (2018) showed the utility of press references and in situ images taken by witnesses on reconstructing tornado damage paths. They pointed out the necessity of geo-referencing the locations where photos were taken and the damaged elements, using GIS tools and triangulation methods. Furthermore, Holzer et al. (2018) provided useful indications for current field studies, such as visiting affected areas as soon as possible and also providing an estimation of the wind intensity for each damaged element given by the pair damage indicator–degree of damage (DI–DoD) from the EF scale (WSEC, 2006), similarly to other authors such as Burgess et al. (2014).

During the first decade of the current century, the use of GPS receivers or similar systems was extended to in situ damage assessments to geolocate gathered data, as discussed in Edwards et al. (2013). Moreover, aerial imagery from helicopters or aeroplanes (e.g. Fujita, 1981; Bech et al., 2009) and high-resolution satellites (e.g. Molthan et al., 2014; Chernokulsky and Shikhov, 2018) has also been frequently used to analyse damage swaths. Recently, drones have been raised as a new device which might be useful to, at least, complement surface surveys (Bai et al., 2017).

3 Methodology

The methodology to carry out damage surveys must be efficient, allowing us to visit the affected area in the shortest time possible. It must also be easily reproducible, and its results should be accurate. Geolocating damage using pictures or videos recorded with smartphones or cameras with a Global Navigation Satellite System such as GPS fulfils these conditions (Edwards et al., 2013). Nevertheless, as it happens with other types of damage assessments, there are inherent uncertainties that should be taken into account when analysing field data (Beven et al., 2018), like possible GPS location errors or ambiguous application of intensity rating assessments due to EF scale limitations, which are discussed on Sect. 4.

In Table 1 the main devices needed to carry out field studies throughout the proposed methodology are summarized. Moreover, as indicated in Bunting and Smith (1993) and Gayà (2018), water, food, comfortable footwear, a rain jacket, spare clothes and a mobile phone spare battery are recommended, because affected areas may be far away from inhabited locations. As surveyor displacements longer than a few kilometres can be required, a well-equipped, preferably all terrain, car is necessary to save time between points of damage. Nevertheless, difficult-access areas may be found along the track, because of muddy roads and fallen trees or simply because of the absence of roads. Especially in these cases, and also to study damaged areas in detail, walking is the basic way to perform the field survey.

Table 1. Devices required to perform strong-convective-wind damage surveys.

Device reference	Device
D1	Smartphone or camera with GPS image geolocation and orientation (azimuth pointing) capabilities
D2	Compass
D3	Tape measure
D4	Hand counter
D5	Suitcase balance

Despite this not always being feasible, it would be ideal that the damage survey team was multidisciplinary, being formed by meteorologists, insurance inspectors, forestry engineers and architects experienced in damage assessments, preferably familiar with damage reporting systems such as the EF scale. This would facilitate an accurate and detailed analysis of the damage and the phenomenon intensity.

The proposed methodology is organized in three stages (Fig. 2). The first step includes pre-in situ damage survey tasks, preparing the actual visit of the damaged area (Sect. 3.1). Secondly, the in situ fieldwork tasks, which include direct gathering of human-made structure and vegetation damage information, and also collection of direct witness experiences (Sect. 3.2). Finally, post-in situ damage assessment tasks are performed, which involve the organization of all the information collected into three deliverables (a text report of the event, a geolocated information table and a data location map; Sect. 3.3).

3.1 Pre-in situ survey tasks

To properly prepare the damage survey, a number of previous tasks must be performed. One of them is planning the route of the fieldwork. As mentioned in Holzer et al. (2018) it is strongly recommended to start in situ damage surveys as soon as possible, especially if urban areas have been affected. Emergency and clearing services may start repair only a few hours after the event, which can alter the quality and quantity of possible information available during the fieldwork. Thus, to optimize time and resources, detailed planning is necessary to carry out the in situ damage assessment.

Firstly, preliminary information should be collected about damage location and images available in the media and social networks, which are the main providers of strong-convective-wind reports today (Hyvärinen and Saltikoff, 2010; Knox et al., 2013; Kryvasheyeu et al., 2016). Collaborative citizen science platforms covering different geographical domains such as the European Severe Weather Database (ESWD;

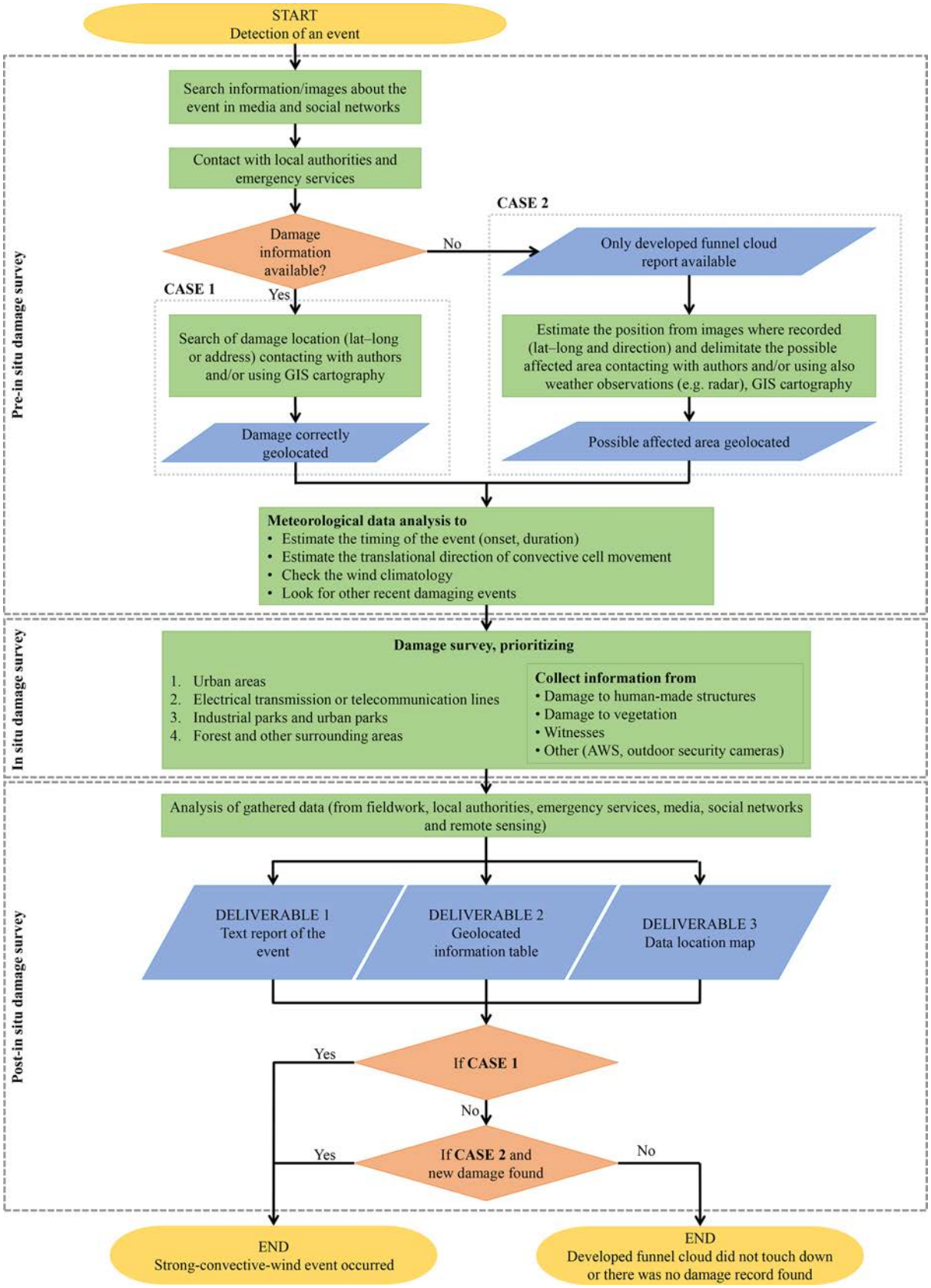

Figure 2. Flow diagram of the structure and application of the proposed methodology to carry out strong-convective-wind fieldwork damage assessment. Start and end are shaded in yellow, processes in green, decisions in orange and inputs–outputs in blue.

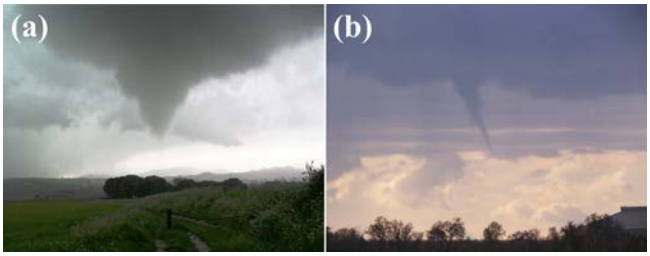

Figure 3. (a) Well-developed funnel cloud observed in Santa Eulàlia de Ronçana (Catalonia) on 4 April 2010 (author: @CalabobosChaser), and **(b)** well-developed funnel cloud observed in Bellpuig (Catalonia) on 1 December 2017 (author: Edgar Aldana). In both cases no evident tornado was actually observed (i.e. touchdown) but nearby damage was reported, suggesting tornado occurrence.

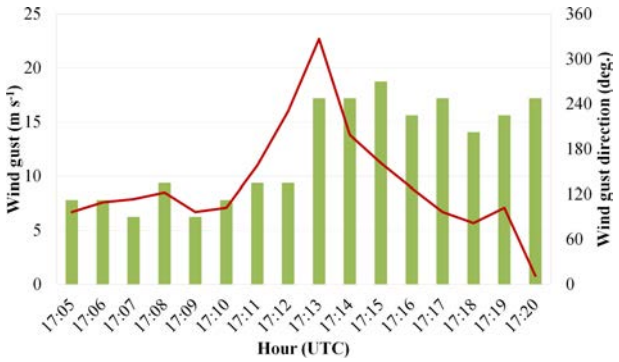

Figure 4. Wind gust (red line) and wind gust direction (green bars) registered by an AWS in Mataró (Catalonia) with 1 min temporal resolution data. The AWS was located 240 m west of the estimated centre of the EF0 tornado track, on 23 November 2016. Data source: Meteomar, Consell Comarcal del Maresme.

Dotzek et al., 2009), the severe weather database of the Spanish Meteorological Agency (SINOBAS; Gutiérrez et al., 2015) or the meteorological spotters platform of the Meteorological Service of Catalonia (XOM; Ripoll et al., 2016) are also examples of valuable sources of tornado and downburst reports.

Contacting emergency services and local authorities can also provide valuable information, as they may record detailed damage data, especially if an urban area is affected. This kind of information may be crucial for post-in situ damage study because clearing services might start arrangement tasks before the in situ visit is started. Occasionally, they may take aerial damage recordings, which can be very useful to complement the damage survey assessment.

To consider performing an in situ damage survey, the report must contain information about damage and/or a well-developed funnel cloud (i.e. a funnel cloud extending down below cloud base at least 50 % of the distance between the cloud base and the ground level). Funnel clouds (Fig. 3) are a typical feature of tornadic storms, though sometimes they may form without developing a tornado, i.e. when the rotating air column associated with the funnel does not reach the ground. When damage reports are available (Case 1 in Fig. 2), their location should be found by contacting their authors and/or using GIS cartography, proceeding as described in Holzer et al. (2018). Applications such as Google Street View can be very useful to carry out this task.

Nevertheless, if damage reports are not available but only developed funnel cloud images are reported (Case 2 in Fig. 2), then authors have to be asked for the location where photos were taken and their orientation. If for any reason this information is not accessible, it should be estimated from meteorological observations such as weather radar and satellite imagery (e.g. comparing radar images and the location of precipitation features observed in photos of the event with respect to the funnel cloud, as described by Wakimoto and Lew, 1993; Wakimoto and Liu, 1998; Zehnder et al., 2007) and GIS cartography. Then, from the triangulation of those pictures of the funnel cloud it is possible to preliminarily identify a possibly affected area, which can be more precisely delimited when the number of photos or videos from different perspectives is high (Rasmussen et al., 2003). However, at this stage it has to be kept in mind it is possible that the funnel cloud may have not produced damage, either due to the lack of human-made structures or trees in the area intercepted by the tornado or because the strong rotation associated with the funnel cloud actually did not touch down. This possibility will be verified during the in situ survey tasks.

Analysis of satellite and weather radar imagery is required to estimate the approximate timing of the event and the movement of the convective parent storm that may have produced the phenomenon. That information should be considered in order to extend the initial evidence of a preliminary damage path (looking for possible initial and ending damage path points) and to assess the consistence of reports by eyewitnesses.

On the other hand, existing AWSs in the area of interest can play an important role in determining the phenomenon type and the timing of the event and also in estimating the wind strength (Letchford and Chay, 2002; Karstens et al., 2010). Therefore, it is strongly recommended to search and locate all weather stations in the area of study, requesting the data with the maximum temporal resolution and performing basic quality control (time consistency and comparison with official observations) before use. High-temporal-resolution wind data series during the passage of a tornado are usually characterized by a sudden increase in wind speed and a swift direction shift, as is shown in Fig. 4. By contrast, although a downburst event is also described by a wind strengthening, there is a predominant wind direction without relevant changes (Orf et al., 2012).

Another important task before starting the actual in situ damage assessment is to check the wind climatology of the studied area, particularly in windy regions (because of either

the orography or the prevailing synoptic conditions; Feuerstein et al., 2011). In this case, human-made structures and vegetation are adapted to resist strong winds – sometimes from specific directions – and wind speed thresholds over which an element can be damaged may be higher than in non-windy regions. Therefore, if a weak tornado or microburst affects a region usually influenced by strong winds, it is possible that little or no damage is found. Similarly, the application of an intensity damage scale in very windy regions may require some adjustments – i.e. increasing the wind speed thresholds for specific damages – as discussed in Feuerstein et al. (2011).

On some occasions, the studied area may have been affected recently by another damaging windstorm or by a heavy snowfall which may have produced widespread damage in forests – for example due to wet snow as described in Bech et al. (2013) and Llasat et al. (2014). In those cases, the data collection process may be hampered by possible overlapping damage, and, consequently, great care must be taken to identify the most recent damage event. A possible way to mitigate this problem is asking locals about previous events and paying attention to the dryness from affected trees and broken branches, which can indicate if forest damage is recent or not.

3.2 In situ survey tasks

To avoid alterations of the damage scenario due to clearing services, the fieldwork should preferably start on the most resilient areas, i.e. where socio-economic activity is more intense and the areas are more likely to recover quickly. The proposed priority order is to visit urban areas first, then damaged electrical transmission or telecommunication lines, industrial parks and urban parks, and, finally, forest and other surrounding areas (Fig. 2).

As a general principle, the highest possible number of relevant damaged elements should be analysed in the affected area, both human-made structures and natural (vegetation) elements. Moreover, if any previously unknown AWS is detected during the fieldwork, it should be considered to contact its owner asking for data. The same process should be carried out for outdoor security cameras, which may record the event and could provide valuable information in order to determine which phenomenon took place. Interviews with eyewitnesses, which can provide key information about the event and other damaged areas, are also very important.

All the in situ measurements are related to geo-referenced damaged elements. To reduce the time of registering data in order to proceed to other affected areas, it is proposed to take a photo from the measuring device clearly showing the data (Fig. 5), following the order proposed in Table 2 (from V5 to V10). After that, a photo of the damaged element should be taken, whose metadata already contain latitude and longitude. Therefore, surveyors can associate each measure with each geolocated element during the post-in situ tasks when organizing the records gathered in the fieldwork.

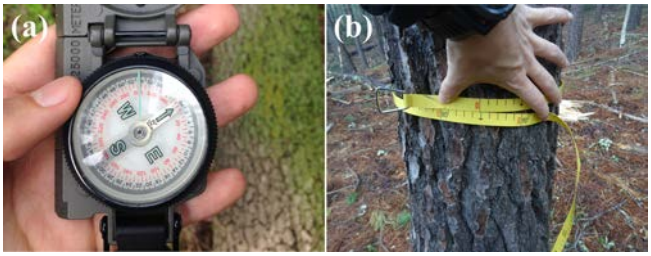

Figure 5. (a) Measure of the fall direction of a tree and **(b)** measure of trunk diameter during the damage survey of an EF1 tornado on 13 October 2016 in Llinars del Vallès (Catalonia) and an EF2 tornado on 7 January 2018 in Darnius (Catalonia), respectively (author: Oriol Rodríguez).

Note also that Table 2 lists maximum uncertainties recommended for each measure type reflecting possible maximum errors in the field survey measures as suggested in Beven et al. (2018). Particular uncertainty values listed in Table 2 are consistent with the resolution of data presented in several severe weather databases such as NOAA/SPC (2019), ESWD (Dotzek et al., 2009), SINOBAS (Gutiérrez et al., 2015), KERAUNOS (2020) and Gayà (2018), where damage path width is usually expressed with a resolution of ± 10 m (i.e. damage location uncertainty must be smaller than $\pm 1 \times 10^{-4}$°). Furthermore, uncertainties listed also take into account surveyors' experience and the data resolution from previous studies – e.g. direction of fallen trees and windborne debris are typically presented with 5° range (Bech et al., 2009, 2011, 2015).

3.2.1 Human-made structure damage assessment

Human-made structural damage analysis is essential to estimate the phenomenon wind intensity, for example using the EF scale. As explained in WSEC (2006), the Enhanced Fujita scale considers several degrees of damage (DoD) from a total of 23 damage indicators (DIs) related to constructions and three DIs from other human-made structures that can be used to determine the 3 s wind gust speed associated with this damage.

In the present methodology it is proposed to geolocate every damaged structure in the affected area, whose coordinates (latitude and longitude) can be obtained from the GPS receiver of the photo camera (with a precision greater than $\pm 1 \times 10^{-4}$°; see Table 2). It is also convenient to take one or more pictures from each damaged element, both general and detailed views that may be of interest to evaluate the damage intensity (Marshall et al., 2012; Roueche and Prevatt, 2013). These photos should also be used during the post-in situ damage survey analysis to study which type of strong-convective-wind phenomenon caused the damage.

Table 2. Variables and maximum uncertainties recommended for data descriptors for damaged human-made structures and vegetation elements. The first four variables are required for all damaged elements (both human-made structures and vegetation). Dragged distance, direction and weight of windborne debris should be measured if possible for relevant and representative elements (e.g. fragment of panel roof). Fallen tree direction and trunk diameter should be measured in the case of uprooted and snapped trees, respectively. Degraded state or previous weakness of damaged elements should also be reported.

Index	Variable	Uncertainty	Comments
V1	Latitude	$\pm 1 \times 10^{-4}$°	Measured with GPS camera.
V2	Longitude	$\pm 1 \times 10^{-4}$°	Measured with GPS camera.
V3	Damage indicator (DI)	–	Determined during the post-in situ damage survey using intensity rating scales such as the EF scale.
V4	Degree of damage (DoD)	–	Determined during the post-in situ damage survey using intensity rating scales such as the EF scale.
V5	Fallen tree direction	±5°	In the case of uprooted trees. Measured with a compass.
V6	Dragged direction object	±5°	Direction of the displacement. Measured with a compass or GIS tools.
V7	Trunk diameter	±5 cm	In the case of snapped trees. The trunk perimeter is measured with a tape measure and then the diameter can be calculated.
V8	Dragged distance object	±1 m	Distance between the final position and the origin of an object displaced by the wind. Measured with a tape measure or GIS tools.
V9	Weight of windborne debris	±10 %	Weight of an object of interest moved by the wind. In the case of small objects, measured with a balance if possible.
V10	Previous weakness	–	Description of deficiencies that can increase the vulnerability of elements to strong winds.

Moreover, for each affected human-made structure, the pair of DI–DoD data values should be provided by using an intensity rating scale such as the EF scale, as proposed by several authors such as Burgess et al. (2014) and Holzer et al. (2018). This task can be carried out during the damage survey, but it is recommended that it be performed during the post-in situ damage assessment analysis. The main reason is to optimize the time and sources devoted to the in situ survey. In the case that no DI could be associated with the damaged element, it should be explicitly shown as "unrated".

It is highly recommendable to check the maintenance status of the damaged human-made structures to avoid a biased intensity determination. Previous weaknesses or deficiencies in construction can make structures more vulnerable to strong winds, and so a higher degree of damage might be caused for an expected wind speed (Doswell et al., 2009). For example, if an absence of anchors or the presence of rust on metal beams from a roof are observed, this should be explicitly documented by pictures and a brief description to be taken into account when a damage rating scale is applied, as already proposed by Fujita (1992).

The estimated trajectory and distance covered by windborne debris, as well as its size and weight, may also provide valuable information to estimate wind velocity associated with the studied phenomenon (Knox et al., 2013). Therefore, it is recommended to measure the dragged or flying distance and direction of objects of interest, if origin and final locations are known, using a tape measure or GIS tools (Table 2). It is also interesting to document its weight, either estimated consulting the bibliography or measuring it with a portable balance in the case of small objects (the relative error should be less than 10 %).

3.2.2 Forest damage assessment

As mentioned in previous studies (see for example Holland et al., 2006 or Bech et al., 2009), the maximum wind field (direction and intensity) associated with a strong-convective-wind event can be approximately derived from the fallen-tree pattern. Therefore, if a substantial number of trees are damaged to produce a clear damage pattern, a detailed forest damage study is recommended. As described in detail in the Appendix, if fallen trees present a convergence and rotational pattern along a linear path, it is likely it was caused by a tornado, whereas if a divergent damage pattern, mostly non-linear, is observed, the most likely cause is a downburst. This analysis is especially interesting for those cases where there is no image nor direct witness of the phenomenon to determine the damage origin.

The forest damage survey should be carried out similarly to the human-made structure damage assessment, taking pictures of every relevant damaged vegetation element and reg-

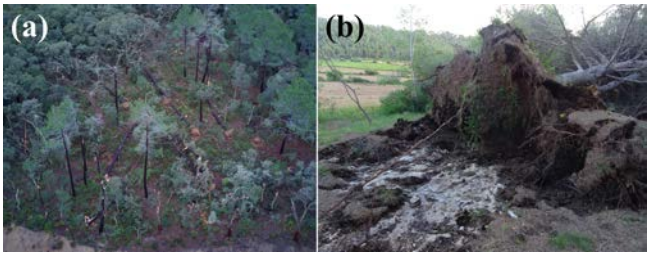

Figure 6. (a) Drone image of a mixed Mediterranean forest in Darnius (Catalonia) where most pine trees were blown down, whereas cork oaks were only slightly affected with broken branches, by an EF2 tornado, on 7 January 2018 (author: Jonathan Carvajal). **(b)** Pine blown down by an EF0 tornado in Perafort (Catalonia) in a very thin, moist soil area, on 14 October 2018 (author: Oriol Rodríguez).

istering its location (latitude and longitude). In the case of uprooted trees, the fall direction (azimuth) should be measured using a compass with, at least, 5° of precision (see Table 2). However, it should be noted that tree fall directions may be influenced by local factors and might not be representative of the wind direction. For example, trees falling on a steep-slope terrain (favouring one fall direction over others) or the presence of another nearby tree falling first can alter the tree direction with respect to the dominant wind. Therefore, in these cases it is recommended not to consider the data. In the case of snapped trees, trunk diameters should be measured with a measuring tape (with a minimum resolution of 5 cm; Table 2). These data can help in the damage rating task. However, as there may be a large number of damaged trees in a forest area, it is advisable to collect data from the most representative ones (for example, where tree fall direction changes or converges, probably indicating the effects of air rotation, or where damage is most significant and surrounding damaged trees to delimitate the damage swath width).

Damage in forest areas can also be useful to evaluate the phenomenon intensity. The EF scale (WSEC, 2006) describes different wind velocity ranges for five degrees of damage (DoD), namely small limbs broken, large branches broken, trees uprooted, trunks snapped and trees debarked with only stubs of the largest branches remaining. As wind effect on trees also depends on the tree species (Foster, 1988; Fig. 6a), the EF scale also distinguishes between softwood and hardwood trees. Thus, DI–DoD pairs for each analysed vegetation element should be provided.

Moreover, soil characteristics can affect tree stability; in the case of very moist soil, or thin soil over rocky subsoil, trees can be uprooted more easily, as is illustrated in Fig. 6b. Trees' health can also alter the resistance to strong winds. As is done for human-made structures, these debilities must be stated in the report. In order to refine intensity rating tasks in forests, it is recommended to calculate the ratio of affected trees in $50\,\mathrm{m} \times 50\,\mathrm{m}$ areas if possible; this can be related to the EF scale, according to Godfrey and Peterson (2017). High-resolution aerial imagery (i.e. from helicopter or drone) can be useful to carry out this task. This analysis is especially interesting in the most severely affected forest area of the damage swath.

Most tornado damage paths are less than 5 km long; for example, in Spain only 25 % of identified tornado tracks are longer than 5 km (Gayà, 2018). Therefore, a detailed forest damage analysis is usually possible. However, in cases where damage is widespread, a complete detailed analysis may not be feasible. In this case, it is recommended to study discontinuous segments every 250–500 m along the expected damage swath. This allows estimation of the path width and identification of the damage continuity. In addition, as previously commented, aerial images can enhance the forest damage analysis, especially in the case of large damage tracks and difficult-access areas (Karstens et al., 2013). Alternative approaches to surveys over widespread damaged forest areas are satellite image processing, as recently developed by Molthan et al. (2014), Chernokulsky and Shikhov (2018), Shikhov and Chernokulsky (2018), and Shikhov et al. (2019).

3.2.3 Witness enquiries

Direct witnesses, if available, are an important source of information often essential to determine which type of strong-convective-wind phenomenon occurred. Witnesses' experience of the event and their possible knowledge of other casual witnesses in nearby damaged locations can be very useful to complement a damage survey. In Bunting and Smith (1993) and Gayà (2018) it is noted that a direct witness may have been emotionally or physically affected by the phenomenon (for example private property damaged or loved ones injured) so it is necessary to be respectful and careful during the enquiry.

It is important to let witnesses explain their experience of the event in their own words, and interviewers should avoid using key words such as tornado, downburst or gust front, particularly in those cases when the phenomenon type is not known yet. The terms used by the witness may provide valuable clues about what happened. In addition, it is necessary to consider that previous media reports can alter the explanation of witnesses; for example, if the event has already been described as a tornado in the media, even if evidence of rotation is not found in the damaged area, people will probably say that a tornado has occurred.

A brief and concise enquiry, with specific questions but allowing open answers that may unveil relevant information, is proposed. Recommended questions are shown in Table 3. Moreover, on some occasions a direct witness may have taken photos or videos of the phenomenon that can be helpful for the study. When pictures are available, they should be treated as described in Sect. 3.1.

Table 3. Witness questionnaire (reference and question).

Question reference	Question
Q1	At what time did the phenomenon occur?
Q2	Where were you when the phenomenon took place?
Q3	How long did the strongest winds last? (Some seconds, around 1 min, several minutes, etc.)
Q4	During the phenomenon, did you hear any special or rare noise?
Q5	What was the weather like before, during and after the phenomenon? (Light rain, heavy rain, small hail, large hail, snow, no precipitation.)
Q6	Have you noticed other areas with damage?
Q7	Do you remember any previous similar phenomenon in this area?

3.3 Post-in situ survey tasks and deliverables

When the in situ damage survey is completed, the event analysis should be complemented revising meteorological remote-sensing data, which can now be compared with the records obtained in the survey. The information collected by direct witnesses, pictures and videos usually allows us to restrict the event occurrence to a temporal window of about 15 min to 2 h. Satellite imagery and data from Doppler radar, lightning detection systems and AWS (particularly if located within or close to the damage swath) from the period of interest can provide the necessary information to verify that the identification of the convective structure as that responsible for the damage performed during the pre-in situ damage survey was correct. In particular, the starting and ending time of the event can be estimated by checking the time when the convective structure passed over the initial and the final points of the damage swath, respectively, with an error typically less than 5 min. It is recommended to perform this comparison with Doppler radar observations, if available, with data in original polar coordinates keeping the highest spatial resolution (see for example Bech et al., 2009, 2011, 2015). In some cases, it is even possible to estimate the mean translational velocity and direction of the convective cell, knowing the distances between initial and final damage paths and the starting and ending times of the event. This can be very useful to compare theoretical surface wind vortex models with observed damage patterns over forest areas (Bech et al., 2009; see the Appendix for further details).

Finally, all the information gathered needs to be organized and archived in an easily interpretable way to analyse the strong-convective-wind event. In the following subsections, three final deliverables are proposed to achieve this objective: (i) a standardized text report of the event, (ii) a geolocated information table and (iii) a data location map. These deliverables are illustrated explicitly with the example of the 15 October 2018 Malgrat de Mar–Massanes tornado case (see location in Fig. 1), provided as the Supplement. Then, according to the flow diagram shown in Fig. 2, in Case 1 and in Case 2 and new damage found, it can be concluded that a damaging strong-convective-wind event (tornado, downburst, straight-line winds) occurred, whereas if a developed funnel cloud was reported and during the fieldwork no damage was found, it might be deduced that the funnel cloud did not touch down or there was not any exposed and/or vulnerable element in the tornado track to be damaged.

3.3.1 Text report of the event

The text report of the event should be an overview of the analysed episode, including a brief description of the information gathered during the fieldwork and the main conclusions from the analysis of these data. The proposed deliverable is divided into seven parts.

- *General event information*. This includes geographic data of the analysed meteorological phenomenon following current international standards for disaster report losses (De Groeve et al., 2014), such as names and codes of country (ISO 3166-1 alpha-3 specification), regions or provinces (NUTS code), and municipalities (LAU code). This part must also contain the start and end dates and time (in UTC) of the event and hazard classification according to the Integrated Research on Disaster Risk Peril Classification and Hazard Glossary (IRDR, 2014), including the family, the main event and the peril type.

- *Fieldwork information*. This describes specific data about team members, including their affiliation and email address. Moreover, date and time of the visits, estimation of the fieldwork coverage over the total affected area, and a brief description of difficult-access areas should also be provided.

- *Initial sources of information*. This contains information available (web pages and links) in media and social networks and developed funnel cloud images (if any), together with a brief explanation of the initial information gathered before starting the damage survey.

- *Meteorological conditions*. This part describes weather conditions before, during and after the event according to direct witnesses, the visibility (darkness, precipitation), AWS data (location and a summary of the most relevant recorded data), and other data of interest derived from an overview of remote-sensing tools.

- *Damage observed*. A general description of the observed damage is given (i.e. the most common and the most relevant seen during the fieldwork), including the maximum DoD for every DI noticed.

- *Direct witness inquiries*. This part summarizes witness enquiries (which should also be attached entirely apart).

It should contain, if available, the duration of the strong winds and a brief description of the experience of each witness.

– *Characterization of the event*. This final section contains the length and average and maximum width of the damage swath, the maximum wind intensity (specifying the intensity scale used), the translational direction and other data of interest such as the convective cell translation velocity.

3.3.2 Geolocated information table

A geolocated information table providing disaggregated data for each point of damage is proposed, similarly as in Holzer et al. (2018). It should contain all relevant geolocated information gathered during the fieldwork and also damage locations provided by local authorities, emergency services, media and social networks, which have been previously collected and analysed. To better organize the information displayed, seven different location types (L1 to L7; see Table 4) are considered. Note that L1 to L3 (vegetation and human-made structures) correspond to point-of-damage locations so that, if possible, they should include information about intensity rating (DI–DoD), according to Sect. 3.2. The rest of the locations describe positions of AWS, witnesses, pictures or windborne debris.

3.3.3 Data location map

The third deliverable consists of a map or a KML file format containing geolocated information gathered during the field survey in order to allow further graphical analysis, for example using Google Earth software (Gorelick et al., 2017). It is proposed that each of the seven location types presented in Sect. 3.3.2 is represented with a different icon, with a specific colour for points of damage (L1 to L3 from Table 4) depending on its intensity. Moreover, in the case of damage in trees with fall direction (L1) it is convenient to display an arrow icon on the map, whose direction should be the fall direction. Thereby, a tree damage pattern analysis to discriminate between damage caused by a tornado or by a downburst should be easily carried out. Damage swath characteristics (length and width) should also be calculated using the data location map.

As an example, Fig. 7 shows the data location map of part of the fieldwork carried out on 25 March 2012 to study the EF1 tornado that affected the municipalities of Castellnou de Seana and Ivars d'Urgell (Catalonia) on 21 March 2012 (Bech et al., 2015). It displays the information contained in a fallen tree damage-point type (in this case, latitude, longitude, tree fall direction, DI–DoD, a brief description and a photo) and in the unofficial Ivars d'Urgell AWS location (here latitude, longitude, AWS type and maximum wind speed plot), which registered a maximum wind gust of 26.4 $\mathrm{m\,s^{-1}}$ during the event.

4 Discussion

The proposed methodology is formulated in a convenient, feasible and detailed way so it can be readily used, but its practical application may present some weaknesses. Among the advantages of the proposed methodology is the relative simplicity of the devices required (Table 1), which are neither unusual nor expensive tools, so meteorological services, public research institutions and private entities may perform systematic damage surveys of reported events, analysing even suspicious developed funnel clouds for which it is previously unknown if they reached the ground. Moreover, the easy-to-reproduce fieldwork process and the generation of the proposed three final deliverables support the main objectives of the in situ damage assessment, which are identifying the phenomenon type, estimating wind intensity, and characterizing the event and the damage swath. Besides, the methodology is also intended to optimize time during in situ measurements in order to make possible visiting the whole affected area as soon as possible to avoid the alteration of the damage scenario by clearing services, as stated in Sect. 3.1.

Surface in situ analysis provides more detailed information than aerial surveys or analysis based only on remote-sensing data. For instance, minor damage to vegetation and to human-made structures is more easily detected (e.g. Marshall et al., 2012). In addition, it is possible to study in detail the soil state in forest areas and the degraded state or previous weaknesses of damaged elements, which are essential to assess the wind intensity, and measuring data of interest such as snapped trunk diameter or small windborne debris weight. On the other hand, tornado outbreaks and widespread events (such as derechos – e.g. Peterson, 2019; Chmielewski et al., 2020) may be cases where it is challenging to apply the methodology. Nevertheless, in Sect. 3.2 some methods to mitigate these problems have been provided, such as making a discontinuous analysis in forest areas, studying transversal stripes along the damage track every 250 to 500 m if possible. Another option would be to distribute areas to be analysed among the members of the surveyor team to carry out several field studies in parallel. Especially in those cases, and also in complex-terrain events, aerial imagery could be useful to complement surface data, providing an overview of the damaged area and information from difficult-access zones.

On the other hand, the geolocation of damaged elements and data of interest has a strong dependence on GPS signal reception. Geolocation accuracy depends on a number of factors including local terrain geometry, quality of the receiver antenna system or number of satellites observed. Photo cameras and smartphones have location errors usually ranging from 5 to 20 m, typically being the greatest in deep valleys, or close to large buildings or structures blocking satellite signals. To minimize geolocation errors, it is recommended to check the accuracy with manually selected reference locations and, if necessary, to correct damage locations on the summary map and on the geolocated information table. This

Table 4. Information location types (reference, description and data that should be presented).

Location reference	Description	Data
L1	Damage to trees with fall direction	Latitude, longitude, DI–DoD, previous weaknesses, fall direction
L2	Damage to trees without fall direction	Latitude, longitude, DI–DoD, previous weaknesses, trunk diameter (if snapped tree)
L3	Damage to human-made structures	Latitude, longitude, DI–DoD, previous weaknesses
L4	AWS location	Latitude, longitude, data (maximum wind gust, direction of maximum wind gust and hour)
L5	Witness location	Latitude and longitude of the witness location at the moment of the meteorological event and a brief description of their experience
L6	Image of the phenomenon	Latitude and longitude of the point where the image was recorded and orientation
L7	Windborne debris	Latitude, longitude, distance and direction of the displacement, size and weight of the object if measured

is feasible in urban or peri-urban areas, where buildings or other elements are easily identifiable using high-resolution aerial images such as orthophotos, but not in forests or other natural areas without evident references where this verification may not be possible.

The estimation of wind intensity of convective origin is based on damage rating scales, which relate the damage observed with the wind speed. Despite the proposed methodology being illustrated using the EF scale, it should be noted that other intensity scales could be used such as the TORRO scale (Meaden et al., 2007). The practical application of the EF scale has some limitations (Doswell et al., 2009), in spite of the progress made some years ago by introducing a more detailed intensity rating scale (WSEC, 2006) compared to the original and simpler Fujita scale (Fujita, 1981, 1992; Doswell, 2003). The Enhanced Fujita scale, developed in the USA, is mainly based on the damage caused by wind to standard US buildings and elements (schools, hospitals, automobile showrooms, etc.), so-called damage indicators (DIs). When applied to areas outside the USA many DIs may not exist, hampering its application as discussed in detail in Feuerstein et al. (2011) and Holzer et al. (2018). Moreover, there are elements which are susceptible to damage such as traffic signals, walls and fences, trash bins, and vehicles, which are not included on the EF scale.

The data gathered can have several uses, apart from contributing to build-up of homogeneous severe weather databases, which at the same time enhance the knowledge about tornado, downburst and straight-line wind occurrence. Insurance and reinsurance companies can be one of the major benefitted sectors from results of field studies, which usually need to know the area affected by a strong-convective-wind event and its intensity to cover compensations and, in some specific cases as in Spain, the phenomenon type (De Groeve et al., 2014).

Data collected from damage to buildings (general photos and detailed pictures of deficiencies or previous weaknesses) may also contribute to study exposure and vulnerability of constructions in an area of interest and also to assess the failure modes (e.g. north-eastern Italy; Zanini et al., 2017; Pipinato, 2018), as pointed out in De Groeve et al. (2013, 2014). Moreover, the identification of typical damaged buildings using the information provided in the set of final deliverables can give a guideline for adapting intensity rating scales, such as the EF scale, outside of the USA, partially solving those deficiencies in assessing wind intensity. In this line of work, some authors have propounded new damage indicators to append to the above-mentioned scale using information derived from tens of field studies (Mahieu and Wesolek, 2016); to adapt them to typical human-made structures from other countries, as recently reported in Canada (Environment Canada, 2013) or Japan (Japan Meteorological Agency, 2015); or even to develop a standardized international Fujita scale, as proposed in Groenemeijer et al. (2019). Furthermore, in some articles it has been discussed how to assess wind intensity throughout effects on vehicles, with data given by field studies (Paulikas et al., 2016), similarly to here. As provided in the geolocated information map, where each point of damage with its DI–DoD pair is given, it is possible to assess the degree of damage severity along the damage swath of a tornadic event. This information can be very valuable to analyse the impact of tornadoes in future

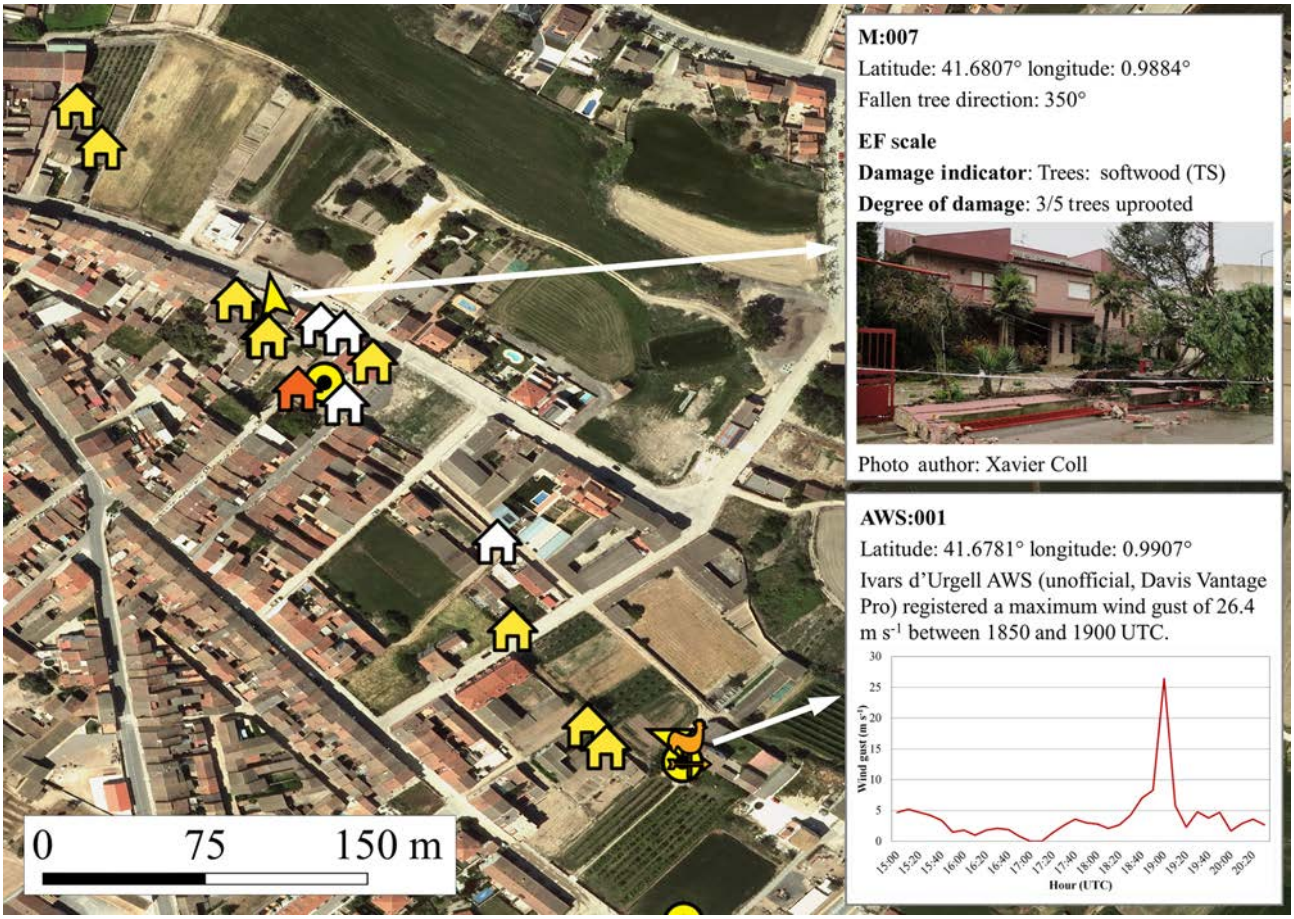

Figure 7. Data location map and two examples of recorded information from the 21 March 2012 EF1 Ivars d'Urgell (Catalonia) tornado track. Map symbols indicate locations of AWS (orange weathervane), damage to human-made structures (house icon) and fallen trees or damaged vegetation elements (arrow and circle icon if no direction is available, respectively). Icon colours indicate damage intensity using the EF scale: EF0 (yellow), EF1 (orange) and unrated (white). The background orthophoto is from the Institut Cartogràfic i Geològic de Catalunya (ICGC), http://www.icc.cat (last access: 1 September 2019), under a CC BY 4.0 license.

projected scenarios, for example modelling damaged areas in tornado paths using the data provided by field studies and assessing the possible consequences under different expected urban conditions (Ashley et al., 2014; Rosencrants and Ashley, 2015).

5 Summary and concluding remarks

In situ damage survey data are used to study the consequences of natural hazards, such as floods or damaging strong convective winds. The latter can be specifically characterized carrying out field studies, estimating the damage path length and width and also the intensity of the event. Moreover, through an analysis of the data gathered it might be possible to clarify which phenomenon caused the damage (tornado, downburst or straight-line winds) in case neither images nor direct witness reports exist.

The purpose of this article is to provide an easily reproducible methodology to carry out surface strong-convective-wind event damage surveys, which optimize time and economic resources. It is mainly based on collecting geolocated information about damaged human-made structures and vegetation, with the final aim of representing the damage scenario to study the event from a meteorological point of view. Complementary data from AWSs close to the affected area and witness reports should also be gathered if available, and remote-sensing data should be used to get a deeper understanding of the convective storm event. With all this information, three final deliverables are generated (a standardized text report of the event, a table consisting of detailed geolocated information, and a map or a file in KML format).

This methodology is based on previous studies and has been refined during the elaboration of 136 strong-convective-wind damage surveys carried out in Spain between 2004 and 2018. Known limitations of its application include geolocation errors of damage, applicability of the EF scale outside

the USA and difficulties in analysing extensive events or complex topography areas. Nevertheless, surface-based detailed data provided, such as previously degraded state of damaged elements, minor damage to human-made structures and vegetation, snapped tree trunk diameter, and soil state in forest areas, might be helpful to better analyse event consequences compared to other methodologies. In any case, the field survey data obtained are valuable for further analysis, complementing detailed meteorological case studies based on operational remote sensing such as Doppler weather radar data, surface observations and numerical weather prediction model output. Moreover, the methodology proposed may contribute to standardize detailed field surveys, which are essential to build up and maintain robust and homogeneous databases of severe weather phenomena.

Appendix A: Tornado vs. downburst damage patterns

The determination of the damaging wind phenomenon (tornado, downburst or straight-line winds) can be rather challenging in some cases. As reported in previous studies (Hall and Brewer, 1959; Holland et al., 2006; Bech et al., 2009; Beck and Dotzek, 2010; Rhee and Lombardo, 2018), it can be assumed that the direction of fallen trees indicates the direction of maximum wind speed in strong-convective-wind events, provided there are no influences from the terrain (i.e. slope favouring a specific fall direction) or from another tree fall interacting with the tree considered. Despite the fact that real wind damage patterns can be very complex due to their interaction with topography or with other nearby events (Forbes and Wakimoto, 1983; Cannon et al., 2016), theoretical idealized damage swath patterns of both tornado and downburst wind fields can be compared with observed damage patterns in order to look for similarities to assess their possible origin.

As explained in previous studies (e.g. Holland et al., 2006; Bech et al., 2009), a simple approximation to describe a tornado vortex wind field near the surface is given by the Rankine vortex model. This approach combines an inner rigidly rotating core with an outer region with decreasing rotation speed. The wind field velocity module is defined in polar coordinates by Eq. (A1):

$$v(r) = \begin{cases} \frac{v_{\max} r}{R} & \text{if } r \le R \\ \frac{v_{\max} R}{r} & \text{if } r > R \end{cases}, \tag{A1}$$

where $v(r)$ is the wind velocity as a function of the distance to the centre of the vortex r, $v_{\max}$ is the maximum wind velocity and R is the vortex radius where $v(r) = v_{\max}$.

Note that according to Eq. (A1), the Rankine vortex can describe, in simple terms, only a rotating vortex and its nearby environment, i.e. a stationary vortex. To model real tornadoes, a Rankine vortex with both tangential and radial wind components is combined with a translational movement, i.e. a homogeneous wind field. As described in Bech et al. (2009), according to Peterson (1992), two parameters are used to characterize this model: parameter G, which is the ratio between tangential velocity and translational velocity, and parameter α, which is the angle between radial velocity and tangential velocity, with 0° corresponding to a pure inflow, 90° to a pure tangential case and 180° to a pure outflow.

Examples of two-dimensional wind fields with different parameter configurations are shown in Fig. A1, including their associated damage swath pattern shown as a rectangular panel below each two-dimensional wind field. The damage swath pattern is obtained computing the maximum wind vector of the wind field along the y axis, as the examples assume a northern translation of the vortex. In the first row (Fig. A1a, b, and c), translational velocity is one-fourth the tangential velocity ($G = 4$) and, in the second row (Fig. A1d, e and f), translational velocity is equal to tangential velocity ($G = 1$).

In Fig. A1a, where tangential and inflow velocities are equal ($\alpha = 45°$), a convergence damage pattern is identified, whereas in Fig. A1b, where the radial component is zero ($\alpha = 90°$, i.e. pure tangential flow), the damage swath presents a rotational pattern. Figure A1c presents pure outflow with no tangential velocity ($\alpha = 180°$), exhibiting a similar divergence pattern as Fig. A1f, in the damage swath, which could correspond to a classical downburst pattern.

Thus, based on this simple model, if fallen tree patterns present convergence or rotation, it can be assumed that a vortex caused the damage, whereas a divergent pattern would suggest the effects of a downburst. Similarly, the way debris is spread or how a roof is collapsed or lifted can indicate winds either with a rotation and upward pattern (i.e. a tornado) or with a divergent and downward pattern (i.e. a downburst) – see Rhee and Lombardo (2018) for a more detailed discussion.

Nevertheless, it is also noticeable that in cases where tangential and translational velocities are similar ($G \approx 1$; see for example the second row of the Fig. A1), damage swaths may present only little differences among them. This can occur in weak (EF0 or EF1) tornado or downburst events that affect a small area. In these cases, damage may also be sparse, scattered and unconnected, which makes any damage pattern consistent with a tornado or a microburst unidentifiable (Bech et al., 2009; Rhee and Lombardo, 2018). Then, even a detailed damage survey, if there are neither images nor direct witnesses, may not be sufficient to determine which type of phenomena caused the damage. This situation of inconclusive results regarding the phenomenon type occurred in 7 % of the 136 damage surveys carried out in Spain by the authors between 2004 and 2018.

As a real example, the case shown in Fig. A2 presents fallen poplar trees following a convergence pattern: on the right-hand side of the damage swath, trees are blown down to the west, whereas on the left-hand side they are uprooted to the north. Comparing this real case and idealized cases (Fig. A1), this damage pattern matches the damage swath caused by a vortex with $G = 4$ and $\alpha = 45°$ well (Fig. A1a). This fact along with other evidence confirm the hypothesis that damage was caused by a tornado, as presented in the Supplement. Moreover, it is remarkable that these vortex characteristics are also coherent with the damage rated as the lower EF1 bound and the mean translational velocity of $12\,\mathrm{m\,s^{-1}}$, estimated using radar data from the Meteorological Service of Catalonia (not shown).

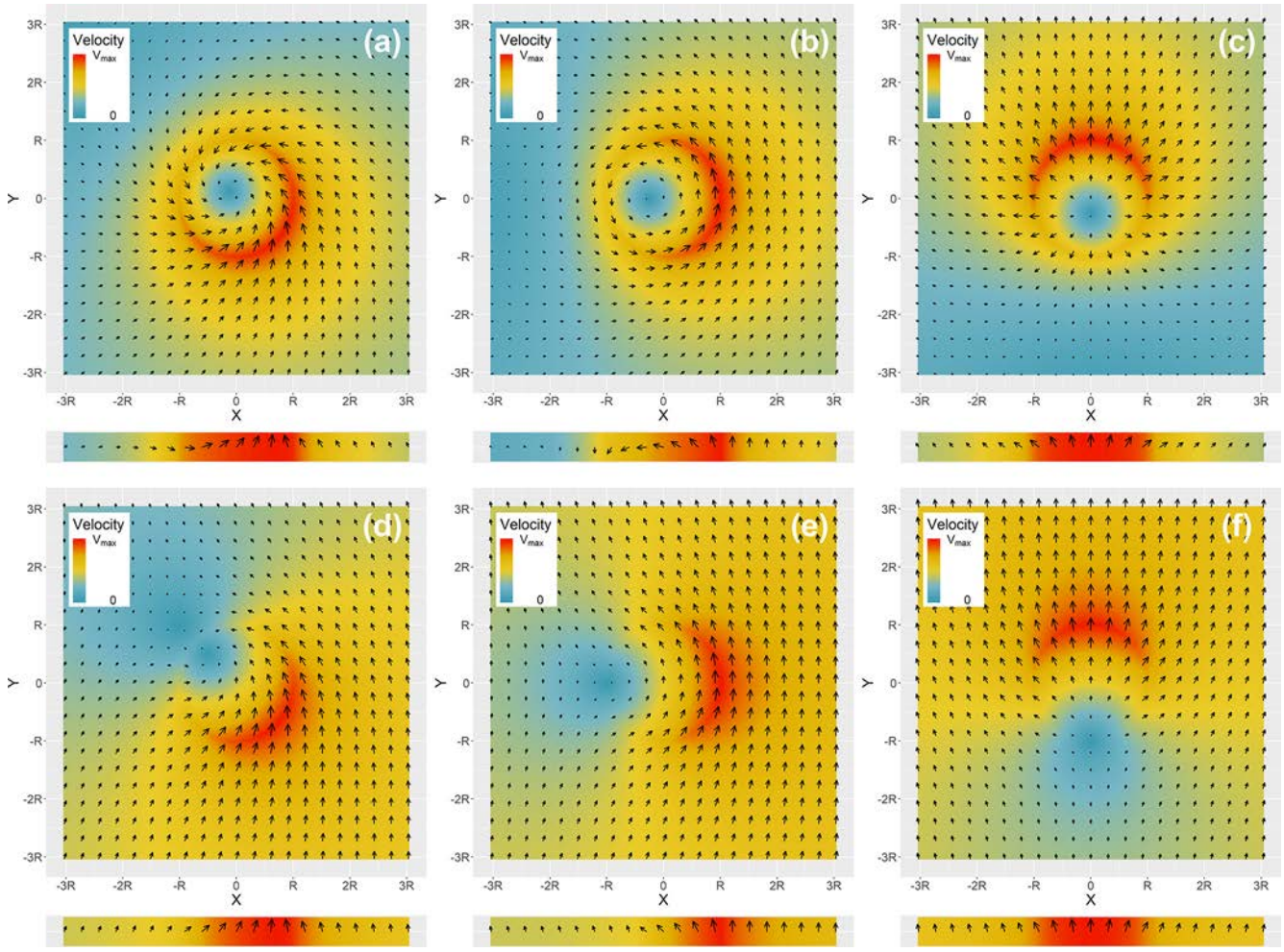

Figure A1. Two-dimensional near-surface horizontal wind fields and damage swaths for the cases: **(a)** $G = 4$ and $\alpha = 45°$, **(b)** $G = 4$ and $\alpha = 90°$, **(c)** $G = 4$ and $\alpha = 180°$, **(d)** $G = 1$ and $\alpha = 45°$, **(e)** $G = 1$ and $\alpha = 90°$, and **(f)** $G = 1$ and $\alpha = 180°$. Adapted from Figs. 3 and 4 of Bech et al. (2009).

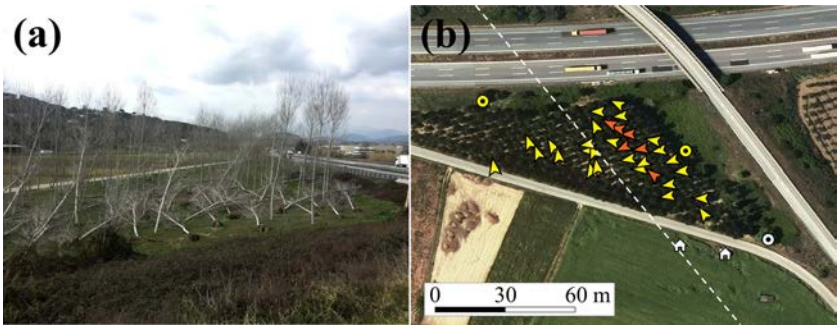

Figure A2. **(a)** A poplar plantation from Fogars de la Selva (Catalonia) affected by the 15 October 2018 EF1 Malgrat de Mar–Massanes tornado, and **(b)** fallen-tree directions of the same poplar plantation. Map symbols indicate locations of damage in human-made structures (house icon) and fallen tree or damaged vegetation elements (arrow or circle icon if no direction is available). Icon colours indicate damage intensity: EF0 (yellow), EF1 (orange) and unrated (white). The white discontinuous line separates the right-hand and the left-hand sides of the damage swath where predominant tree fall directions are west and north, respectively. The background orthophoto is from the Institut Cartogràfic i Geològic de Catalunya (ICGC), http://www.icc.cat, under a CC BY 4.0 license.

Data availability. The data used in this paper are available from the authors upon request.

Supplement. The supplement related to this article is available online at: https://doi.org/10.5194/nhess-20-1513-2020-supplement.

Author contributions. SC proposed and drafted the initial idea, and OR, JB, JdDS and DG contributed to develop the methodology according to their own experience on in situ damage surveys. OR and JB prepared the paper, with contributions from all co-authors.

Competing interests. The authors declare that they have no conflict of interest.

Acknowledgements. The authors gratefully acknowledge individuals supporting wind damage assessments carried out during these years, especially Joan Arús, Andrés Cotorruelo, Petra Ramos and particularly Miquel Gayà for his pioneering systematic studies of tornadoes in Spain. We also thank the Consorcio de Compensación de Seguros (CCS) and the Water Research Institute (IdRA) of the University of Barcelona for support and also the three anonymous reviewers for their comments and suggestions that improved the present article. This research was performed with partial funding from the projects CGL2015-65627-C3-2-R (MINECO/FEDER), CGL2016-81828-REDT (AEI) and RTI2018-098693-B643-C32 (AEI).

Financial support. This research has been supported by the Ministerio de Economía y Competitividad (grant no. CGL2015-65627-C3-2-R) and the Agencia Estatal de Investigación (grant nos. CGL2016-81828-REDT, RTI2018-098693-B643-C32).

Review statement. This paper was edited by Ricardo Trigo and reviewed by three anonymous referees.

References

Antonescu, B., Schultz, D. M., Lomas, F., and Kühne, T.: Tornadoes in Europe: Synthesis of the observational datasets, Mon. Weather Rev., 144, 2445–2480, https://doi.org/10.1175/MWR-D-15-0298.1, 2016.

Antonescu, B., Schultz, D. M., Holzer, A., and Groenemeijer, P.: Tornadoes in Europe: An underestimated threat, B. Am. Meteorol. Soc., 98, 713–728, https://doi.org/10.1175/BAMS-D-16-0171.1, 2017.

Ashley, W. S., Strader, S., Rosencrants, T. D., and Krmenec, A. J.: Spatiotemporal Changes in Tornado Hazard Exposure: The Case of the Expanding Bull's-Eye Effect in Chicago, Illinois, Weather Clim. Soc., 6, 175–193, https://doi.org/10.1175/WCAS-D-13-00047.1, 2014.

Bai, L., Meng, Z., Huang, L., Yan, L., Li, Z., Mai, X., Huang, Y., Yao, D., and Wang, X.: An Integrated Damage, Visual, and Radar Analysis of the 2015 Foshan, Guangdong, EF3 Tornado in China Produced by the Landfalling Typhoon Mujigae (2015), B. Am. Meteorol. Soc., 98, 2619–2640, https://doi.org/10.1175/BAMS-D-16-0015.1, 2017.

Bech, J., Pascual, R., Rigo, T., Pineda, N., López, J. M., Arús, J., and Gayà, M.: An observational study of the 7 September 2005 Barcelona tornado outbreak, Nat. Hazards Earth Syst. Sci., 7, 129–139, https://doi.org/10.5194/nhess-7-129-2007, 2007.

Bech, J., Gayà, M., Aran, M., Figuerola, F., Amaro, J., and Arús, J.: Tornado damage analysis of a forest area using site survey observations, radar data and a simple analytical vortex model, Atmos. Res., 93, 118–130, https://doi.org/10.1016/j.atmosres.2008.10.016, 2009.

Bech, J., Pineda, N., Rigo, T., Aran, M., Amaro, J., Gayà, M., Arús, J., Montanyà, J., and van der Velde, O.: A Mediterranean nocturnal heavy rainfall and tornadic event. Part I: Overview, damage survey and radar analysis, Atmos. Res., 100, 621–637, https://doi.org/10.1016/j.atmosres.2010.12.024, 2011.

Bech, J., Pineda, N., Rigo, T., and Aran, M.: Remote sensing analysis of a Mediterranean thundersnow and low-altitude heavy snowfall event, Atmos. Res., 123, 305–322, https://doi.org/10.1016/j.atmosres.2012.06.021, 2013.

Bech, J., Arús, J., Castán, C., Pineda, N., Rigo, T., Montanyà, J., and van der Velde, O.: A study of the 21 March 2012 tornadic quasi linear convective system in Catalonia, Atmos. Res., 158–159, 192–209, https://doi.org/10.1016/j.atmosres.2014.08.009, 2015.

Beck, V., and Dotzek, N.: Reconstruction of Near-Surface Tornado Wind Fields from Forest Damage, J. Appl. Meteorol. Clim., 49, 1517–1537, https://doi.org/10.1175/2010JAMC2254.1, 2010.

Beven, K. J., Aspinall, W. P., Bates, P. D., Borgomeo, E., Goda, K., Hall, J. W., Page, T., Phillips, J. C., Simpson, M., Smith, P. J., Wagener, T., and Watson, M.: Epistemic uncertainties and natural hazard risk assessment – Part 2: What should constitute good practice?, Nat. Hazards Earth Syst. Sci., 18, 2769–2783, https://doi.org/10.5194/nhess-18-2769-2018, 2018.

Bunting, W. F. and Smith, B. E.: A guide for conducting damage surveys. NOAA Tech. Memo. NWS-SR-146, Scientific Services Division, Southern Region, Fort Worth, TX, USA, 44 pp., 1993.

Burgess, D., Ortega, K., Stumpf, G., Garfield, G., Kartens, C., Meyer, T., and Smith, B.: 20 May 2013 Moore, Oklahoma, Tornado: Damage Survey and Analysis, Weather Forecast., 29, 1229–1237, https://doi.org/10.1175/WAF-D-14-00039.1, 2014.

Cannon, J. B., Hepinstall-Cymerman, J., Godfrey, C. M., and Peterson, C. J.: Landscape-scale characteristics of forest tornado damage in mountainous terrain, Landscape Ecol., 31, 2097–2114, https://doi.org/10.1007/s10980-016-0384-8, 2016.

Chernokulsky, A. and Shikhov, A.: 1984 Ivanovo tornado outbreak: Determination of actual tornado tracks with satellite data, Atmos. Res., 207, 111–121, https://doi.org/10.1016/j.atmosres.2018.02.011, 2018.

Chmielewski, T., Szer, J., and Bobra, P.: Derecho wind storm in Poland on 11–12 August 2017: results of the post-disaster investigation, Environ. Hazards, 0, 1–21, https://doi.org/10.1080/17477891.2020.1730154, 2020.

De Groeve, T., Poljansek, K., and Ehrlich, D.: Recording disasters losses: recommendation for a European approach. JRC Scientific and Policy Report, available at: http://publications.jrc.ec.europa.

eu/repository/bitstream/111111111/29296/1/lbna26111enn.pdf (last access: 2 December 2019), 2013.

De Groeve, T., Poljansek, K., Ehrlich D., and Corbane C.: Current status and best practices for disaster loss data recording in EU Member States. JRC Scientific and Policy Report, available at: http://publications.jrc.ec.europa.eu/repository/bitstream/JRC92290/lbna26879enn.pdf (last access: 2 December 2019), 2014.

Doswell III, C. A.: A guide to F-scale damage assessment, NOAA Rep., 101 pp., available at: http://www.wdtb.noaa.gov/courses/ef-scale/lesson2/FinalNWSF-scaleAssessmentGuide.pdf (last access: 19 March 2020), 2003.

Doswell III, C. A., Brooks, H. E., and Dotzek, N.: On the implementation of the enhanced Fujita scale in the USA, Atmos. Res., 93, 554–563, https://doi.org/10.1016/j.atmosres.2008.11.003, 2009.

Dotzek, N., Groenemeijer, P., Feuerstein, B., and Holzer, A. M.: Overview of ESSL's severe convective storms research using the European Severe Weather Database ESWD, Atmos. Res., 93, 575–586, https://doi.org/10.1016/j.atmosres.2008.10.020, 2009.

Edwards, R.: Frequently Asked Questions about Tornadoes, Storm Prediction Center (NOAA), available at: https://www.spc.noaa.gov/faq/tornado/index.html, last access: 19 March 2020.

Edwards, R., LaDue, J. G., Ferree, J. T., Scharfenberg, K., Maier, C., and Coulbourne, W. L.: Tornado Intensity Estimation: Past, Present, and Future, B. Am. Meteorol. Soc., 94, 641–653, https://doi.org/10.1175/BAMS-D-11-00006.1, 2013.

Environment Canada: Enhanced Fujita Scale Damage Indicators and Degrees Of Damage, available at: https://www.canada.ca/en/environment-climate-change/services/seasonal-weather-hazards/enhanced-fujita-scale-wind-damage.html (last access: 11 August 2019), 2013.

Farnell, C., Busto, M., Aran, M., Andrés, A., Pineda, N., and Torà, M.: Study of the hailstorm of 17 September 2007 at the Pla d'Urgell. Part one: fieldwork and analysis of hailpads, Tethys, 6, 67–79, https://doi.org/10.3369/tethys.2009.6.05, 2009.

Feuerstein, B., Groenemeijer, P., Dirksen, E., Hubrig, M., Holzer, A. M., and Dotzek, N.: Towards an improved wind speed scale and damage description adapted for Central Europe, Atmos. Res., 100, 547–564, https://doi.org/10.1016/j.atmosres.2010.12.026, 2011.

Forbes, G. S. and Wakimoto, R. M.: A Concentrated Outbreak of Tornadoes, Downbursts and Microbursts, and Implications Regarding Vortex Classification, Mon. Weather Rev., 111, 220–236, https://doi.org/10.1175/1520-0493(1983)111<0220:ACOOTD>2.0.CO;2, 1983.

Foster, D. R.: Species and stand response to catastrophic wind in Central New England, USA, J. Ecol., 76, 135–151, https://doi.org/10.2307/2260458, 1988.

Fujita, T. T.: Tornadoes and downbursts in the context of generalized planetary scales, J. Atmos. Sci., 38, 1511–1534, https://doi.org/10.1175/1520-0469(1981)038<1511:TADITC>2.0.CO;2, 1981.

Fujita, T. T.: Mystery of severe storms. Wind Research Laboratory Research Paper 239, Dept. of Geophysical Sciences, University of Chicago, Chicago, IL, USA, 298 pp., 1992.

Gayà, M.: The 1886 tornado of Madrid, Atmos. Res., 83, 201–210, https://doi.org/10.1016/j.atmosres.2005.10.017, 2007.

Gayà, M.: Els Fiblons a Espanya: Climatologia i catàleg de tornados i trombes (Whirlwinds in Spain: Climatology and Catalog of Tornadoes and Waterspouts, in Catalan), 2nd edn., Edicions UIB, Palma, Spain, 619 pp., 2018.

Gayà, M., Llasat, M.-C., and Arús, J.: Tornadoes and waterspouts in Catalonia (1950–2009), Nat. Hazards Earth Syst. Sci., 11, 1875–1883, https://doi.org/10.5194/nhess-11-1875-2011, 2011.

Godfrey, C. M. and Peterson, C. J.: Estimating Enhanced Fujita Scale Levels Based on Forest Damage Severity, Weather Forecast., 32, 243–252, https://doi.org/10.1175/WAF-D-16-0104.1, 2017.

Gorelick, N., Hancher, M., Dixon, M., Ilyushchenko, S., Thau, D., and Moore, R.: Google Earth Engine: Planetary-scale geospatial analysis for everyone, Remote Sens. Environ., 202, 18–27, https://doi.org/10.1016/j.rse.2017.06.031, 2017.

Groenemeijer, P., Holzer, A. M., Hubrig, M., Kühne, T., Kaltenberger, R., Soriano, J. D., Bock, L., Guitiérrez, D., van de Ploeg, B., Strommer, G., and Schreiner, T.: The International Fujita Scale: A Globally Applicable Scale for Tornado and Wind Damage Classification, 10th European Conference on Severe Storms, 4–8 November 2019, Kraków, Poland, 2019.

Gutiérrez, D., Riesco, J., and Ponce, S.: SINOBAS, a tool for collaborative mapping applied to observation of "singular" weather phenomena, 15th EMS Annual Meeting & 12th European Conference on Applications of Meteorology (ECAM), 7–11 September 2015, Sofia, Bulgaria, EMS2015-413, 2015.

Hall, F. and Brewer, R. D.: A sequence of tornado damage patterns, Mon. Weather Rev., 87, 207–216, 1959.

Holland, A. P., Riordan, A. J., and Franklin, E. C.: A simple model for simulating tornado damage in forests, J. Appl. Meteorol. Clim., 45, 1597–1611, https://doi.org/10.1175/JAM2413.1, 2006.

Holzer, A. M., Schreiner, T. M. E., and Púčik, T.: A forensic reanalysis of one of the deadliest European tornadoes, Nat. Hazards Earth Syst. Sci., 18, 1555–1565, https://doi.org/10.5194/nhess-18-1555-2018, 2018.

Hyvärinen, O. and Saltikoff, E.: Social Media as a Source of Meteorological Observations, Mon. Weather Rev., 138, 3175–3184, https://doi.org/10.1175/2010MWR3270.1, 2010.

IRDR: Peril Classification and Hazard Glossary, Integrated Research on Disaster Risk, 28 pp., available at: http://www.irdrinternational.org/2014/03/28/irdr-peril-classification-and-hazard-glossary/ (last access: 27 December 2019), 2014.

Japan Meteorological Agency (JMA): Guidelines for the Japanese Enhanced Fujita Scale, 113 pp., available at: https://www.data.jma.go.jp/obd/stats/data/bosai/tornado/kaisetsu/jefscale_en.html (last access: 11 August 2019), 2015.

Karstens, C. D., Samaras, T. M., Lee, B. D., Gallus, W. A., and Finley, C. A.: Near-Ground Pressure and Wind Measurements in Tornadoes, Mon. Weather Rev., 138, 2570–2588, https://doi.org/10.1175/2010MWR3201.1, 2010.

Karstens, C. D., Gallus, W. A., Lee, B. D., and Finley, C. A.: Analysis of Tornado-Induced Tree Fall Using Aerial Photography from the Joplin, Missouri, and Tuscaloosa–Birmingham, Alabama, Tornadoes of 2011, J. Appl. Meteorol. Clim., 52, 1049–1068, https://doi.org/10.1175/JAMC-D-12-0206.1, 2013.

KERAUNOS: Les tornades en France (Tornadoes in France, in French), available at: http://www.keraunos.org/climatologie/les-tornades-en-france.html, last access: 17 April 2020.

Knox, J. A., Rackley, J. A., Black, A. W., Gensini, V. A., Butler, M., Dunn, C., Gallo, T., Hunter, M. R., Lindsey, L., Phan, M., Scroggs, R., and Brustad, S.: Tornado Debris Characteristics And Trajectories During The 27 April 2011 Super Outbreak As Determined Using Social Media Data, B. Am. Meteorol. Soc., 94, 1371–1380, https://doi.org/10.1175/BAMS-D-12-00036.1, 2013.

Kryvasheyeu, Y., Chen, H., Obradovich, N., Moro, E., Van Hentenryck, P., Fowler, J., and Cebrian M.: Rapid assessment of disaster damage using social media activity, Sci. Adv., 3, e1500779, https://doi.org/10.1126/sciadv.1500779, 2016.

Lemon, L. R., Stan-Sion, A., Soci, C., and Cordoneanu, E.: A strong, long-track, Romanian tornado, Atmos. Res., 67–68, 391–416, https://doi.org/10.1016/S0169-8095(03)00063-2, 2003.

Letchford, C. W. and Chay, M. T.: Pressure distributions on a cube in a simulated thunderstorm downburst. Part B: moving downburst observations, J. Wind. Eng. Ind. Aerodyn., 90, 733–753, https://doi.org/10.1016/S0167-6105(02)00163-0, 2002.

Li, L., Yang, J., Lin, C.-Y., Chua, C. T., Wang, Y., Zhao, K., Wu, Y.-T., Liu, P. L.-F., Switzer, A. D., Mok, K. M., Wang, P., and Peng, D.: Field survey of Typhoon Hato (2017) and a comparison with storm surge modeling in Macau, Nat. Hazards Earth Syst. Sci., 18, 3167–3178, https://doi.org/10.5194/nhess-18-3167-2018, 2018.

Llasat, M. C., Turco, M., Quintana-Seguí, P., and Llasat-Botija, M.: The snow storm of 8 March 2010 in Catalonia (Spain): a paradigmatic wet-snow event with a high societal impact, Nat. Hazards Earth Syst. Sci., 14, 427–441, https://doi.org/10.5194/nhess-14-427-2014, 2014.

Mahieu, P. and Wesolek, E.: Tornado Rating in Europe with the EF-scale, KERAUNOS, 65 pp., available at: http://www.keraunos.org/tornado-rating-in-europe-with-the-enhanced-fujita-scale.pdf (last access: 11 August 2019), 2016.

Marshall, T. P.: Tornado damage survey at Moore, Oklahoma, Weather Forecast., 17, 582–598, https://doi.org/10.1175/1520-0434(2002)017<0582:TDSAMO>2.0.CO;2, 2002.

Marshall, T. P., Davis, W., and Runnels, S.: Damage survey of the Joplin tornado, 26th Conference on Severe Local Storm, 5–8 November 2012, Nashville, TN, USA, 6.1, available at: https://ams.confex.com/ams/26SLS/webprogram/Manuscript/Paper211662/Joplinmerger.pdf (last access: 11 August 2019), 2012.

Mateo, J., Ballart, D., Brucet, C., Aran, M., and Bech, J.: A study of a heavy rainfall event and a tornado outbreak during the passage of a squall line over Catalonia, Atmos. Res., 93, 131–146, https://doi.org/10.1016/j.atmosres.2008.09.030, 2009.

McDonald, J. R. and Marshall, T. P.: Tornado Damage Documentation, Institute for Disaster Research Publication 1984-20, Texas Tech University, USA, 27 pp., 1984.

Meaden, G. T., Kochev, S., Kolendowicz, L., Kosa-Kiss, A., Marcinoniene, I., Sioutas, M., Tooming, H., and Tyrrell, J.: Comparing the theoretical versions of the Beaufort scale, the T-Scale and the Fujita scale, Atmos. Res., 83, 446–449, https://doi.org/10.1016/j.atmosres.2005.11.014, 2007.

Meng, Z. and Yao, D.: Damage Survey, Radar, and Environment Analyses on the First-Ever Documented Tornado in Beijing during the Heavy Rainfall Event of 21 July 2012, Weather Forecast., 29, 702–724, https://doi.org/10.1175/WAF-D-13-00052.1, 2014.

Miller, P. W. and Mote, T. L.: Characterizing severe weather potential in synoptically weakly forced thunderstorm environments, Nat. Hazards Earth Syst. Sci., 18, 1261–1277, https://doi.org/10.5194/nhess-18-1261-2018, 2018.

Molinari, D., Menoni, S., Aronica, G. T., Ballio, F., Berni, N., Pandolfo, C., Stelluti, M., and Minucci, G.: Ex post damage assessment: an Italian experience, Nat. Hazards Earth Syst. Sci., 14, 901–916, https://doi.org/10.5194/nhess-14-901-2014, 2014.

Molthan, A. L., Bell, J. R., Cole, T. A., and Burks, J. E.: Satellite-based identification of tornado damage tracks from the 27 April 2011 severe weather outbreak, J. Oper. Meteor., 2, 191–208, https://doi.org/10.15191/nwajom.2014.0216, 2014.

NOAA/SPC: U.S. tornadoes (1950–2018), available at: https://www.spc.noaa.gov/wcm (last access: 17 April 2020), 2019.

Orf, L., Kantor, E., and Savory, E.: Simulation of a downburst-producing thunderstorm using a very high-resolution three-dimensional cloud model, J. Wind Eng. Ind. Aerodyn., 104–106, 547–557, https://doi.org/10.1016/j.jweia.2012.02.020, 2012.

Paulikas, M. J., Schmidlin, T. W., and Marshall, T. P.: The Stability of Passenger Vehicles at Tornado Wind Intensities of the (Enhanced) Fujita Scale, Weather Clim. Soc., 8, 85–91, https://doi.org/10.1175/WCAS-D-15-0051.1, 2016.

Peterson, C. J.: Damage diversity as a metric of structural complexity after forest wind disturbance, Forests, 10, 85, https://doi.org/10.3390/f10020085, 2019.

Peterson, R. E.: Johannes Letzmann: a pioneer in the study of tornadoes, Weather Forecast., 7, 166–184, https://doi.org/10.1175/1520-0434(1992)007<0166:JLAPIT>2.0.CO;2, 1992.

Pipinato, A.: Recent northeast Italian tornado events: lesson learned for improving structures, Nat. Hazards, https://doi.org/10.1007/s11069-018-3380-2, 2018.

Rasmussen, E. N., Davies-Jones, R., and Holle, R. L.: Terrestrial Photogrammetry of Weather Images Acquired in Uncontrolled Circumstances, J. Atmos. Ocean. Tech., 20, 1790–1803, https://doi.org/10.1175/1520-0426(2003)020<1790:TPOWIA>2.0.CO;2, 2003.

Rhee, D. M. and Lombardo, F. T.: Improved near-surface wind speed characterization using damage patterns, J. Wind. Eng. Ind. Aerodyn., 180, 288–297, https://doi.org/10.1016/j.jweia.2018.07.017, 2018.

Riesco, J., Polvorinos, F., Núñez, J. A., Soriano, J. D., and Jiménez, C.: Climatología de tornados en España Peninsular y Baleares (Tornado Climatology in the Peninsular Spain and Balearic Islands, in Spanish), Spanish Meteorological Agency (AEMet), 83 pp., available at: http://www.aemet.es/documentos/es/conocermas/publicaciones/Climatologia_tornados/Climatologia_tornados.pdf (last access: 11 August 2019), 2015.

Ripoll, R., del Amo, X., and Vendrell, R.: The weather observers network of the Meteorological Service of Catalonia, WMO Technical Conference on Meteorological and Environmental Instruments and Methods of Observation (CIMO TECO 2016), 27–30 September 2016, Madrid, Spain, P2(57), 2016.

Rodríguez, O. and Bech, J.: Sounding-derived parameters associated with tornadic storms in Catalonia, Int. J. Climatol., 38, 2400–2414, https://doi.org/10.1002/joc.5343, 2018.

Rosencrants, T. D. and Ashley, W. S.: Spatiotemporal analysis of tornado exposure in five US metropolitan areas, Nat. Hazards, 78, 121–140, https://doi.org/10.1007/s11069-015-1704-z, 2015.

Roueche, D. B. and Prevatt, D. O.: Residential Damage Patterns Following the 2011 Tuscaloosa, AL and Joplin, MO Tornadoes, J. Disaster Res., 8, 1061–1067, 2013.

Sánchez-Laulhé, J. M.: El tornado de Málaga del 1 de Febrero de 2009 (The 1 February 2009 tornado of Malaga), Spanish Meteorological Agency (AEMet), 3 pp., available at: https://repositorio.aemet.es/bitstream/20.500.11765/2724/1/TyC_2009_24_03.pdf (last access: 11 August 2019), 2013 (in Spanish).

Shikhov, A. and Chernokulsky, A.: A satellite-derived climatology of unreported tornadoes in forested regions of northeast Europe, Remote Sens. Environ., 204, 553–567, https://doi.org/10.1016/j.rse.2017.10.002, 2018.

Shikhov, A. N., Perminova, E. S., and Perminov, S. I.: Satellite-based analysis of the spatial patterns of fire-and storm-related forest disturbances in the Ural region, Russia, Nat. Hazards, 97, 283–308, https://doi.org/10.1007/s11069-019-03642-z, 2019.

Strader, S. M., Ashley, W., Irizarry, A., and Hall, S.: A climatology of tornado intensity assessments, Meteorol. Appl., 22, 513–524, https://doi.org/10.1002/met.1482, 2015.

Taszarek, M., Brooks, H. E., and Czernecki, B.: Sounding-Derived Parameters Associated with Convective Hazards in Europe, Mon. Weather Rev., 145, 1511–1528, https://doi.org/10.1175/MWR-D-16-0384.1, 2017.

Verbout, S. M., Brooks, H. E., Leslie, L. M., and Schultz, D. M.: Evolution of the US tornado database: 1954–2003, Weather Forecast., 21, 86–93, https://doi.org/10.1175/WAF910.1, 2006.

Wakimoto, R. M. and Lew, J. K.: Observations of a Florida Waterspout during CaPE, Weather Forecast., 8, 412–423, https://doi.org/10.1175/1520-0434(1993)008<0412:OOAFWD>2.0.CO;2, 1993.

Wakimoto, R. M. and Liu, C.: The Garden City, Kansas, Storm during VORTEX 95. Part II: The Wall Cloud and Tornado, Mon. Wea. Rev., 126, 393–408, https://doi.org/10.1175/1520-0493(1998)126<0393:TGCKSD>2.0.CO;2, 1998.

Wakimoto, R. M., Wienhoff, Z., Bluestein, H. B., and Reif, D.: The Dodge City Tornadoes on 24 May 2016: Damage Survey, Photogrammetric Analysis Combined with Mobile Polarimetric Radar Data, Mon. Weather Rev., 146, 3735–3771, https://doi.org/10.1175/MWR-D-18-0125.1, 2018.

Wesolek, E. and Mahieu, P.: The F4 tornado of August 3, 2008, in Northern France: Case study of a tornadic storm in a low CAPE environment, Atmos. Res., 100, 649–656, https://doi.org/10.1016/j.atmosres.2010.09.003, 2011.

WSEC: A Recommendation for an Enhanced Fujita Scale (EF-scale), Wind Science and Engineering Center, 111 pp., available at: http://www.spc.noaa.gov/faq/tornado/EFScale.pdf (last access: 11 August 2019), 2006.

Wurman, J., Kosiba, K., and Robinson, P.: In situ, Doppler radar, and video observations of the interior structure of a tornado and the wind–damage relationship, B. Am. Meteorol. Soc., 94, 835–846, https://doi.org/10.1175/BAMS-D-12-00114.1, 2013.

Zanini, M. A., Hofer, L., Faleschini, F., and Pellegrino, C.: Building damage assessment after the Riviera del Brenta tornado, northeast Italy, Nat. Hazards, 86, 1247–1273, https://doi.org/10.1007/s11069-017-2741-6, 2017.

Zehnder, J. A., Hu, J., and Razdan, A.: A Stereo Photogrammetric Technique Applied to Orographic Convection, Mon. Weather Rev., 135, 2265–2277, https://doi.org/10.1175/MWR3401.1, 2007.

2.2 Reanàlisi de traces de danys associades a episodis de vent fort d'origen convectiu mitjançant imatges aèries d'alta resolució

2.2.1 Resum de l'article

Al següent treball es mostra la potencial contribució de les ortofotografies a l'hora de detectar i analitzar traces de danys causades per episodis de vent fort d'origen convectiu. Mitjançant la comparativa de les imatges anteriors i posteriors a un esdeveniment es poden observar canvis en la cobertura vegetal i en les construccions. Fins i tot és possible estudiar el camp de vent a partir de la direcció de caiguda dels arbres identificats amb l'ajut d'ortofotografies, sobretot en zones forestals.

Tal com passa amb les dades obtingudes fruit de l'elaboració de treballs de camp, l'anàlisi d'aquest tipus d'imatges sol fer possible conèixer quin fenomen meteorològic ha tingut lloc i caracteritzar la traça de danys. Per tant, contribueixen a la construcció de bases de dades homogènies i robustes de fenòmens de temps violent.

Per a mostrar el valor afegit que aporten les imatges aèries d'alta resolució en l'estudi de les traces de danys, s'analitza l'episodi de temps violent que hi va haver la matinada del 2 de novembre de 2008 al Camp de Tarragona i es compara amb els resultats publicats en estudis anteriors. Per a fer-ho s'utilitzen les ortofotografies de l'ICGC dels anys 2008 i 2009, que tenen una resolució espacial de 50 i 25 cm, respectivament. L'estudi es complementa amb l'anàlisi de les dades Doppler de velocitat radial del radar de Tivissa-Llaberia (LMI) de la Xarxa de Radars (XRAD) del SMC i d'una estació meteorològica particular ubicada al centre de la traça de danys a Reus.

Es conclou que aquella matinada hi va haver dos tornados. El primer va afectar la franja compresa entre els municipis de Salou (el Tarragonès) i l'Aleixar (el Baix Camp), mentre que el segon ho va fer entre el Pla de Santa Maria (l'Alt Camp) i Sarral (la Conca de Barberà). L'ús de l'escala EF, i de la relació entre la longitud i l'amplada de la traça de danys i de la ràtio d'arbres tombats amb la intensitat dels fiblons permet estimar que el tornado de Salou-l'Aleixar va ser d'intensitat EF2 i el del Pla de Santa Maria-Sarral d'intensitat EF3, essent el darrer el més intens registrat a Catalunya.

Aquest article dona resposta a l'objectiu general **OG1** i a l'objectiu específic **OE2**.

2.2.2 Article

Rodríguez O. i Bech J. (2020): Reanalysing strong-convective wind damage paths using high-resolution aerial images. *Natural Hazards*, **104(1)**: 1021–1038. doi:10.1007/s11069-020-04202-6.

Natural Hazards (2020) 104:1021–1038
https://doi.org/10.1007/s11069-020-04202-6

ORIGINAL PAPER

Reanalysing strong-convective wind damage paths using high-resolution aerial images

Oriol Rodríguez[1] · **Joan Bech**[1]

Received: 31 March 2020 / Accepted: 21 July 2020 / Published online: 31 July 2020

Abstract
High-resolution aerial imagery may provide very detailed information about strong-convective wind events, which can be very useful to enhance and make more robust severe weather databases. Through an aerial analysis, unknown affected areas can be unveiled, large damaged zones or complex terrain events can be mapped, and in situ damage surveys can be completed. Comparing aerial orthophotographs or high-resolution satellite imagery taken before and after the event, damage to forest associated with EF1 + intensities rated with the Enhanced Fujita scale is easily observable. It is also possible to detect repaired parts on some types of roofs and buildings due to the occurrence of weak events and major damage on human-made structures in case of significant episodes. To illustrate the added value of using orthophotographs in forensic damage survey analysis, the 2 November 2008 strong-convective wind event in Catalonia (NE Iberian Peninsula) is revisited. Confirming previous studies, two different damage swaths, associated with the passage of two supercells during the early morning, are clearly identified in high-resolution aerial images. The additional information provided by orthophotograph analysis allowed extending the two damage paths and increasing the damage intensity of the event. It is concluded that both damage tracks are related to tornadoes, which are rated as an EF2 and an EF3, the second being the strongest tornado ever registered in Catalonia, one of the most tornado-prone regions of southern Europe.

Keywords Tornado · Remote sensing · Orthophotographs · Damaging winds · Severe storms

1 Introduction

Strong-convective surface winds (i.e. tornadoes and downbursts) are classified as microscale meteorological phenomena (Orlanski 1975), i.e. with characteristic length scales from 2 km to 200 m and time scales of a few minutes. Despite their small spatial scale and short life cycle, they have a high damaging potential. For example, in the USA tornadoes

✉ Oriol Rodríguez
orodriguez@meteo.ub.edu

[1] Department of Applied Physics – Meteorology, University of Barcelona, Barcelona, Martí i Franquès, 1, 08028 Barcelona, Catalonia, Spain

cause every year 75 fatalities, 1050 people injured and economical losses around 1275 M€ on average (NWS 2020). In Europe, their impact is smaller, but nevertheless on average every year they cause 5 fatalities, 70 injured people and more than 15 M€ on damage (Antonescu et al. 2017).

Meteorological services, public research institutions and private entities work to build up robust and consistent databases of strong-convective wind events to study their temporal and spatial distribution, frequency, intensity and damage swaths characteristics (see, for example, Gayà 2018; SPC 2020; ESWD 2020). Currently, initial event detection is mainly based on spotter observations and social media reports (Hyvärinen and Saltikoff 2010). That is the reason why strong-convective wind databases lack information in low-densely populated areas, mountain zones and deforested areas, especially in case of weak events (Potvin et al. 2019). This lack of detailed information hampers the analysis of severe weather case studies in complex orography areas, where remote sensing data may be available and numerical simulations may be performed but observed damaged on ground may be limited or almost inexistent.

Remote-sensing tools such as high-resolution satellite images or aerial orthophotographs (Karstens et al. 2010; Lee et al. 2010; Ermert et al. 2013; Wagner et al. 2019; Burow et al. 2020) can be helpful to notice past events by detecting damaged elements (forests, buildings), independently from the population density or the orography of the area. With its use, it is possible to unveil affected areas previously unknown (Shikhov and Chernokulsky 2018), to analyse in detail widespread events with large damaged areas or complex orography (Molthan et al. 2011, 2014; Chernokulsky and Shikhov 2018; Womble et al. 2018; Shikhov et al. 2019) and to complete in situ damage surveys (Bunting and Smith 1993; Rodríguez et al. 2020). Moreover, numerical case studies of severe storms in complex terrain areas (see, for example, Mulholland et al. 2019; León-Cruz et al. 2019; Barrett et al. 2020) could potentially benefit from more complete ground damage observations.

Damage revealed by this kind of information is mainly associated with severe storms affecting forests (Fig. 1a, b) rated as EF1 or greater level from the EF-scale (Enhanced Fujita scale, WSEC 2006). Moreover, in high-resolution aerial image time series, it is also possible to observe changes before and after a damaging wind event in roofs or other human-made structures, even for weak cases. As examples, Fig. 1c, d shows damage on roofs associated with tornadoes. Note that in the first case, two different tornadic events in years 2005 and 2006 (described in Bech et al. 2007 and Mateo et al. 2009, respectively), damaged the same industrial building. Nevertheless, the use of aerial orthophotographs also presents some limitations, because if the affected areas are crop fields or deforested zones, damage might be completely undetectable.

The aim of this article is to present the potential contribution of using orthophotographs taken before and after a strong-convective wind event and also additional radar imagery and surface weather stations data on characterizing damage paths. This is illustrated here revisiting the 2 November 2008 Camp de Tarragona region (Catalonia) severe weather event. This case study was previously analysed in Bech et al. (2011) and Pineda et al. (2011), where the synoptic scale configuration is presented, the results of an in situ damage survey assessment are explained and convective cells are characterized using remote-sensing tools. Two damage swaths were located in the area of study: the first one between Salou and Reus and extending to the north, and the other between el Pla de Santa Maria and Sarral (Fig. 2). The second was attributed to an F2 tornado, according to the Fujita scale (Fujita 1981).

This paper is structured as follows. Firstly, in Sect. 2, the region of study is described and an overview of the reanalysed event is presented. Then, in Sect. 3,

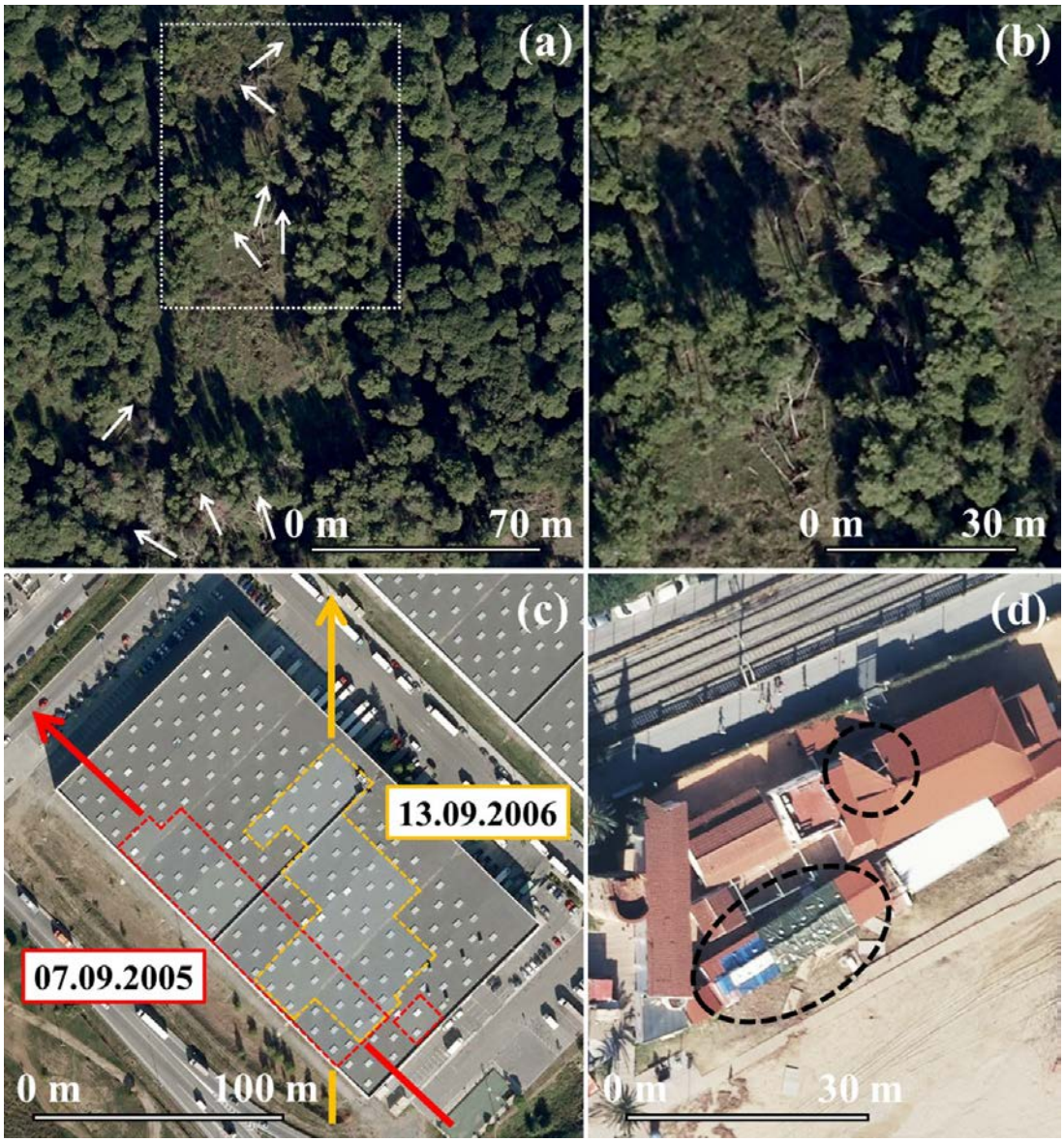

Fig. 1 **a** Pines blown down by the EF1 13 September 2006 tornado in Gavà (Catalonia; 41.274° N, 2.031° E), with arrows indicating their fall direction, **b** zoom from the marked area in **a** with a dotted rectangle, **c** damaged factory roof in Sant Boi de Llobregat (Catalonia; 41.321° N, 2.038° E) by the EF2 7 September 2005 el Prat de Llobregat–Sant Boi de Llobregat tornado and the EF1 13 September 2006 Gavà–Sant Feliu de Llobregat tornado and **d** damaged beach restaurant roof in Montgat (Catalonia; 41.466° N, 2.281° E) by the EF0 20 October 2019 tornado (disturbances marked by discontinuous circles). Orthophotographs from the Cartographic and Geologic Institute of Catalonia (ICGC)

sources of orthophotographs, radar and Automatic Weather Station (AWS) data and the procedure to analyse wind damage by its use are introduced. Next, Sect. 4 reanalyses the 2 November 2008 strong-damaging convective-wind event in Camp de Tarragona and results are compared with previous studies. Finally, discussion and conclusions are presented in Sect. 5, summarizing results and providing recommendations for future work.

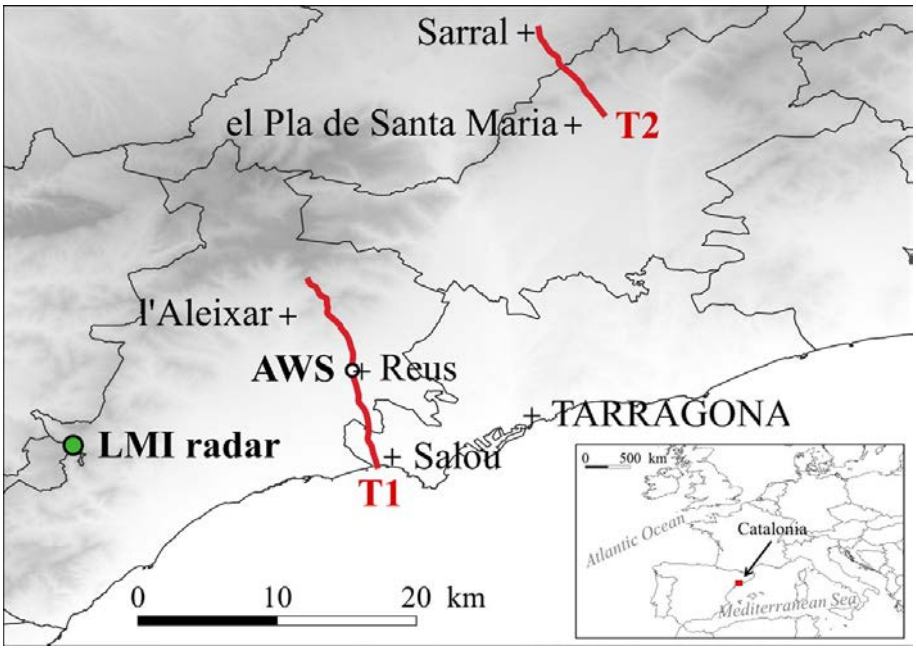

Fig. 2 South-western Europe (insert) showing the region of study marked with a red square. Zoomed map of the region of study shows locations of LMI radar (green circle), AWS (white circle), damage tracks (T1 and T2, red lines) and towns cited in the text

2 Region of study and overview of the event

Camp de Tarragona is a littoral flat area about 2700 km^2 located in southern Catalonia (north-east of the Iberian Peninsula), delimited by the pre-littoral mountain range in the north and west, with peaks between 700 and 1200 m (Fig. 2). It is also a high-densely populated region, consisting of the second most inhabited metropolitan area of Catalonia and smaller villages in the mountainous zone, with 515,000 inhabitants on 2018 (IDES-CAT 2020). The population increases even more during summer in coastal touristic towns, and also due to the high density of holiday resorts, making the region more vulnerable to natural hazards.

The region of study presents the highest lightning activity of the Catalan coast (del Moral et al. 2020). Moreover, according to Gayà (2018) and Rodríguez and Bech (2018), this is one of the most prone regions of the Iberian Peninsula to tornadoes. Since 1900 until 2019, almost 38 tornadoes (5 of them rated as significant, i.e. EF2 or stronger) and 64 waterspouts have been observed there. Nevertheless, a vast majority of those events (23 tornadoes and 54 waterspouts) have been reported between 2000 and 2019, an increase in reports favoured by the emergence of internet and social networks (Hyvärinen and Saltikoff 2010). Thus, according to data from the last 20 years, the yearly tornado density in Camp de Tarragona is 4.3 tornadoes year^{-1} 10,000 km^{-2}, comparable to Kansas, Mississippi or Alabama States in the USA (NCDC 2020).

The severe weather event revisited in this paper occurred during 2 November 2008 early morning and was characterized at synoptic scale by an upper level trough over SW Europe and the intensification of a surface low-pressure centre over the eastern Iberian coast, as described in detail in Bech et al. (2011) and Trapero et al. (2013). Organized convection produced local flash floods due to precipitation amounts exceeding 20 to 40 mm in 30 min, and locally even more than 100 mm in 24 h. Strong wind gusts (>20 m s^{-1}) produced some

minor-sparse damage in several locations from central and south Catalonia, and also two delimited swaths of severe damage were observed in Camp de Tarragona (Fig. 8 from Bech et al. 2011).

3 Data and methodology

3.1 Sources of data

To analyse the effects of the 2 November 2008 convective-damaging wind event in Camp de Tarragona area, open access orthophotographs from the Cartographic and Geologic Institute of Catalonia (ICGC) have been used. These RGB images cover all the country with a spatial resolution of 25 to 50 cm and are updated yearly since 2011. The high spatial resolution allows to distinguish in detail human-made structures and forest areas, discriminating individual trees or vegetation elements. Prior to this, orthophotographs covered partially the territory and updates were discontinuous. They are available at the internet site: https://www.icgc.cat/en/Public-Administration-and-Enterprises/Downloads/Aerial-photos-and-orthophotos/Conventional-orthophoto.

Radar data have also been analysed to perform this study, using observations from the Radar Network (XRAD) from the Meteorological Service of Catalonia (SMC). XRAD radar systems provide a complete scan every 6 min—see Altube et al. (2015) for further details. In this case, Tivissa-Llaberia radar (LMI) data (41.092° N, 0.863° E) have been used, being the closest radar to the affected areas. Damage paths are relatively close to the radar (between 20 and 50 km away), and more importantly, they are not affected by beam blockage obstructing the coverage (Fig. 2), a common problem in other parts of XRAD.

No official AWS was located near the two damage paths. However, a non-official AWS from a Meteorological spotter was situated in the centre of the first damage swath (at 41.156° N, 1.101° E), in the north-west of the Reus urban nucleus, and registered the event. Therefore, and taking into account its limitations, surface wind and atmospheric pressure observations from this AWS have been also analysed in this article. The station, a Davis Vantage Pro2 (see Table 1 for wind measurement specifications, Davis 2020), measured temperature, dew point, humidity, wind speed, wind gust, wind direction, atmospheric pressure and precipitation. The data were saved with 1-min temporal resolution for all the variables unless for atmospheric pressure, which was saved every 15 min. This AWS is part of the Meteoclimatic network (Gutierrez-Corea et al. 2013), where is labelled as a high-quality station (i.e. for the anemometer and wind vane, located at the top of the building, at least at 1.5 m above the ground, without obstacles—trees, other buildings—in the horizontal plane).

Table 1 Update interval, range and accuracy of anemometer and wind vane Davis Vantage Pro 2

	Anemometer	Wind vane
Update interval	2.5–3.0 s	2.5–3.0 s
Range	0–89 m s^{-1}	1°–360°
Accuracy	±0.9 m s^{-1} or ±5% (whatever is greater)	±3°

3.2 Procedure

When a damaging wind event of convective origin is reported, the first step consists in gathering as much information as possible about the affected area (i.e. damaged human-made structure or forest locations), preferably performing an in situ damage survey (Rodríguez et al. 2020). Together with the data provided by meteorological spotters and local media, then it is possible to start the search of damage swaths in orthophotographs in a delimitated area. This initial task is relatively straightforward but it is essential to locate damaged areas consistent with previous information to proceed with the study.

The comparison of orthophotographs or high-resolution satellite images taken before and after the strong wind event is especially useful to find damage in forest areas, and also in human-made structures (Fig. 1). Major damage is easily perceived, whereas damage caused by the weakest events (mainly EF0) may not be detected at all.

After the damage swath is found, the next step consists in its analysis. First, it is necessary to determine if damage was caused by a tornado or a downburst, in case of being unknown. The near surface wind field associated with the event can usually be estimated by the trees damage pattern (Holland et al. 2006). If there exists a convergence or rotation pattern in the falling direction of trees, damage is likely a vortex in translational movement (i.e. tornado), whereas if the pattern of fallen trees is divergent, the origin of damage is likely a downburst (Fujita 1981; Bech et al. 2009; Beck and Dotzek 2010).

Damage path length and maximum and mean damage path width are usually measured to characterize an event. Moreover, wind speed is also evaluated throughout an analysis of the damage detected in the affected area. This task, which is frequently performed with surface observations, can be also carried out using high-resolution aerial imagery. Calculating the ratio of damaged trees in 100 m × 100 m areas (Godfrey and Peterson 2017) the wind intensity can be estimated approximately using the EF-scale (WSEC 2006). Moreover, Brooks (2004) related tornado damage swath length and width with the tornado intensity (here, using the F-scale; Fujita 1981) following a Weibull distribution, which is described by:

$$f(x) = \left(\frac{\alpha}{\beta}\right)\left(\frac{x}{\beta}\right)^{\alpha-1} \exp\left[-\left(\frac{x}{\beta}\right)^{\alpha}\right] \tag{1}$$

where α and β are two parameters that define the distribution, whose values for each intensity level for the USA are given in the above-mentioned article. According to Shikhov and Chernokulsky (2018), considering the damage path length and width as independent variables, it is possible to calculate the probability of exceeding an intensity level given these two measurements of a tornado track (see "Appendix"). Note that each of these two methods use different rating scales (F-scale and EF-scale) to estimate tornado intensity. Although EF-scale is the most widespread used at present (Doswell et al. 2009), we have kept the use of F-scale when performing the Weibull distribution analysis to maintain the consistency with Brooks (2004).

Radar data can be used to identify the convective cell or parent storm associated with the wind damage, and also to determine the approximate timing of the event and the velocity of translational movement. As explained in Wilson et al. (1980), in a Doppler velocity radar data analysis, it may be possible to identify signatures related to rotation, as a velocity couplet, or a divergence pattern, which is typically related to downbursts. This information may be complemented with orthophotographs damage analysis to check if all damage-related elements are consistent.

In case of available AWS surface data from the damaged area, they must be analysed to compare maximum wind gusts recorded with damage intensity, which may complement the previous high-resolution aerial images and radar study. Moreover, if the temporal resolution of AWS data is 1 min or lesser, it might be possible to discriminate between the passage of a tornado or another type of strong-convective wind by analysing the evolution of wind speed and direction to confirm previous findings.

4 The 2 November 2008 Camp de Tarragona tornadic event

4.1 Orthophotographs analysis

The 2 November 2008 severe weather event reported in Camp de Tarragona was previously studied in Bech et al. (2011) and Pineda et al. (2011). A fieldwork to analyse strong-convective wind damage was carried out in Salou (41.075° N, 1.122° E) and in Miralcamp residential area, in Cabra del Camp municipality (41.391° N, 1.303° E). Using also remote-sensing tools and analysing the synoptic situation, the study concluded that two areas were severely damaged due to strong-convective wind (marked in their Fig. 8). In the case of Cabra del Camp, damage was attributed to an F2 tornado.

4.1.1 Damage swaths identification

Comparing orthophotographs recorded before and after the event, it has been found two narrow damaged areas, longer than expected according to previous studies. The first one (T1 in Fig. 2) extended through the municipalities of Salou, Vila-seca, Reus, Castellvell del Camp, Almoster and l'Aleixar; the second, between el Pla de Santa Maria, Cabra del Camp, Barberà de la Conca and Sarral.

The information provided by local media during the following days after the episode has been very useful to geolocate points of damage in towns such as Salou and Reus, which were directly affected by the first event. Orthophotographs show the absence of existing trees before the event, and other changes such as roof replacements in several farms; all these recognized differences could be attributed to wind damage.

In the mountainous area situated between Castellvell del Camp and l'Aleixar municipalities, a large number of pines were uprooted or snapped (see Fig. 3a, b; 41.205° N, 1.080° E). Fallen trees followed a convergence and rotation pattern, which is compatible with the passage of a strong wind vortex (Fujita 1981; Bech et al. 2009; Beck and Dotzek 2010). Therefore, it is highly probable that damage was caused by a tornado.

The second damaged area (T2 in Fig. 2) was located in a complex terrain forest zone. The fallen trees direction in Miralcamp residential area showed a convergence and rotation pattern, as discussed in Bech et al. (2011). Nevertheless, more damage has been detected to the north supported by additional orthophotographs analysis. Over that area a large extension of pine forest severely damaged has been examined in detail.

Figure 4a, b (41.422° N, 1.276° E) shows a major continuous damage path of 300 to 400 m width, which is delimited with a white discontinuous line. Moreover, minor-sparsely damage areas are also localized around the main damaged area, exceeding 500 m width in total. Therefore, the size of the damage track is greater than the value initially determined.

Independently, some scattered minor damage, mainly on trees, has been also found over all the analysed area due to strong winds that affected the Camp de Tarragona and

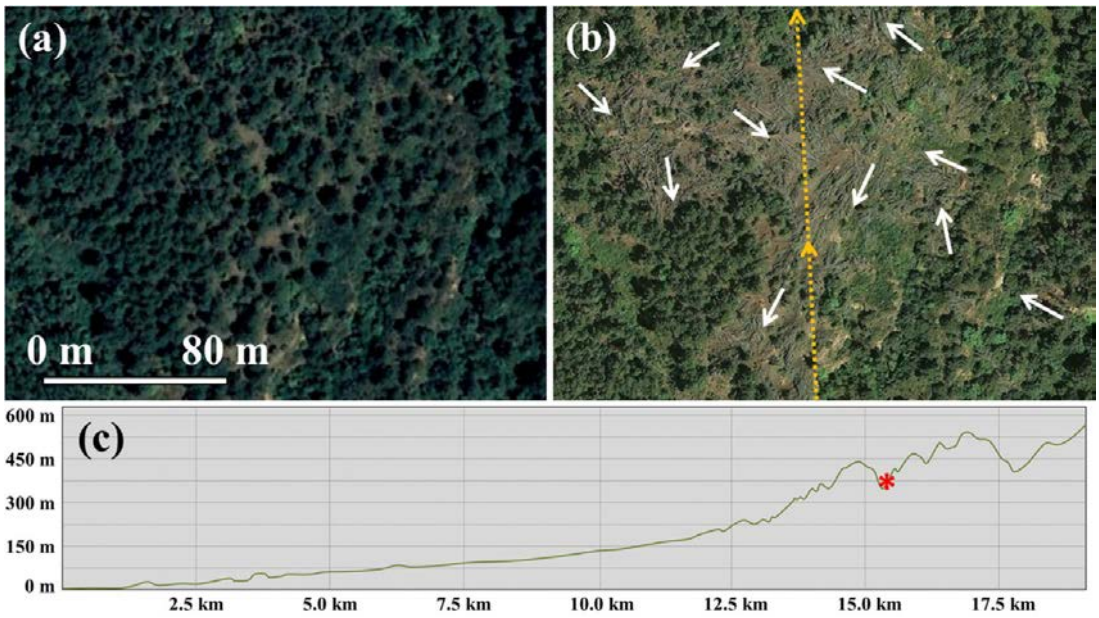

Fig. 3 Pine forest damaged in Salou–l'Aleixar tornado **a** before the event orthophotograph and **b** after the event orthophotograph, where arrows indicate the main fallen trees directions and dotted line with arrows indicates the vortex centre movement. **c** Altitudinal evolution of the tornado track, where the location of the analysed area in panels **a** and **b** is indicated with a red asterisk

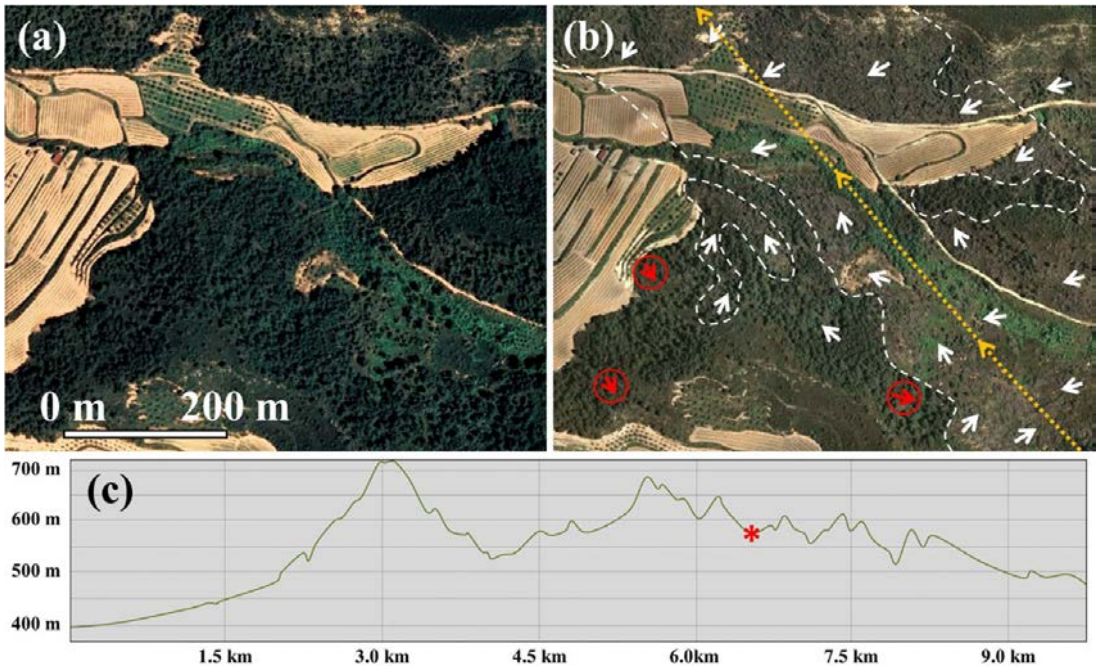

Fig. 4 Pine forest damaged in el Pla de Santa Maria–Sarral tornado **a** before the event orthophotograph and **b** after the event orthophotograph, where arrows indicate the main fallen trees directions, dashed lines delimitate the major damaged area and dotted line with arrows indicates the vortex centre movement. Fallen trees by Klaus winter storm are also indicated with circled arrows. **c** Altitudinal evolution of the tornado track, where the location of the analysed area in panels **a** and **b** is indicated with a red asterisk

pre-littoral mountain range during the early morning of 2 November 2008. The AWS network of the SMC registered peaks of 15 to 20 m s^{-1} in several locations, and maximum wind gusts of 20 to 30 m s^{-1} in elevated areas (above 500 m above sea level, ASL).

As analysed posterior-tornadoes orthophotographs were recorded some months later than the event, it has been detected the overlap of another strong wind episode. Some of the observed damage in forest areas was caused very likely by the Klaus storm, which affected the north of Iberia and southern France on 23 and 24 January 2009 causing strong synoptic north-westerly winds (Liberato et al. 2011; Bertotti et al. 2012). Nevertheless, as the predominant wind direction was the opposite in both events, it has been relatively easy to discriminate the origin of most of forest damage, due to differences on falling trees direction (see red circled arrows in Fig. 4b).

4.1.2 Tornadoes intensity estimation

In Bech et al. (2011), several images from the damage observed in both analysed areas are shown. In Salou, strong winds blew down trees, broke windows, damaged roofs and pulled out railing balconies. In Miralcamp residential area, a large number of trees were uprooted or snapped, mobile homes were damaged, and even four metal truss towers from a high-voltage power line located at the top of a mountain range collapsed. According to that, previous estimates of the wind intensity using the F-scale, concluded that damage observed in Salou and Miralcamp was compatible with F1 and F2 winds, respectively (Table 2).

The EF-scale (Doswell et al. 2009) provides a larger number and more detailed damage descriptors than the original F-scale (28 damage indicators with 3 to 12 degrees of damage, WSEC 2006), although its limitations on applying it out of the USA (e.g. Feuerstein et al. 2011; Rodríguez et al. 2020). An updated EF-scale damage assessment performed by reanalysing images from media and Bech et al. (2011) data strongly suggests that Salou–l'Aleixar and el Pla de Santa Maria–Sarral tornadoes can be rated as EF1 and EF3, respectively. This intensity increase is supported by the identification of degree of damage 3 from softwood trees (TS) damage indicator in the first tornado damage path, and degree of damage 6 from electrical transmission line (ETL) damage indicator in the second one—see details of damage indicators in WSEC (2006). Note that for the first tornado there was not any in situ field survey nor images from the most damaged area according to orthophotographs analysis, located between Reus and l'Aleixar. That probably caused an underestimation on intensity rating.

Moreover, as stated in Sect. 3.2, it is possible to assess wind-damage intensity throughout orthophotographs analysis. Godfrey and Peterson (2017) related the ratio of blown down trees in 100 m × 100 m forest areas with the intensity of tornado using the EF-scale. In the Salou–l'Aleixar event, only the last part of the track was throughout a pine forest

Table 2 Intensity rating for each event according to Bech et al. (2011), to the EF-scale reanalysis using media and Bech et al. (2011) damage images, and using Godfrey and Peterson (2017), and Brooks (2004) and Shikhov and Chernokulsky (2018) approaches

Event	Bech et al. (2011)	EF-scale reanalysis	Godfrey and Peterson (2017)	Brooks (2004) and Shikhov and Chernokulsky (2018)
Salou–l'Aleixar	F1	EF1	EF1/EF2	F3 ($p > 0.9$)
el Pla de Santa Maria–Sarral	F2	EF3	EF2/EF3	F3 ($p > 0.9$)

area. There, some sectors with 50 to 70% of damage have been observed during the orthophotographs analysis, which is compatible to EF1 to EF2 categories (Fig. 3b). However, in el Pla de Santa Maria–Sarral event forest damage was more substantial than in the first one. There were areas with 60 to 80% of pines blown down or snapped, a proportion of damage which is related to EF2 to EF3 categories (Fig. 4b, Table 2).

On the other hand, in Brooks (2004) and Shikhov and Chernokulsky (2018), it is proposed another method to estimate the tornado intensity (here, with F-scale) using the length and width of the damage swath. Although tornadic events analysed in the present article occurred in complex terrain area (Figs. 3c and 4c) and the orography could have influenced on the nonlinearity of the last part of the Salou–l'Aleixar tornado track and also on the variability of both damage paths width (Cannon et al. 2016), damage swath length and width could be estimated. Thus, Salou–l'Aleixar tornado damage was concentrated in an area 18.9 km long and 470 m (maximum) wide, whereas el Pla de Santa Maria–Sarral tornado was in a 9.8 km per 675 m area (see Table 3 for further details). Thereby, the probability of reaching F3 intensity was 93% for T1 and 95% for T2 (see Fig. 5), according to Weibull parameters determined by Brooks (2004) for the USA (Table 2).

In accordance with the above discussion, the first tornado would be rated as EF2, and the second one as EF3, both being stronger than what was concluded in previous studies. It is remarkable that only around 6% of tornadoes in Catalonia are significant (i.e. EF2 or stronger; Rodríguez and Bech 2018), and no EF3 had ever been registered in the region (Gayà 2018). Due to the intensity of the event, and the fact that some important towns such as Salou and Reus were affected, 4 people were directly injured by tornadoes and economic losses reached 5.8 M€ according to CCS, the reinsurance public company of Spain.

4.2 Radar and AWS data analysis

To further confirm the results of the orthophotographs study, in this section, radar and AWS data are briefly analysed. Figure 6 shows Doppler radial velocity radar Plan Position Indicator (PPI) images from the Meteorological Service of Catalonia (SMC) LMI weather radar, and the two tornado tracks described above overlaid. It can be noticed the presence of a velocity couplet in Salou area at 0300 UTC (Fig. 6a) that was moving to the north (Fig. 6b) crossing Reus between 0312 and 0318 UTC (Fig. 6c, d) and reaching l'Aleixar area at 0330 UTC (Fig. 6f), coinciding with the first damage swath. Another velocity couplet was observed east of Tarragona at 0300 UTC (Fig. 6a), also moving to the north (Fig. 6b–e). At 0330 UTC was located close to el Pla de Santa Maria (Fig. 6f), the starting point of the second damage path, which is consistent with the analysis performed in Bech et al. (2011). In both cases, the velocity couplets indicate cyclonic rotation.

It is remarkable that velocity values in both circulations were significant, which is related to strong rotation. Doppler radial wind speed of the lowest PPI radar scan was over 20 m s^{-1}, with local maximums reaching 35 m s^{-1}. PPI heights over the damage areas were 1.1 km ASL over Salou–l'Aleixar and 1.5 km ASL over Pla de Santa Maria–Sarral. Therefore, it can be concluded that the two convective cells had associated a mesocyclone (i.e. exhibited supercell characteristics) as detailed in Bech et al. (2011), and damage was related to the passage of both cyclonic circulations. It should be noted that this analysis is possible because of two reasons. Firstly, the two damaged areas are relatively close to the radar (about 20 and 50 km, respectively), so the storm rotation can be well resolved. Secondly, the radar beam blockage in the area of interest is not relevant, unlike other parts of Catalonia as discussed in Bech et al. (2003) or Trapero et al. (2009).

Table 3 Tornado touchdown and dissipation time, maximum intensity, track length, damage path maximum and mean width and damage losses (data from CCS) for Salou–l'Aleixar and el Pla de Santa Maria–Sarral tornadoes

Tornado	Touchdown time (UTC)	Dissipation time (UTC)	Maximum intensity (EF)	Track length (km)	Damage swath maximum width (m)	Damage swath mean width (m)	Damage losses (M€)
Salou–l'Aleixar	0259	0327	2	18.9	470	240	4.82
el Pla de Santa Maria–Sarral	0332	0341	3	9.8	675	330	1.00

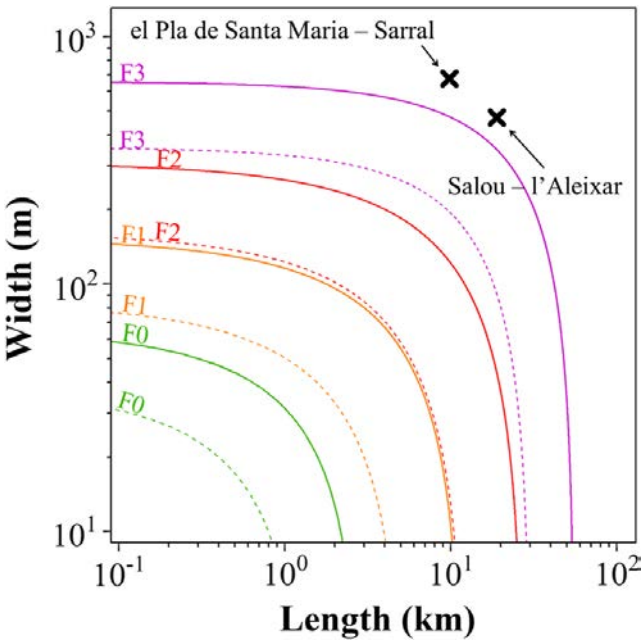

Fig. 5 Probability that, given the length and maximum width of a tornado damage path, its maximum intensity exceeds a given F-scale intensity (F0 in green, F1 in orange, F2 in red and F3 in violet). Dashed and continuous lines indicate probability levels of 70% and 90%, respectively. The case studies are marked with a cross; figure based on Shikhov and Chernokulsky (2018)

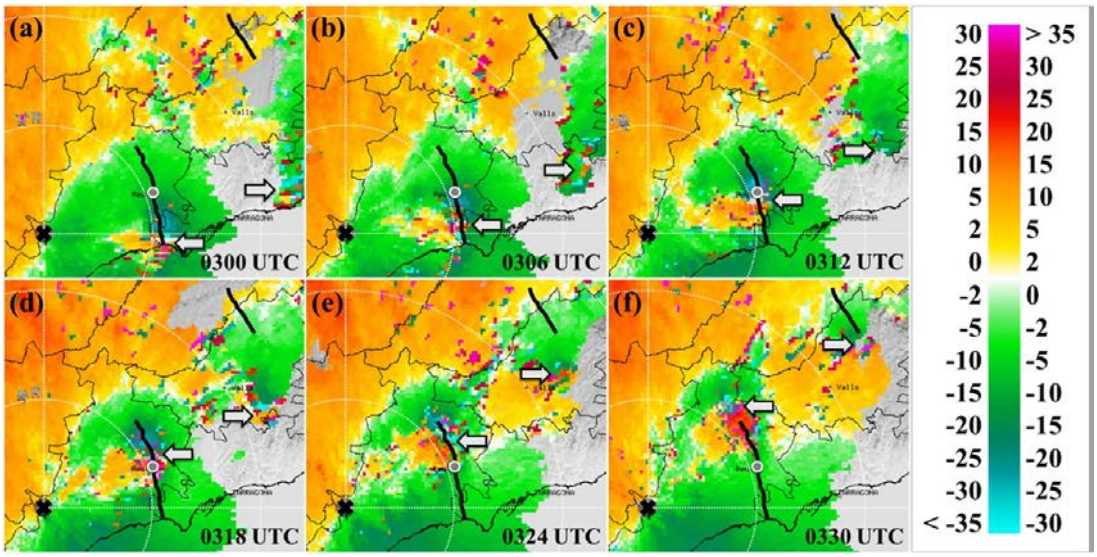

Fig. 6 0.6° PPI scans showing Doppler radial velocity (m s^{-1}) from LMI C-band weather radar (SMC) from **a** 0300 UTC, **b** 0306 UTC, **c** 0312 UTC, **d** 0318 UTC, **e** 0324 UTC and **f** 0330 UTC. The radar location is marked with a cross, Reus – Doctor Vilaseca Avenue AWS location is marked with a grey dot, tornado tracks are shown as black-thick lines, velocity couplets locations are indicated with arrows, and distance rings are plotted at 20 km interval as white-dotted circles

Combining the information from radar images and the location of damaged points, it is also possible to estimate the approximate touch down and dissipation tornado timing, and its translational velocity. The storm that affected the Salou–l'Aleixar area formed over the Mediterranean Sea and arrived at Salou at 0259 UTC. The tornado was on land until 0328 UTC, almost 28 min duration. The other tornado touched down at 0332 UTC and lasted 9 min, until it dissipated close to Sarral at 0341 UTC. Moreover, according to these timings and also to damage tracks, translational velocity for both supercells during the tornado life

cycle can be estimated. Thus, the Salou–l'Aleixar tornado parent storm moved at 11 m s^{-1}, whereas the el Pla de Santa Maria–Sarral moved at 17 m s^{-1}.

A non-official AWS located in the centre on width of the damage path of the Salou–l'Aleixar tornado, in the north-western urban nucleus of Reus, registered a sudden wind increase at 0315 UTC (see Table 4), at the same time that the velocity couplet detected by the radar passed over the area (Fig. 6c, d). Moreover, the maximum wind gust of 31.3 m s^{-1} coincided with a wind shift from NE to SW. This is compatible with the passage of a vortex in translational movement (Wurman et al. 2013; Fox-Hughes et al. 2018), discarding the possibility of a downburst (Lin et al. 2007), which is coherent with the findings of the orthophotographs analysis. Furthermore, the maximum wind gust registered by the AWS is also compatible with reported damage in the area, where tree branches were broken, some trees were uprooted and weak damage in asbestos or tiles roofs was observed (not shown).

As stated in Sect. 3.1, atmospheric pressure data were registered with 15-min resolution being the records closest to the strongest winds 997.8 hPa (0300 UTC), 992.9 hPa (0315 UTC) and 996.8 hPa (0330 UTC). The passage of the tornado over the AWS is estimated around 0315 UTC according to wind speed and Doppler radar data, but the exact time is unknown, so 0315 UTC atmospheric pressure may not be the minimum value associated to the tornado centre. Should higher temporal resolution wind and atmospheric pressure data were available, maximum tornado wind speed could be estimated by making simple assumptions such as cyclostrophic flow balance conditions and a Rankine or Burgers vortex model (e.g. Lorenz 2016; Franzese et al. 2020).

5 Discussion and conclusions

Remote-sensing tools are an essential source of information about strong-convective wind events damage paths. Comparing orthophotographs of the affected area before and after an event may reveal damage on human-made structures and also on forest areas, complementing in situ fieldwork surveys. That gives an overview of all the damage track, even from difficult access areas where local damage assessments may not be carried out. High-resolution images make possible the identification of uprooted trees and the estimation of their direction of fall, yielding information that may be used to discriminate if damage was caused by a tornado or a downburst. The length and width of damage swath and the ratio of blown down trees in forest areas, which are typically related to the tornado intensity, can be also determined.

Table 4 Reus – Doctor Vilaseca Avenue AWS minute maximum wind speed and direction data between 0312 and 0318 UTC

Time (UTC)	Max. wind gust (m s^{-1})	Max. wind gust direction (deg.)
0312	10.3	123
0313	11.6	63
0314	11.2	85
0315	31.3	39
0316	31.3	220
0317	17.0	278
0318	19.7	214

Nevertheless, this approach also presents some limitations. For example, as the periodicity of ICGC orthophotographs is one year, damage caused by several strong-wind events may overlap in the same image, as shown in Sect. 4.1.1. That can hamper significantly the analysis. However, in some occasions, the predominant wind flows from each event are from different directions, which can help to discriminate the damage origin. On the other hand, damage caused by very weak events (i.e. mainly EF0 causing only broken branches, tiles removal or sparsely uprooted trees) is unobservable throughout this kind of analysis, thus illustrating the necessity of in situ damage surveys specially to assess minor damage and degraded state or previous weakness of damaged elements (Gayà 2018; Rodríguez et al. 2020). Moreover, in events that do not generate broad blown down trees areas, it may not be feasible to find wind damage patterns clear enough to discriminate the damage origin (i.e. tornado or downburst).

As an example, the 2 November 2008 severe weather event occurred in Camp de Tarragona region (Catalonia) has been reanalysed using orthophotographs. Forest damage has shown a convergent and rotation fallen tree pattern in both Salou–l'Aleixar and el Pla de Santa Maria–Sarral damage swaths, which is compatible with disturbances caused by a vortex in movement (i.e. tornado) confirming, in the second case, the results from the previous in situ damage survey carried out in a damaged residential area. Radar and AWS data have been also analysed to corroborate those findings.

The first damage swath started in Salou beach and extended 18.9 km to the NNW, affecting the municipalities of Reus, Castellvell del Camp and l'Aleixar with a maximum width of 470 m and 240 m average width. The starting point of the other track was located in el Pla de Santa Maria and extended north-westerly across Cabra del Camp, Barberà de la Conca and Sarral, being 9.8 km long, 330 m average width and 675 m maximum width.

A deep analysis of the ratio of uprooted or snapped trees in forest areas, and also taking into account the relation among the damage swath length and width and tornado strength, make possible to estimate tornado intensity. The Salou–l'Aleixar tornado has been rated as EF2 and the el Pla de Santa Maria–Sarral as EF3, being the strongest registered in Catalonia until 2019.

Combining orthophotographs information with radar data, it has been confirmed that both damage paths were related to the passage of mesocyclones. The first one moved onshore in Salou at 0259 UTC and arrived at l'Aleixar at 0327 UTC where no more wind damage was observed, with a translational velocity of 11 m s^{-1}. The second arrived at the damaged area in el Pla de Santa Maria at 0332 UTC and passed over Sarral at 0341 UTC, with a mean velocity of 17 m s^{-1}. Moreover, data from a non-official AWS located in Reus, in the track of the first tornado, confirmed a suddenly reinforce of the wind (maximum wind gust of 31.3 m s^{-1}) and wind shift, which is consistent with a tornado passage.

The case presented here illustrates well the potential added-value that aerial high-resolution orthophotographs can provide to complement in situ wind damage surveys. A more complete description of damages considering aerial orthophotographs will therefore improve severe weather database reports enhancing our understanding of hazards posed by severe thunderstorms and also will allow a better interpretation of both remote sensing data (e.g. Doppler weather radar observations, lightning signatures) and numerical weather prediction analysis of severe weather case studies.

Acknowledgements The authors thank Tomeu Rigo (Meteorological Service of Catalonia), who provided Doppler radar data, Miquel Soro (Cartographic and Geologic Institute of Catalonia) for helpful comments about ICGC orthophotographs, and Eduard Marimon, for Reus – Doctor Vilaseca Avenue Automatic Weather Station data. This research was performed under the framework of the HyMeX (HYdrological cycle in the Mediterranean EXperiment) programme and with partial funding from projects

CGL2015-65627-C3-2-R (MINECO/FEDER), CGL2016-81828-REDT (AEI) and RTI2018-098693-B643-C32 (AEI), and also from the Water Research Institute (IdRA) of the University of Barcelona.

Funding This study was funded by CGL2015-65627-C3-2-R (MINECO/FEDER), CGL2016-81828-REDT (AEI), RTI2018-098693-B643-C32 (AEI), Water Research Institute (IdRA) of the University of Barcelona.

Data availability The data used in this paper are available from the authors upon request.

Compliance with ethical standards

Conflict of interest The authors declare that they have no conflict of interest.

Appendix: Wind intensity versus damage path width and length

Given a Weibull distribution (Brooks 2004):

$$f(x) = \left(\frac{\alpha}{\beta}\right)\left(\frac{x}{\beta}\right)^{\alpha-1} \exp\left[-\left(\frac{x}{\beta}\right)^{\alpha}\right], \tag{2}$$

the cumulative distribution function is:

$$F(x) = 1 - \exp\left[-\left(\frac{x}{\beta}\right)^{\alpha}\right]. \tag{3}$$

Considering the damage path length and width as independent variables (Shikhov and Chernokulsky 2018):

$$P_{LW} = P_L + P_W - P_L P_W \tag{4}$$

where P_{LW} is the probability of exceeding an F-scale intensity given the length (L) and width (W) of the damage path, P_L is the probability of exceeding an F-scale intensity given the length (L) (i.e. cumulative distribution function for L, $F(x = L)$) and P_W is the probability of exceeding an F-scale intensity given the width (W) (i.e. cumulative distribution function for W, $F(x = W)$).

Replacing P_L by the cumulative distribution function for the length and P_W by the cumulative distribution function for the length in Eq. 4:

$$P_{LW} = 1 - \exp\left[-\left(\frac{L}{\beta_L}\right)^{\alpha_L}\right] + 1 - \exp\left[-\left(\frac{W}{\beta_W}\right)^{\alpha_W}\right] - \left\{1 - \exp\left[-\left(\frac{L}{\beta_L}\right)^{\alpha_L}\right]\right\}\left\{1 - \exp\left[-\left(\frac{W}{\beta_W}\right)^{\alpha_W}\right]\right\} \tag{5}$$

$$P_{LW} = 1 - \exp\left[-\left(\frac{L}{\beta_L}\right)^{\alpha_L} - \left(\frac{W}{\beta_W}\right)^{\alpha_W}\right] \tag{6}$$

and, arranging the equation to present it as function (W) depending on length (L), it is:

$$W(L) = \beta_W\left[-\left(\frac{L}{\beta_L}\right)^{\alpha_L} - \ln\left(1 - P_{LW}\right)\right]^{1/\alpha_W}. \tag{7}$$

Then, it is possible to make the plot presented in the manuscript (Fig. 5), using α_L, β_L (for length), and α_W, β_W (for width) from Brooks (2004) for each F-scale degree, and being $P_{LW} = 0.70$ for discontinuous lines and $P_{LW} = 0.90$ for continuous lines.

References

Altube P, Bech J, Argemí O, Rigo T (2015) Quality control of antenna alignment and receiver calibration using the sun: adaptation to midrange weather radar observations at low elevation angles. J Atmos Ocean Tech 32:927–942. https://doi.org/10.1175/JTECH-D-14-00116.1

Antonescu B, Schultz DM, Holzer A, Groenemeijer P (2017) Tornadoes in Europe: an underestimated threat. Bull Am Meteor Soc 98:713–728. https://doi.org/10.1175/BAMS-D-16-0171.1

Barrett BS, Marin JC, Jacques-Coper M (2020) A multiscale analysis of the tornadoes of 30–31 May 2019 in south-central Chile. Atmos Res 236:104811. https://doi.org/10.1016/j.atmosres.2019.104811

Bech J, Codina B, Lorente J, Bebbington D (2003) The sensitivity of single polarization weather radar beam blockage correction to variability in the vertical refractivity gradient. J Atmos Ocean Tech 20(6):845–855. https://doi.org/10.1175/1520-0426(2003)020<0845:TSOSPW>2.0.CO;2

Bech J, Pascual R, Rigo T, Pineda N, López JM, Arús J, Gayà M (2007) An observational study of the 7 September 2005 Barcelona tornado outbreak. Nat Hazard Earth Syst 7(1):129–139. https://doi.org/10.5194/nhess-7-129-2007

Bech J, Gayà M, Aran M, Figuerola F, Amaro J, Arús J (2009) Tornado damage analysis of a forest area using site survey observations, radar data and a simple analytical vortex model. Atmos Res 93(1–3):118–130. https://doi.org/10.1016/j.atmosres.2008.10.016

Bech J, Pineda N, Rigo T, Aran M, Amaro J, Gayà M, Arús J, Montanyà J, van der Velde O (2011) A Mediterranean nocturnal heavy rainfall and tornadic event. Part I: overview, damage survey and radar analysis. Atmos Res 100(4):621–637. https://doi.org/10.1016/j.atmosres.2010.12.024

Beck V, Dotzek N (2010) Reconstruction of near-surface tornado wind fields from forest damage. J Appl Meteorol Clim 49:1517–1537. https://doi.org/10.1175/2010JAMC2254.1

Bertotti L, Bidlot JR, Bunney C, Cavaleri L, Delli Passeri L, Gomez M, Lefèvre JM, Paccagnella T, Torrisi L, Valentini A, Vocino A (2012) Performance of different forecast systems in an exceptional storm in the Western Mediterranean Sea. Quart J R Meteor Soc 138:34–55. https://doi.org/10.1002/qj.892

Brooks HE (2004) On the relationship of tornado path length and width to intensity. Weather Forecast 19:310–319. https://doi.org/10.1175/1520-0434(2004)019<0310:OTROTP>2.0.CO;2

Bunting WF, Smith BE (1993) A guide for conducting damage surveys. NOAA Tech. Memo. NWS-SR-146, Scientific Services Division, Southern Region, Fort Worth, TX. https://repository.library.noaa.gov/view/noaa/7317/noaa_7317_DS1.pdf. Accessed 31 March 2020

Burow D, Herrero HV, Ellis KN (2020) Damage analysis of three long-track tornadoes using high-resolution satellite imagery. Atmosphere 11(6):613. https://doi.org/10.3390/atmos11060613

Cannon JB, Hepinstall-Cymerman J, Godfrey CM, Peterson CJ (2016) Landscape-scale characteristics of forest tornado damage in mountainous terrain. Landsc Ecol 31:2097–2114. https://doi.org/10.1007/s10980-016-0384-8

Chernokulsky A, Shikhov A (2018) 1984 Ivanovo tornado outbreak: determination of actual tornado tracks with satellite data. Atmos Res 207:111–121. https://doi.org/10.1016/j.atmosres.2018.02.011

Davis (2020) Wireless vantage Pro2™ & vantage Pro2™ plus stations. https://www.davisinstruments.com/product_documents/weather/spec_sheets/6152_62_53_63_SS.pdf. Accessed 1 July 2020

Doswell CA III, Brooks HE, Dotzek N (2009) On the implementation of the enhanced Fujita scale in the USA. Atmos Res 93(1–3):554–563. https://doi.org/10.1016/j.atmosres.2008.11.003

del Moral A, Llasat MC, Rigo T (2020) Connecting flash flood events with radar-derived convective storm characteristics on the northwestern Mediterranean coast: knowing the present for better future scenarios adaptation. Atmos Res 238:104863. https://doi.org/10.1016/j.atmosres.2020.104863

Ermert J, Koch B, Dees M, Zhao W, Hetzenecker M, Scharrer K, Amaro D (2013) Mapping of forest damages caused by a tornado 2012 in Gera, Germany using Terrasar-X change detection. https://pdfs.semanticscholar.org/db85/38cead0196153ead4c45e609a024a2c4dc62.pdf. Accessed 31 March 2020

European Severe Weather Database (ESWD) (2020) https://eswd.eu/. Accessed 20 March 2020

Feuerstein B, Groenemeijer P, Dirksen E, Hubrig M, Holzer AM, Dotzek N (2011) Towards an improved wind speed scale and damage description adapted for Central Europe. Atmos Res 100(4):547–564

Fox-Hughes P, Barnes-Keoghan I, Porter A (2018) Observations of a tornado at an Automatic Weather Station in northern Tasmania. J South Hemisph Earth Syst Sci 68:215–230. https://doi.org/10.22499/3.6801.012

Franzese G, Della Rocca V, Esposito F (2020) Resolution of the size/distance degeneracy of the dust devils signals observed with a stationary meteorological station. Aeolian Res 44:100594. https://doi.org/10.1016/j.aeolia.2020.100594

Fujita TT (1981) Tornadoes and downbursts in the context of generalized planetary scales. J Atmos Sci 38:1511–1534. https://doi.org/10.1175/1520-0469(1981)038<1511:TADITC>2.0.CO;2

Gayà M (2018) Els Fiblons a Espanya: Climatologia i catàleg de tornados i trombes (Whirlwinds in Spain: Climatology and Catalog of Tornadoes and Waterspouts). Second edition. Universitat de les Illes Balears. **(in Catalan)**

Godfrey CM, Peterson CJ (2017) Estimating enhanced Fujita scale levels based on forest damage severity. Weather Forecast 32:243–252. https://doi.org/10.1175/WAF-D-16-0104.1

Gutierrez-Corea FV, Manso-Callejo MA, Vázquez-Hoehne A (2013) Assessment of the availability of near-real time open weather data provided by networks of surface stations in Spain. Earth Sci Inform 6:145–163. https://doi.org/10.1007/s12145-013-0120-8

Holland AP, Riordan AJ, Franklin EC (2006) A simple model for simulating tornado damage in forests. J Appl Meteorol Clim 45:1597–1611. https://doi.org/10.1175/JAM2413.1

Hyvärinen O, Saltikoff E (2010) Social media as a source of meteorological observations. Mon Weather Rev 138:3175–3184. https://doi.org/10.1175/2010MWR3270.1

Institut d'Estadística de Catalunya (IDESCAT) (2020) Official statistics of Catalonia. https://www.idescat.cat/?lang=en. Accessed 20 March 2020

Karstens CD, Samaras TM, Gallus WA, Finley CA, Lee BD (2010) Analysis of near-surface wind flow in close proximity to tornadoes. Preprints, In: 25th conference on severe local storms, Denver, CO, American Meteorological Society, P10.12. https://ams.confex.com/ams/pdfpapers/176188.pdf. Accessed 20 March 2020

Lee BD, Finley CA, Karstens CD, Samaras TM (2010) Surface observations of the rear-flank downdraft evolution associated with the Aurora, NE tornado of 17 June 2009. Preprints, In: 25th conference on severe local storms, Denver, CO, American Meteorological Society, P10.12. https://ams.confex.com/ams/pdfpapers/176133.pdf. Accessed 20 March 2020

León-Cruz JF, Carbajal N, Pineda-Martínez LF (2019) The role of complex terrain in the generation of tornadoes in the west of Mexico. Nat Hazards 97(1):335–353. https://doi.org/10.1007/s11069-019-03647-8

Liberato MLR, Pinto JG, Trigo IF, Trigo RM (2011) Klaus—an exceptional winter storm over northern Iberia and southern France. Weather 66(12):330–334. https://doi.org/10.1002/wea.755

Lin WE, Orf LG, Savory E, Novacco C (2007) Proposed large-scale modelling of the transient features of a downburst outflow. Wind Struct 10(4):315–346. https://doi.org/10.12989/was.2007.10.4.315

Lorenz RD (2016) Heuristic estimation of dust devil vortex parameters and trajectories from single-station meteorological observations: application to InSight at Mars. Icarus 271:326–337. https://doi.org/10.1016/j.icarus.2016.02.001

Mateo J, Ballart D, Brucet C, Aran M, Bech J (2009) A study of a heavy rainfall event and a tornado outbreak during the passage of a squall line over Catalonia. Atmos Res 93(1–3):131–146. https://doi.org/10.1016/j.atmosres.2008.09.030

Molthan A, Jedlovec G, Carcione B (2011) NASA satellite data assist in tornado damage assessments. Eos 92(40):337–339. https://doi.org/10.1029/2011EO400002

Molthan AL, Bell JR, Cole TA, Burks JE (2014) Satellite-based identification of tornado damage tracks from the 27 April 2011 severe weather outbreak. J Oper Meteor 2(16):191–208. https://doi.org/10.15191/nwajom.2014.0216

Mulholland JP, Nesbitt SW, Trapp RJ (2019) A case study of terrain influences on upscale convective growth of a supercell. Mon Weather Rev 147(12):4305–4324. https://doi.org/10.1175/MWR-D-19-0099.1

National Climatic Data Center (NCDC) (2020) U.S. Tornado Climatology. https://www.ncdc.noaa.gov/climate-information/extreme-events/us-tornado-climatology. Accessed 20 March 2020

National Weather Service (NWS) (2020) Weather related fatality and injury statistics. https://www.weather.gov/hazstat. Accessed 20 March 2020

Orlanski I (1975) A rational subdivision of scales for atmospheric processes. Bull Am Meteorol Soc 56(5):527–530

Pineda N, Bech J, Rigo T, Montanyà J (2011) A Mediterranean nocturnal heavy rainfall and tornadic event. Part II: total lightning analysis. Atmos Res 100(4):638–648. https://doi.org/10.1016/j.atmosres.2010.10.027

Potvin CK, Broyles C, Skinner PS, Brooks HE, Rasmussen E (2019) A Bayesian hierarchical modeling framework for correcting reporting bias in the U.S. Tornado Database Weather Forecast 34:15–30. https://doi.org/10.1175/WAF-D-18-0137.1

Rodríguez O, Bech J (2018) Sounding-derived parameters associated with tornadic storms in Catalonia. Int J Climatol 38:2400–2414. https://doi.org/10.1002/joc.5343

Rodríguez O, Bech J, Soriano JD, Gutiérrez D, Castán S (2020) A methodology to conduct wind damage field surveys for high-impact weather events of convective origin. Nat Hazards Earth Syst Sci 20(5):1513–1531. https://doi.org/10.5194/nhess-20-1513-2020

Shikhov A, Chernokulsky A (2018) A satellite-derived climatology of unreported tornadoes in forested regions of northeast Europe. Remote Sens Environ 204:553–567. https://doi.org/10.1016/j.rse.2017.10.002

Shikhov AN, Perminova ES, Perminov SI (2019) Satellite-based analysis of the spatial patterns of fire-and storm-related forest disturbances in the Ural region, Russia. Nat Hazards 97(1):283–308. https://doi.org/10.1007/s11069-019-03642-z

Storm Prediction Center (SPC) (2020) Prototype interactive local storm reports display. https://www.spc.noaa.gov/climo/reports/today.html. Accessed 20 March 2020

Trapero L, Bech J, Rigo T, Pineda N, Forcadell D (2009) Uncertainty of precipitation estimates in convective events by the Meteorological Service of Catalonia radar network. Atmos Res 93(1–3):408–418. https://doi.org/10.1016/j.atmosres.2009.01.021

Trapero L, Bech J, Lorente J (2013) Numerical modelling of heavy precipitation events over Eastern Pyrenees: analysis of orographic effects. Atmos Res 123:368–383. https://doi.org/10.1016/j.atmosres.2012.09.014

Wagner M, Doe RK, Johnson A, Chen Z, Das J, Cerveny RS (2019) Unpiloted aerial systems (UASs) application for tornado damage surveys: benefits and procedures. Bull Am Meteor Soc 100:2405–2409. https://doi.org/10.1175/BAMS-D-19-0124.1

Wilson J, Carbone R, Baynton H, Serafin R (1980) Operational application of meteorological doppler radar. Bull Am Meteorol Soc 61:1154–1168. https://doi.org/10.1175/1520-0477(1980)061<1154:OAOMDR>2.0.CO;2

Wind Science and Engineering Center (WSEC) (2006) A recommendation for an enhanced Fujita scale (EF-scale). https://www.spc.noaa.gov/faq/tornado/EFScale.pdf. Accessed 20 March 2020

Womble JA, Wood RL, Mohammadi ME (2018) Multi-scale remote sensing of tornado effects. Front Built Environ 4:66. https://doi.org/10.3389/fbuil.2018.00066

Wurman J, Kosiba K, Robinson P (2013) In situ, Doppler radar, and video observations of the interior structure of a tornado and the wind-damage relationship. Bull Am Meteorol Soc 94:835–846. https://doi.org/10.1175/BAMS-D-12-00114.1

Capítol 3

Base de dades de tornados i mànegues marines a Catalunya

3.1 Una visió general dels episodis de tornados i mànegues marines a Catalunya (2000-2019)

3.1.1 Resum de l'article

En aquest article es presenta una base de dades que conté 105 tornados i 329 trombes marines registrats a Catalunya entre els anys 2000 i 2019. La informació prové de diverses fonts, entre les quals destaquen els observadors meteorològics, els mitjans de comunicació, les publicacions ja existents (Gayà, 2018) i, sobretot durant la segona meitat del període d'estudi, les xarxes socials. Cadascun dels episodis incorporats a la base de dades ha passat per un procés de validació que consisteix a confirmar la presència de convecció mitjançant eines de teledetecció i a confirmar que els danys foren causats per un fibló i no per cap altre fenomen. A banda, s'utilitzen les tècniques descrites al Capítol 2 per a analitzar les traces de danys.

Amb les dades recollides es duu a terme una anàlisi de la distribució espacial i temporal dels tornados i les mànegues marines. A més, s'examinen els *outbreaks* (episodis de sis o més fiblons formats per un mateix sistema d'escala sinòptica) i els episodis múltiples (dos o més fiblons formats per una mateixa cèl·lula convectiva), es caracteritzen les traces de danys i s'estudia l'impacte socioeconòmic per tal d'aconseguir una descripció completa d'aquests tipus de fenòmens i de les seves conseqüències.

Els resultats que es deriven de l'anàlisi de la base de dades mostren que la mitjana anual de tornados i de mànegues marines a Catalunya és de 5,3 i de 16,5, respectivament, fet que dona lloc a una de les densitats de fiblons per unitat d'àrea més elevades de la conca mediterrània. La zona de la regió d'estudi més afectada per aquests fenòmens correspon al sector central del litoral i prelitoral, incloent-hi les àrees metropolitanes de Barcelona i de Tarragona. La majoria de tornados i de trombes marines tenen lloc entre els mesos d'agost i novembre, i la franja horària en la qual s'observen amb major freqüència és a la tarda. Al llarg del període d'estudi s'han detectat diversos *outbreaks*, essent el més destacable el dels dies 7 i 8 de setembre de 2005, amb un total de 21 vòrtexs (Bech et al., 2007). La majoria dels tornados són febles (d'intensitat EF0 o EF1) i la traça de danys associada sol ser inferior als 5 km de llargada i als 200 m d'amplada màxima. Tot i això, ocasionalment es produeixen episodis significatius (EF2+) amb traces que poden superar els 10 km de llarg i els 500 m d'ample. Independentment, fins a 26 persones han estat ferides de manera directa o indirecta per tornados, i s'estima que els fiblons han causat danys per valor de 30,8 M€ al llarg d'aquests 20 anys.

La llista de casos que conformen la base de dades (data, hora, latitud, longitud i intensitat màxima segons l'escala EF) s'adjunta com a Apèndix en aquest mateix treball. La intenció no

és altra que pugui ser utilitzada per a futurs estudis, tal com s'ha fet per a elaborar els articles que constitueixen el Capítol 4.

Aquest article dona resposta a l'objectiu general **OG1** i a l'objectiu específic **OE3**.

3.1.2 Article

Rodríguez O., Bech J., Arús J., Castán S., Figuerola F. i Rigo T. (2021): An overview of tornado and waterspout events in Catalonia (2000-2019). *Atmospheric Research*, **250**: 105415. doi:10.1016/j.atmosres.2020.105415.

Nota: per error de l'editorial de la revista, el primer paràgraf de la secció 1 (*Introduction*) apareix duplicat a la versió publicada de l'article. En aquest sentit, s'ha sol·licitat la correcció a l'editorial.

Atmospheric Research 250 (2021) 105415

Contents lists available at ScienceDirect

Atmospheric Research

journal homepage: www.elsevier.com/locate/atmosres

An overview of tornado and waterspout events in Catalonia (2000–2019)

Oriol Rodríguez [a,*], Joan Bech [a], Joan Arús [b], Salvador Castán [c], Francesc Figuerola [d], Tomeu Rigo [d]

[a] Department of Applied Physics – Meteorology, University of Barcelona, Barcelona, Catalonia, Spain
[b] DT Catalonia, Spanish Meteorological Agency, Barcelona, Catalonia, Spain
[c] Agencia Pericial, Cornellà de Llobregat, Catalonia, Spain
[d] Meteorological Service of Catalonia, Barcelona, Catalonia, Spain

ARTICLE INFO

Keywords:
Tornado
Waterspout
Severe weather
Climatology
Mediterranean
Europe

ABSTRACT

Tornado climatologies are essential to enhance our knowledge about their frequency and spatial distribution, together with their damage path characteristics. Due to their small spatiotemporal scale, tornado detection is strongly linked to visual observations. Therefore, social networks have become one of the most important sources of severe weather reports during the present century, including tornadoes, improving their detection and increasing the number of observed cases compared to previous decades. This article presents an analysis of tornado and waterspout events reported between 2000 and 2019 in Catalonia (NE Iberian Peninsula), one of the southern European regions where these phenomena are most frequent. The study includes 105 tornadoes and 329 waterspouts reported in a 32,000 km^2 area, and therefore, it presents one of the highest tornado and waterspout densities in the Mediterranean basin according to recent climatologies. Remote-sensing tools such as weather radar, lightning detection and satellite imagery have been used to validate each event. Moreover, fieldwork performed after several tornado cases and the use of high-resolution aerial imagery have provided information to characterise damage paths, including the length and width of the damage swath and the maximum intensity according to the Enhanced Fujita Scale. Finally, a list of the analysed events is provided for further research.

1. Introduction

Tornadoes, which are the most intense wind phenomenon on Earth (AMS, 2020), occur mainly between 20° and 60° of latitude (Goliger and Milford, 1998). It is well known that central and eastern USA present favourable conditions for tornadic storms (Brooks et al., 2003; Taszarek et al., 2020), but in other parts of the world such as Europe they also occur frequently. Several significant events –i.e., F2/EF2 or stronger according to Fujita scale (Fujita (1981)) and Enhanced Fujita scale (WSEC (2006)) respectively– causing injuries and fatalities, have been reported across the continent throughout history (e.g., Gayà, 2007; Holzer et al., 2018), as well as tornado outbreaks such as the 24–25 June 1967 (Antonescu et al., 2020), 23 November 1981 (Apsley et al., 2016) or 9 June 1984 (Chernokulsky and Shikhov, 2018).

Tornadoes, which are the most intense wind phenomenon on Earth (AMS, 2020), occur mainly between 20° and 60° of latitude (Goliger and Milford, 1998). It is well known that central and eastern USA present favourable conditions for tornadic storms (Brooks et al., 2003; Taszarek et al., 2020), but in other parts of the world such as Europe they also occur frequently. Several significant events –i.e., F2/EF2 or stronger according to Fujita scale (Fujita (1981)) and Enhanced Fujita scale (WSEC (2006)) respectively– causing injuries and fatalities, have been reported across the continent throughout history (e.g., Gayà, 2007; Holzer et al., 2018), as well as tornado outbreaks such as the 24–25 June 1967 (Antonescu et al., 2020), 23 November 1981 (Apsley et al., 2016) or 9 June 1984 (Chernokulsky and Shikhov, 2018).

The first European tornado climatology was published during the second decade of the 20th centuranty by Wegener (1917), including 258 reports between 1456 and 1913 (Antonescu et al., 2019). Overtime, technological advances had contributed to the improvement of tornado detection, increasing the number of reports and making possible a better description of their temporal and spatial distribution. Recent climatologies show that in the Mediterranean basin there are some tornado density hotspots (Antonescu et al., 2017), probably related to local

* Corresponding author at: Department of Applied Physics – Meteorology, Faculty of Physics, University of Barcelona, Martí i Franquès, 1, 08028 Barcelona, Catalonia, Spain.
E-mail address: orodriguez@meteo.ub.edu (O. Rodríguez).

https://doi.org/10.1016/j.atmosres.2020.105415
Received 24 August 2020; Received in revised form 5 November 2020; Accepted 5 December 2020
Available online 9 December 2020

complex topography enhancing mesoscale favourable conditions, as reported in several case studies (e.g., Homar et al., 2003; Matsangouras et al., 2014a, 2016; Miglietta and Rotunno, 2016). In Antonescu et al. (2017), Gayà (2018) and Grieser and Haines (2020) it is shown that the maximum tornado frequency in the western Mediterranean is located between Catalonia and Balearic Islands.

Gayà et al. (2011) provided the first analysis of tornado and waterspout occurrence in Catalonia, covering the 1950–2009 period. They identified the central part of the littoral as the area where tornado frequency is maximum. A similar pattern was found in Gayà (2018), where the period of study was extended up to 2012. Occasionally, significant events have been reported in the region (Ramis et al., 1999; Aran et al., 2009; Bech et al., 2009, 2011; Pineda et al., 2011; del Moral et al., 2020a) and also tornado outbreaks have affected high-densely populated areas, such as Barcelona and Tarragona metropolitan areas (Bech et al., 2007; Mateo et al., 2009). The high socioeconomical impact of these events and their frequency have motivated the recent study of tornadic storms vertical profile characteristics (Rodríguez and Bech, 2018, 2020a) and, together with the occurrence of other severe weather phenomena, the development of nowcasting tools to predict severe thunderstorms (Farnell et al., 2017).

During the last two decades, the exponential use and dissemination of severe weather information on internet, smartphones and social networks, and even some movies such as "Twister" (Rauhala et al., 2012) increased the general interest in tornadoes all over the world. Moreover, the local improvement on radar coverage and data quality (Altube et al., 2015, 2017) and the installation of a lightning detection network (Pineda and Montanyà, 2009) in the early 2000 in Catalonia has also helped to better identify convective storms and severe weather events in the region of study. An increasing number of post-event surface damage surveys (Rodríguez et al., 2020) and the use of high-resolution aerial imagery on detecting tornado-related damage swaths (Rodríguez and Bech, 2020b) also contributed to enlarge the number of tornado and waterspout reports compared to the late 20th century.

The main goal of this article is to present a homogeneous and robust dataset of tornado and waterspout reports registered from 2000 to 2019 in Catalonia, analysing their main spatial and temporal features. This 20-year period is comparable to other recent tornado climatologies carried out in Europe (Matsangouras et al., 2014b; Miglietta and Matsangouras, 2018; Sioutas and Doe, 2019; Leitão and Pinto, 2020) and gathers results from technological advances on severe weather observations, decreasing the number of unreported events and providing a comprehensive updated analysis of one of the European tornado hotspots.

This paper is organized as follows. In Section 2 the region of study is presented and the tornado and waterspout database is introduced, detailing information sources and the validation and recording process of each event. Then, in Section 3 results are discussed, showing the spatial and temporal distribution of tornadoes and waterspouts, tornado outbreaks and multiple tornado or waterspout events, damage swath characteristics and socioeconomic impact in terms of injured people and damage loss estimation. Finally, in Section 4 a summary, conclusions and proposals for future work are presented. Moreover, an Appendix lists individual tornado and waterspout events analysed in this study (date and time, coordinates of touchdown and intensity rating) provided for open use in further studies.

2. Data and methodology

2.1. Region of study

Catalonia, which is located in the north-east of the Iberian Peninsula (Fig. 1), is a 32,000 km^2 region divided into 42 counties, with a population of 7.7 million (IDESCAT, 2020). Pyrenees and Pre-Pyrenees mountain ranges extend in the north, from east to west, with peaks exceeding 3100 m and 2600 m, respectively. Moreover, parallel to the coast there are the Littoral (700 m) and Pre-Littoral (1700 m) mountain ranges with flat areas between them, whereas western Catalonia is dominated by the Ebro depression, which is a large flat area. The interaction of complex topography with low-level moist-warm air from the Mediterranean Sea and upper-level cold air advections from higher latitudes produces –mainly during the warm season– severe convective storms (Calvo-Sancho and Martín, 2020; Martín et al., 2020), sometimes with large hail (Farnell et al., 2009), strong winds (López, 2007) and

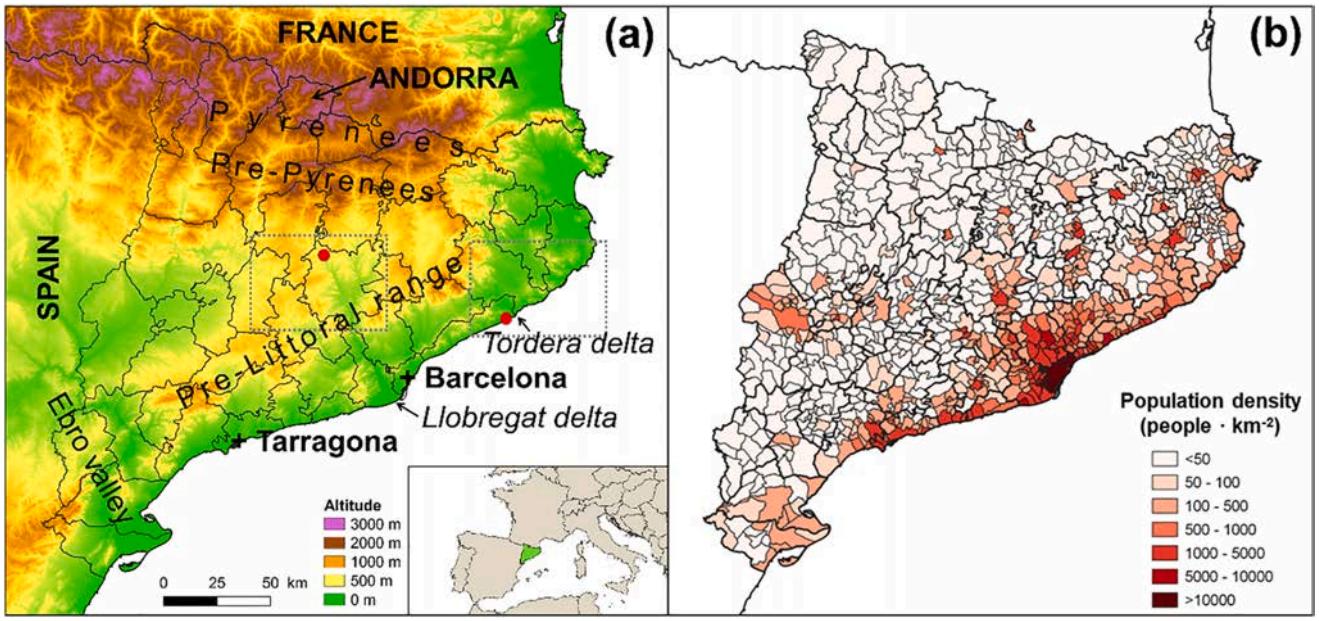

Fig. 1. (a) Topographical map of Catalonia showing Barcelona and Tarragona cities, and Tordera and Llobregat deltas location. County borders are indicated with thick black lines. Moreover, the selected area of the cases shown in Fig. 4 is marked with grey-dotted rectangles and tornado location is indicated with red dots. The insert, shows the location of the region of study (shaded in green) in SW Europe. (b) Municipal population density map of Catalonia (source of data: Cartographic and Geologic Institute of Catalonia ICGC and Statistics Institute of Catalonia IDESCAT).

tornadoes.

2.2. Tornado and waterspout database

The tornado and waterspout database consists of 434 individual vortices (i.e., a tornado or a waterspout) observed from 2000 to 2019 in Catalonia and the surrounding sea area. The database follows the *Glossary of Meteorology* (AMS, 2020) definition for tornado "A rotating column of air, in contact with the surface, pendant from a cumuliform cloud, and often visible as a funnel cloud and/or circulating debris/dust at the ground" (105 (24%) cases in the dataset) and waterspout "In general, any tornado over a body of water" (329 (76%) events). In the database, waterspouts that make landfall are considered tornadoes, representing 41 (39%) of tornado events. As indicated above, note that in this article the term vortex is used to refer to individual tornadoes or waterspouts, not to rotating structures within a tornado as in other studies (Wurman et al., 2014).

Generally, for each tornado, date, hour, location (i.e. latitude, longitude, and affected municipalities and counties) and the intensity estimation using the EF-scale (WSEC, 2006) are provided. If available, starting and ending latitude and longitude of damage track, the damage path length and width, the number of injuries and fatalities and the damage loss estimation are also recorded. For waterspout events (e.g., Fig. 2) date, hour, and location are registered.

2.3. Sources of tornado and waterspout reports

Reports of tornadoes and waterspouts have been collected from meteorological spotters and casual witness observations, emergency services (firefighters, police and civil protection) and mass media during all the period of study. Furthermore, the internet and social networks have become a crucial source of unusual meteorological observations hardly captured by operational observing networks (Hyvärinen and Saltikoff, 2010; Grasso et al., 2017), particularly in severe weather events (e.g., Kahraman and Markowski, 2014; Kirk, 2014; Rigo and Farnell, 2019; Chernokulsky et al., 2020), being an essential source of information about tornadoes and waterspouts during the second decade of the period of study (Fig. 3). This is reflected in the creation, during the last years, of several citizen collaborative platforms such as the European Severe Weather Database (ESWD; Dotzek et al., 2009) from the European Severe Storms Laboratory (ESSL), the Reporting System of Singular Atmospheric Observations (SINOBAS; Gutiérrez et al., 2015) from the Spanish Meteorological Agency (AEMET) and the Meteorological Spotters Network (XOM; Ripoll et al., 2016) from the Meteorological Service of Catalonia (SMC); the three platforms provided part of tornado and waterspout reports included in the database. All this information was combined with the catalogue of tornadoes and waterspouts of Spain described by Gayà (2018), which contains cases up to 2012.

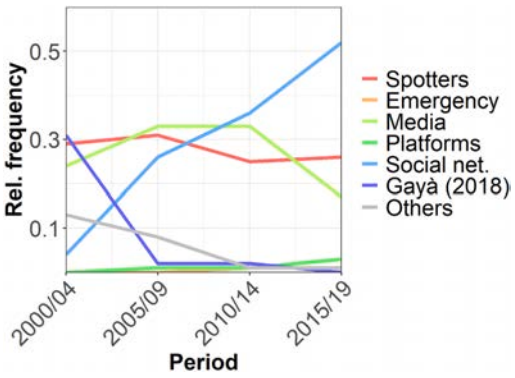

Fig. 3. Relative frequency of selected report sources: meteorological spotters, emergency services, media, citizen collaborative platforms, social networks, Gayà (2018) and others for each 5-year windows during 2000–2019.

2.4. Validation and recording of reported events

A validation process is necessary to avoid introducing erroneous or duplicated reports into severe weather databases (Dotzek et al., 2009). The validation followed here to build up the database consists of two steps:

1. Confirming that atmospheric convection was present during the day and time of the reported event
2. Confirming that damage was really caused by a tornado instead of other strong winds of convective origin (in case of reported damage and if no images of the funnel cloud and/or swirling debris are available).

The first step is carried out making a visual analysis of satellite data, C-band Doppler radar observations (Altube et al., 2015, 2017) and lightning data (Pineda and Montanyà, 2009) from the SMC, according to geographical and temporal information of each report. The main goal is to identify the parent-convective storm that spawned the tornado or the

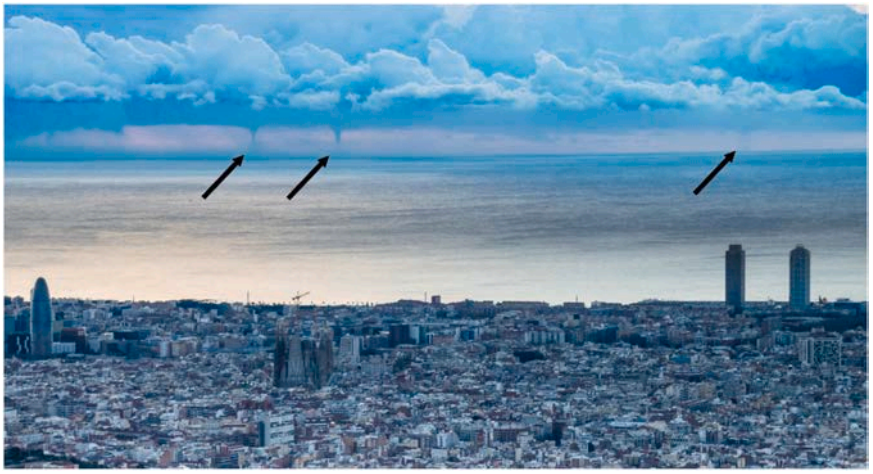

Fig. 2. Three waterspouts (indicated with black arrows) formed around 50 km off-coast in front of Barcelona, during the 7 March 2018 waterspout outbreak. Author: Alfons Puertas.

waterspout. Weather radar imagery is of special interest, as it may reveal classical features associated to supercell storms (Wilson et al., 1980; Zrnić et al., 1985) either in the radar reflectivity field such as hook-echoes or on radial Doppler wind fields such as mesocyclonic velocity couplets (Fig. 4a), although in many cases these features may not be detectable (Fig. 4b) or simply they may not be present in case of non-mesocyclonic tornadoes (Wakimoto and Wilson, 1989). On the other hand, it should be taken into account that waterspouts can be associated with fair weather conditions (i.e., light- or non-precipitation nor lightning; Matsangouras et al., 2017; Miglietta, 2019), making possible the identification of the parent-convective storm only using satellite imagery such as infrared (10.80 μm) or visible (0.60 μm) channels. With this analysis it is generally feasible to estimate the timing of the event (usually with an uncertainty lesser than 5 min) and even the approximate location of waterspouts over the sea. This task was performed manually so it was time-consuming and, occasionally, results were inconclusive due to unavailable data (especially during the first five years of study) or, in case of extensive and long-lived convective systems, when it was not possible to identify the particular parent-storm.

The confirmation of tornado occurrence instead of other damaging winds of convective origin, in case no image of the phenomenon was available (step 2), is performed after mapping and examining the reported damage of each event. Consequently, this step is not carried out for waterspouts remaining all their life-cycle offshore. The information used to fulfil this analysis has been gathered by performing in-situ damage surveys (Rodríguez et al., 2020), when it has been possible. Therefore, 37% reported tornadic events between 2000 and 2009 and 63% of cases between 2010 and 2019 have been analysed in-situ (e.g., Bech et al., 2011; Bech et al., 2015). Moreover, 25 and 50 cm-spatial resolution orthophotographs from the Cartographic and Geologic Institute of Catalonia (ICGC) have been also used to assess damage swaths (Rodríguez and Bech, 2020b), looking for changes on forest coverage and on human-made structures comparing images taken before and after events, similarly to Karstens et al. (2010), Molthan et al. (2014, 2020) and Shikhov and Chernokulsky (2018). The study of damage patterns in forest areas (i.e., direction of fallen trees) can provide valuable clues for distinguishing damage caused by tornadoes, downbursts or straight-line winds (Fujita, 1981; Bech et al., 2009; Rhee and Lombardo, 2018). Long-narrow tracks with a convergent or rotational damage pattern and great damage gradient are compatible with tornadoes, whereas short-wide, divergent damage swath with a lesser damage gradient are more likely associated with downbursts (Bunting and Smith, 1993).

Then, only those cases for which all the validation process is completed are introduced in the database. Furthermore, the information recorded for each event is complemented by characterising the damage swath, when the identification of the track is possible. This analysis has been performed using data gathered during fieldworks and orthophotograph imagery, but also using information provided by emergency services and local authorities about geolocated damaged elements. On the other hand, data about injuries and fatalities has been obtained from

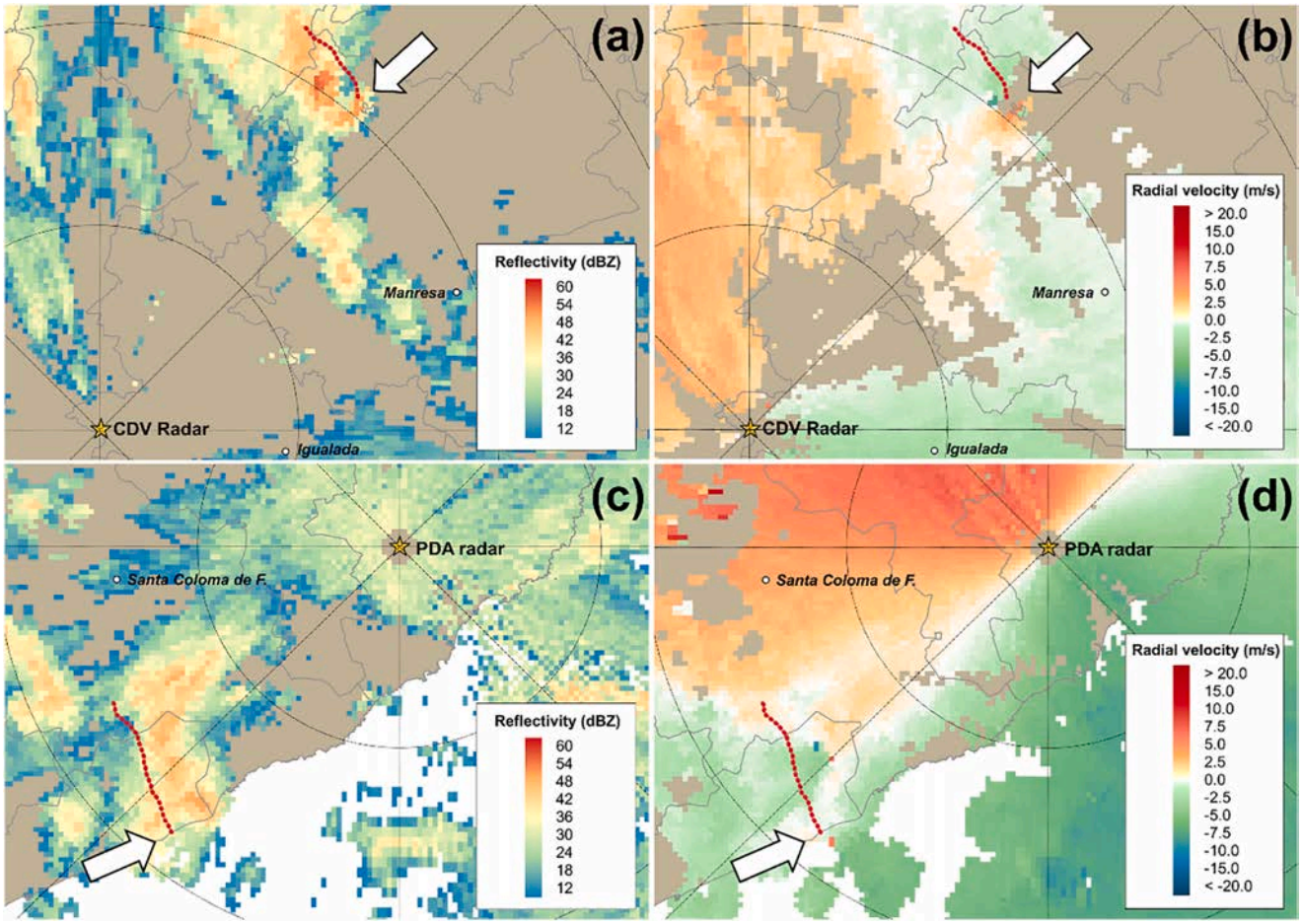

Fig. 4. Radar reflectivity (left column) and radial Doppler velocity (right column) weather radar PPIs (0.6° antenna elevation). Panels (a) and (b) were observed by the CDV radar (41.60° N, 1.40° E) on 7 January 2018 at 0054 UTC and panels (c) and (d) by the PDA radar (41.89° N, 3.00° E) on 15 October 2018 at 0136 UTC. Images show radar locations (stars), county capitals (white dots), tornado tracks (red-discontinuous lines), parent-storms (white arrows), and 20-km range rings and azimuths centred on each radar.

media.

Finally, the maximum intensity of each event has been estimated. To carry out this task we analysed damage observed in photographs from media and from fieldwork when performed. For each relevant element damaged, the EF-scale to assess wind intensity has been applied, proceeding as in Bech et al. (2015). The EF-scale consists of 28 damage indicators (type of construction or element, such as mobile homes, hospitals or trees) and 3 to 12 degree of damage for each one. Combining both parameters, a wind velocity range is given, which can be related to EF categories (WSEC, 2006; Mahieu and Wesolek, 2016). In contrast, F-scale, which was broadly used before 2007, is based on typical damage descriptions associated with F0 to F5 categories (Fujita, 1981). Therefore, the EF-scale makes possible a more detailed damage intensity rating instead of the original F-scale, despite limitations on its use specially outside the USA (Doswell III et al., 2009).

2.5. Damage loss estimation

Achieving realistic data of direct tornado damage loss is a non-trivial task; see for example discussions in Edwards et al. (2013) or Antonescu et al. (2017). In the present article, damage loss estimation has been carried out using data from the *Consorcio de Compensación de Seguros* (CCS), local administrations and expert assessment. CCS provided damage compensation data, as it is the public reinsurance company of Spain which covers the damage to insured properties due to several natural disasters, including tornadoes since 2004. Due to policy coverage limitations, there is a difference of 13% between the compensation assumed by the insurance company throughout the CCS and the real cost of the damage (Martínez-Gomariz et al., 2019). Therefore, a correction factor based on this figure has been applied to CCS data to estimate the real insured properties damage cost caused by tornadoes.

Nevertheless, apart from the absence of tornado damage compensations data before 2004, there is also a lack of data for several events. This may be either by damage on uninsured properties (and therefore not covered by the CCS) or because the event caused minor or no damage which was not claimed to the CCS.

Damage loss estimation carried out by local administrations has also been used to complement the present analysis. These data have been taken into account instead of CCS data when this estimation was higher and when there were no CCS data for an event. This situation is especially common in rural areas where the ratio of uninsured properties is notably higher than in urban areas.

Finally, in case of no data availability from CCS nor local administrations, data from an expert assessment has been used, derived from the analysis of information gathered during in-situ damage surveys, similarly to Martínez-Gomariz et al. (2020). All these data have been converted to 31 December 2019 reference value to enable a consistent comparison.

3. Results and discussion

3.1. Spatial distribution

Tornado density in Catalonia is 1.65 tornadoes year^{-1} 10^{-4} km^{-2}, which is similar to Colorado (1.54) and Ohio (1.75) states in the USA, slightly higher than other Mediterranean countries such as Italy (1.23) or Greece (1.20), and higher than other European countries (Table 1). Nevertheless, the UK (1.92) is the European state where tornado density is the highest, although this value is far from the US Great Plains, reaching the maximum in Kansas (4.45 tornadoes year^{-1} 10^{-4} km^{-2}). If only significant events (i.e., EF2 or stronger according to the EF-scale, WSEC, 2006 – see Section 3.4) are taken into account, then the density is 0.13 events year^{-1} 10^{-4} km^{-2} in the region of study. As stated in Table 1, this value is slightly smaller than those reported in Ohio (0.21), Germany (0.19) or Portugal (0.19), and clearly smaller than in Kansas (0.37). In contrast, it is higher than for Italy (0.08) or Colorado (0.05).

Similarly, the density of waterspouts normalized per year and 100 km of coastal line in Catalonia is 5.0, which is higher than in Croatia (3.0, Renko et al., 2016), in Greece (2.1, Matsangouras et al., 2014b), in Germany (2.1, Kühne et al., 2017), in Italy (0.9, Miglietta and Matsangouras, 2018) and in Portugal (0.2 in mainland, Leitão and Pinto, 2020). Nevertheless, if only near-coastal waterspouts are considered (i.e., located less than 10 km offshore), the density decreases to 2.7, which is similar to some of the previous-mentioned countries.

The spatial distribution of tornadoes is not homogeneous throughout the region of study (Fig. 5a). The highest density is found on the littoral and the pre-littoral, especially the central sector, being coherent with previous studies (Gayà et al., 2011; Gayà, 2018). There are some hotspots close to delta rivers such as Tordera and Llobregat (indicated in Fig. 1a) and also in the flat area surrounding Tarragona, where several waterspouts were reported to landfall. In those regions the mean number of events per year in 0.2° grid cells is between 0.40 and 0.55 (i.e. around one tornado every 2 years). Moreover, a few isolated cases have been observed in the rest of Catalonia, and only a couple has been reported in the Pyrenees and Pre-Pyrenees during the period of study.

The waterspout spatial distribution follows a similar pattern than that of coastal tornadoes, with maximum density between Barcelona and Tarragona, where between 1 and 2 events per year are reported in coastal grid cells (Fig. 5b). However, in both extremes of the littoral, especially in the northern one, the waterspout density is significantly lower. It is noticeable that the central area of the littoral and pre-littoral is the most populated area of the region of study (Fig. 1b). In this 4800 km^2 area (15% of Catalonia surface) live 5.6 M inhabitants (73% of the population). Therefore, an important question here is: is there a bias on tornado spatial distribution caused by population density?

To answer this question, we reviewed previous research in the region of study devoted to the analysis of the spatial distribution of lightning strikes and convective storm structures –both independent from population density–, and hailstorms, assuming that tornadoes are usually related to deep-moist convection. Even though, it should be taken into account that in some occasions, they can be formed within fair weather

Table 1
Tornado density, significant tornado density, period and reference of data for selected USA States and Countries.

State / Country	Period	Tornado density (y^{-1} 10^{-4} km^{-2})	Significant tornado density (y^{-1} 10^{-4} km^{-2})	Reference
Kansas	2000–2018	4.45	0.37	NOAA/SCP (2019)
United Kingdom	1981–2010	1.92	–	Kirk (2014)
Ohio	2000–2018	1.75	0.21	NOAA/SCP (2019)
Catalonia	2000–2019	1.65	0.13	This article
Colorado	2000–2018	1.54	0.05	NOAA/SCP (2019)
USA	2000–2018	1.24	0.13	NOAA/SCP (2019)
Italy	2007–2016	1.23	0.08	Miglietta and Matsangouras (2018)
Greece	2000–2019	1.20	–	Sioutas and Doe (2019)
Germany	2002–2016	1.12	0.19	Kühne et al. (2017)
Portugal (mainland)	2001–2019	0.67	0.19	Leitão and Pinto (2020)

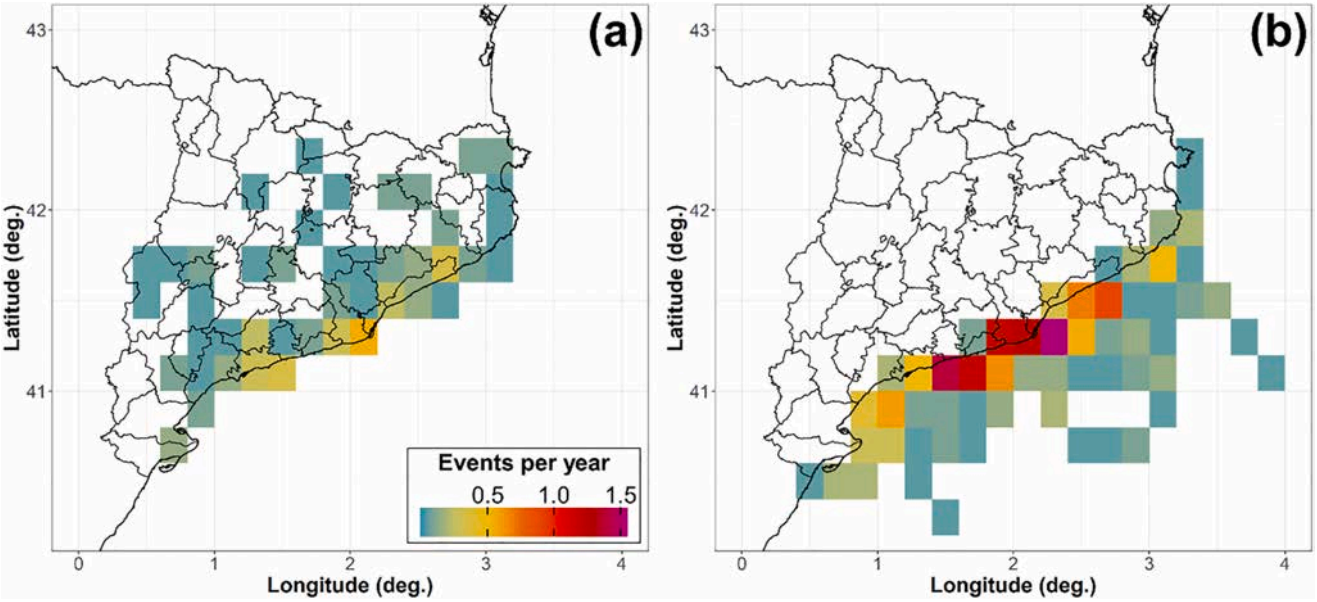

Fig. 5. Number of tornadoes per year, based on initial touchdown (a), and number of waterspouts per year (b) in a 0.2° per 0.2° grid.

conditions mainly offshore, limiting partially the following discussion.

In Pineda and Soler (2015) it is shown that the maximum lightning density (more than 3 cloud to ground flashes $year^{-1}$ km^{-2}) is located in the Pre-Pyrenees, especially in the central and eastern sector. It coincides with the area where hailstorms (Rigo and Farnell, 2019) and convective storm structures (del Moral et al., 2017) frequency is the highest, pointing out this subregion as the most favourable for deep convection. Nevertheless, this area does not present the highest tornado density, as previously described. The low number of reported events in Pyrenees and Pre-Pyrenees could be explained by complex topography, which reduces the visibility, and the low population-density, hindering the direct visual observations (Schuster et al., 2005; Saltikoff et al., 2010; Potvin et al., 2019). Moreover, the lightning monthly distribution could also provide another explanation for that. According to Pineda and Soler (2015), the thunderstorm season in this subregion starts on late spring and finishes on late summer, and their formation is usually related to the diurnal heating cycle combined with sea surface temperature seasonal cycle (Pastor et al., 2018) and upslope breezes (Callado and Pascual, 2005). During warm season, Jet Stream and associated surface lows are weaker and move farther north (Koch et al., 2006), favouring low-shear environments in the region, whereas tornadic storms are usually associated with moderate to high shear and helicity conditions, especially in low-levels (Taszarek et al., 2017; Rodríguez and Bech, 2018, 2020a). Therefore, the lack of environments with instability overlapping with high shear could hamper tornado formation in Pyrenees and Pre-Pyrenees.

On the other hand, lightning density presents a secondary maximum in the Tarragona area, extending north-east in front of the coast up to Barcelona (del Moral et al., 2020b), whereas in northern littoral there is a minimum. This distribution is related with northern surface synoptic wind situations, when the orographic effect of the Pyrenees favours the formation of a convergence zone in the central Catalan littoral between the tramontane flow from the northern coast and the mistral flow in the southern region, which is channelled by the Ebro valley (Peña et al., 2011; Gonzalez et al., 2018). In case of vertical instability, the presence of a convergence line can initiate convection, and furthermore can support waterspout formation (Miglietta, 2019). Therefore, it could explain the tornado and waterspout maximum in the central sector of the littoral and pre-littoral, although population distribution may also contribute to draw the pattern shown in Fig. 5b.

3.2. Temporal distribution

Between 5 and 6 tornadoes are reported in 3 to 4 days every year on average in Catalonia, which provides a ratio of 1.4 tornadoes per tornadic day (i.e. a day with at least one tornado reported). The number of waterspouts per year is notably higher, between 16 and 17, observed in 9 to 10 days. Thus, the number of waterspouts per waterspout day (i.e. a day with at least one waterspout reported) is 1.8, being comparable to other Mediterranean countries such as Greece (1.7, Sioutas and Doe, 2019) or Croatia (2.4, Renko et al., 2016). Even so, the yearly tornado and waterspout standard deviation is 3.3 and 10.2, respectively, which indicates that there is a large interannual variability, as shown in Fig. 6a, b. Thus, the number of tornadoes per year ranges from 1 tornado in 2000 to 13 in 2018 and the annual number of waterspouts, from 3 in 2000 to 38 in 2016. On the other hand, the annual numbers of tornado days and waterspout days are more homogeneous (Fig. 6c), presenting a yearly standard deviation of 2.3 days and 4.0 days, respectively. This difference on annual behaviour between the number of individual tornadoes and waterspouts and the number of days when they were observed, especially for the latter, is because of the occurrence of multiple events and outbreaks. These events can occasionally generate more than 5 tornadoes or waterspouts in a single day (see Section 3.3 for further discussion).

Interestingly, it can be observed that, whereas 65% of reported tornadoes between 2000 and 2009 were rated as EF0, the percentage raised up to 80% for the next ten years, a figure consistent with previous studies (e.g., Verbout et al., 2006; Gayà, 2018). Moreover, 42% of those EF0 reported during the first decade were mainly concentrated in the five most populated counties, whereas between 2010 and 2019 it was only 29%. Similarly, the ratio of waterspouts observed far-away from the coast (i.e., 10 km or more offshore) also increased from 27% for the first decade to 53% for the second. These differences are a consequence of the improvement of the detection of low-impact events (weak tornadoes and far-offshore waterspouts) during the period of study. As explained in Section 2.3, the expansion of internet and social networks, the increasing number of smartphones, the consolidation of remote-sensing networks, the growing interest on severe weather, together with the increase of Catalonia population from 6.2 M inhabitants in 2000 to 7.7 M people in 2019 (IDESCAT, 2020) have likely contributed to a better observation of this kind of events.

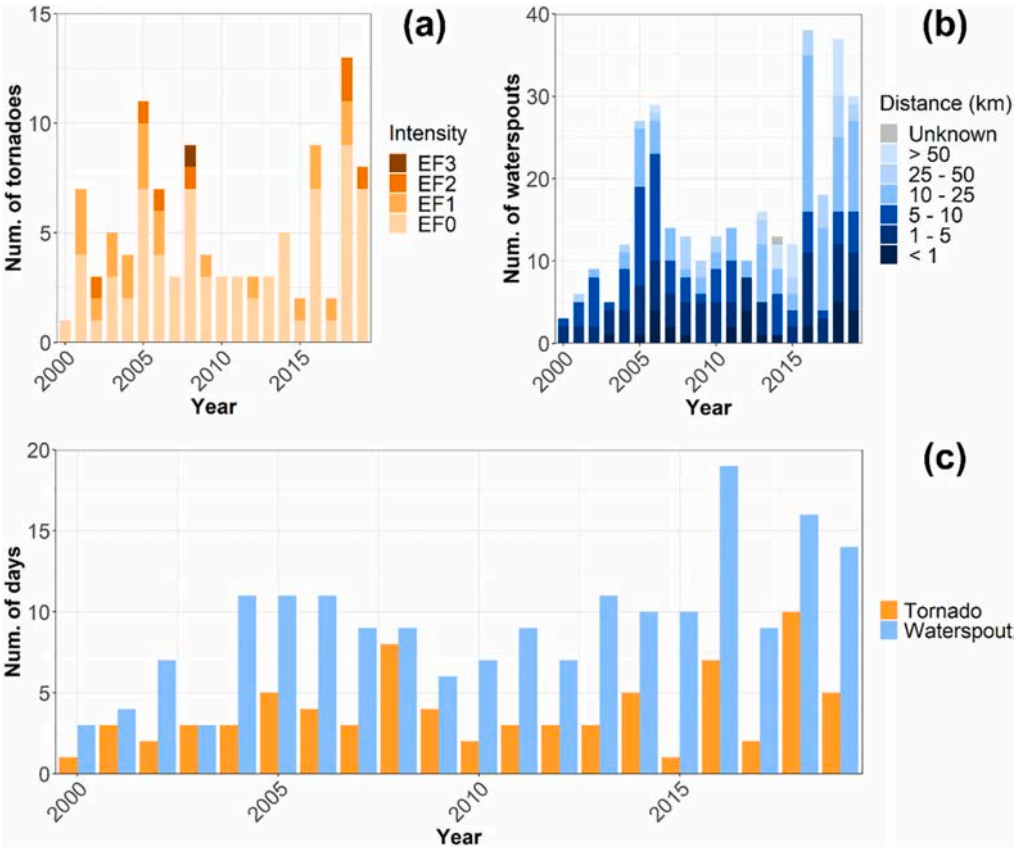

Fig. 6. Number of tornadoes depending on their intensity (a), number of waterspouts depending on their distance from the coast-line (b), and number of tornado days and waterspout days (c) per year reported between 2000 and 2019.

Both tornado and waterspout events have a similar seasonal and monthly distribution (Fig. 7). Although they can occur at any time of the year, a vast majority have been observed in autumn (56% of tornadoes and 60% of waterspouts) and in summer (19% and 21%). In contrast, winter (10% and 9%) and spring (15% and 10%) are the less favourable seasons for their occurrence. The tornado season in the area of study runs from August to November (69% of the tornadic cases), reaching the peak in October. On the other hand, a secondary tornado activity maximum is observed between April and May (12%). This result is similar to that previously found by Gayà et al. (2011), although the maximum has been shifted towards autumn. The monthly distribution presented here is similar to other Mediterranean countries such as Greece (Matsangouras et al., 2014b) or Italy (Miglietta and Matsangouras, 2018), but differs from central and northern Europe, where

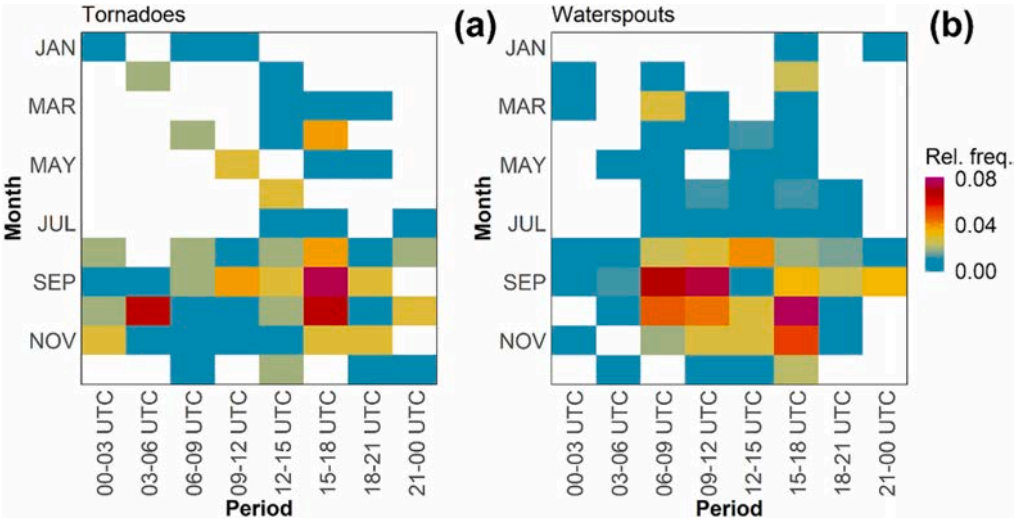

Fig. 7. Hourly and monthly relative frequency of tornadoes (a) and waterspouts (b).

tornadoes are usually observed between June and August (Groenemeijer and Kühne, 2014; Antonescu et al., 2016). Differences between central and northern Europe and the region of study can be explained by the influence of the Mediterranean Sea shifting the maximum convective activity towards autumn and the more frequent presence of the jet stream later in the season compared to higher latitudes. Regarding waterspout seasonal patterns, 75% of waterspouts are also reported during the August to November period, but the most active month is September.

The hourly distribution of tornadic events in the area of study (Fig. 7a) shows that they are more common during afternoon (especially between 15 and 18 UTC), when 44% (29%) of the reported cases were detected. This pattern, which is comparable to that for inland lightning strikes presented in Pineda and Soler (2015), can be explained by the diurnal solar heating cycle, that supports deep convection and tornadogenesis as stated in other studies for several regions (e.g., Kirk, 2014; Chen et al., 2018; Chernokulsky et al., 2020). In contrast, some differences are observed when our results are compared to Gayà et al. (2011) findings, where a secondary maximum on tornado activity was presented between 09 and 12 UTC (not observed here) and the highest tornadic events frequency was detected during early afternoon instead of the late-afternoon. These differences might be due to the smaller size of the sample data of the above-mentioned study (54 tornadoes) respect to the 105 hourly-determined events analysed here.

Unsurprisingly, waterspouts are mostly observed also during the diurnal period (Fig. 7b) which could be expected given their mostly visual detection. Their hourly distribution presents two maxima: during the morning (06–12 UTC) and in the late afternoon (15–18 UTC). This pattern, with a relative minimum during early afternoon (12–15 UTC), is consistent with previous works (Gayà et al., 2011) and also with the Balearic Sea lightning hourly distribution (Pineda and Soler, 2015), which presents a decay on the number of strikes during this 3-h window.

The lowest tornado and waterspout frequency is observed during the nocturnal period, between 21 and 06 UTC, when only 25% tornadoes and 10% waterspouts have been reported. The lack of visibility due to the darkness and the smaller number of potential eye-witness during night (Potvin et al., 2019) contribute to draw this pattern. Moreover, meteorological factors such as inland thunderstorm daily cycle activity also presents the daily minimum during this period (Pineda and Soler, 2015), supporting the low frequency of nocturnal tornadic events. In contrast, the highest occurrence of offshore lightning events is observed during night, which does not fit with the small number of waterspouts detected during darkness hours. Therefore, that discrepancy could suggest that nocturnal waterspouts are more underreported than nocturnal tornadoes.

3.3. Outbreaks and multiple events

The Glossary of Meteorology (AMS, 2020) defines tornado outbreak as "multiple tornado occurrences associated with a particular synoptic-scale system". Nevertheless, some authors restrict the term tornado outbreak for those events in which 5 or more (Pautz, 1969), 6 or more (Galway, 1975) or 10 or more (Galway, 1977) tornadoes are reported, whether others such as Hagemeyer (1997) also presents a temporal-window restriction (4 or more tornadoes in a lapse time of 4 h or less). In this section, we follow Galway (1975) outbreak definition, but taking both tornado and waterspout occurrences into account. According to the classification presented in the previous-mentioned article, in terms of number of tornadoes per outbreak, there are three main outbreak classes: small (6 to 10), moderate (11 to 20) and large (more than 20).

From 2000 to 2019 75 events with 2 or more individual tornados or waterspouts have been registered in Catalonia, 17 of which can be considered outbreaks (Fig. 8). The vast majority of them (82%) were small, 2 were moderate and 1 was large. The most extensive one was on 7 and 8 September 2005, when at least 21 individual vortices (7 tornadoes and 14 waterspouts), the strongest one rated as an EF2, mainly affected the Barcelona international airport and its surrounding area (12 km SW Barcelona, in Llobregat delta), causing the interruption of air traffic operations for 1 h (Bech et al., 2007). The low number of moderate and large outbreaks could be explained by the relatively small size of the area of study compared to similar researches.

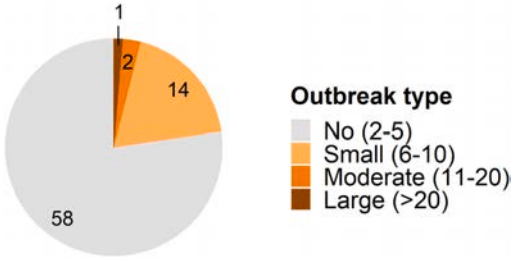

Fig. 8. Frequency of tornado outbreak type, according to Galway (1975) categories ("Small outbreak", "Moderate outbreak" and "Large outbreak") including both tornadoes and waterspouts. "No-outbreak" type includes events in which 2 to 5 vortices formed in the same synoptic-scale system.

The duration of outbreaks is higher than those presented in previous studies for other countries (e.g., Galway, 1977). The average is 27 h, and the median 25 h. The main reason is that they usually occur when a cut-off low is located in the centre or south of the Iberian Peninsula, which is a synoptic situation that can persist for some days (e.g., Romero et al., 2000; Homar et al., 2002).

In some occasions, several tornadoes or waterspouts may be formed by a single convective storm and sometimes they can be observed simultaneously (Sioutas et al., 2013; Miglietta et al., 2020), being more common for waterspouts (see Fig. 2 as an example). In order to analyse these cases, a multiple event is defined here as the one where two or more tornadoes or waterspouts formed within a particular convective storm during its life cycle.

The database reveals that 158 vortices have been observed during 54 multiple events, 13 corresponding to tornadoes and 145 to waterspouts. The mean elapsed time between the formation of the first and the last reported vortex is 30 min, although 6% of cases exceeded 1 h. In 52% of them, two vortices where reported, and only in 7% of them more than 5 individual vortices were formed (Table 2), a figure similar to the one reported for Italy by Miglietta and Matsangouras (2018). The two largest events occurred on 7 September 2005 between 1715 and 1818 UTC, when 4 tornadoes and 4 waterspouts affected the Llobregat delta, and on 7 March 2018 between 0613 and 0646 UTC, when 8 waterspouts formed around 50 km off-coast in front of the central Catalan littoral area (Fig. 2).

The number of reported multiple events has increased during the period of study. Between 2000 and 2009 21 cases were detected, whereas between 2010 and 2019 the number raised up to 33. This difference is related to the increasing number of available images of reported events and the ease to contact with their authors, facilitating the identification of non-simultaneous tornadoes or waterspouts formed

Table 2
Frequency of multiple events reported from 2000 to 2019 depending on the number of vortices (individual tornado or waterspout) formed by a particular convective storm.

Number of vortices	Frequency
2	28
3	15
4	6
5	1
6	2
7	0
8	2

within the same convective storm.

3.4. Damage path characteristics

Damage assessments classified 72% tornadoes as EF0, 20% as EF1 and 8% as EF2 or stronger. Only one EF3 event has been observed during this 20-years period, registered on 2 November 2008 30 km northern Tarragona (Rodríguez and Bech, 2020b). The percentage of EF0 is clearly higher than in previous studies (43% in Gayà et al., 2011), whereas the ratio of EF1 is significantly smaller (44% in that work). This could be explained by the differences between the period of study of the above-mentioned works, which extends between 1950 and 2009, and the analysed here. As stated in Section 3.1, smartphones, internet and social networks, among others, have favoured reporting weak events compared to decades ago, increasing the percentage of EF0 tornadoes on databases (e.g., Verbout et al., 2006).

Despite the lack of violent events (i.e., EF4/EF5), the proportions presented here show some similarities to USA tornadoes (Fig. 9). Nevertheless, it can be observed that, whereas the ratio of EF0 in Catalonia is higher than in the USA, the proportion of EF1 is smaller. That could be explained by the high number of tornadoes formed offshore in the dataset (39% of the total), which are usually non-mesocyclonic (Markowski and Richardson, 2009). Therefore, whereas, 78% of waterspouts making landfall have been rated as EF0, 17% as EF1 and 5% as EF2+, 68% of formed-inland events have been rated as EF0, 22% as EF1, and 10% as EF2+, being this second distribution more similar to the USA data (not shown).

Around 42% of the analysed damage paths are shorter than 1 km. From them, more than a half correspond to tornadoes formed offshore that weaken when move onshore. The vast majority of tornado tracks are smaller than 5 km (82%), and only 7% are larger than 10 km, being consistent with previous studies (Gayà et al., 2011; Gayà, 2018). The longest damage path in the database is 45.5 km, which corresponds to the 7 January 2018 tornado, formed in NE Catalonia (Rodríguez et al., 2018). Comparing these results to the USA data (NOAA/SPC, 2019), it is noteworthy that, in general, damage swaths are longer than in Catalonia (i.e., 73% are shorter than 5 km and 14% are longer than 10 km).

Similarly to short damage tracks, the narrowest paths are usually related with waterspouts that move onshore. Then, more than 50% of the 50 m or less-wide swaths are due to tornadoes formed over the sea. 79% of the studied damage paths are narrower than 200 m, and only occasionally are wider than 500 m (6% of the cases). Proportions presented here are similar to the USA data, where 85% of tornado tracks do not overcome 200 m width and only 4% of them exceed 500 m.

Furthermore, stronger tornadoes are usually related with longer and wider damage paths than weaker tornadoes. Brooks (2004) reported a statistical relation based on Weibull distribution between tornado intensity (there, using the F-scale, Fujita, 1981) and length and width of tornado path with data from the USA. As presented in Fig. 10, the track length of weak tornadoes is generally smaller than 10 km, whereas the majority of significant events surpass this threshold. Regarding the damage swath width, while very few weak tornadoes produce a path wider than 200 m, EF2+ events mostly exceed 400 m width. The 50th percentile of track length and width for EF0 is 0.6 km and 35 m, for EF1 is 3.9 km and 145 m, and for EF2+ is 12.4 km and 485 m.

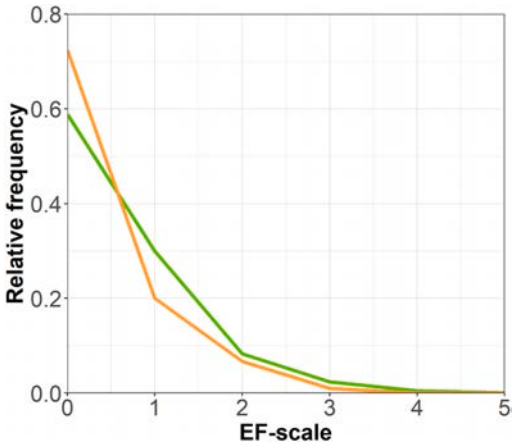

Fig. 9. Relative frequency of tornadoes depending on their intensity according to EF-scale in Catalonia (orange) and USA (green, NOAA/SPC, 2019).

Tornado damage tracks are usually oriented from south to north and present differences depending on their origin. Fig. 11 shows orientation distributions for tornadoes formed inland (a) and offshore (b). Tornadoes which touchdown inshore, usually move from the 3rd quadrant to the 1st (49%) and from the 2nd quadrant to the 4th (33%), although the predominant directions of movement are SSW to NNE (20%) and SSE to NNW (18%). This pattern has also been observed in other Mediterranean countries such as Greece (Sioutas, 2011) or Italy (Miglietta and Matsangouras, 2018). On the other hand, waterspouts can make landfall when move perpendicular to the coast, which is mostly oriented east and south-east in the area of study. Therefore, around 35% of tornadoes formed over the sea that hit land move from SE to NW and 30% from SSE to NNW. The orientation of damage paths is related to the typical synoptic pattern under which tornadic activity occurs in the region of study, which is usually characterised by southerly mid- and upper-level winds due to a deep through or a low located west from Catalonia (e.g., Aran et al., 2009; Bech et al., 2011, 2015).

3.5. Socioeconomic impact

Between 2000 and 2019 no fatalities due to tornadoes were registered in the region of study. The last deathly tornadic event reported was on 27 November 1930 between Tarragona and la Selva del Camp (Gayà, 2018). Nevertheless, at least 26 people have been injured during the period of study (Table 3). Most of them (22) were associated to urban events, where the population density is high, a factor which is positively correlated to casualties (Donner, 2007). The rest (4), were located in campings, where constructions (mobile homes, vans, bungalows) are more vulnerable than in urban areas, as it is indicated in Eidson et al. (1990). The most common injury types were bruises, cuts and fractures, similar than reported in other studies (e.g., Brown et al., 2002).

All these injuries have been caused by 6 individual tornadoes (around 6% of the total), which in general have been rated as EF1+. Only one person was injured by an EF0 tornado, during the 7 and 8 September 2005 outbreak (Bech et al., 2007). Moreover, a vast majority of injuring events (4) occurred during daytime hours (between 06 and 18 UTC). From the present dataset it stands out the case of the 18 October 2017 tornado that hit Valls, a 24,000 inhabitants town located 20 km north of Tarragona, which caused 13 people injured.

The annual number of injured people is highly irregular, being a typical pattern of rare events (Table 3). This is because injuring tornadoes are usually restricted to the occurrence of two simultaneous conditions which do not concur every year, as previously pointed out: (i) the tornado intensity is normally greater than EF0 (it corresponds to 28% of all reported events), and (ii) the tornado generally hits urban areas.

Damage loss estimation also presents a large interannual variability (Fig. 12). This behaviour, which is observed in other tornado datasets (Antonescu et al., 2017; NOAA/SPC, 2019) and other natural disasters (e.g., Barredo et al., 2012), obviously depends on the characteristics of each event and the affected area (Romanic et al., 2016). Here, great damage losses are usually related to EF1+ events hitting high-densely populated areas or important infrastructures (see for example year 2006, when an EF1 tornado affected several towns close to Barcelona; Mateo et al., 2009).

Between 2004 and 2019, the CCS paid 20.0 M€ on reinsurance

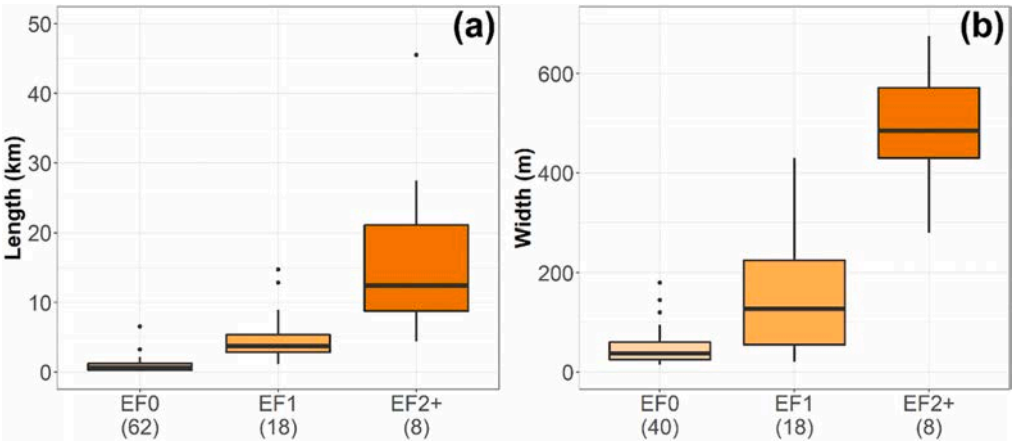

Fig. 10. Boxplots showing the track length (a) and width (b) for tornadoes reported in Catalonia depending on the EF-scale. It is represented 25th, 50th, and 75th percentiles and outlier points (exceeding the distance to the 25th or 75th percentile by 1.5 times the inter-quartile range). In brackets it is shown the number of paths for each EF category.

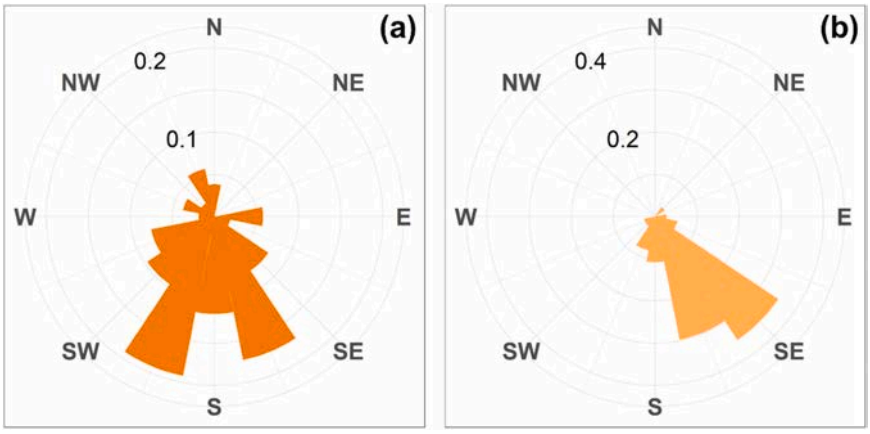

Fig. 11. Relative frequency of tornado path directions for inland (a) and offshore (b) touchdown cases.

Table 3
List of tornados and their intensity according to the EF-scale causing injuries during 2000–2019.

Date	EF	Injuries	Reference
7 September 2005	1	2	Bech et al. (2007)
7 September 2005	0	1	Bech et al. (2007)
13 September 2006	1	3	Mateo et al. (2009)
2 November 2008	2	4	Bech et al. (2011)
18 October 2017	1	13	Bech et al. (2018)
22 October 2019	2	3	–

compensations for tornado-related damage on insured properties (updated on 31 December 2019; light-grey columns in Fig. 12), although the real cost of repairing the covered damage is estimated on 22.5 M€ (dark-grey columns in Fig. 12). Nevertheless, taking into account data from local administration and expert assessment, the sum of the global damage loss estimation during the analysed 20-years period rises up to 30.8 M€ (red columns in Fig. 12). This figure, which implies an average of 1.5 M€ per year, is one magnitude order smaller than CCS floods compensations paid in Catalonia between 1996 and 2015 (21.8 M€ per year; Cortès et al., 2018).

The difference between CCS paid amounts and the global cost estimation is greater for rural tornadoes than for urban events. This might be caused by a lack of insurances covering part of rural buildings such as farms and warehouses. On those cases, the Public Reinsurance Company does not compensate damage. This situation is illustrated by a case in 2018, when a long-track tornado affected a rural area in northern Catalonia (Rodríguez et al., 2018). Local administration estimated damage losses on 4.3 M€, whereas CCS only covered 0.7 M€ (16%).

On years when at least one significant tornado is reported, the damage loss estimation surpasses 1 M€ (Fig. 6a and red columns in Fig. 12). Ten individual events produced estimated damage higher than 1 M€. From those, two caused damage greater than 5 M€ (13 September 2006 EF1 tornado 18 km SW Barcelona, and 2 November 2008 EF2 tornado 12 km SW Tarragona). In contrast, no EF0 event caused estimated losses greater than 0.5 M€.

4. Conclusions and final remarks

In this article, tornado and waterspout events reported in Catalonia (NE Iberian Peninsula) between 2000 and 2019 have been analysed. During the second half of the period of study, social networks were the main source of severe weather information, enlarging the number of waterspouts (especially formed far-away from the coast) and EF0 tornadoes (mainly in lower densely-populated areas) reports. A total of 105 tornadoes (41 of them formed offshore) and 329 waterspouts have been observed during this 20-years period, which yields yearly averages of 5.3 tornadoes year^{-1} and 16.5 waterspout year^{-1} respectively. Areal and linear density over the region and the coast are, respectively, 1.65

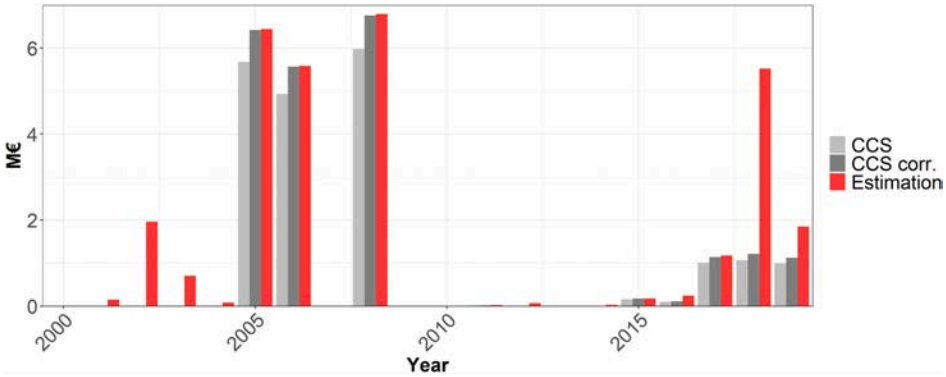

Fig. 12. Yearly tornadic events costs: CCS compensations, corrected (+13%) CCS compensations, and total damage-loss estimations (in Million Euros homogenized to 31 December 2019).

tornadoes year^{-1} 10^{-4} km^{-2} and 5.0 waterspouts year^{-1} 10^{-2} km^{-1}, slightly higher than in other Mediterranean countries.

Most tornadoes and waterspouts have been detected in the central sector of the littoral and pre-littoral, coinciding with the most populated area of the region. Nevertheless, meteorological and geographical factors such as the formation of mesoscale convergence lines in northerly situations due to the orographic effect of the Pyrenees, and the combination of increasing wind-shear environments during late summer and autumn with the period of highest instability due to high sea surface temperature might provide favourable conditions for tornado formation in this zone. In fact, 69% tornadoes and 75% waterspouts have been reported between August and November, similarly with previous studies. Moreover, tornadoes have usually occurred between 15 and 18 UTC, being related to deep-moist convection supported by the solar diurnal heating cycle. In contrast, waterspouts have been mainly observed during the morning (06–12 UTC) and late afternoon (15–18 UTC), presenting a secondary minimum during early afternoon, which is consistent with lightning climatology in the Balearic sea. Nevertheless, lightning activity over the western Mediterranean is maximum between 18 and 06 UTC, which would suggest that nocturnal waterspouts are much more underreported than nocturnal tornadic events.

During the period of study, 17 tornado outbreaks were identified, two of them qualified as moderate (between 11 and 20 vortices formed within the same synoptic system) and one, as large (more than 20 vortices). Moreover, 158 tornadoes and waterspouts were associated with 54 multiple events. The observation of five or more independent vortices in this kind of events is rare, representing 6% of the total, whereas the most common reported multiple events are those with only two independent vortices (52%).

Most tornadoes (92%) observed in Catalonia were weak (EF0/EF1), and only 8% were significant (EF2+). The strongest tornado took place 30 km north of Tarragona on 2 November 2008 and reached EF3 intensity. Most damage paths have been less than 5 km long (82%) and 200 m wide (79%), and a positive correlation between tornado strength and damage swath size has been observed. The tornado tracks studied presented a direction usually ranging from SE-NW to SW-NE, being the SE-NW direction the predominant for waterspouts that make landfall, due to the coast orientation.

Only 6 of the reported tornado events, mostly EF1+, caused injuries. In total, 26 people were injured, mainly with bruises, cuts and fractures, and no fatalities were registered. The damage loss estimation raised up to 30.8 M€, with a median of 1.5 M€ per year, which is one magnitude order smaller than floods compensations payed by the reinsurance public company of Spain in the area of study.

The analysis performed here may contribute to deepen in the knowledge of tornado and waterspouts frequency and characteristics in this hotspot area of the western Mediterranean. Moreover, the data provided in the appendix is available for the scientific community, and may be useful to validate and test nowcasting products and develop new studies to enhance tornadic storms forecasting and surveillance systems.

Future work could also include a more detailed weather radar analysis to objectively identify radar signatures supporting convective storm organization, allowing to distinguish supercell vs. non-supercell tornado features. Further studies could also expand the analysis of outbreaks to the rest of the Mediterranean slope of the Iberian Peninsula, Balearic Islands, southern France and even NW of Italy. Finally, a larger database including more years could also attempt to study possible temporal trends in the data set.

Declaration of Competing Interest

The authors declare that they have no known competing financial interests or personal relationships that could have appeared to influence the work reported in this paper.

Acknowledgments

We thank weather spotters, casual witnesses, meteorologists from the Meteorological Service of Catalonia and the Spanish Meteorological Agency, and weather presenters from Catalan media for reporting us tornado and waterspout events. We also appreciate the fire-fighters of the Government of Catalonia and Local Administration for providing tornado-related incidents, and the *Consorcio de Compensación de Seguros* (CCS) for providing data about tornado damage compensations. This study has been carried out into the framework of the HyMeX (HYdrological cycle in the Mediterranean EXperiment) international research programme and with partial support from projects CGL2015-65627-C3-2-R (MINECO/FEDER), CGL2016-81828-REDT (AEI) and RTI2018-098693-B-C32 (AEI), and the Water Research Institute (IdRA) of the University of Barcelona.

Appendix A

Here, it is provided a list of individual tornado and waterspout events analysed in the present article for open use in further research (see Table A1).

Table A1
Individual tornado and waterspouts analysed in this study including for each item listed the number (#), UTC Date and Time (in YYYY/MM/DD HH:mm format), Latitude (°), Longitude (°) and Enhanced Fujita intensity (EF) for tornadoes or W for waterspouts. In five waterspout cases, time was not available.

Item (#)	Date & Time (UTC)	Lat (°)	Lon (°)	EF/W (n/W)
001	2000/06/11 17:00	41.245	2.060	W
002	2000/12/21 13:30	41.497	2.576	W
003	2000/12/23 06:50	42.338	3.040	0
004	2000/12/23 11:55	41.570	2.566	W
005	2001/04/19 08:32	41.698	2.848	0
006	2001/04/27 16:00	42.000	2.284	0
007	2001/08/31 14:30	41.223	1.934	W
008	2001/08/31 14:30	41.219	1.948	W
009	2001/08/31 14:30	41.210	1.971	W
010	2001/10/20 03:00	41.659	2.405	1
011	2001/10/20 03:15	42.033	2.455	1
012	2001/10/20 03:45	42.247	2.883	1
013	2001/10/20 04:00	42.344	3.064	0
014	2001/10/20 10:15	41.621	2.692	0
015	2001/10/20 13:50	41.735	3.133	W
016	2001/11/09 07:30	41.308	2.724	W
017	2001/11/16 08:15	41.454	2.297	W
018	2002/06/05 16:30	41.632	2.858	W
019	2002/08/03 –:–	41.139	1.554	W
020	2002/08/08 16:35	41.701	2.994	W
021	2002/08/27 –:–	41.510	2.476	W
022	2002/09/16 07:00	40.614	0.911	W
023	2002/09/16 07:00	40.629	0.939	W
024	2002/10/10 07:30	41.363	2.299	W
025	2002/10/10 15:45	41.125	1.759	W
026	2002/10/21 15:48	41.641	0.605	1
027	2002/10/21 16:15	42.009	1.392	2
028	2002/11/15 16:30	41.428	2.422	W
029	2002/11/20 09:41	41.483	2.337	0
030	2003/08/17 07:30	41.280	1.246	0
031	2003/08/17 08:30	41.708	1.845	1
032	2003/08/17 09:00	41.788	2.226	1
033	2003/08/17 09:02	41.359	2.219	W
034	2003/08/17 –:–	41.501	2.489	W
035	2003/08/23 01:10	41.186	1.569	0
036	2003/09/04 17:00	40.988	0.931	W
037	2003/09/22 06:45	41.765	3.087	W
038	2003/09/22 06:45	41.758	3.083	W
039	2003/10/01 01:45	41.128	1.137	0
040	2004/07/05 15:45	41.472	0.443	1
041	2004/07/10 09:49	40.999	1.126	W
042	2004/08/05 00:20	41.265	1.997	0
043	2004/08/05 01:45	41.137	1.647	W
044	2004/08/10 12:00	41.130	1.495	W
045	2004/08/29 13:30	41.021	1.299	W
046	2004/08/30 06:24	40.990	1.026	W
047	2004/08/30 06:29	40.987	1.052	W
048	2004/09/20 11:00	41.382	2.213	W
049	2004/10/18 11:00	41.011	1.483	W
050	2004/10/30 18:00	42.028	3.228	W
051	2004/11/01 16:00	41.218	1.934	W
052	2004/11/10 18:30	40.998	2.202	W
053	2004/11/22 13:30	41.147	1.640	W
054	2004/12/01 20:45	41.147	1.422	1
055	2004/12/01 21:00	41.216	1.740	0
056	2005/01/29 16:30	41.132	1.753	W
057	2005/08/02 18:00	41.104	1.548	W
058	2005/09/07 17:05	41.261	1.932	1
059	2005/09/07 17:15	41.264	1.995	0
060	2005/09/07 17:23	41.228	2.162	W
061	2005/09/07 17:29	41.280	2.086	2
062	2005/09/07 17:30	41.533	2.637	W
063	2005/09/07 17:30	41.540	2.648	W
064	2005/09/07 17:39	41.210	2.256	W
065	2005/09/07 17:48	41.292	2.117	1
066	2005/09/07 17:52	41.239	2.234	W
067	2005/09/07 17:52	41.229	2.266	W
068	2005/09/07 18:00	41.534	2.511	W
069	2005/09/07 18:10	41.595	2.716	W
070	2005/09/07 18:18	41.315	2.114	0
071	2005/09/07 20:00	41.593	2.602	0

(*continued on next page*)

Table A1 (*continued*)

Item (#)	Date & Time (UTC)	Lat (°)	Lon (°)	EF/W (n/W)
072	2005/09/08 05:00	41.164	1.889	W
073	2005/09/08 05:45	40.896	0.834	W
074	2005/09/08 07:30	41.506	2.208	1
075	2005/09/08 12:40	41.028	1.872	W
076	2005/09/08 13:00	41.172	1.821	W
077	2005/09/08 14:00	41.119	1.755	W
078	2005/09/08 15:30	41.044	1.297	W
079	2005/10/05 08:10	41.399	2.362	W
080	2005/10/13 07:00	41.780	3.033	0
081	2005/10/13 12:40	41.214	1.820	W
082	2005/10/14 11:15	41.289	2.205	W
083	2005/10/15 14:00	41.243	1.980	W
084	2005/10/15 15:45	41.468	2.297	W
085	2005/11/13 13:28	41.139	1.622	W
086	2005/11/13 16:40	41.126	1.539	W
087	2005/11/14 16:45	40.830	1.835	W
088	2005/11/14 20:15	41.636	2.730	0
089	2005/11/14 20:15	41.663	2.784	0
090	2005/11/15 08:58	41.239	1.976	W
091	2005/11/15 08:58	41.212	2.128	W
092	2005/11/15 14:50	41.724	0.837	0
093	2005/11/15 14:50	40.853	1.040	W
094	2006/02/19 08:45	41.102	1.495	W
095	2006/02/21 15:30	41.190	2.692	W
096	2006/02/21 16:15	41.230	2.021	W
097	2006/02/21 16:15	41.215	2.006	W
098	2006/02/21 16:15	41.223	2.014	W
099	2006/02/21 17:00	41.230	2.028	W
100	2006/08/10 18:30	41.526	2.634	W
101	2006/08/11 14:00	41.340	2.164	0
102	2006/08/14 09:19	40.686	2.518	W
103	2006/08/15 15:45	41.151	1.663	W
104	2006/08/16 06:00	40.532	0.845	W
105	2006/08/16 15:30	41.056	1.062	W
106	2006/08/16 15:55	41.095	1.320	W
107	2006/08/16 17:00	41.168	1.488	0
108	2006/09/12 07:30	41.444	2.690	W
109	2006/09/13 08:20	41.169	1.743	W
110	2006/09/13 08:50	41.589	2.592	0
111	2006/09/13 09:00	41.052	1.516	W
112	2006/09/13 09:05	41.097	1.514	W
113	2006/09/13 09:15	41.134	1.402	1
114	2006/09/13 09:30	41.196	1.497	0
115	2006/09/13 10:28	41.242	1.876	W
116	2006/09/13 10:30	41.260	1.945	W
117	2006/09/13 10:30	41.260	1.948	W
118	2006/09/13 10:30	41.229	1.971	W
119	2006/09/13 10:49	41.267	2.029	1
120	2006/09/18 09:46	41.356	2.349	W
121	2006/09/18 10:45	41.463	2.436	W
122	2006/09/18 10:45	41.456	2.469	W
123	2006/09/18 11:00	41.561	2.642	W
124	2006/09/18 11:00	41.556	2.630	W
125	2006/10/11 08:30	41.192	1.754	W
126	2006/10/11 08:30	41.182	1.734	W
127	2006/10/14 –:–	41.738	3.083	W
128	2006/10/14 –:–	40.961	0.981	W
129	2006/10/18 13:21	41.729	2.141	2
130	2007/05/01 08:00	41.202	1.723	W
131	2007/05/01 14:04	41.483	2.644	W
132	2007/05/01 14:45	41.790	3.167	W
133	2007/06/18 15:45	41.236	1.995	W
134	2007/08/12 20:00	41.232	1.864	W
135	2007/08/12 21:30	41.574	2.542	0
136	2007/08/19 10:05	41.164	1.491	W
137	2007/08/21 17:40	41.345	2.035	0
138	2007/08/22 07:30	41.206	1.870	W
139	2007/08/22 07:30	41.212	1.892	W
140	2007/08/24 11:45	40.506	0.676	W
141	2007/08/24 11:45	40.501	0.660	W
142	2007/08/24 12:00	40.933	1.395	W
143	2007/09/27 20:00	41.402	2.315	W
144	2007/10/05 04:00	41.271	1.986	0
145	2007/10/08 09:48	41.484	2.563	W
146	2007/10/10 19:50	41.092	1.949	W

(*continued on next page*)

Table A1 (*continued*)

Item (#)	Date & Time (UTC)	Lat (°)	Lon (°)	EF/W (n/W)
147	2008/03/04 12:30	41.957	2.632	0
148	2008/03/09 16:45	41.137	1.502	W
149	2008/03/09 16:45	41.135	1.494	W
150	2008/03/09 16:45	41.131	1.485	W
151	2008/04/17 15:27	41.469	2.189	0
152	2008/05/10 18:42	40.648	0.615	0
153	2008/05/11 06:20	40.749	0.937	W
154	2008/05/17 09:47	41.723	1.550	0
155	2008/05/19 15:05	41.218	1.840	W
156	2008/06/17 12:15	41.397	1.798	0
157	2008/07/12 15:50	41.044	1.248	W
158	2008/08/25 18:45	41.131	1.367	0
159	2008/09/13 18:00	41.233	2.508	W
160	2008/09/13 18:00	41.246	2.523	W
161	2008/09/13 18:00	41.252	2.485	W
162	2008/09/25 07:30	41.295	2.633	W
163	2008/09/26 10:45	41.076	1.976	W
164	2008/10/17 16:45	41.249	1.903	W
165	2008/11/01 01:45	41.686	2.816	0
166	2008/11/02 02:59	41.074	1.122	2
167	2008/11/02 03:32	41.375	1.315	3
168	2008/11/06 13:15	41.506	2.626	W
169	2009/04/01 16:30	41.127	1.727	W
170	2009/04/10 13:55	41.664	2.785	0
171	2009/04/11 14:15	41.090	1.347	W
172	2009/04/11 15:27	41.307	2.341	W
173	2009/08/09 12:30	41.397	2.237	W
174	2009/08/09 15:05	42.227	1.734	1
175	2009/08/25 15:45	41.604	0.419	0
176	2009/09/14 15:28	41.397	2.262	W
177	2009/09/14 17:04	41.257	2.072	W
178	2009/09/30 06:00	41.225	1.858	W
179	2009/09/30 06:00	41.181	2.043	W
180	2009/10/09 06:30	40.809	1.174	W
181	2009/10/09 06:30	40.817	1.177	W
182	2009/10/21 03:35	41.131	1.369	0
183	2010/04/04 15:35	41.626	2.238	0
184	2010/07/23 19:10	41.252	1.983	W
185	2010/08/12 19:00	41.138	1.472	W
186	2010/08/19 16:30	40.511	0.578	W
187	2010/09/20 07:10	41.277	2.132	W
188	2010/09/21 08:15	41.366	2.316	W
189	2010/09/26 18:00	41.461	2.326	W
190	2010/10/11 14:25	41.265	1.583	0
191	2010/10/11 15:00	41.612	1.242	0
192	2010/10/11 15:25	41.284	2.369	W
193	2010/10/11 15:45	41.232	2.030	W
194	2010/10/11 15:48	41.011	2.144	W
195	2010/10/11 16:06	41.013	1.948	W
196	2010/10/11 16:36	41.115	1.618	W
197	2010/10/11 16:54	41.061	1.502	W
198	2010/10/11 17:15	41.198	1.996	W
199	2011/04/24 09:00	40.608	0.827	W
200	2011/06/01 17:40	41.289	2.150	W
201	2011/07/12 21:50	41.134	1.380	0
202	2011/09/03 21:10	41.306	2.170	W
203	2011/09/24 05:30	41.264	1.964	0
204	2011/10/22 15:35	41.846	3.108	0
205	2011/10/22 16:34	41.839	3.125	W
206	2011/10/23 12:30	41.443	2.415	W
207	2011/11/02 15:00	41.053	1.099	W
208	2011/11/05 15:00	41.060	1.577	W
209	2011/11/05 15:00	41.053	1.563	W
210	2011/11/05 15:00	41.049	1.550	W
211	2011/11/05 15:30	41.094	1.546	W
212	2011/11/05 15:30	41.096	1.541	W
213	2011/11/05 15:30	41.100	1.533	W
214	2011/11/06 14:25	41.832	3.119	W
215	2011/12/27 14:34	41.441	2.857	W
216	2012/03/21 18:45	41.657	0.996	1
217	2012/04/06 08:00	40.983	0.923	W
218	2012/04/14 15:30	42.027	3.138	0
219	2012/04/19 15:10	41.912	3.213	W
220	2012/05/20 09:45	42.137	2.436	0
221	2012/09/02 00:00	41.216	1.830	W

(*continued on next page*)

Table A1 (*continued*)

Item (#)	Date & Time (UTC)	Lat (°)	Lon (°)	EF/W (n/W)
222	2012/10/12 17:40	41.134	1.409	W
223	2012/10/13 08:30	41.086	1.872	W
224	2012/10/21 12:54	41.031	1.129	W
225	2012/10/21 16:45	41.359	2.440	W
226	2012/10/27 16:45	41.440	2.262	W
227	2012/10/27 16:51	41.381	2.229	W
228	2012/10/27 16:55	41.307	2.168	W
229	2013/06/08 13:55	41.362	1.293	0
230	2013/06/18 13:35	41.320	0.875	0
231	2013/07/16 14:15	41.726	1.449	0
232	2013/08/08 00:49	41.294	2.431	W
233	2013/08/17 11:15	41.021	1.667	W
234	2013/08/28 14:20	41.180	1.609	W
235	2013/09/07 11:15	41.011	1.342	W
236	2013/09/10 21:06	41.287	2.139	W
237	2013/09/10 21:07	41.274	2.182	W
238	2013/09/10 21:24	41.248	2.259	W
239	2013/09/30 10:30	41.597	3.327	W
240	2013/10/06 15:05	41.384	2.359	W
241	2013/10/06 15:56	41.213	2.319	W
242	2013/10/07 06:10	40.390	1.538	W
243	2013/10/10 17:00	41.418	3.213	W
244	2013/10/19 10:15	41.037	1.513	W
245	2013/10/19 10:15	40.898	1.456	W
246	2013/11/17 10:55	41.236	2.038	W
247	2013/11/17 14:00	41.176	1.695	W
248	2014/05/30 16:36	41.253	1.321	0
249	2014/06/25 06:45	41.712	3.242	W
250	2014/07/29 14:30	41.246	2.181	W
251	2014/09/04 09:30	40.994	1.059	W
252	2014/09/05 19:05	41.560	2.267	0
253	2014/09/14 10:08	40.947	0.977	W
254	2014/09/14 10:15	40.971	0.894	0
255	2014/09/16 05:30	40.469	0.740	W
256	2014/09/16 23:40	41.387	2.274	W
257	2014/09/18 07:30	-	-	W
258	2014/09/23 12:55	42.065	2.311	0
259	2014/11/03 14:37	41.641	2.760	W
260	2014/11/26 08:45	41.115	1.550	W
261	2014/11/28 01:10	41.113	1.229	0
262	2014/12/06 13:54	41.448	2.696	W
263	2014/12/09 03:50	40.702	2.869	W
264	2014/12/09 03:50	40.697	2.849	W
265	2014/12/09 03:51	40.731	2.796	W
266	2015/01/31 23:37	41.459	3.440	W
267	2015/01/31 23:38	41.459	3.481	W
268	2015/02/01 00:17	41.308	3.657	W
269	2015/02/01 00:51	41.082	3.995	W
270	2015/06/13 18:10	41.078	1.305	W
271	2015/08/13 16:30	41.349	2.379	W
272	2015/08/15 14:44	41.553	2.664	W
273	2015/08/16 05:15	40.601	1.707	W
274	2015/09/06 22:30	41.243	2.049	W
275	2015/09/10 11:30	41.153	1.525	W
276	2015/09/11 09:00	40.931	1.094	W
277	2015/10/09 07:10	40.635	1.254	W
278	2015/11/02 15:28	41.022	0.959	1
279	2015/11/02 18:00	41.387	1.186	0
280	2016/02/27 04:30	41.234	1.807	0
281	2016/02/27 05:10	41.611	2.658	0
282	2016/02/27 17:45	41.315	2.194	W
283	2016/03/07 02:38	41.286	2.900	W
284	2016/03/21 15:45	41.456	1.814	0
285	2016/06/16 18:40	41.947	3.239	W
286	2016/08/09 21:30	40.710	1.100	W
287	2016/08/09 21:30	40.699	1.072	W
288	2016/09/08 10:45	40.584	1.242	W
289	2016/09/10 01:00	41.615	2.673	0
290	2016/09/10 06:30	40.545	0.871	W
291	2016/09/10 06:33	40.532	0.865	W
292	2016/09/10 06:45	40.525	0.867	W
293	2016/09/14 08:15	41.999	3.270	W
294	2016/09/15 18:03	41.564	3.175	W
295	2016/09/21 05:25	41.481	2.418	W
296	2016/09/23 06:45	40.551	0.782	W

(*continued on next page*)

Table A1 (*continued*)

Item (#)	Date & Time (UTC)	Lat (°)	Lon (°)	EF/W (n/W)
297	2016/09/24 09:00	41.725	3.111	W
298	2016/10/02 08:15	41.255	2.103	W
299	2016/10/03 09:45	40.921	1.358	W
300	2016/10/13 08:00	40.960	1.121	W
301	2016/10/13 08:00	40.945	1.142	W
302	2016/10/13 09:15	41.096	1.751	W
303	2016/10/13 12:00	41.037	1.435	W
304	2016/10/13 15:30	41.638	2.414	1
305	2016/10/13 16:58	41.118	0.746	0
306	2016/10/14 16:45	41.681	2.943	W
307	2016/10/14 16:45	41.680	2.934	W
308	2016/10/14 16:50	41.754	3.083	W
309	2016/10/14 16:50	41.755	3.077	W
310	2016/11/05 17:06	42.022	1.997	1
311	2016/11/07 10:00	41.185	2.361	W
312	2016/11/07 10:00	41.220	2.408	W
313	2016/11/07 10:00	41.218	2.422	W
314	2016/11/23 14:30	41.171	1.659	W
315	2016/11/23 16:12	41.522	2.428	0
316	2016/11/26 08:15	41.245	2.112	W
317	2016/11/26 09:15	41.259	2.275	W
318	2016/11/26 15:09	41.143	1.931	W
319	2016/11/26 16:10	41.098	1.793	W
320	2016/11/26 16:21	41.110	1.766	W
321	2016/11/26 16:32	41.110	1.783	W
322	2016/11/26 16:42	41.138	1.743	W
323	2016/11/26 17:18	41.196	1.681	W
324	2016/11/27 11:03	41.212	1.981	W
325	2016/11/27 11:04	41.196	1.723	W
326	2016/12/04 13:51	40.747	0.661	0
327	2017/01/25 15:55	41.120	1.394	W
328	2017/03/24 10:59	40.749	1.104	W
329	2017/03/24 11:06	40.755	1.116	W
330	2017/03/24 11:15	40.727	1.126	W
331	2017/06/29 10:10	41.821	3.258	W
332	2017/08/10 21:06	41.367	2.425	W
333	2017/09/16 07:43	41.447	2.779	W
334	2017/09/16 21:51	41.135	2.226	W
335	2017/09/22 09:00	41.288	2.284	W
336	2017/10/18 16:00	41.263	1.246	1
337	2017/11/04 10:15	40.944	0.918	W
338	2017/11/04 16:30	41.155	1.457	W
339	2017/12/01 13:25	41.554	0.809	0
340	2017/12/01 16:05	40.985	1.760	W
341	2017/12/01 16:05	41.028	1.786	W
342	2017/12/01 16:25	40.956	1.813	W
343	2017/12/01 16:25	40.951	1.800	W
344	2017/12/01 16:50	41.046	1.807	W
345	2017/12/01 16:50	41.054	1.817	W
346	2017/12/12 15:30	41.085	2.504	W
347	2018/01/07 00:53	41.903	1.702	2
348	2018/01/07 07:22	42.209	2.858	2
349	2018/01/07 09:00	41.581	2.210	0
350	2018/02/04 14:40	40.995	0.929	0
351	2018/02/05 07:30	41.218	1.828	W
352	2018/02/08 16:10	41.103	1.524	W
353	2018/02/12 15:52	41.109	1.320	W
354	2018/03/07 06:13	41.227	2.927	W
355	2018/03/07 06:13	41.206	2.919	W
356	2018/03/07 06:13	41.172	2.901	W
357	2018/03/07 06:22	41.170	2.967	W
358	2018/03/07 06:25	41.121	3.032	W
359	2018/03/07 06:25	41.031	3.046	W
360	2018/03/07 06:35	41.039	3.137	W
361	2018/03/07 06:35	40.956	3.112	W
362	2018/03/13 08:20	41.585	2.604	W
363	2018/04/13 08:30	41.097	1.160	0
364	2018/05/28 10:35	40.707	0.714	0
365	2018/05/29 04:55	41.512	2.451	W
366	2018/06/06 11:40	41.505	2.610	W
367	2018/06/06 11:40	41.485	2.626	W
368	2018/06/06 13:20	41.758	3.150	W
369	2018/06/06 13:20	41.755	3.141	W
370	2018/06/07 09:27	41.564	3.490	W
371	2018/07/16 06:55	41.383	2.205	W

(*continued on next page*)

Table A1 (*continued*)

Item (#)	Date & Time (UTC)	Lat (°)	Lon (°)	EF/W (n/W)
372	2018/07/16 07:00	41.369	2.180	W
373	2018/08/08 09:00	40.753	1.003	W
374	2018/08/12 18:30	41.153	1.552	W
375	2018/08/17 08:30	40.982	2.261	W
376	2018/08/17 08:30	40.963	2.232	W
377	2018/08/17 08:30	40.950	2.214	W
378	2018/08/17 12:40	41.465	2.340	W
379	2018/08/17 13:45	41.188	1.577	0
380	2018/09/01 17:20	41.186	1.500	0
381	2018/10/08 16:56	41.424	2.281	W
382	2018/10/09 05:47	41.242	2.314	W
383	2018/10/09 05:50	41.181	2.351	W
384	2018/10/09 05:53	41.213	2.385	W
385	2018/10/09 07:28	41.326	2.177	W
386	2018/10/09 09:48	41.249	1.908	W
387	2018/10/09 22:39	41.860	2.659	0
388	2018/10/10 11:17	40.793	0.962	W
389	2018/10/10 11:27	40.823	0.969	W
390	2018/10/10 11:34	40.866	1.010	W
391	2018/10/10 12:01	40.920	1.125	W
392	2018/10/14 19:55	41.165	1.260	1
393	2018/10/14 23:30	41.180	1.253	0
394	2018/10/15 01:39	41.636	2.729	1
395	2018/11/15 07:07	41.571	1.982	0
396	2018/11/15 09:40	41.326	2.202	W
397	2019/04/07 13:45	41.585	2.659	W
398	2019/04/07 13:47	41.576	2.671	W
399	2019/04/07 13:47	41.568	2.672	W
400	2019/04/24 06:56	41.255	2.322	W
401	2019/08/15 22:16	41.381	2.194	0
402	2019/08/27 10:05	41.288	2.232	W
403	2019/08/27 11:54	41.208	1.716	W
404	2019/08/27 12:32	41.051	1.173	W
405	2019/08/27 12:35	41.089	1.215	W
406	2019/08/27 13:05	40.767	0.851	W
407	2019/09/07 11:15	41.105	1.844	W
408	2019/09/08 08:24	41.229	2.239	W
409	2019/09/08 11:28	41.093	2.149	W
410	2019/09/08 14:35	41.280	2.084	0
411	2019/09/08 14:40	41.312	2.091	0
412	2019/09/08 15:47	41.342	2.150	0
413	2019/09/08 16:15	41.331	2.161	0
414	2019/09/08 16:45	41.299	2.164	W
415	2019/09/09 21:59	41.367	2.407	W
416	2019/09/09 22:03	41.316	2.339	W
417	2019/09/09 22:18	41.409	2.463	W
418	2019/09/09 22:43	41.321	2.410	W
419	2019/09/10 08:30	40.756	1.530	W
420	2019/09/10 08:30	40.748	1.516	W
421	2019/09/10 15:45	41.107	0.675	0
422	2019/09/28 07:00	40.994	1.592	W
423	2019/10/16 06:00	42.387	3.376	W
424	2019/10/20 03:35	41.465	2.280	0
425	2019/10/21 08:45	41.332	2.349	W
426	2019/10/21 09:37	41.353	2.407	W
427	2019/10/22 13:47	40.982	0.994	W
428	2019/10/22 23:53	41.710	2.533	2
429	2019/10/23 11:22	41.240	1.995	W
430	2019/10/23 11:59	41.260	2.010	W
431	2019/10/23 13:45	41.833	3.173	W
432	2019/10/23 16:39	41.195	1.830	W
433	2019/11/08 02:32	41.222	3.052	W
434	2019/11/14 14:05	41.473	2.485	W

References

Altube, P., Bech, J., Argemí, O., Rigo, T., 2015. Quality control of Antenna alignment and receiver calibration using the sun: Adaptation to Midrange Weather Radar observations at low elevation angles. J. Atmos. Ocean. Technol. 32, 927–942. https://doi.org/10.1175/JTECH-D-14-00116.1.

Altube, P., Bech, J., Argemí, O., Rigo, T., Pineda, N., Collis, S., Helmus, J., 2017. Correction of dual-PRF Doppler velocity outliers in the presence of aliasing. J. Atmos. Ocean. Technol. 34 (7), 1529–1543. https://doi.org/10.1175/JTECH-D-16-0065.1.

AMS, 2020. Glossary of Meteorology. American Meteorological Society. http://glossary.ametsoc.org (last access 4 November 2020).

Antonescu, B., Schultz, D.M., Lomas, F., Kühne, T., 2016. Tornadoes in Europe: synthesis of the observational datasets. Mon. Weather Rev. 144, 2445–2480. https://doi.org/10.1175/MWR-D-15-0298.1.

Antonescu, B., Schultz, D.M., Holzer, A., Groenemeijer, P., 2017. Tornadoes in Europe: an underestimated threat. Bull. Am. Meteorol. Soc. 98, 713–728. https://doi.org/10.1175/BAMS-D-16-0171.1.

Antonescu, B., Ricketts, H.M., Schultz, D.M., 2019. 100 years later: reflecting on Alfred Wegener's contributions to Tornado research in Europe. Bull. Am. Meteorol. Soc. 100, 567–578. https://doi.org/10.1175/BAMS-D-17-0316.1.

Antonescu, B., Púčik, T., Schultz, D.M., 2020. Hindcasting the first Tornado forecast in Europe: 25 June 1967. Weather Forecast. 35, 417–436. https://doi.org/10.1175/WAF-D-19-0173.1.

Apsley, M.L., Mulder, K.J., Schultz, D.M., 2016. Reexamining the United Kingdom's Greatest Tornado outbreak: forecasting the limited extent of Tornadoes along a cold front. Weather Forecast. 31, 853–875. https://doi.org/10.1175/WAF-D-15-0131.1.

Aran, M., Amaro, J., Arús, J., Bech, J., Figuerola, F., Gayà, M., Vilaclara, E., 2009. Synoptic and mesoscale diagnosis of a tornado event in Castellcir, Catalonia, on 18th October 2006. Atmos. Res. 93 (1–3), 147–160. https://doi.org/10.1016/j.atmosres.2008.09.031.

Barredo, J.L., Saurí, D., Llasat, M.C., 2012. Assessing trends in insured losses from floods in Spain 1971–2008. Nat. Hazards Earth Syst. Sci. 12, 1723–1729. https://doi.org/10.5194/nhess-12-1723-2012.

Bech, J., Pascual, R., Rigo, T., Pineda, N., López, J.M., Arús, J., Gayà, M., 2007. An observational study of the 7 September 2005 Barcelona tornado outbreak. Nat. Hazards Earth Syst. Sci. 7 (1), 129–139. https://doi.org/10.5194/nhess-7-129-2007.

Bech, J., Gayà, M., Aran, M., Figuerola, F., Amaro, J., Arús, J., 2009. Tornado damage analysis of a forest area using site survey observations, radar data and a simple analytical vortex model. Atmos. Res. 93 (1–3), 118–130. https://doi.org/10.1016/j.atmosres.2008.10.016.

Bech, J., Pineda, N., Rigo, T., Aran, M., Amaro, J., Gayà, M., Arús, J., Montanyà, J., van der Velde, O., 2011. A Mediterranean nocturnal heavy rainfall and tornadic event. Part I: Overview, damage survey and radar analysis. Atmos. Res. 100 (4), 621–637. https://doi.org/10.1016/j.atmosres.2010.12.024.

Bech, J., Arús, J., Castán, S., Pineda, N., Rigo, T., Montanyà, J., van der Velde, O., 2015. A study of the 21 March 2012 tornadic quasi linear convective system in Catalonia. Atmos. Res. 158–159, 192–209. https://doi.org/10.1016/j.atmosres.2014.08.009.

Bech, J., Rodríguez, O., Altube, P., Rigo, T., Pineda, N., Castán, S., Arús, J., Montanyà, J., 2018. Doppler radar observations of two tornadic thunderstorm cases in the Western Mediterranean region. In: 10th European Conference on Radar in Meteorology and Hydrology, p. 111. https://doi.org/10.18174/454537.

Brooks, H.E., 2004. On the relationship of tornado path length and width to intensity. Weather Forecast. 19, 310–319. https://doi.org/10.1175/1520-0434(2004)019<0310:OTROTP>2.0.CO;2.

Brooks, H.E., Lee, J.W., Craven, J.P., 2003. The spatial distribution of severe thunderstorm and tornado environments from global reanalysis data. Atmos. Res. 67–68, 73–94. https://doi.org/10.1016/S0169-8095(03)00045-0.

Brown, S., Archer, P., Kruger, E., Mallonee, S., 2002. Tornado-related deaths and injuries in Oklahoma due to the 3 May 1999 Tornadoes. Weather Forecast. 17, 343–353. https://doi.org/10.1175/1520-0434(2002)017<0343:TRDAII>2.0.CO;2.

Bunting, W.F., Smith, B.E., 1993. A guide for conducting damage surveys. In: NOAA Tech. Memo. NWS-SR-146, Scientific Services Division, Southern Region, Fort Worth, TX (44 pp).

Callado, A., Pascual, R., 2005. Diagnosis and modelling of a summer convective storm over Mediterranean Pyrenees. Adv. Geosci. 2, 273–277. https://doi.org/10.5194/adgeo-2-273-2005.

Calvo-Sancho, C., Martín, Y., 2020. The influence of synoptic weather patterns in supercell formation in Spain. In: EGU General Assembly Conference Abstracts, p. 40.

Chen, J., Cai, X., Wang, H., Kang, L., Zhang, H., Song, Y., Zhu, H., Zheng, W., Li, F., 2018. Tornado climatology of China. Int. J. Climatol. 38 (5), 2478–2489. https://doi.org/10.1002/joc.5369.

Chernokulsky, A., Shikhov, A., 2018. 1984 Ivanovo tornado outbreak: Determination of actual tornado tracks with satellite data. Atmos. Res. 207, 111–121. https://doi.org/10.1016/j.atmosres.2018.02.011.

Chernokulsky, A., Kurgansky, M., Mokhov, I., Shikhov, A., Azhigov, I., Selezneva, E., Zakharchenko, D., Antonescu, B., Kühne, T., 2020. Tornadoes in Northern Eurasia: from the Middle age to the information era. Mon. Weather Rev. 148 (8), 3081–3110. https://doi.org/10.1175/MWR-D-19-0251.1.

Cortès, M., Turco, M., Llasat-Botija, M., Llasat, M.C., 2018. The relationship between precipitation and insurance data for floods in a Mediterranean region (Northeast Spain). Nat. Hazards Earth Syst. Sci. 18, 857–868. https://doi.org/10.5194/nhess-18-857-2018.

del Moral, A., Llasat, M.C., Rigo, T., 2017. Identification of anomalous motion of thunderstorms using daily rainfall fields. Atmos. Res. 185, 92–100. https://doi.org/10.1016/j.atmosres.2016.11.001.

del Moral, A., Weckwerth, T.M., Rigo, T., Bell, M.M., Llasat, M.C., 2020a. C-Band Dual-Doppler retrievals in complex Terrain: improving the knowledge of severe storm dynamics in Catalonia. Remote Sens. 12 (18), 2930. https://doi.org/10.3390/rs12182930.

del Moral, A., Llasat, M.C., Rigo, T., 2020b. Connecting flash flood events with radar-derived convective storm characteristics on the Northwestern Mediterranean coast: knowing the present for better future scenarios adaptation. Atmos. Res. 238, 104863. https://doi.org/10.1016/j.atmosres.2020.104863.

Donner, W.R., 2007. The political ecology of disaster: An analysis of factors influencing U.S. tornado fatalities and injuries, 1998–2000. Demography 44 (3), 669–685. https://doi.org/10.1353/dem.2007.0024.

Doswell III, C.A., Brooks, H.E., Dotzek, N., 2009. On the implementation of the enhanced Fujita scale in the USA. Atmos. Res. 93, 554–563. https://doi.org/10.1016/j.atmosres.2008.11.003.

Dotzek, N., Groenemeijer, P., Feuerstein, B., Holzer, A.M., 2009. Overview of ESSL's severe convective storms research using the European Severe Weather Database ESWD. Atmos. Res. 93, 575–586. https://doi.org/10.1016/j.atmosres.2008.10.020.

Edwards, R., LaDue, J.G., Ferree, J.T., Scharfenberg, K., Maier, C., Coulbourne, W.L., 2013. Tornado intensity estimation: past, present, and future. Bull. Am. Meteorol. Soc. 94 (5), 641–653. https://doi.org/10.1175/BAMS-D-11-00006.1.

Eidson, M., Lybarger, J.A., Parsons, J.E., Maccormack, J.N., Freeman, J.I., 1990. Risk factors for Tornado injuries. Int. J. Epidemiol. 19 (4), 1051–1056. https://doi.org/10.1093/ije/19.4.1051.

Farnell, C., Busto, M., Aran, M., Andrés, A., Pineda, N., Torà, M., 2009. Study of the hailstorm of 17 September 2007 at the Pla d'Urgell. Part one: fieldwork and analysis of hailpads. Tethys 6, 67–79. https://doi.org/10.3369/tethys.2009.6.05.

Farnell, C., Rigo, T., Pineda, N., 2017. Lightning jump as a nowcast predictor: Application to severe weather events in Catalonia. Atmos. Res. 183, 130–141. https://doi.org/10.1016/j.atmosres.2016.08.021.

Fujita, T.T., 1981. Tornadoes and downbursts in the context of generalized planetary scales. J. Atmos. Sci. 38 (8), 1511–1534. https://doi.org/10.1175/1520-0469(1981)038<1511:TADITC>2.0.CO;2.

Galway, J.G., 1975. Relationship of Tornado deaths to severe weather watch areas. Mon. Weather Rev. 103, 737–741. https://doi.org/10.1175/1520-0493(1975)103<0737:ROTDTS>2.0.CO;2.

Galway, J.G., 1977. Some climatological aspects of tornado outbreaks. Mon. Weather Rev. 105, 477–484. https://doi.org/10.1175/1520-0493(1977)105<0477:SCAOTO>2.0.CO;2.

Gayà, M., 2007. The 1886 tornado of Madrid. Atmos. Res. 83 (2–4), 201–210. https://doi.org/10.1016/j.atmosres.2005.10.017.

Gayà, M., 2018. Els Fiblons a Espanya: Climatologia i catàleg de Tornados i Trombes (Whirlwinds in Spain: Climatology and Catalogue of Tornadoes and Waterspouts), Second edition. Universitat de les Illes Balears. (619 pp. in Catalan).

Gayà, M., Llasat, M.C., Arús, J., 2011. Tornadoes and waterspouts in Catalonia (1950–2009). Nat. Hazards Earth Syst. Sci. 11, 1875–1883. https://doi.org/10.5194/nhess-11-1875-2011.

Goliger, A.M., Milford, R.V., 1998. A review of worldwide occurrence of tornadoes. J. Wind Eng. Ind. Aerodyn. 74–76, 111–121. https://doi.org/10.1016/S0167-6105(98)00009-9.

Gonzalez, S., Callado, A., Werner, E., Escribà, P., Bech, J., 2018. Coastally trapped disturbances caused by the tramontane wind on the northwestern Mediterranean: numerical study and sensitivity to short-wave radiation. Q. J. R. Meteorol. Soc. 144 (714), 1321–1336. https://doi.org/10.1002/qj.3320.

Grasso, V., Zaza, I., Zabini, F., Pantaleo, G., Nesi, P., Crisci, A., 2017. Weather events identification in social media streams: tools to detect their evidence in Twitter. Peer J. Preprints 5. https://doi.org/10.7287/peerj.preprints.2241v2 e2241v2.

Grieser, J., Haines, P., 2020. Tornado risk climatology in Europe. Atmosphere 11 (7), 768. https://doi.org/10.3390/atmos11070768.

Groenemeijer, P., Kühne, T., 2014. A climatology of Tornadoes in Europe: results from the European severe weather database. Mon. Weather Rev. 142, 4775–4790. https://doi.org/10.1175/MWR-D-14-00107.1.

Gutiérrez, D., Riesco, J., Ponce, S., 2015. SINOBAS, a tool for collaborative mapping applied to observation of "singular" weather phenomena. In: 15th EMS Annual Meeting & 12th European Conference on Applications of Meteorology: EMS2015-413.

Hagemeyer, B.C., 1997. Peninsular florida Tornado outbreaks. Weather Forecast. 12, 399–427. https://doi.org/10.1175/1520-0434(1997)012<0399:PFTO>2.0.CO;2.

Holzer, A.M., Schreiner, T.M.E., Púčik, T., 2018. Forensic re-analysis of one of the deadliest European tornadoes. Nat. Hazards Earth Syst. Sci. 18, 1555–1565. https://doi.org/10.5194/nhess-18-1555-2018.

Homar, V., Romero, R., Ramis, C., Alonso, S., 2002. Numerical study of the October 2000 torrential precipitation event over eastern Spain: analysis of the synoptic-scale stationarity. Ann. Geophys. 20, 2047–2066.

Homar, V., Gayà, M., Romero, R., Ramis, S., Alonso, S., 2003. Tornadoes over complex terrain: an analysis of the 28th August 1999 tornadic event in eastern Spain. Atmos. Res. 67–68, 301–317. https://doi.org/10.1016/S0169-8095(03)00064-4.

Hyvärinen, O., Saltikoff, E., 2010. Social media as a source of meteorological observations. Mon. Weather Rev. 138, 3175–3184. https://doi.org/10.1175/2010MWR3270.1.

IDESCAT, 2020. Official Statistics of Catalonia. https://www.idescat.cat/?lang=en (last access 21 August 2020).

Kahraman, A., Markowski, P.M., 2014. Tornado climatology of Turkey. Mon. Weather Rev. 142, 2345–2352. https://doi.org/10.1175/MWR-D-13-00364.1.

Karstens, C.D., Samaras, T.M., Gallus, W.A., Finley, C.A., Lee, B.D., 2010. Analysis of near-surface wind flow in close proximity to tornadoes. In: 25th Conference on Severe Local Storms. P10.12. Available online at. http://ams.confex.com/ams/pdfpapers/176188.pdf.

Kirk, P.J., 2014. An updated tornado climatology for the UK: 1981–2010. Weather 69 (7), 171–175.

Koch, P., Wernli, H., Davies, H.C., 2006. An event-based jet-stream climatology and typology. Int. J. Climatol. 26 (3), 283–301. https://doi.org/10.1002/joc.1255.

Kühne, T., Kollmohr, A., Hubrig, M., Sävert, T., Schlenczek, O., Simon, W., Wichmann, H., 2017. Statistical analysis of the spatial and temporal distribution of tornadoes in Germany. In: 9th European Conference on Severe Storms: ECSS2017-132.

Leitão, P., Pinto, P., 2020. Tornadoes in Portugal: an overview. Atmosphere 11, 679. https://doi.org/10.3390/atmos11070679.

López, J.M., 2007. A Mediterranean derecho: Catalonia (Spain), 17th August 2003. Atmos. Res. 83 (2–4), 272–283. https://doi.org/10.1016/j.atmosres.2005.08.008.

Mahieu, P., Wesolek, E., 2016. Tornado Rating in Europe with the EF-scale, KERAUNOS, 65 pp., available at. http://www.keraunos.org/tornado-rating-in-europe-with-the-enhanced-fujita-scale.pdf (last access: 20 August 2020).

Markowski, P.M., Richardson, Y.P., 2009. Tornadogenesis: our current understanding, forecasting considerations, and questions to guide future research. Atmos. Res. 93 (1–3), 3–10. https://doi.org/10.1016/j.atmosres.2008.09.015.

Martín, Y., Cívica, M., Pham, E., 2020. Constructing a supercell database in Spain using publicly available two-dimensional radar images and citizen science. Ann. Am. Assoc. Geogr. 1–21 https://doi.org/10.1080/24694452.2020.1812371 (In press).
Martínez-Gomariz, E., Guerrero-Hidalga, M., Russo, B., Yubero, D., Gómez, M., Castán, S., 2019. Development and application of depth damage and sealing coefficient curves to estimate urban flooding economic impact on Spanish urban areas. Ingeniería del Agua 23 (4), 229–245. https://doi.org/10.4995/ia.2019.12137.
Martínez-Gomariz, E., Forero-Ortiz, E., Guerrero-Hidalga, M., Castán, S., Gómez, M., 2020. Flood depth-damage curves for Spanish Urban areas. Sustainability 12 (7), 2666. https://doi.org/10.3390/su12072666.
Mateo, J., Ballart, D., Brucet, C., Aran, M., Bech, J., 2009. A study of a heavy rainfall event and a tornado outbreak during the passage of a squall line over Catalonia. Atmos. Res. 93 (1–3), 131–146. https://doi.org/10.1016/j.atmosres.2008.09.030.
Matsangouras, I.T., Pytharoulis, I., Nastos, P.T., 2014a. Numerical modeling and analysis of the effect of complex Greek topography on tornadogenesis. Nat. Hazards Earth Syst. Sci. 14 (7), 1905–1919. https://doi.org/10.5194/nhess-14-1905-2014.
Matsangouras, I.T., Nastos, P.T., Bluestein, H.B., Sioutas, M.V., 2014b. A climatology of tornadic activity over Greece based on historical records. Int. J. Climatol. 34 (8), 2538–2555. https://doi.org/10.1002/joc.3857.
Matsangouras, I.T., Nastos, P.T., Pytharoulis, I., 2016. Study of the tornado event in Greece on March 25, 2009: Synoptic analysis and numerical modeling using modified topography. Atmos. Res. 169 (B), 566–583. https://doi.org/10.1016/j.atmosres.2015.08.010.
Matsangouras, I.T., Nastos, P.T., Bluestein, H.B., Pytharoulis, I., Papachristopoulou, K., Miglietta, M.M., 2017. Analysis of waterspout environmental conditions and of parent-storm behaviour based on satellite data over the southern Aegean Sea of Greece. Int. J. Climatol. 37 (2), 1022–1039. https://doi.org/10.1002/joc.4757.
Miglietta, M.M., 2019. Waterspouts: a Review. Reference Module in Earth Systems and Environmental Sciences. https://doi.org/10.1016/B978-0-12-409548-9.12414-5.
Miglietta, M.M., Matsangouras, I.T., 2018. An updated "climatology" of tornadoes and waterspouts in Italy. Int. J. Climatol. 38, 3667–3683. https://doi.org/10.1002/joc.5526.
Miglietta, M.M., Rotunno, R., 2016. An EF3 multivortex tornado over the ionian region: is it time for a dedicated warning system over italy? Bull. Am. Meteorol. Soc. 97, 337–344. https://doi.org/10.1175/BAMS-D-14-00227.1.
Miglietta, M.M., Arai, K., Kusunoki, K., Inoue, H., Adachi, T., Niino, H., 2020. Observational analysis of two waterspouts in northwestern Italy using an OPERA Doppler radar. Atmos. Res. 234, 104692. https://doi.org/10.1016/j.atmosres.2019.104692.
Molthan, A.L., Bell, J.R., Cole, T.A., Burks, J.E., 2014. Satellite-based identification of tornado damage tracks from the 27 April 2011 severe weather outbreak. J. Oper. Meteor. 2 (16), 191–208. https://doi.org/10.15191/nwajom.2014.0216.
Molthan, A.L., Schultz, L.A., McGrath, K.M., Burks, J.E., Camp, J.P., Angle, K., Bell, J.R., Jedlovec, G.J., 2020. Incorporation and use of earth remote sensing imagery within the NOAA/NWS damage assessment toolkit. Bull. Am. Meteorol. Soc. 101, E323–E340 (doi.10.1175).
NOAA/SPC, 2019. U.S. Tornadoes (1950–2018). https://www.spc.noaa.gov/wcm/ (last access 17 February 2020).
Pastor, F., Valiente, J.A., Palau, J.L., 2018. Sea surface temperature in the mediterranean: trends and spatial patterns (1982–2016). Pure Appl. Geophys. 175 (11), 4017–4029. https://doi.org/10.1007/978-3-030-11958-4_18.
Pautz, M.E., 1969. Severe Local Storms Occurrences, 1955–1967. ESSA Tech. Memo. WBTM FCST12, Washington, DC (77 pp).
Peña, J.C., Aran, M., Cunillera, J., Amaro, J., 2011. Atmospheric circulation patterns associated with strong wind events in Catalonia. Nat. Hazards Earth Syst. Sci. 11, 145–155. https://doi.org/10.5194/nhess-11-145-2011.
Pineda, N., Montanyà, J., 2009. Lightning detection in Spain: The particular case of Catalonia. In: Betz, H.-D., Schumann, U., Laroche, P. (Eds.), Lightning: Principles, Instruments and Applications. Springer, pp. 161–185.
Pineda, N., Soler, X., 2015. The influence of the Mediterranean Sea on the annual lightning distribution in Catalonia. In: 5th International Conference on Meteorology and Climatology of the Mediterranean, pp. 36–37.
Pineda, N., Bech, J., Rigo, T., Montanyà, J., 2011. A Mediterranean nocturnal heavy rainfall and tornadic event. Part II: Total lightning analysis. Atmos. Res. 100 (4), 638–648. https://doi.org/10.1016/j.atmosres.2010.10.027.
Potvin, C.K., Broyles, C., Skinner, P.S., Brooks, H.E., Rasmussen, E., 2019. A Bayesian hierarchical modeling framework for correcting reporting bias in the U.S. Tornado database. Weather Forecast. 34, 15–30. https://doi.org/10.1175/WAF-D-18-0137.1.
Ramis, C., López, J., Arús, J., 1999. Two cases of severe weather in Catalonia (Spain). A diagnostic study. Meteorol. Appl. 6 (1), 11–27. https://doi.org/10.1017/S1350482799000869.
Rauhala, J., Brooks, H.E., Schultz, D.M., 2012. Tornado climatology of Finland. Mon. Weather Rev. 140, 1446–1456. https://doi.org/10.1175/MWR-D-11-00196.1.
Renko, T., Kuzmić, J., Šoljan, V., Mahović, N.S., 2016. Waterspouts in the Eastern Adriatic from 2001 to 2013. Nat. Hazards 82, 441–470. https://doi.org/10.1007/s11069-016-2192-5.
Rhee, D.M., Lombardo, F.T., 2018. Improved near-surface wind speed characterization using damage patterns. J. Wind Eng. Ind. Aerodyn. 180, 288–297. https://doi.org/10.1016/j.jweia.2018.07.017.
Rigo, T., Farnell, C., 2019. Using maximum Vertical Integrated Liquid (VIL) maps for identifying hail-affected areas: an operative application for agricultural purposes. Tethys 16, 15–24. https://doi.org/10.3369/tethys.2019.16.02.
Ripoll, R., del Amo, X., Vendrell, R., 2016. The weather observers network of the Meteorological Service of Catalonia. In: WMO Technical Conference on Meteorological and Environmental Instruments and Methods of Observation (CIMO TECO 2016). P2(57).
Rodríguez, O., Bech, J., 2018. Sounding-derived parameters associated with tornadic storms in Catalonia. Int. J. Climatol. 38, 2400–2414 (doi.1002/joc.5343).
Rodríguez, O., Bech, J., 2020a. Tornadic environments in the Iberian Peninsula and the Balearic Islands based on ERA5 reanalysis. Int. J. Climatol. 1–21 https://doi.org/10.1002/joc.6825 (In press).
Rodríguez, O., Bech, J., 2020b. Reanalysing strong-convective wind damage paths using high-resolution aerial images. Nat. Hazards 104, 1021–1038. https://doi.org/10.1007/s11069-020-04202-6.
Rodríguez, O., Bech, J., Castán, S., Arús, J., 2018. El Tornado del 7 de Gener de 2018: de l'Alt Empordà al Rosselló. Treball de Camp i anàlisi de les Destrosses (the 7 January 2018 Tornado: From Alt Empordà to Rosselló. Fieldwork and Damage Analysis). XXIV Jornades de Meteorologia Eduard Fontserè, p. 140 (in Catalan).
Rodríguez, O., Bech, J., Soriano, J.D., Gutiérrez, D., Castán, S., 2020. A methodology to conduct wind damage field surveys for high-impact weather events of convective origin. Nat. Hazards Earth Syst. Sci. 20 (5), 1513–1531. https://doi.org/10.5194/nhess-20-1513-2020.
Romanic, D., Refan, M., Wu, C.H., Michel, G., 2016. Oklahoma tornado risk and variability: a statistical model. Int. J. Disast. Risk Re. 16, 19–32. https://doi.org/10.1016/j.ijdrr.2016.01.011.
Romero, R., Doswell, C.A., Ramis, C., 2000. Mesoscale numerical study of two cases of long-lived quasi-stationary convective systems over Eastern Spain. Mon. Weather Rev. 128, 3731–3751. https://doi.org/10.1175/1520-0493(2001)129<3731:MNSOTC>2.0.CO;2.
Saltikoff, E., Tuovinen, J.P., Kotro, J., Kuitunen, T., Hohti, H., 2010. A climatological comparison of radar and ground observations of hail in Finland. J. Appl. Meteorol. Climatol. 49 (1), 101–114. https://doi.org/10.1175/2009JAMC2116.1.
Schuster, S.S., Blong, R.J., Speer, M.S., 2005. A hail climatology of the greater Sydney area and New South Wales, Australia. Int. J. Climatol. 25 (12), 1633–1650. https://doi.org/10.1002/joc.1199.
Shikhov, A., Chernokulsky, A., 2018. A satellite-derived climatology of unreported tornadoes in forested regions of Northeast Europe. Remote Sens. Environ. 204, 553–567. https://doi.org/10.1016/j.rse.2017.10.002.
Sioutas, M.V., 2011. A tornado and waterspout climatology for Greece. Atmos. Res. 100 (4), 344–356. https://doi.org/10.1016/j.atmosres.2010.08.011.
Sioutas, M., Doe, R.K., 2019. Significant tornado and strong waterspout climatology of Greece. In: 10th European Conference on Severe Storms: ECSS2019-214.
Sioutas, M., Szilagyi, W., Keul, A., 2013. Waterspout outbreaks over areas of Europe and North America: Environment and predictability. Atmos. Res. 123, 167–179. https://doi.org/10.1016/j.atmosres.2012.09.013.
Taszarek, M., Brooks, H.E., Czernecki, B., 2017. Sounding-derived parameters associated with convective hazards in Europe. Mon. Weather Rev. 145, 1511–1528. https://doi.org/10.1175/MWR-D-16-0384.1.
Taszarek, M., Allen, J.T., Púčik, T., Hoogewind, K.A., Brooks, H.E., 2020. Severe convective storms across Europe and the United States. Part II: ERA5 environments associated with Lightning, large hail, severe wind, and tornadoes. J. Clim. 33, 10263–10286. https://doi.org/10.1175/JCLI-D-20-0346.1.
Verbout, S.M., Brooks, H.E., Leslie, L.M., Schultz, D.M., 2006. Evolution of the U.S. Tornado Database: 1954–2003. Weather Forecast. 21, 86–93. https://doi.org/10.1175/WAF910.1.
Wakimoto, R.M., Wilson, J.W., 1989. Non-supercell tornadoes. Mon. Weather Rev. 117 (6), 1113–1140. https://doi.org/10.1175/1520-0493(1989)117<1113:NST>2.0.CO;2.
Wegener, A., 1917. Wind- Und Wasserhosen in Europa (Tornadoes and Waterspouts in Europe). Vieweg (301 pp).
Wilson, J., Carbone, R., Baynton, H., Serafin, R., 1980. Operational application of meteorological doppler radar. Bull. Am. Meteorol. Soc. 61, 1154–1168. https://doi.org/10.1175/1520-0477(1980)061<1154:OAOMDR>2.0.CO;2.
WSEC, 2006. A Recommendation for an Enhanced Fujita Scale (EF-scale). http://www.spc.noaa.gov/faq/tornado/EFScale.pdf (last access 21 August 2020).
Wurman, J., Kosiba, K., Robinson, P., Marshall, T., 2014. The role of multiple-vortex tornado structure in causing storm researcher fatalities. Bull. Am. Meteorol. Soc. 95 (1), 31–45. https://doi.org/10.1175/BAMS-D-13-00221.1.
Zrnić, D.S., Burgess, D.W., Hennington, L.D., 1985. Automatic detection of mesocyclonic shear with doppler radar. J. Atmos. Ocean. Technol. 2, 425–438. https://doi.org/10.1175/1520-0426(1985)002<0425:ADOMSW>2.0.CO;2.

Capítol 4

Entorns favorables per a la formació de tornados i mànegues marines

4.1 Paràmetres derivats de radiosondatges associats a tornados a Catalunya

4.1.1 Resum de l'article

A l'estudi que es presenta a continuació s'analitza un conjunt de 333 radiosondatges associats a diversos tipus de temps a Catalunya: dies sense precipitació (DD), dies de tempesta sense tornado (NTTD), dies de tornado EF0 (EF0), dies de tornado EF1 o superior (EF1+) i dies de mànega marina (WAT). Per a fer aquest treball, s'utilitzen dades de radiosondatge de les estacions de Barcelona (08190), Palma (08302), Saragossa (08160), Múrcia (08430) i Nîmes (07645) del període 2000-2016. A l'hora de seleccionar el radiosondatge més representatiu per als casos de tornado i de tromba marina s'empra el *proximity-inflow method* proposat per Rasmussen i Blanchard (1998).

S'estudien una dotzena de paràmetres per a caracteritzar els entorns. Per una banda, s'analitzen els paràmetres termodinàmics, com la CAPE, que en aquest article es calcula mitjançant l'ús de la parcel·la SB. Per altra banda, s'estudien els cinemàtics, com el WS per als estrats 0-1 km, 0-3 km i 0-6 km, l'SRH per als estrats 0-1 km i 0-3 km i el BRNSHR. A més, també es testegen alguns paràmetres compostos, com l'EHI per a l'estrat 0-1 km, el VGP per a l'estrat 0-4 km, l'SCP, l'STP i l'UTI. Per a estudiar les diferències que hi ha en els valors que prenen els paràmetres en funció del tipus de temps, es duu a terme el test de Kolmogorov-Smirnov (KS).

Els resultats mostren que la CAPE és un paràmetre que no presenta diferències estadísticament significatives entre la majoria de tipus de temps, especialment pel que fa als entorns favorables per a la tornadogènesi respecte als dies de tempesta sense tornado. Independentment, s'observa que hi ha una relació directa entre la intensitat dels fiblons i el WS, especialment per a l'estrat 0-3 km. Es comprova que els paràmetres compostos SCP i STP solen presentar valors clarament més baixos que als EEUU, on s'utilitzen en la predicció operativa de supercèl·lules i de tornados. Aquest fet implica que, especialment l'STP, no és un paràmetre d'utilitat per a discriminar entre condicions favorables per a fiblons EF1+ i per a tempestes sense tornado. En canvi, l'UTI mostra un comportament que afavoreix la identificació d'entorns favorables per a la tornadogènesi, ja que presenta valors significativament diferents per als episodis de fibló, sobretot per als casos més intensos, respecte a la resta de tipus de temps. Finalment, es proposen uns llindars per a distingir els entorns favorables per a la formació de tornados d'intensitat EF1 o superior dels entorns de tempesta sense tornado per als paràmetres WS i SRH, ambdós per als estrats 0-1 km i 0-3 km, així com per a l'EHI, el VGP, l'SCP i l'UTI.

Aquest article dona resposta als objectius generals **OG2** i **OG3** i als objectius específics **OE4** i **OE5**.

4.1.2 Article

Rodríguez O. i Bech J. (2018): Sounding-derived parameters associated with tornadic storms in Catalonia. *International Journal of Climatology*, **38**: 2400–2414. doi:10.1002/joc.5343.

INTERNATIONAL JOURNAL OF CLIMATOLOGY
Int. J. Climatol. **38**: 2400–2414 (2018)
Published online 20 November 2017 in Wiley Online Library
(wileyonlinelibrary.com) DOI: 10.1002/joc.5343

Sounding-derived parameters associated with tornadic storms in Catalonia

Oriol Rodríguez* and Joan Bech

Department of Applied Physics – Meteorology, University of Barcelona, Spain

ABSTRACT: Catalonia, a southern Europe coastal region in the western Mediterranean basin, is regularly affected by severe local storms which every year produce an average of 5 tornadoes and 12 waterspouts, based on data recorded from 2000 to 2016. Despite these tornadoes mostly being weak – not exceeding EF1 on the enhanced Fujita (EF) damage intensity scale – they occasionally reach stronger intensities, posing an evident threat to population and socio-economic activity, particularly in densely populated coastal conurbations such as Tarragona or Barcelona. This study provides analysis of upper air conditions that favour the formation of tornadic storms in the region, considering five different stations in Spain and France to build a database of 333 soundings which included 49 tornadic soundings, 104 waterspout soundings (WAT) as well as non-tornadic thunderstorms and dry period soundings. For each one, 12 different parameters were calculated and analysed to test their potential capacity to discriminate non-tornadic from tornadic environments and also to assess the feasibility of stratifying tornado intensity (EF0, and EF1 or stronger, on the EF scale). The results indicate that storm-relative helicity for the layer 0–3 km, with a threshold value of 150 $m^2 s^{-2}$, wind shear for the same layer, with a threshold of 15 m s^{-1}, and composite parameters such as the supercell composite parameter with a threshold of 1.2 and universal tornadic index with a threshold of 0.3 are all useful to distinguish between non-tornadic thunderstorms and EF1 or stronger tornadic events. These results contribute to a better description of the climatology of upper air conditions that favour tornadic storms in the region and can also help operational weather forecasting and surveillance tasks, thus increasing situational awareness in severe convective weather events.

KEY WORDS tornado; waterspout; thunderstorm; Mediterranean; Europe; upper air conditions; radiosonde

Received 1 February 2017; Revised 11 October 2017; Accepted 12 October 2017

1. Introduction

For decades, tornadoes have been studied in detail in the United States due to their high frequency, intensity, and dramatic economic and social impact. However, tornadoes and their effects are also present in other middle-latitude zones. Two recent studies (Antonescu *et al.*, 2016, 2017) demonstrate that tornadoes are also frequent and potentially dangerous in Europe, with around 240 tornadoes per year: a figure consistent with that previously given by Dotzek (2003) and even with the pioneering work of Wegener (1917). Similarly, there have been specific studies of tornado climatology in several European countries (e.g. Rauhala *et al.,* 2012; Matsangouras *et al.,* 2014; Mulder and Schultz, 2015).

In the Iberian Peninsula (southwest Europe, Figure 1), Catalonia, NE Spain, is the region where tornadoes and waterspouts are most frequent (Gayà *et al.,* 2011; Gayà, 2015; Riesco Martín *et al.,* 2015). Antonescu *et al.* (2017) examined tornado reports from 1950 to 2015 in Europe (their figure 1) and found that, in general, they are common along the western Mediterranean continental coast. In Catalonia, with an area of 32 000 km^2 and the surrounding coastal waters, every year there are an average of 5 tornadoes and 12 waterspouts (Figure 2). This means that the normalized number of tornadoes is 1.5 per 10^4 km^2 per year, which is similar to the figure for the UK (1.7, Mulder and Schultz, 2015) or Belgium (1.2, Frique, 2012). Other Mediterranean countries, such as Greece (Matsangouras *et al.,* 2014), have a smaller normalized number of tornadoes per year (1.0), but the normalized number of waterspouts per year is comparable to that in Catalonia in some cases. Averaging the continental coastline of each country into 100 km segments, the proportion of waterspouts per 100 km of coast per year is 3.8 in Catalonia, 3.0 in Croatia (Renko *et al.,* 2016), and 2.1 in Greece (Matsangouras *et al.,* 2014). In contrast, in central and eastern Europe, the normalized number of tornadoes is significantly lower, as in Germany (0.7, Bissolli *et al.,* 2007), Finland (0.5, Rauhala *et al.,* 2012), Poland (0.3, Taszarek and Brooks, 2015), or Romania (0.3, Antonescu and Bell, 2015). Note that the tornado climatologies cited above for different countries refer to a temporal period similar to that of the present study.

Most tornadoes in Catalonia are weak, EF0 or EF1 on the enhanced Fujita (EF) scale (Doswell *et al.,* 2009), and

* Correspondence to: O. Rodríguez, Department of Applied Physics – Meteorology, Faculty of Physics, University of Barcelona, Martí i Franquès, 1, 08028 Barcelona, Spain.
E-mail: orodriguez@meteo.ub.edu

Figure 1. Map of southwest Europe, showing the study region, Catalonia, the five sounding stations with their WMO codes, which are marked with crosses, and the location of the cities of Barcelona and Tarragona: the areas of Catalonia where tornadoes and waterspouts are most frequent.

only 6% of them (five events) have been classified as significant tornadoes (all of them EF2) – see, for example, the case studies of Ramis *et al.* (1997), Aran *et al.* (2009), and Bech *et al.* (2009, 2011). Tornadoes usually occur near the Mediterranean coast, where most of the population of Catalonia live. For example, the tornado outbreaks of 7 September 2005 (Bech *et al.,* 2007) and 13 September 2006 (Mateo *et al.,* 2009) affected the metropolitan area of Barcelona and Tarragona, respectively. The high population density, as well as the important concentration of transport infrastructures including airports, ports, high-speed railway lines, and highways, makes these areas highly vulnerable. It is therefore important to anticipate environmental conditions that favour tornadic events and to forecast potentially dangerous situations, as already highlighted by some authors (Rauhala and Schultz, 2009; Miglietta and Rotunno, 2016; Antonescu *et al.,* 2017).

It is important to note the distinction between non-mesocyclonic and mesocyclonic – i.e. linked to a supercell – tornadoes (e.g. Brady and Szoke, 1989; Wakimoto and Wilson, 1989; Markowski and Richardson, 2010). As the strongest tornadoes are mesocyclonic, specific effort was devoted to characterizing supercell environments. There are several parameters which are traditionally calculated from sounding data in order to describe the thermodynamic instability and vertical wind shear (WS) of an air mass, which are basic ingredients of severe local storms (Johns and Doswell, 1992). Since 1990, some composite parameters have been proposed to discriminate between non-tornadic thunderstorms, tornadic thunderstorms, and supercell environments; these include the energy helicity index (EHI) (Davies, 1993), the supercell composite parameter (SCP), the significant tornado parameter (STP) (Thompson *et al.,* 2003), and the universal tornadic index (UTI) (Taszarek and Kolendowicz, 2013). Because most of these parameters were originally developed in the United States, where tornadic environments are not necessarily the same as in Europe, applying them elsewhere is not straightforward and it may be necessary to modify the parameter thresholds or even develop new parameters.

Several studies in the United States determine supercell and tornado sounding-derived parameter thresholds using radiosonde data (Rasmussen and Blanchard, 1998; Monteverdi *et al.,* 2003; Craven and Brooks, 2004; Grams *et al.,* 2012). They conclude that large vertical WS, high surface-based convective potential energy (SBCAPE) values and low lifting condensation level (LCL) favour the formation of significant tornadoes. Similar articles have been published for different European countries or regions (Gayà *et al.,* 2001; Giaiotti *et al.,* 2007; Groenemeijer and van Delden, 2007; Romero *et al.,* 2007). The main differences in their findings, with respect to those of the United States, are that SBCAPE and also composite parameter values are not as high. Moreover, there are studies of environmental conditions that specifically favour waterspouts (Sioutas and Keul, 2007; Renko *et al.,* 2016; Matsangouras *et al.,* 2017), which are usually related with shallow convection.

Here, we report a study of several radiosonde-derived parameters for waterspout and tornadic events in Catalonia. No previous study has examined environments for tornadic storms and waterspouts specifically for this region in detail. Moreover, as tornadoes are usually weak in this area (EF0 or EF1) and only occasionally significant (EF2), differences between EF0 and stronger tornado environments are studied; unlike previous studies which determined thresholds for significant tornadoes (Romero *et al.,* 2007). Our results contribute to a deeper understanding of tornadic and waterspout environments in one of the most tornado-prone regions in southern Europe (Antonescu *et al.,* 2017) and also help weather forecasting and surveillance tasks in the area.

The organization of the article is as follows. Section 2 provides a description of the data sets employed, the radiosounding selection method, and the parameters calculated. Section 3 offers results and discussion; and finally Section 4 presents a summary of the main findings and conclusions.

2. Data and methodology

2.1. Tornado and waterspout database

The tornado and waterspout database used in this study has been built from cases that occurred in Catalonia from 2000 to 2016. The starting year was chosen because it is the first complete year with Barcelona radiosonde launches available twice a day. All the information on tornadoes and waterspouts (occurrence, date, time, location, and damage) was collected from local media, eyewitnesses, and wind damage surveys. In the most recent events, internet sites and social networks were the main sources of information. Moreover, cases available in the European Severe Weather Database (ESWD) – http://www.eswd.eu and see

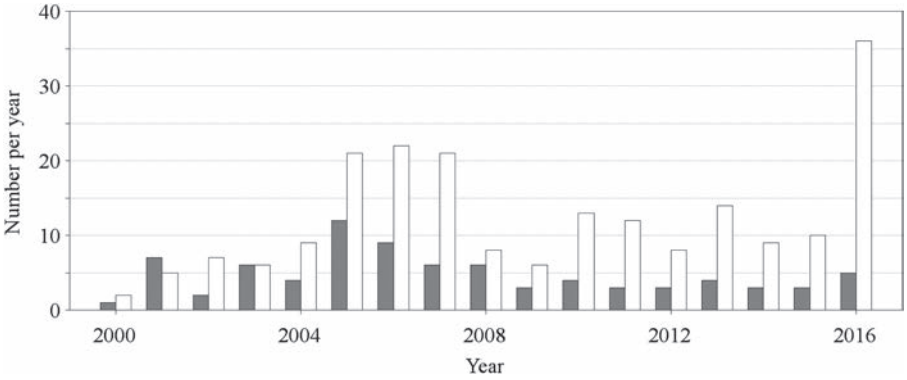

Figure 2. Number of tornadoes (in grey) and waterspouts (in white) per year in Catalonia for the period (2000–2016), according to the database used in this study.

Dotzek *et al.* (2009a) for details – with QC1 or QC2 quality control level were also included, as well as additional cases from Gayà (2015) for the period 2000–2012.

The database follows the *Glossary of Meteorology* definitions of tornado and waterspout, i.e. a tornado is 'a rotating column of air, in contact with the surface, pendant from a cumuliform cloud, and often visible as a funnel cloud and/or circulating debris/dust at the ground' (American Meteorological Society, 2017a), and a waterspout is 'a tornado over a body of water' (American Meteorological Society, 2017b). Moreover, in our database, waterspouts that originated over water but hit land were considered tornadoes and not waterspouts. According to these definitions, there were 81 tornadoes (distributed among 57 days) and 209 waterspouts (on 122 different days) in Catalonia from 2000 to 2016. On 13 occasions, at least one tornado and at least one waterspout coexisted on the same day. In addition, there were 21 possible tornado cases that could not be corroborated by eyewitnesses and their damage spatial distribution did not allow us to distinguish if they were caused by a tornado or a downburst event. These cases are not considered in this article.

2.2. Sounding database

The sounding database consists of 333 soundings corresponding to the nearest 12-h window to the event, as described in Section 2.3. Soundings are categorized as:

- Dry-period sounding (DRY, 90 soundings): associated with days without precipitation, lightning or any waterspout or tornado events in a radius of 50 km around the Barcelona sounding station, for all months in the period 2000–2016, according to the Meteorological Service of Catalonia (SMC) rain gauge network.
- Non-tornadic thunderstorm sounding (NTT, 90 soundings): associated with two or more lightning flashes detected by the lightning detection network of the SMC (Pineda *et al.,* 2007) for the period 2003–2016 in a radius of 50 km around the Barcelona sounding station, but without any reported tornadoes or waterspouts.
- WAT (104 soundings): associated with one or more waterspouts.
- EF0 tornado sounding (EF0, 28 soundings): associated with one or more EF0 tornadoes.
- EF1 or stronger tornado sounding (EF1+, 21 soundings): associated with one or more EF1 or stronger tornadoes, even if weaker tornadoes were also present.

Note that EF0 and EF1+ are mutually exclusive: If, in a 12-h window, one EF0 and one EF1 tornado are present, the sounding will belong to the EF1+ class. In contrast, WAT and EF0 or EF1+ are not mutually exclusive: If one tornado and one waterspout coexist in a 12-h window, the sounding will belong to both WAT and the maximum tornado intensity class (EF0 or EF1+).

The specification of DRY and NTT soundings required choosing, for each one, four variables: year, month, day, and time (0000 and 1200 UTC). The selection of month and time followed the monthly and hourly distribution resulting from the combination of all WAT, EF0, and EF1+ soundings. The year and the day of month selection was random throughout the period 2000–2016 for DRY soundings and the period 2003–2016 for NTT soundings, limited by the lightning observations mentioned above.

2.3. Radiosonde selection method: proximity-inflow method

Several methodologies have been proposed in the past to find representative soundings to study severe weather events such as hailstorms, thunderstorms, severe wind gusts or tornadoes. The greater the distance or the time that elapses between the sounding launch and the event, the less representative the air mass in the selected sounding (Potvin *et al.,* 2010). That is why all of them limit the distance and the elapsed time between the sounding and the event (Monteverdi *et al.,* 2003; Taszarek and Kolendowicz, 2013). Some of them are much more restrictive with the distance between the sounding station and the event (Groenemeijer and van Delden, 2007) than others (Matsangouras *et al.,* 2017).

In this study, to select WAT, EF0, and EF1+ sounding classes, the proximity-inflow method was used. This procedure was originally described and employed by Rasmussen and Blanchard (1998) and is also used by

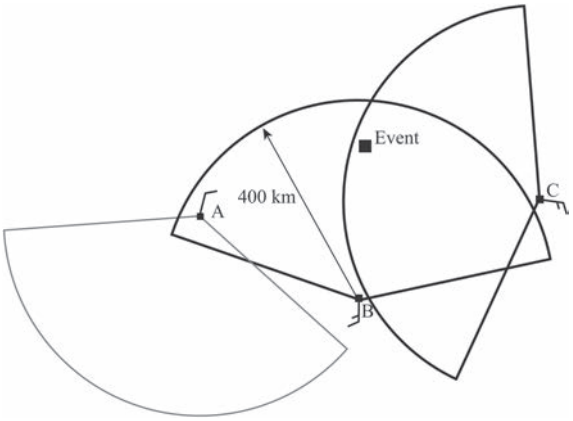

Figure 3. Scheme of the proximity-inflow method from Rasmussen and Blanchard (1998). A, B, and C are sounding stations whose inflow area is determined by the low-level wind, which is also represented with a wind barb. As an example, the event marked with a black square is assigned to B and C soundings; of them, the one with the highest SBCAPE would be selected.

Rasmussen (2003) and Renko *et al.* (2016). It consists of three steps:

(1) Consider sounding stations closer than 400 km to the event location.
(2) Use the mean wind vector from the first 500 m above ground level (AGL), considering a 150° sector centred on the wind vector. If the event is within this sector, then the sounding is considered representative and it is selected.
(3) If there are two or more possible soundings selected, the one with the highest SBCAPE is chosen.

This method is schematically represented in Figure 3. The original temporal selection criteria of the proximity-inflow method considered a 9-h window starting 6 h before and finishing 3 h after each event. As we only have 0000 and 1200 UTC soundings, some time periods would not be covered (0300–0600 and 1500–1800 UTC: the latter corresponding to the period of maximum tornadic climatological occurrence). To minimize these gaps, we advanced the time window 3 h: extending the previous 6-h period to 9 h and removing the 3-h period after the event.

Because of the 400 km distance criteria, this method allows us to enlarge our sounding database, because of the relatively low density of the sounding station network in the western Mediterranean compared, for example, with central Europe. However, using a sounding far from the tornado occurrence may reduce the representativeness of the air mass studied. Nevertheless, it is important to note that 60% of WAT, EF0, and EF1+ soundings were launched closer than 100 km to events, and 96% of them closer than 250 km.

Following the proposed method, five sounding stations closer than 400 km to the events studied were used (Figure 1): Barcelona (08190), Palma (08302), Zaragoza (08160), Murcia (08430), and Nîmes (07645). The stations belong to the SMC (Barcelona), Météo France (Nîmes), and the Spanish Meteorological Agency, AEMET (in the case of the other three). As can be seen in Table 1, the stations at Barcelona and Palma are used to describe almost all of the WAT, EF0, and EF1+ soundings (145 of 154) because of their position with respect to the event locations and the low-level predominant wind flow in these events; tornadoes and waterspouts in Catalonia are generally formed in SE to SW low-level advections (Gayà *et al.,* 2011).

With the method described, 87% of WAT, EF0, and EF1+ soundings were satisfactorily assigned. The remaining assignments were not possible for two reasons: two WAT and two EF0 cases had no sounding station in the direction of the low-level wind flow, and for the others (16 WAT, 6 EF0, and 2 EF1+), there were no sounding data available or the data were incomplete.

Table 2 lists the number of soundings for each class after the application of the proximity-inflow method and the inclusion of the DRY and NTT classes described in Section 2.2.

2.4. Sounding-derived parameters

A preliminary selection of parameters to be analysed in this study was performed based on their capacity to differentiate non-tornadic thunderstorms from tornadic or waterspout events, considering significant statistical differences between NTT and EF1+ sounding classes – *p*-values equal or lower than 0.100 with the Kolmogorov–Smirnov test (Wilks, 2011); see Appendix and Table A1 for more details. The resulting parameters were WS 0–6, 0–3, and 0–1 km layers (WS_{06}, WS_{03}, and WS_{01}), bulk Richardson number shear (BRNSHR), storm-relative helicity (SRH) 0–3 and 0–1 km layers (SRH_{03} and SRH_{01}), EHI 0–1 km layer (EHI_{01}), vorticity generation parameter (VGP) 0–4 km layer (VGP_{04}), SCP, STP, and UTI. One additional parameter relevant in previous studies was also included: SBCAPE (e.g. Kaltenböck *et al.,* 2009; Taszarek and Kolendowicz, 2013). All of them are listed and referenced in Table 3. In this study, all height values are calculated AGL and the virtual temperature correction was applied to the SBCAPE calculations (Doswell and Rasmussen, 1994).

Finally, as discussed extensively by Doswell and Schultz (2006), it is important to remark that the parameters described above summarize some characteristics of the severe weather environment in a single number. Forecasters need to know how to interpret these parameters and should be aware of their limitations and the fact that they can only contribute to understanding the situation if employed with additional background context.

3. Results and discussion

3.1. Surface-based convective available potential energy

The lowest SBCAPE values were associated with DRY soundings. Most of these soundings did not exceed 100 J kg^{-1}, and only 19% surpassed 1000 J kg^{-1}

Table 1. Characteristics of the sounding stations used in this study, including the number of soundings we expected to analyse (needed), the number of soundings that were available with complete and coherent data (available), and the number of available 0000 and 1200 UTC soundings used for WAT, EF0, and EF1+.

WMO ID and name station	Lat. (°)	Lon. (°)	Alt. (m)	No. soundings needed (available)	No. soundings available 0000 UTC	No. soundings available 1200 UTC
08190 Barcelona	41.62	2.20	98	111 (105)	38	67
08302 Palma	39.61	2.71	41	47 (40)	22	18
08160 Zaragoza	41.66	−1.01	258	15 (6)	2	4
08430 Murcia	38.00	−1.16	62	3 (2)	1	1
07645 Nîmes	43.85	4.40	60	1 (1)	0	1

Table 2. Number of 0000 and 1200 UTC soundings for each category.

Sounding class	Number of 0000 UTC sounding	Number of 1200 UTC sounding	Total number
DRY	32	58	90
NTT	32	58	90
WAT	46	58	104
EF0	10	18	28
EF1+	7	14	21

(Figure 4). The other sounding types had higher values: 28% of NTT, 34% of WAT, 32% of EF0, and 38% of EF1+ exceeded 1000 J kg^{-1}.

Interestingly, all EF2 cases in our database were related to SBCAPE values higher than 400 J kg^{-1} (not shown). However, as expected, high values of this parameter alone are not a sufficient condition for tornado or waterspout formation: Almost half the NTT soundings exceeded 400 J kg^{-1} and occasionally 3000 J kg^{-1}, without any tornadic event.

Differences found between NTT, WAT, EF0, and EF1+ values were not statistically significant (Table A1), illustrating that SBCAPE is not a good tornadic discriminator. This parameter is useful to differentiate between DRY and the rest of the sounding classes, which indicates that SBCAPE correctly characterizes convection. Nevertheless, higher values were not directly related to stronger tornadoes. This is consistent with other studies under similar conditions in Europe (Giaiotti *et al.,* 2007; Groenemeijer and van Delden, 2007; Taszarek and Kolendowicz, 2013) and in other areas of the world (Monteverdi *et al.,* 2003).

3.2. Wind shear

3.2.1. WS 0–6 km (WS_{06})

High WS is a necessary condition for organized convective storm systems formation as helps to decouple the updraft and downdraft currents. It leads to long-lived storm cells and, at the same time, helps them evolve into organized systems such as multicells or supercells (Rasmussen and Blanchard, 1998).

Thompson *et al.* (2003) determined that WS_{06} values over 20 m s^{-1} are favourable environments for supercells. As can be seen in Figure 5(a), only 44% of EF0 soundings surpassed 20 m s^{-1}. However, the percentage of EF1+ with greater values is higher: 52%. There is a direct relation between high WS_{06} values and tornado intensity.

NTT and WAT soundings have similar WS_{06} values, so they cannot be discriminated by using this variable. More than 75% of each of these sounding classes did not overcome 23 m s^{-1}, similarly to the findings in Renko *et al.* (2016). However, the WS_{06} median for EF0 soundings was slightly higher than for WAT, the 75th percentile is substantially higher. However, the 25th percentile is identical, presumably because the EF0 category included waterspout cases that hit land, which represent 54% of EF0 soundings.

The EF1+ WS_{06} 25th percentile is substantially higher than for the rest of the sounding types. The 25th, 50th, and 75th percentiles for this category are, respectively, 16.8, 22.4, and 27.7 m s^{-1}. These values are consistent with the results presented in Groenemeijer and van Delden (2007) and Taszarek and Kolendowicz (2013) showing that on average, with the other variables equal: the greater the WS, the higher the probability of a stronger tornado.

3.2.2. WS 0–3 km (WS_{03})

The WS_{03} median of EF1+ soundings is 16.0 m s^{-1}, higher than the threshold proposed in Taszarek *et al.* (2017), of 15.0 m s^{-1}, and also higher than the 75th percentile of the other sounding types. The same happens between the 25th percentile of EF1+, 12.9 m s^{-1}, and the medians of the other classes, which are between 8.7 and 11.8 m s^{-1} (Figure 5(b)). Therefore, WS_{03} allows us to discern better than WS_{06} does between tornadic and non-tornadic soundings, especially between EF1+ and the rest.

The difference between NTT and EF1+ and between EF0 and EF1+ soundings are statistically significant at a 98% level of confidence. This supports the notion that WS_{03} is a good parameter to discriminate tornadic (EF1+) from non-tornadic storms and also to distinguish weaker tornadoes from the rest of them, which is consistent with Taszarek *et al.* (2017).

However, with this parameter, it is not possible to find differences between NTT, WAT, and EF0 soundings. The WS_{03} values of these three sounding categories are similar, even though EF0 tends to reach slightly higher values, as already reported by Monteverdi *et al.* (2003). It is also interesting that the WS_{03} 25th percentile for EF0 waterspouts that hit land is 6.9 m s^{-1} (not shown); a value that is similar to 25th percentile for the WAT sounding type:

Table 3. Sounding-derived parameters used in this study, where g is the acceleration due to gravity, LFC is the level of free convection, EL is the equilibrium level, $T_{v_{LP}}$ is the lifting parcel virtual temperature, T_{v_e} is the environmental virtual temperature, **v** is the horizontal wind vector, $\overline{U}$ is the density-weighted speed of the mean wind vector in the layer 0–6 km, U_0 is the speed of the mean wind vector in the layer from the surface to 500 m, **k** is the upwards unitary vector, **c** is the storm motion vector, S is the mean shear (which is the hodograph length divided by the depth of the level studied), MUCAPE is the most unstable convective available potential energy, MLLCL is the mixed-layer lifting condensation level, $CAPE_{03}$ is the convective available potential energy integrated up to 3 km, and AMR_{500} is the average mixing ratio in the lowest 500 m. EHI_{01}, SCP, STP, and UTI are dimensionless. Note that in this study, WS_{0z} is calculated using $z = 6$ km, $z = 3$ km, and $z = 1$ km; and SRH_{0z} using $z = 3$ km and $z = 1$ km.

Parameter	Equation	Reference
SBCAPE ($J\,kg^{-1}$)	$SBCAPE = g\int_{LFC}^{EL}\frac{T_{v_{LP}}(z)-T_{v_e}(z)}{T_{v_e}(z)}dz$	Moncrieff and Miller (1976)
WS_{0z} ($m\,s^{-1}$)	$WS_{0z} = \lvert\mathbf{v}_z - \mathbf{v}_0\rvert$	Weisman and Klemp (1982)
BRNSHR ($m^2\,s^{-2}$)	$BRNSHR = \frac{1}{2}\left(U - U_0\right)^2$	Weisman and Klemp (1982)
SRH_{0z} ($m^2\,s^{-2}$)	$SRH_{0z} = -\int_0^z \mathbf{k}\cdot\left[(\mathbf{v}-\mathbf{c})\times\frac{\partial\mathbf{v}}{\partial z}\right]dz$	Davies-Jones *et al.* (1990)
EHI_{01}	$EHI_{01} = \frac{SBCAPE\cdot SRH_{01}}{160\ 000}$	Davies (1993)
VGP_{04} ($m\,s^{-2}$)	$VGP_{04} = S\sqrt{SBCAPE} = \left(\int_0^{4\text{ km}}\frac{\partial v}{\partial z}dz / \int_0^{4\text{ km}}dz\right)\sqrt{SBCAPE}$	Rasmussen and Blanchard (1998)
SCP	$SCP = \left(\frac{MUCAPE}{1000\text{ J kg}^{-1}}\right)\left(\frac{SRH_{03}}{100\text{ m}^2\text{s}^{-2}}\right)\left(\frac{BRNSHR}{40\text{ m}^2\text{s}^{-2}}\right)$	Thompson *et al.* (2003)
STP	$STP = \left(\frac{MLCAPE}{1000\text{ J kg}^{-1}}\right)\left(\frac{WS_{06}}{20\text{ m s}^{-1}}\right)\left(\frac{SRH_{01}}{100\text{ m}^2\text{ s}^{-2}}\right)\left(\frac{2000-MLLCL}{1500\text{ m}}\right)$	Thompson *et al.* (2003)
UTI	$UTI = \frac{\left\{\left[\frac{SBCAPE\cdot SRH_{01}}{200}\cdot\frac{5(WS_{06}-20)+\left(\frac{2000-LCL}{10}\right)}{100}\right]\right\}+CAPE_{03}+\frac{SRH_{01}}{4}}{1000}\cdot\frac{WS_{01}}{12}\cdot\frac{AMR_{500}}{10}$	Taszarek and Kolendowicz (2013)

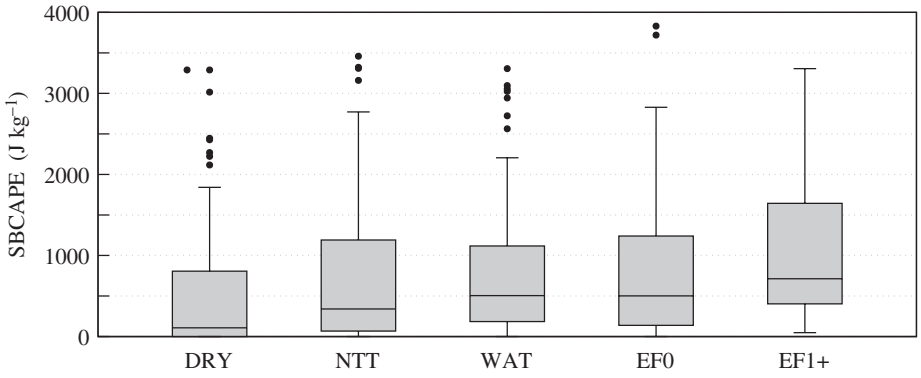

Figure 4. Boxplots of SBCAPE values showing 25th, 50th, and 75th percentiles and outlier points (exceeding the distance to the 25th or 75th percentile by 1.5 times the inter-quartile range); outliers with repeated values are stacked horizontally. The whiskers indicate the maximum and the minimum values that fall within the range between the 25th or 75th percentile, and 1.5 times the inter-quartile distance.

6.5 $m\,s^{-1}$. However, for EF0 tornadoes formed inland, this percentile is considerably higher: 9.1 $m\,s^{-1}$.

3.2.3. WS 0–1 km (WS_{01})

Several previous studies concluded that low-level WS can be used to discriminate well between significant tornadoes and non-tornadic storms (Thompson *et al.,* 2003; Grams *et al.,* 2012). In Figure 6, it can be seen that WS_{01} shows no significant differences between DRY, NTT, WAT, and EF0 soundings, while they are clearly higher for EF1+ soundings.

In convective storm forecasting, a threshold of 10 $m\,s^{-1}$ for low-level WS is considered to identify environments that favour significant tornadic storms (Craven and Brooks, 2004). Applying this figure to our database, we find that only a small proportion of tornadoes surpass the threshold: 22% of EF0 soundings and 29% of EF1+ soundings.

For DRY, NTT, and WAT soundings, most WS_{01} values range from 3.0 to 8.0 $m\,s^{-1}$. This interval is similar to that of the EF0 soundings, whose 25th and 75th percentiles are 4.8 and 9.2 $m\,s^{-1}$, respectively. Again, conditions for the weakest tornadoes or waterspout formation are not really different from those in non-tornadic thunderstorm cases.

Once more, the main differences in WS_{01} values are between EF1+ soundings and the other classes. Also, it is important to note that none of the five EF2 cases contained in our data set was related to WS_{01} values below 8.1 $m\,s^{-1}$ (not shown), which coincides with the EF1+ 50th percentile. According to these results: the greater the WS_{01} value, the stronger the tornado.

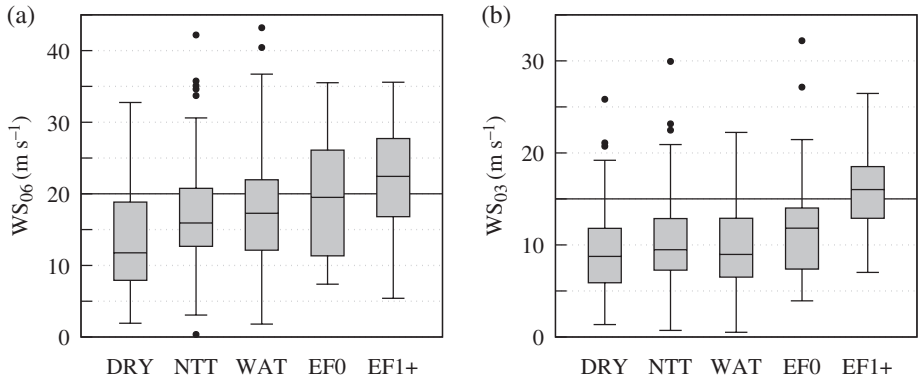

Figure 5. As Figure 4, but for WS_{06} (a) and WS_{03} (b), where the solid lines are reference 20 m s^{-1} (Thompson *et al.,* 2003) and 15 m s^{-1} (Taszarek *et al.,* 2017) thresholds, respectively.

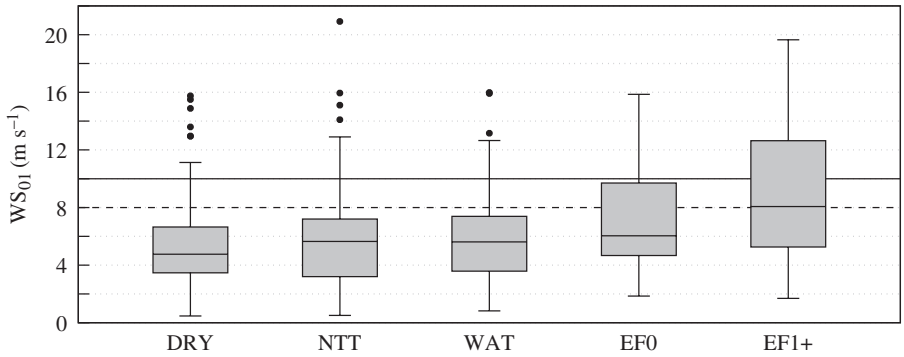

Figure 6. As Figure 4, but for WS_{01} where the solid line is the reference Craven and Brooks (2004) threshold (10 m s^{-1}) and the new threshold value (8 m s^{-1}) proposed in Section 3.5 is plotted as a dashed line.

3.2.4. Bulk Richardson number shear

BRNSHR is a parameter which assesses mid-level mesocyclone development and tornado potential. Stensrud *et al.* (1997) reports that values over 40 m^2 s^{-2} provide a favourable environment for mesocyclones, which is consistent with the BRNSHR values computed for the five EF2 cases in our database (not shown). Thompson *et al.* (2003) situates the threshold to discern between significant tornadic and non-tornadic storms at 50 m^2 s^{-2}. In our case, 44% of EF0 soundings in the database surpass this 50 m^2 s^{-2} threshold, whereas 81% of EF1+ soundings exceed it (Figure 7). However, around half the NTT soundings have BRNSHR values above this threshold too. So, for our data set, BRNSHR is not a good discriminator between non-tornadic thunderstorms and weak tornadic soundings, which are usually non-mesocyclonic tornadoes.

As BRNSHR is a parameter directly related with low-level and mid-level WS, one can expect a similar distribution to those of WS_{03} and WS_{01} (Figures 5(b) and 6). So, as with those parameters, BRNSHR values are clearly greater for EF1+ soundings than for the rest, with significant differences at a 97% level of confidence. However, there are no significant differences between DRY, NTT, WAT, and EF0.

3.3. Storm-relative helicity

3.3.1. SRH 0–3 km (SRH_{03})

SRH assesses the potential for cyclonic rotation in the updraft of right-moving supercells, which is why it is one of the most commonly studied of several sounding-derived parameters associated with severe weather (e.g. Doswell and Evans, 2003; Thompson *et al.,* 2003; Groenemeijer and van Delden, 2007).

DRY and WAT soundings have similar values of SRH_{03}. As shown in Figure 8(a), their 25th percentile is 10 and 19 m^2 s^{-2}, and their 75th percentile is 80 and 90 m^2 s^{-2}, both respectively. These results for WAT soundings are consistent with Renko *et al.* (2016). Although the 25th percentile for NTT and EF0 soundings is similar to that for DRY and WAT, their 75th percentile is significantly higher, surpassing 100 m^2 s^{-2}.

For EF1+ cases, SRH_{03} values are higher. The median for this sounding type is 187 m^2 s^{-2}, and 19% overpass the threshold of 250 m^2 s^{-2} proposed by Thompson *et al.* (2003), which is used to discriminate between significant tornadic and non-tornadic storms. The highest values of SRH_{03} are in EF2 soundings, as is also commented on the above-mentioned article and in Kaltenböck *et al.* (2009). Four of the five EF2 soundings of our database surpassed an SRH_{03} of 180 m^2 s^{-2} (not shown).

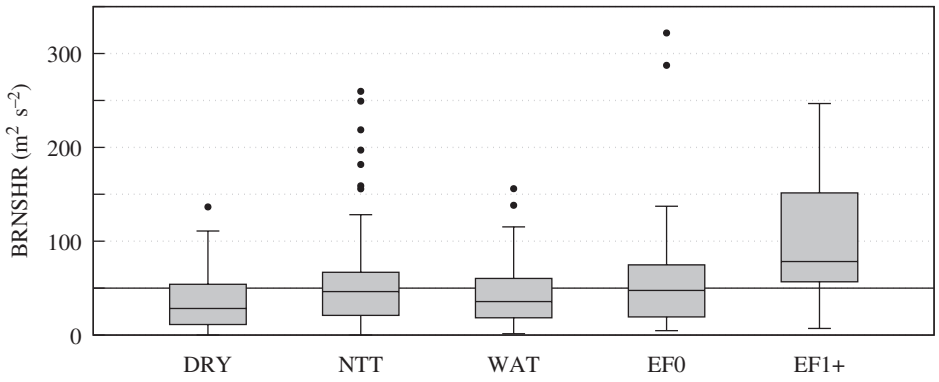

Figure 7. As Figure 4, but for BRNSHR where the solid line is the reference threshold value (50 m^2 s^{-2}) proposed by Thompson *et al.* (2003).

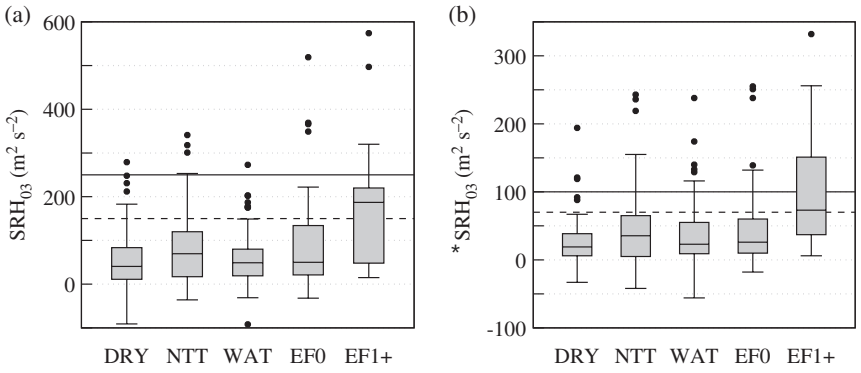

Figure 8. As Figure 4, but for SRH_{03} (a), where the solid line (250 m^2 s^{-2}) is the Thompson *et al.* (2003) threshold and the dashed line is the proposed threshold (150 m^2 s^{-2}), and SRH_{01} (b), where the solid line (100 m^2 s^{-2}) is the Thompson *et al.*'s (2003) threshold and the dashed line is the proposed threshold (70 m^2 s^{-2}).

It is important to note that SRH_{03} values for WAT soundings present a very similar distribution to those for DRY soundings, whose values are lower than for NTT and EF0 soundings. This could be explained by the fact that waterspouts do not need strong mid-level helicity for their formation, which is consistent with the results in Renko *et al.* (2016).

Therefore, SRH_{03} is a good discriminator between tornadic EF1+ and non-tornadic storms. However, this parameter cannot be used to differentiate weak tornadoes and waterspouts from non-tornadic thunderstorm events, due to their similar values.

3.3.2. SRH 0–1 km (SRH_{01})

In general terms, the SRH_{01} boxplots follow a similar pattern to those of SRH_{03} for the different sounding categories. So, there are no statistically significant differences between DRY, NTT, WAT, and EF0 soundings (Table A1), whose SRH_{01} range is, in general, between 5 and 65 m^2 s^{-2} (Figure 8(b)).

Although more than 48% of EF1+ soundings have SRH_{01} values which are into the range of non-tornadic and EF0 soundings, more than 40% of EF1+ soundings exceed the SRH_{01} value of 100 m^2 s^{-2}; the threshold for significant tornadoes proposed by Thompson *et al.* (2003). This percentage is clearly higher than the percentage of EF1+ events surpassing the 250 m^2 s^{-2} SRH_{03} threshold. In fact, four of the five EF2 tornadoes were associated with SRH_{01} values higher than 100 m^2 s^{-2} (not shown).

There are significant differences between EF0 and EF1+, with a confidence level of 96%, and between NTT and EF1+, with a confidence level of 97%. Based on this, SRH_{01} discriminates well between significant and non-significant tornadoes and also between significant tornadic storms and non-tornadic storms. As for SRH_{03}, WAT and EF0 soundings cannot be differentiated from NTT.

3.4. Composite parameters

3.4.1. Surface-based EHI 0–1 km (EHI_{01})

A threshold of 1.0 is recommended for EHI_{01} to discern between significant and non-significant tornadoes (see Thompson *et al.,* 2003 for mixed-layer EHI), but in our database, values over 1.0 are infrequent, even for EF1+ soundings: None of the EF2 cases surpassed this value (not shown), and only 6% of the total tornado cases (EF0 and EF1+ sounding types) exceeded it. The percentage is lower for NTT (1%), WAT (3%), and DRY (0%), as can be seen in Figure 9(a).

The highest values of EHI_{01} correspond to EF1+ soundings, which are significantly different from the rest, with

*Nota: aquest títol hauria de ser SRH_{01}, en comptes d'SRH_{03}.

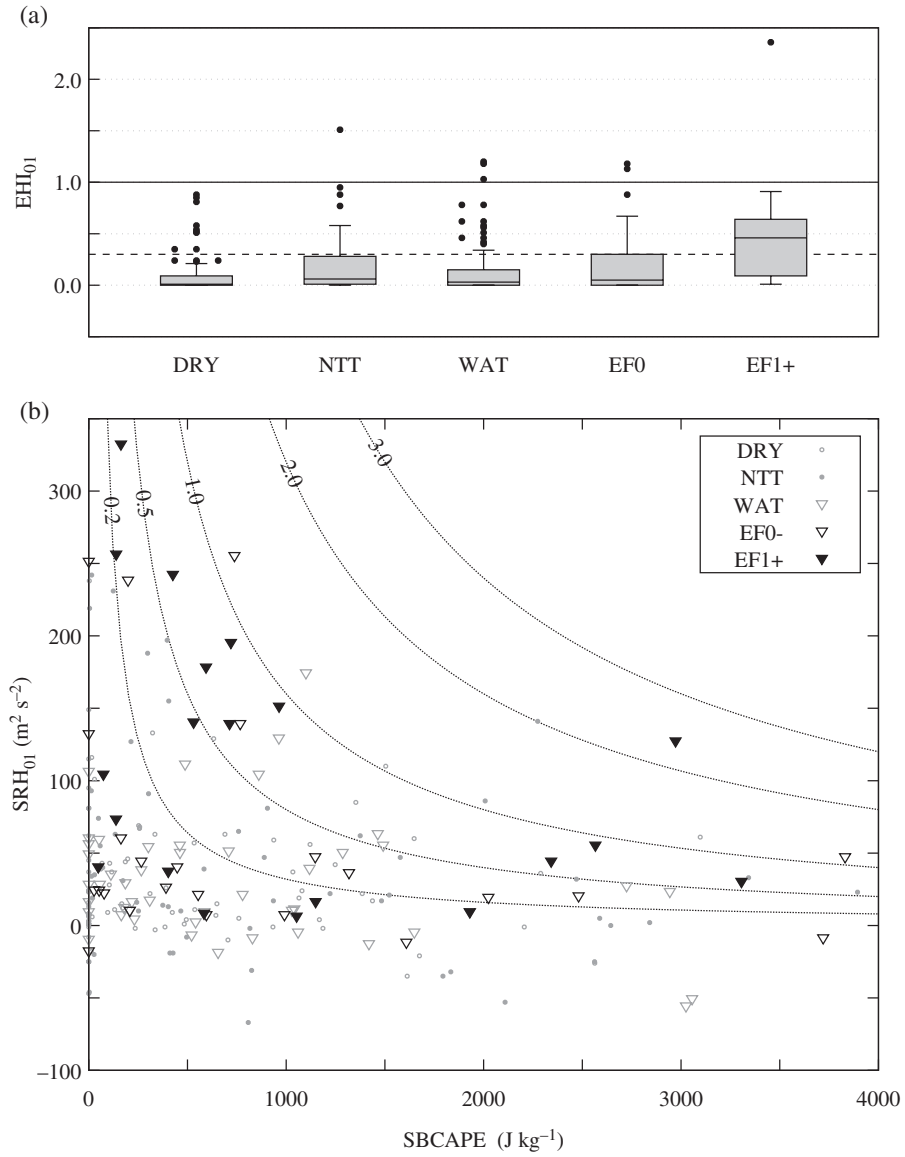

Figure 9. As Figure 4, but for EHI_{01} (a), where the solid line (1.0) is the Thompson *et al.* (2003) reference threshold and the dashed line is the proposed threshold (0.3), and (b), a scatter diagram of DRY (grey contour, white circles), NTT (grey circles), WAT (grey contour, white triangles), EF0 (black contour, white triangles), and EF1+ (black triangles) soundings, plotting SRH_{01} and SBCAPE, where the dotted grey lines are constant EHI_{01} values (0.2, 0.5, 1.0, 2.0, and 3.0).

a total of 48% of them exceeding EHI_{01} values of 0.5 due to high SBCAPE or high SRH_{01} values. More specifically, Figure 9(b) shows that for EF1+ soundings, when SBCAPE is not greater than 1000 J kg^{-1}, SRH_{01} reaches values over 80 m^2 s^{-2}; whereas SRH_{01} is not necessarily as high when SBCAPE exceeds 1000 J kg^{-1}. It can also be seen that there are few DRY, NTT, WAT, and EF0 cases that exceeded an EHI_{01} of 0.5, while most EF1+ soundings were around or over this value.

For the other types of soundings, EHI_{01} values were lower, with 75% of EF0 and NTT cases having an EHI_{01} between 0.0 and 0.3, values for WAT soundings ranging between 0.0 and 0.2, and DRY soundings usually not surpassing 0.1. All these values are very similar to each other, so EHI_{01} is not a good discriminator for weak tornadoes and waterspouts, as reported in Gayà *et al.* (2001) for the Balearic Islands, which are a geographical neighbour of our study region. However, this parameter is useful to discern soundings associated with EF1+ tornadoes.

3.4.2. *VGP 0–4 km (VGP_{04})*

The VGP gives an account of the rate of stretching and tilting of horizontal vorticity by the updraft from a convective cell. As expected from its definition, this parameter reaches its highest values for WAT, EF0, and especially for EF1+ (Figure 10(a)). Around 50% of WAT and EF0 cases had values greater than 0.200 m s^{-2}, and more

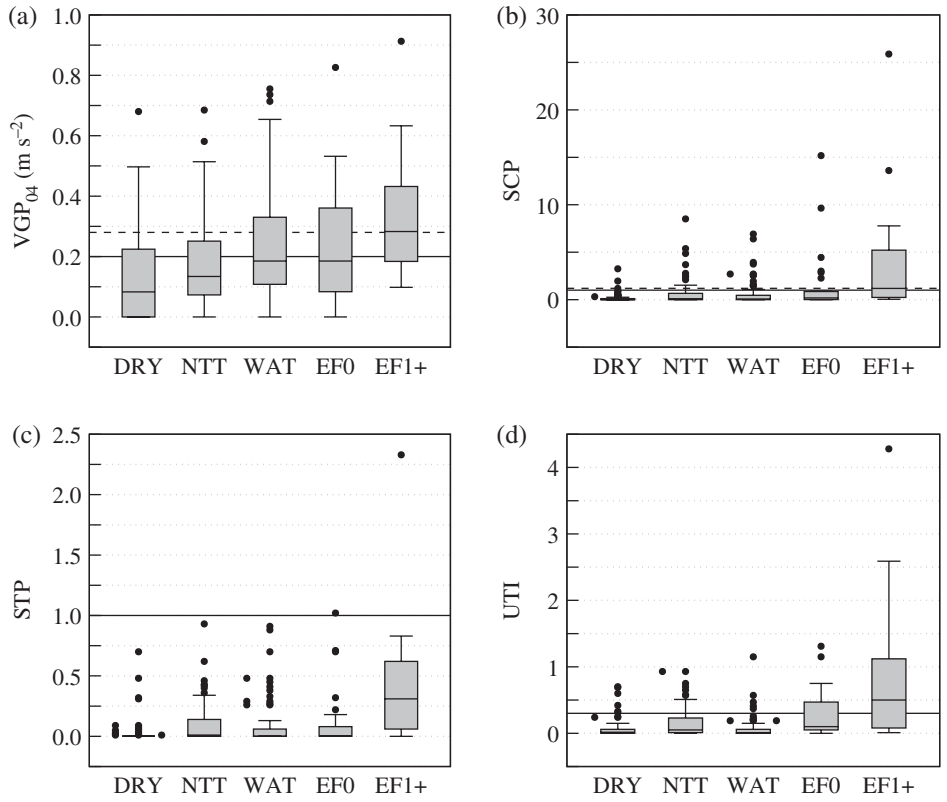

Figure 10. As Figure 4, but for VGP_{04} (a), where the solid line is the Thompson – Storm Prediction Center – threshold (0.200 m s^{-2}) and the dashed line is the proposed threshold (0.280 m s^{-2}); SCP (b), where the solid line is the Thompson *et al.* (2003) threshold (1.0) and the dashed line is the proposed threshold (1.2); STP (c), where the solid line is Thompson *et al.* (2003) threshold (1.0), and UTI (d), where the solid line is Taszarek and Kolendowicz (2013) threshold (0.3).

than one fourth of our EF1+ soundings even surpassed 0.400 m s^{-2}. Meanwhile, DRY and NTT soundings rarely had VGP_{04} values greater than 0.150 m s^{-2}. These results suggest that higher values of VGP_{04} produce environments that are more favourable for tornadic phenomena (waterspouts or tornadoes) and the greater the VGP_{04}, the stronger the tornado. Specifically, there are significant differences between NTT and WAT, with a confidence level of 95%, and between NTT and EF1+, with a confidence level of 99% (Table A1). However, there are no significant differences between NTT and EF0.

Thompson (Storm Prediction Center, http://www.spc.noaa.gov/sfctest/help/sfcoa.html) considered that VGP_{04} values exceeding 0.200 m s^{-2} suggest an increasing possibility of tornadic storms. This value was surpassed by 67% of our EF1+ soundings, including all the EF2 cases (not shown), 43% of EF0 soundings, and 45% of WAT soundings. However, 34% of NTT and 27% of DRY soundings also had VGP_{04} values higher than 0.200 m s^{-2}, which causes a high number of false alarms based solely on this threshold.

Rasmussen and Blanchard (1998) proposed a VGP_{04} value of 0.310 m s^{-2} to discriminate between supercells with significant tornadoes and supercells without significant tornadoes. In total, 47% of our EF1+, 32% of EF0, and 29% of WAT soundings had values of VGP_{04} greater than this threshold, while only 20% of NTT and 11% of DRY surpassed it.

3.4.3. *Supercell composite parameter (SCP)*

The SCP is a parameter that was originally created to discern between environmental conditions that were favourable or not for supercells. However, when calculated with our sounding database (Figure 10(b)), it proved useful in discriminating between EF1+ tornadoes and non-tornadic storms, in agreement with Grams *et al.* (2012). The main reason for this is that the ratio of EF1+ tornadoes linked to a mesocyclone is probably higher than that of EF0 and waterspouts (Markowski and Richardson, 2010). The median SCP value for EF1+ was 1.2, whereas for the other sounding types, SCP values are considerably lower and below 0.5 for the following proportions: 94% of DRY, 71% of NTT, 77% of WAT, and 71% of EF0.

In Thompson *et al.*'s (2003) study, an SCP threshold value of 1.0 is recommended to discriminate between supercell and non-supercell storm environments. This value was exceeded by 62% of our EF1+ cases, and by all our five EF2 cases (not shown), whereas the percentage was clearly lower for the other sounding types. Despite this, the threshold produced some false alarms when used

for discerning tornadic EF1+ from non-tornadic thunderstorms, due to the 17% of NTT soundings that surpassed 1.0.

3.4.4. *Significant tornado parameter (STP)*

In the United States, where significant tornadoes are much more common than in Catalonia, the STP threshold for discriminating between significant and non-significant tornadoes is set at 1.0 (Thompson *et al.,* 2003).

It can be seen that our DRY, NTT, WAT, and EF0 soundings all had low STP values: below 0.5 (Figure 10(c)). The highest values were for EF1+, but despite this, only one sounding in this category surpassed the threshold of 1.0. The ratio of soundings with STP values higher than 0.5 is greater: about one third of the EF1+ events. This implies that there are significant differences between EF1+ and the other sounding types, but it is not useful to discriminate between NTT and EF0 or WAT.

Low STP values, even for significant tornadoes, are not rare in Europe compared to the United States. For example, Kaltenböck *et al.* (2009) obtain similar results for a larger database with more significant tornadoes. The main reason might be that the STP equation takes different parameters into account – mixed-layer convective available potential energy (MLCAPE), WS_{06}, SRH_{01}, and mixed-layer lifting condensation level (MLLCL) – which are normalized with the US thresholds. These are notably different for Europe and particularly for the western Mediterranean area, as has been seen throughout this article. Moreover, some of these parameters, such as MLCAPE or MLLCL, do not present significant differences between NTT and EF1+ soundings in our database (not shown). This is why they are not included in this study. Furthermore, the fact that significant and violent tornadoes in Europe are not as frequent as in the United States may be a consequence of the lack of extremely high CAPE and SRH values.

3.4.5. *Universal tornadic index (UTI)*

The UTI is a dimensionless index (Taszarek and Kolendowicz, 2013) originally developed in Poland, and its authors propose a value of 0.30 as a threshold to discriminate between tornadic and non-tornadic storms. Sixty-seven percent of our EF1+ soundings, including the five EF2 cases (not shown), exceeded this threshold. The percentage is considerably lower for EF0: only 26% of EF0 have a UTI equal to or higher than 0.30 (Figure 10(d)).

While DRY, NTT, and WAT soundings presented low UTI values and the differences between them were not statistically significant, EF0 and EF1+ soundings reached higher UTI values and their *p*-values, compared to the other sounding classes, were below 0.100 (Table A1). The EF0 median, 0.10, was higher than the 75th percentile of the DRY and WAT data, and 33% of EF0 soundings had a UTI higher than the 75th percentile of NTT. The EF1+ cases had the highest values: 53% were greater than 0.50.

If EF0 tornadoes are separated according to their surface origin (over water or inland), then the UTI differences become significant. These differences are clearly illustrated by 75th percentile values: While for EF0 events formed over water, it is 0.27, for EF0 tornadoes formed inland, it is 0.47 (not shown). Interestingly, this parameter shows that environmental conditions for waterspout formation, even if they hit land, are different from the conditions for tornado formation inland and, at the same time, similar to those of NTT soundings.

Therefore, the UTI is useful to discern between tornadic and non-tornadic storms, especially if they produce significant tornadoes, using the same thresholds proposed for tornadoes in Poland in Taszarek and Kolendowicz (2013).

3.5. EF1+ *versus* non-tornadic thunderstorms

In this section, thresholds for different parameters have been calculated to discriminate EF1+ tornadic events from non-tornadic thunderstorms, according to the sounding-derived parameter database. The threshold calculation was performed by considering two conditions regarding EF1+ and NTT sounding distributions: (1) The threshold value was equal to or lower than the EF1+ median value and (2) the threshold was equal to or higher than the 75th percentile of the NTT value. These two criteria were used to ensure a reasonable hit rate for EF1+ and few false alarms for NTT. As explained in previous sections, of the set of sounding categories, only the EF1+ soundings presented significantly different values in all the parameters. This is the reason why thresholds for EF0 and WAT cases have not been established. The parameters that verified the two conditions given above are shown in Table 4.

Table 4. Seventy-fifth percentile of NTT, 50th percentile of EF1+, proposed thresholds, percentage of NTT below the proposed threshold, and percentage of EF1+ over the threshold, for selected parameters.

Parameter (units)	75 percentile (NTT)	50 percentile (EF1+)	Proposed threshold	Perc. NTT below (%)	Perc. EF1+ over
WS_{03} ($m\,s^{-1}$)	12.9	16.0	15.0	86	57
WS_{01} ($m\,s^{-1}$)	7.2	8.1	8.0	79	52
SRH_{03} ($m^2\,s^{-2}$)	122	187	150	82	57
SRH_{01} ($m^2\,s^{-2}$)	65	73	70	78	52
EHI_{01}	0.3	0.5	0.3	79	57
VGP_{04} ($m\,s^{-2}$)	0.249	0.283	0.280	80	52
SCP	0.7	1.2	1.2	86	52
UTI	0.23	0.50	0.30	82	67

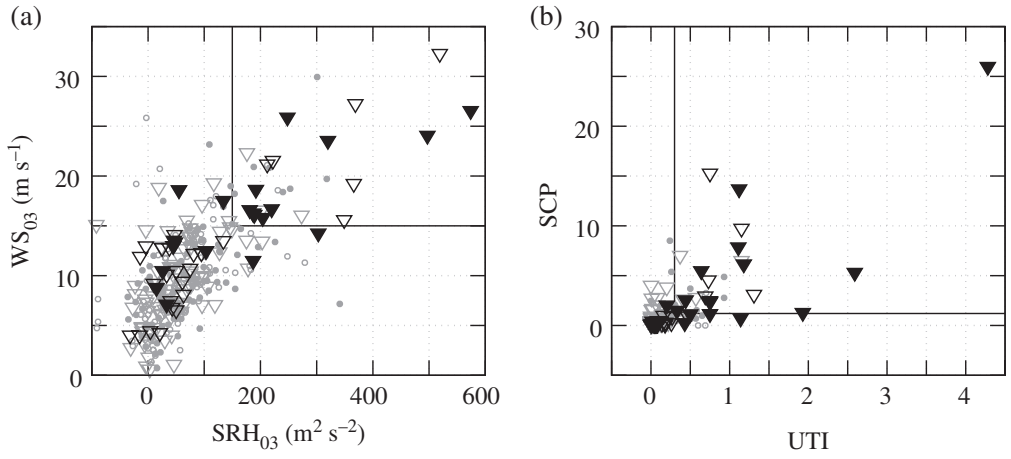

Figure 11. As Figure 9(b), but plotting WS_{03} and SRH_{03} values where the solid lines are the new SRH_{03} and WS_{03} thresholds (a), and relating SCP and UTI values where the solid lines are the new UTI and SCP thresholds (b).

Comparing the parameters that provide the best discrimination for tornadic events in Catalonia (SRH_{03}, WS_{03}, SCP, and UTI), according to the statistical analysis (Tables 4 and A1), it can be seen that usually most soundings associated with EF1+ tornadoes exceed the suggested thresholds at the same time. In Figure 11(a), which shows a scatterplot of SRH_{03} *versus* WS_{03} for all soundings, it can be seen that 45% of EF1+ soundings surpassed both thresholds. The ratio is lower for EF0 (22%), as could be expected for these weaker tornadoes. Moreover, 5% of WAT, 10% of NTT, and 1% of DRY soundings had SRH_{03} and WS_{03} values over 150 m^2 s^{-2} and 15.0 m s^{-1}, respectively, at the same time.

Similar results are obtained plotting UTI *versus* SCP values for all the soundings (Figure 11(b)): 48% of EF1+ cases have a UTI over 0.30 and an SCP greater than 1.2. However, the number of EF0 events that meet both conditions is only 22%. Just 9% of NTT, 4% of WAT, and 2% of DRY surpass the two thresholds concurrently.

4. Summary and conclusions

After examining 12 different parameters in 333 soundings including the environments of 49 tornadic storms, 104 waterspout events, 90 non-tornadic thunderstorms and 90 dry periods from 17 years in Catalonia (NE Spain) it has been found that:

- High SBCAPE values are not necessarily linked with tornadic storms; weak tornadoes and waterspouts with SBCAPE values under 400 J kg^{-1} can be formed, as is also reported in several articles as Groenemeijer and van Delden (2007).
- In general, the greater the WS, the stronger the tornado. This is especially valid for mid-level WS, which is consistent with Taszarek *et al.* (2017). Proposed thresholds for WS_{03} and WS_{01} to detect EF1+ cases are 15 and 8 m s^{-1}, respectively.
- Waterspout environments are more frequent than those of tornado events. Most studied parameters do not present differences between WAT and NTT soundings; this is a similar result to those of Matsangouras *et al.* (2017) and Renko *et al.* (2016): Only VGP_{04} presents values which are significantly different.
- Waterspouts that hit land (54% of EF0 tornado cases) present substantially different mid-level WS values and UTI values from EF0 tornadoes formed inland. EF0 tornadoes formed over water do not present such high WS_{03} and UTI values as those that are formed over land. Future analysis with an enlarged database would allow us to consider a specific new class for tornadoes that are originated as waterspouts, in order to discriminate these differences in more detail.
- STP is not useful to differentiate tornadic and non-tornadic soundings. Nevertheless, if EF0 cases are ignored, then it is possible to find differences in STP values between EF1+ and the other sounding types. Moreover, in other articles, such as Kaltenböck *et al.* (2009), it is found that STP tends to be smaller in Europe than in the United States for significant tornadoes due to the lack of extreme CAPE and SRH values.
- UTI presents significant differences between NTT and EF1+ soundings. More than 65% of EF1+ cases, including the five EF2 tornadic events, surpassed the threshold of 0.3, while 82% of NTT did not reach it. Moreover, the higher the UTI value, the stronger the tornado. Median UTI values for EF0 and EF1+ are 0.10 and 0.50, respectively.
- Other composite parameters such as EHI_{01} and SCP are good at discriminating between NTT and EF1+ soundings. EF1 and EF2 tornadoes typically reach values higher than 0.3 for EHI_{01} and 1.2 for SCP. These values are lower than in Thompson *et al.*'s (2003) study, but this discrepancy could be explained by two characteristics of our database: A probable large proportion

of non-mesocylonic tornadoes and the fact that most of them do not exceed EF1.

Despite the relatively small size of the current tornado database and the low density of the radiosonde network in the western Mediterranean area, these results can contribute to enhancing situational awareness and both convective storm forecasting and surveillance tasks, in the region of study, and they can also complement similar climatological studies of upper air conditions for tornadic and waterspout events.

Acknowledgements

We are grateful to many individuals who helped us to build the tornado and waterspout database used in this study, in particular Joan Arús, Salvador Castán, Miquel Gayà, Dani Ramírez, and Tomeu Rigo; and also to Crispín Parra, Manel Massagué, and Ignacio Rico, whose photos enabled us to include in the database a large number of tornadic events, especially nocturnal waterspouts. We also appreciate the radiosonde data from the Meteorological Service of Catalonia (SMC), Spanish Meteorological Service (AEMET), and Météo-France. This study was performed within the framework of the HyMeX (HYdrological cycle in the Mediterranean EXperiment) programme, with partial funding from projects CGL2015-65627-C3-2-R (MINECO/FEDER) and CGL2016-81828-REDT (MINECO), and also from the Water Research Institute (IdRA) of the University of Barcelona.

Appendix

The *p*-values of the Kolmogorov–Smirnov test for all the parameters studied are shown in Table A1. Only values below 0.100 are considered to be statistically significant in this article. It can be seen that generally there are significant differences between DRY and WAT soundings, and DRY and EF0 soundings for most of the parameters studied. However, the most significant differences are between DRY and EF1+ soundings, with $p < 0.004$ for all the parameters. Differences are also significant between EF1+ and the rest of the sounding classes for most of the parameters. The poorest differences are between NTT and WAT (only VGP_{04} has a *p*-value below 0.100), and between NTT and EF0, and WAT and EF0 (only UTI presents a *p*-value below 0.100 for these sounding categories).

Table A1. *p*-Values of the Kolmogorov–Smirnov test for every sounding type *versus* WAT, EF0, and EF1+ for all sounding-derived parameters.

Parameter	DRY *vs* WAT	NTT *vs* WAT	DRY *vs* EF0	NTT *vs* EF0	WAT *vs* EF0	DRY *vs* EF1+	NTT *vs* EF1+	WAT *vs* EF1+	EF0 *vs* EF1+
SBCAPE	**0.000**	–	**0.005**	–	–	**0.000**	–	–	–
WS_{06}	**0.001**	–	0.016	–	–	**0.000**	0.025	0.040	–
WS_{03}	–	–	0.088	–	–	**0.000**	**0.000**	**0.000**	0.017
WS_{01}	0.038	–	0.020	–	–	**0.003**	0.025	0.025	–
BRNSHR	0.046	–	–	–	–	**0.000**	**0.004**	**0.000**	0.029
SRH_{03}	–	–	–	–	–	**0.000**	**0.005**	**0.000**	0.060
SRH_{01}	0.036	–	0.095	–	–	**0.000**	0.028	0.012	0.037
EHI_{01}	–	–	0.082	–	–	**0.000**	0.011	0.032	–
VGP_{04}	**0.000**	0.042	0.020	–	–	**0.000**	**0.005**	–	–
SCP	**0.000**	–	**0.000**	–	–	**0.000**	**0.001**	**0.000**	0.048
STP	**0.001**	–	0.016	–	–	**0.000**	**0.001**	**0.000**	**0.005**
UTI	–	–	**0.000**	0.027	**0.000**	**0.000**	**0.000**	**0.000**	0.060

p-Values over 0.100 are not shown. In bold, *p*-values equal to or lower than 0.010.

References

American Meteorological Society. 2017a. *Tornado. Glossary of meteorology*. http://glossary.ametsoc.org/wiki/Tornado (accessed 17 April 2017).

American Meteorological Society. 2017b. *Waterspout. Glossary of meteorology*. http://glossary.ametsoc.org/wiki/Waterspout (accessed 17 April 2017).

Antonescu B, Bell A. 2015. Tornadoes in Romania. *Mon. Weather Rev.* **143**: 689–701. https://doi.org/10.1175/MWR-D-14-00181.1.

Antonescu B, Schultz DM, Lomas F, Kühne T. 2016. Tornadoes in Europe: synthesis of the observational datasets. *Mon. Weather Rev.* **144**: 2445–2480. https://doi.org/10.1175/MWR-D-15-0298.1.

Antonescu B, Schultz D, Holzer A, Groenemeijer P. 2017. Tornadoes in Europe: an underestimated threat. *Bull. Am. Meteorol. Soc.* **98**: 713–728. https://doi.org/10.1175/BAMS-D-16-0171.1.

Aran M, Amaro J, Arús J, Bech J, Figuerola F, Gayà M, Vilaclara E. 2009. Synoptic and mesoscale diagnosis of a tornado event in Castellcir, Catalonia, on 18th October 2006. *Atmos. Res.* **93**: 147–160. https://doi.org/10.1016/j.atmosres.2008.09.031.

Bech J, Pascual R, Rigo T, Pineda N, López JM, Arús J, Gayà M. 2007. An observational study of the 7 September 2005 Barcelona tornado outbreak. *Nat. Hazards Earth Syst. Sci.* **7**: 129–139. https://doi.org/10.5194/nhess-7-129-2007.

Bech J, Gayà M, Aran M, Figuerola F, Amaro J, Arús J. 2009. Tornado damage analysis of a forest area using site survey observations, radar data and a simple analytical vortex model. *Atmos. Res.* **93**: 118–130. https://doi.org/10.1016/j.atmosres.2008.10.016.

Bech J, Pineda N, Rigo T, Aran M, Amaro J, Gayà M, Arús J, Montanyà J, van der Velde O. 2011. A Mediterranean nocturnal heavy rainfall and tornadic event. Part I: overview, damage survey and radar analysis. *Atmos. Res.* **100**: 621–637. https://doi.org/10.1016/j.atmosres.2010.12.024.

Bissolli P, Grieser J, Dotzek N, Welsch M. 2007. Tornadoes in Germany 1950–2003 and their relation to particular weather conditions. *Glob. Planet. Change* **57**: 124–138. https://doi.org/10.1016/j.gloplacha.2006.11.007.

Brady RH, Szoke EJ. 1989. A case study of nonmesocyclone tornado development in northeast Colorado: similarities to waterspout formation. *Mon. Weather Rev.* **117**: 843–856. https://doi.org/10.1175/1520-0493(1989)117<0843:ACSONT>2.0.CO;2.

Craven JP, Brooks HE. 2004. Baseline climatology of sounding derived parameters associated with deep moist convection. *Nat. Weather Digest* **28**: 13–24.

Davies JM. 1993. Hourly helicity, instability, and EHI in forecasting supercell tornadoes. In *17th Conference on Severe Local Storms*, American Meteorological Society, St. Louis, MO.

Davies-Jones RP, Burgess D, Foster M. 1990. Test of helicity as a tornado forecast parameter. In *16th Conference on Severe Local Storms*, American Meteorological Society, Kananaskis Park, Alberta, Canada, 588–592.

Doswell III CA, Evans JS. 2003. Proximity sounding analyses for derechos and supercells: an assessment of similarities and differences. *Atmos. Res.* **67–68**: 117–133. https://doi.org/10.1016/S0169-8095(03)00047-4.

Doswell III CA, Rasmussen EN. 1994. The effect of neglecting the virtual temperature correction on CAPE calculations. *Weather Forecast.* **9**: 625–629. https://doi.org/10.1175/1520-0434(1994)009<0625:TEONTV>2.0.CO;2.

Doswell III CA, Schultz DM. 2006. On the use of indices and parameters in forecasting severe storms. *Electron. J. Severe Storms Meteorol.* **1**: 1–22.

Doswell III CA, Brooks HE, Dotzek N. 2009. On the implementation of the enhanced Fujita scale in the USA. *Atmos. Res.* **93**: 554–563. https://doi.org/10.1016/j.atmosres.2008.11.003.

Dotzek N. 2003. An updated estimate of tornado occurrence in Europe. *Atmos. Res.* **67–68**: 153–161. https://doi.org/10.1016/S0169-8095(03)00049-8.

Dotzek N, Groenemeijer P, Feuerstein B, Holzer AM. 2009. Overview of ESSL's severe convective storms research using the European severe weather database ESWD. *Atmos. Res.* **93**: 575–586. https://doi.org/10.1016/j.atmosres.2008.10.020.

Frique JY. 2012. Les tornades en Belgique (tornadoes in Belgium). Belgorage, 31 pp. (in French), https://dl.dropboxusercontent.com/u/1866013/Documents/Tornades/1779-2012-bilan-climatologique-des-tornades-en-belgique.pdf (accessed 19 April 2017).

Gayà M. 2015. Els fiblons a Espanya: climatologia i catàleg de tornados i trombes (whirlwinds in Spain: climatology and catalog of tornadoes and waterspouts). Universitat de les Illes Balears, Palma, Spain, 441 pp. (in Catalan).

Gayà M, Homar V, Romero R, Ramis C. 2001. Tornadoes and waterspouts in the Balearic Islands: phenomena and environmental characterization. *Atmos. Res.* **56**: 253–267. https://doi.org/10.1016/S0169-8095(00)00076-4.

Gayà M, Llasat M-C, Arús J. 2011. Tornadoes and waterspouts in Catalonia (1950–2009). *Nat. Hazards Earth Syst. Sci.* **11**: 1875–1883. https://doi.org/10.5194/nhess-11-3023-2011.

Giaiotti DB, Giovannoni M, Pucillo A, Stel F. 2007. The climatology of tornadoes and waterspouts in Italy. *Atmos. Res.* **83**: 534–541. https://doi.org/10.1016/j.atmosres.2005.10.020.

Grams JS, Thompson RL, Snively DV, Prentice JA, Hodges GM, Reames LJ. 2012. A climatology and comparison of parameters for significant tornado events in the United States. *Weather Forecast.* **27**: 106–123. https://doi.org/10.1175/WAF-D-11-00008.1.

Groenemeijer PH, van Delden A. 2007. Sounding-derived parameters associated with large hail and tornadoes in The Netherlands. *Atmos. Res.* **83**: 473–487. https://doi.org/10.1016/j.atmosres.2005.08.006.

Johns RH, Doswell CA III. 1992. Severe local storms forecasting. *Weather Forecast.* **7**: 588–612. https://doi.org/10.1175/1520-0434(1992)007<0588:SLSF>2.0.CO;2.

Kaltenböck R, Diendorfer G, Dotzek N. 2009. Evaluation of thunderstorm indices from ECMWF analyses, lightning data and severe storms reports. *Atmos. Res.* **93**: 381–396. https://doi.org/10.1016/j.atmosres.2008.11.005.

Markowski PM, Richardson YP. 2010. *Mesoscale Meteorology in Midlatitudes*. Wiley-Blackwell: Chichester, UK, 273–291.

Mateo J, Ballart D, Brucet C, Aran M, Bech J. 2009. A study of a heavy rainfall event and a tornado outbreak during the passage of a squall line over Catalonia. *Atmos. Res.* **93**: 131–146. https://doi.org/10.1016/j.atmosres.2008.09.030.

Matsangouras IT, Nastos PT, Bluestein HB, Sioutas MV. 2014. A climatology of tornadic activity over Greece based on historical records. *Int. J. Climatol.* **34**: 2538–2555. https://doi.org/10.1002/joc.3857.

Matsangouras IT, Nastos PT, Bluestein HB, Pytharoulis I, Papachristopoulou K, Miglietta MM. 2017. Analysis of waterspout environmental conditions and of parent-storm behaviour based on satellite data over the southern Aegean Sea of Greece. *Int. J. Climatol.* **37**: 1022–1039. https://doi.org/10.1002/joc.4757.

Miglietta MM, Rotunno R. 2016. An EF3 multi-vortex tornado over the Ionian region: is it time for a dedicated warning system over Italy? *Bull. Am. Meteorol. Soc.* **97**: 337–344. https://doi.org/10.1175/BAMS-D-14-00227.1.

Moncrieff MW, Miller MJ. 1976. The dynamics and simulation of tropical cumulonimbus and squall lines. *Q. J. R. Meteorol. Soc.* **102**: 373–394. https://doi.org/10.1002/qj.49710243208.

Monteverdi JP, Doswell CA III, Lipari GS. 2003. Shear parameter thresholds for forecasting tornadic thunderstorms in Northern and Central California. *Weather Forecast.* **18**: 357–370. https://doi.org/10.1175/1520-0434(2003)018<0357:SPTFFT>2.0.CO;2.

Mulder KJ, Schultz DM. 2015. Climatology, storm morphologies, and environments of tornadoes in the British Isles: 1980–2012. *Mon. Weather Rev.* **143**: 2224–2240. https://doi.org/10.1175/MWR-D-14-00299.1.

Pineda N, Rigo T, Bech J, Soler X. 2007. Lightning and precipitation relationship in summer thunderstorms: case studies in the northwestern Mediterranean region. *Atmos. Res.* **85**: 159–170. https://doi.org/10.1016/j.atmosres.2006.12.004.

Potvin CK, Elmore KL, Weiss SJ. 2010. Assessing the impacts of proximity sounding criteria on the climatology of significant tornado environments. *Weather Forecast.* **25**: 921–930. https://doi.org/10.1175/2010WAF2222368.1.

Ramis C, Arús J, López JM, Mestres AM. 1997. Two cases of severe weather in Catalonia (Spain): an observational study. *Meteorol. Appl.* **4**: 207–217. https://doi.org/10.1017/S1350482797000510.

Rasmussen EN. 2003. Refined supercell and tornado forecast parameters. *Weather Forecast.* **18**: 530–535. https://doi.org/10.1175/1520-0434(2003)18<530:RSATFP>2.0.CO;2.

Rasmussen EN, Blanchard DO. 1998. A baseline climatology of sounding-derived supercell and tornado forecast parameters. *Weather Forecast.* **13**: 1148–1164. https://doi.org/10.1175/1520-0434(1998)013<1148:ABCOSD>2.0.CO;2.

Rauhala J, Schultz DM. 2009. Severe thunderstorm and tornado warnings in Europe. *Atmos. Res.* **93**: 369–380. https://doi.org/10.1016/j.atmosres.2008.09.026.

Rauhala J, Brooks HE, Schultz DM. 2012. Tornado climatology of Finland. *Mon. Weather Rev.* **140**: 1446–1456. https://doi.org/10.1175/MWR-D-11-00196.1.

Renko T, Kuzmić J, Šoljan V, Mahović NS. 2016. Waterspouts in the eastern Adriatic from 2001 to 2013. *Nat. Hazards* **82**: 441–470. https://doi.org/10.1007/s11069-016-2192-5.

Riesco Martín J, Polvorinos Pascual F, Núñez Mora JA, Soriano Romero J, Jiménez Alonso C. 2015. Climatología de tornados en España Peninsular y Baleares (climatology of tornadoes in Peninsular Spain and Balearic Islands). Agencia Estatal de Meteorología (AEMet) (in Spanish), http://www.aemet.es/documentos/es/conocermas/publicaciones/Climatologia_tornados/Climatologia_tornados.pdf (accessed 30 November 2016).

Romero R, Gayà M, Doswell CA III. 2007. European climatology of severe convective storm environmental parameters: a test for significant tornado events. *Atmos. Res.* **83**: 389–404. https://doi.org/10.1016/j.atmosres.2005.06.011.

Sioutas MV, Keul AG. 2007. Waterspouts of the Adriatic, Ionian and Aegean Sea and their meteorological environment. *Atmos. Res.* **83**: 542–557. https://doi.org/10.1016/j.atmosres.2005.08.009.

Stensrud DJ, Cirtonas JV Jr, Brooks HE. 1997. Discriminating between tornadic and nontornadic thunderstorms using mesoscale model output. *Weather Forecast.* **12**: 613–632. https://doi.org/10.1175/1520-0434(1997)012<0613:DBTANT>2.0.CO;2.

Taszarek M, Brooks HE. 2015. Tornado climatology of Poland. *Mon. Weather Rev.* **143**: 702–717. https://doi.org/10.1175/MWR-D-14-00185.1.

Taszarek M, Kolendowicz J. 2013. Sounding-derived parameters associated with tornado occurrence in Poland and universal tornadic index. *Atmos. Res.* **134**: 186–197. https://doi.org/10.1016/j.atmosres.2013.07.016.

Taszarek M, Brooks HE, Czernecki B. 2017. Sounding-derived parameters associated with convective hazards in Europe. *Mon. Weather Rev.* **145**: 1511–1528. https://doi.org/10.1175/MWR-D-16-0384.1.

Thompson RL, Edwards R, Hart JA, Elmore KL, Markowski P. 2003. Close proximity soundings within supercell environments obtained from the rapid update cycle. *Weather Forecast.* **18**: 1243–1261. https://doi.org/10.1175/1520-0434(2003)018<1243:CPSWSE>2.0.CO;2.

Wakimoto RM, Wilson JW. 1989. Non-supercell tornadoes. *Mon. Weather Rev.* **117**: 1113–1140. https://doi.org/10.1175/1520-0493(1989)117<1113:NST>2.0.CO;2.

Wegener A. 1917. Wind-und Wasserhosen in Europa (tornadoes and waterspouts in Europe). Friedrich Vieweg and Sohn, Braunschweig, Germany, 301 pp. (in German).

Weisman ML, Klemp JB. 1982. The dependence of numerically simulated convective storms on vertical wind shear and buoyancy. *Mon. Weather Rev.* **110**: 504–520. https://doi.org/10.1175/1520-0493(1982)110<0504:TDONSC>2.0.CO;2.

Wilks DS. 2011. *Statistical Methods in the Atmospheric Sciences*. Academic Press: Oxford, UK, 676 pp.

4.2 Entorns favorables per a la tornadogènesi a la Península Ibèrica i les Illes Balears basats en el reanàlisi ERA5

4.2.1 Resum de l'article

En aquest treball s'analitzen 907 perfils verticals de temperatura, humitat i vent associats a 1102 tornados i mànegues marines registrats a la Península Ibèrica i les Illes Balears entre els anys 1980 i 2018. La zona d'estudi es divideix en dues regions a causa de les diferències en la distribució mensual dels tornados i les mànegues marines: el nord-est de la Península i les Illes Balears (NE), on són més habituals durant l'època càlida (72,9%, maig-octubre), i el sud-oest (SW), on són més freqüents al llarg de l'època freda (73,3%, novembre-abril). Els episodis estudiats s'agrupen en cinc categories: els casos d'intensitat F0 o EF0 ((E)F0), els d'intensitat F1 o EF1 ((E)F1), els fiblons significatius ((E)F2+), els casos dels quals no s'ha pogut conèixer la intensitat (UR) i les trombes marines (WAT).

Les dades utilitzades per a generar els perfils verticals provenen de la reanàlisi ERA5, el darrer de l'ECMWF. Aquesta reanàlisi té una resolució espacial de 0,25°, una resolució temporal d'1 hora i 37 nivells de pressió a més de dades de superfície. A l'hora d'analitzar un episodi, se selecciona el punt de malla més proper i l'hora immediatament anterior a l'esdeveniment.

Com a paràmetres termodinàmics s'estudien la CAPE i la CIN, calculades mitjançant la parcel·la MU. Pel que fa als paràmetres cinemàtics, s'analitzen l'SRH per als estrats 0-1 km i 0-3 km, i el WS per als estrats 0-1 km, 0-3 km i 0-6 km. A més, també s'estudien els paràmetres compostos UTI i WMAXSHEAR. D'aquest darrer, a banda de testejar-ne la versió original, se'n modifica l'equació substituint el terme WS 0-6 km per WS 0-3 km, ja que aquest darrer discrimina d'una manera més clara els entorns en funció de la intensitat dels fiblons. Finalment, també s'analitza la distribució en el nomograma de Szilagyi dels episodis de mànegues marines. Com a la secció anterior, s'ha utilitzat el test de Kolmogorov-Smirnov (KS) per a estudiar les diferències en els paràmetres en funció del tipus de perfil vertical i per a comparar-ho amb Rodríguez i Bech (2018).

Fruit de l'anàlisi dels resultats, s'identifiquen dos casos particulars de perfils verticals associats a episodis de tornados, prèviament descrits per altres autors:

- Cisallament del vent elevat i CAPE baixa (HSLC; típic de l'època freda i, per tant, més habitual al SW)
- Helicitat baixa i LCL elevat (LHHLCL; típic de l'època càlida i, per tant, més freqüent al NE)

S'observa que en general existeix una dependència entre la CAPE i el WS, especialment per a l'estrat 0-3 km, de manera que en entorns molt inestables (CAPE elevada) hi pot haver tornados significatius amb un WS més aviat moderat, mentre que per a una CAPE baixa, cal que el WS sigui marcat. L'índex WMAXSHEAR 0-3 km descriu bé aquest fet i demostra ser útil a l'hora de discriminar els entorns de fiblons significatius (> 500 m^2 s^{-2}) respecte a la resta.

La majoria dels episodis de mànegues marines queden circumscrits dins l'àrea favorable descrita al nomograma de Szilagyi, tant els del NE com els del SW. Més de la meitat dels casos que se situen fora de la zona favorable corresponen a trombes marines de l'època freda, un fet que ja havia estat observat en altres sectors de la conca mediterrània. Això posa de manifest que convindria adaptar el nomograma per a la Mediterrània, ja que originalment fou desenvolupat per a la regió dels Grans Llacs de l'Amèrica del Nord, on a l'època hivernal el gradient de temperatura entre 850 hPa i la superfície dels llacs pot superar els 20 °C.

Aquest article dona resposta als objectius generals **OG2** i **OG3** i als objectius específics **OE5** i **OE6**.

4.2.2 Article

Rodríguez O. i Bech J. (2020): Tornadic environments in the Iberian Peninsula and the Balearic Islands based on ERA5 reanalysis. *International Journal of Climatology*: 1–21. doi:10.1002/joc.6825.

Received: 20 April 2020 | Revised: 28 August 2020 | Accepted: 30 August 2020

DOI: 10.1002/joc.6825

RESEARCH ARTICLE

International Journal of Climatology RMetS

Tornadic environments in the Iberian Peninsula and the Balearic Islands based on ERA5 reanalysis

Oriol Rodríguez | **Joan Bech**

Department of Applied Physics – Meteorology, University of Barcelona, Barcelona, Spain

Correspondence
Oriol Rodríguez, Department of Applied Physics – Meteorology, Faculty of Physics, University of Barcelona, Martí i Franquès, 1, 08028 Barcelona, Spain.
Email: orodriguez@meteo.ub.edu

Funding information
Agencia Estatal de Investigación, Grant/Award Numbers: CGL2016-81828-REDT (AEI), RTI2018-098693-B643-C32 (AEI); Institut de Recerca de l'Aigua (University of Barcelona); Ministerio de Economía, Industria y Competitividad, Gobierno de España, Grant/Award Number: CGL2015-65627-C3-2-R (MINECO/FEDER)

Abstract

A dataset of 907 tornado and waterspout events recorded from 1980 to 2018 was built to study convective environments in the Iberian Peninsula and Balearic Islands (western Mediterranean). The events were grouped into different categories, distinguishing waterspouts and tornadoes that were stratified by intensity according to the Fujita (F) scale and the Enhanced Fujita (EF) scale. The analysis separated the north-east (NE) and south-west (SW) subareas in the region of study, which present different seasonal cycles. For each event, atmospheric profiles from the ERA5 reanalysis data were used to determine convective available potential energy (CAPE), storm-relative helicity (SRH), vertical wind-shear (WS), the Universal Tornadic Index (UTI), and the product of wind-shear and the square root of two times CAPE (WMAXSHEAR). Results showed that the NE events are mostly associated with higher CAPE and lower helicity and wind-shear than the SW events. Thus, a significant number of SW tornadoes are associated with high-shear, low-CAPE environments. Moreover, the low-shear, high-LCL tornado environment, which is common inland during warm-season, is more usual in the NE subarea. Composite parameters such as the UTI and $WMAXSHEAR_{06}$ are good discriminators between significant and weak tornado events, although $WMAXSHEAR_{06}$ presents some limitations for the SW events due to low CAPE and weak differences in the WS (0–6 km) between the (E)F1 and (E)F2+ events. This weakness was resolved by using the 0–3 km WS instead of the 0–6 km WS when calculating the WMAXSHEAR. A new threshold for $WMAXSHEAR_{03}$ is proposed (500 $m^2 \cdot s^{-2}$) to distinguish between significant and non-significant tornado environments. Finally, the Szilagyi Waterspout Nomogram, originally developed for the Great Lakes of North America, was successfully tested in the forecasting of waterspout formation for the first time in the western Mediterranean area, although the technique should be adapted to correctly detect cool-season mid-latitude waterspouts.

KEYWORDS

Balearic Islands, ERA5, Iberian Peninsula, Mediterranean, severe weather, Szilagyi Waterspout Nomogram, tornado, waterspout

1 | INTRODUCTION

Tornadoes are meteorological phenomena that can produce the strongest natural surface winds on Earth. They are classified at the micro-α or micro-β scale (i.e., characteristic time and horizontal length scales ranging from 1 min to 1 hr and 20 m to 2 km; Orlanski, 1975). Thus, they typically affect small areas and their socioeconomic impact is relatively lower than that of other damaging larger-scale weather events such as floods and windstorms (Gall *et al*., 2008; Jahn, 2015; Antonescu *et al*., 2017). Nevertheless, tornado winds can occasionally surpass 100 $m \cdot s^{-1}$ (Fujita, 1971; Wakimoto *et al*., 2015), causing severe damage, injuries and fatalities along their path. Despite recent progress, the precise prediction of their timing and location is still a challenge for operational forecasting systems (Weisman *et al*., 2015). Due to their high impact and low predictability and given the expected increase in the frequency of severe convective storm environments in the present century (Allen *et al*., 2014; Seeley and Romps, 2015; Púčik *et al*., 2017; Viceto *et al*., 2017), it is necessary to increase our understanding of the environmental conditions that favour tornadogenesis.

During the last decades, several studies have analysed upper-air conditions that favour the development of tornadic storms using proximity sounding data (e.g., Maddox, 1976; Rasmussen and Blanchard, 1998; Groenemeijer and van Delden, 2007; Renko *et al*., 2016). Finding the most representative sounding for each tornadic event through proximity criteria (Potvin *et al*., 2010) enables the calculation of thermodynamic, kinematic and their composite parameters, which can be used to characterize the events depending on their intensity or convective mode.

Some studies have also used numerical model analysis (the Rapid Update Cycle, Rasmussen, 2003) and reanalysis data (ERA-40, Romero *et al*., 2007; ERA-Interim, Chernokulsky *et al*., 2019; ERA5, Ingrosso *et al*., 2020). Results from those studies provide valuable thresholds for different severe weather parameters, which may be useful for weather forecasters to identify potential tornadic storm environments. However, there are some limitations to this approach (i.e., threshold exceedance provides guidance, but must be examined in a global context, considering the presence of all the necessary factors or 'ingredients'; Doswell and Schultz, 2006).

The use of reanalysis data instead of real atmospheric sounding measurements increases the temporal resolution (normally, only two soundings per day are launched at radiosonde stations) and spatial resolution (the horizontal grid scale of recent reanalysis data such as from ERA5 [C3S, 2017] is around one order of magnitude smaller than the network density of sounding stations in Europe). Therefore, atmospheric profiles from reanalysis usually provide data from a point (latitude, longitude and time) that is closer to the event of interest than a sounding station does. Nevertheless, direct measurements from soundings provide greater vertical resolution than reanalysis and present a more realistic depiction of the atmospheric boundary layer.

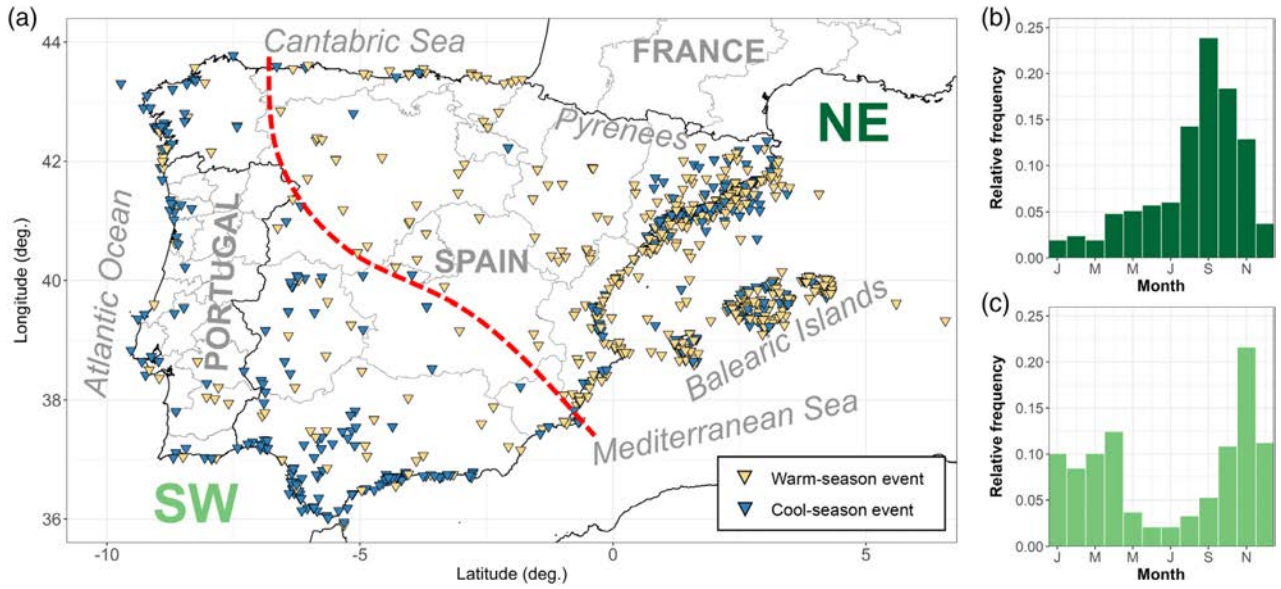

FIGURE 1 (a) Location of the 907 analysed events from 1980 to 2018 on the Iberian Peninsula and Balearic Islands. The dashed line separates the so-called north-east (NE) area, where tornadoes and waterspouts typically occur during warm-season (May–October) and the south-west (SW) area, where they predominate during cool-season (November–April). Relative frequency of tornado and waterspout events in the NE area (b), and the SW area (c) are also shown [Colour figure can be viewed at wileyonlinelibrary.com]

These directly affect the calculation of quantities, which are very sensitive to vertical temperature, dew point and wind profile, especially at low levels (Taszarek *et al*., 2018).

In this article, convective environments prior to tornado formation from events reported in the Iberian Peninsula and Balearic Islands (Figure 1) are characterized. Tornado climatologies of the study area (Leitão, 2003; Gayà, 2011, 2018) show that it is regularly affected by tornadoes and waterspouts (i.e., a tornado occurring over a body of water; Glickman and Zenk, 2000). Moreover, it contains some of the spots where tornadoes occur the most frequently in southern Europe (Figure 1a in Antonescu *et al*., 2017): Balearic Islands, Catalonia (NE Iberia) and the Gulf of Cádiz (SW Iberia). Around 55 million people currently live in this region measuring 630,000 km^2, where significant tornadic storms occasionally have a substantial social impact, with injuries or even fatalities as well as considerable economic losses (Homar *et al*., 2003; Bech *et al*., 2007, 2011; Ramis *et al*., 2009; Sánchez-Laulhé, 2009; Belo-Pereira *et al*., 2017; Rodríguez and Bech, 2020).

Despite the scientific literature containing studies on both the tornado climatologies of Spain and Portugal and also a number of detailed tornadic and waterspout case studies, there have been none to date examining the upper-air environments associated with tornadic storms in this region as a whole. Here, we used ERA5 data (C3S, 2017; Hersbach *et al*., 2020), the latest available reanalysis from the European Centre for Medium-Range Weather Forecasts (ECMWF), which includes tornado and waterspout records occurring in the area from 1980 to 2018. Several thermodynamic, kinematic and composite sounding-derived parameters were calculated from the most representative atmospheric vertical profile for each event. Moreover, we analysed the waterspout distribution in the Szilagyi Waterspout Nomogram (Szilagyi, 2009), which was developed in North America and has already been tested in some European seas, such as the Baltic and the central and eastern Mediterranean (Keul *et al*., 2009; Sioutas *et al*., 2013; Renko *et al*., 2018), but not the western Mediterranean.

The structure of the rest of the article is as follows. In Section 2, tornado and waterspout datasets and the ERA5 reanalysis data are presented, while the parameters calculated from the atmospheric profiles that will be used for further analysis are introduced. In Section 3, results derived from the comparison of the parameter values between the tornado and waterspout events in relation to their intensity are shown and discussed. Finally, in Section 4, conclusions and final remarks are provided, including comments about the potential use of the results in weather surveillance.

2 | DATA AND METHODOLOGY

2.1 | Tornado and waterspout events database

The tornado and waterspout database used to conduct this study consists of 465 individual tornadoes and 637 individual waterspouts that occurred between 1980 and 2018 in the Iberian Peninsula and Balearic Islands. For all of them, the location (latitude and longitude), date and time of occurrence were considered. If available, the intensity according to the Fujita scale (F-scale; Fujita, 1971) or the Enhanced Fujita scale (EF-scale, WSEC, 2006; Doswell *et al*., 2009) was also used. If the intensity was unknown, they were recorded as unrated (UR). In this dataset, a waterspout that moved onshore was considered a tornado and was classified according to its damage rating. This accounted for 34% of the tornadoes analysed.

The database was built by merging data from previous publications (Gayà, 2018; Rodríguez and Bech, 2018, hereafter referred to as RB18) and incorporating information from citizen collaborative platforms. These platforms included the European Severe Weather Database (ESWD, from the European Severe Storm Laboratory, ESSL; Dotzek *et al*., 2009), the Reporting System of Singular Atmospheric Observations (SINOBAS, from the Spanish Meteorological Agency, AEMET; Gutiérrez *et al*., 2015) and the Meteorological Spotters Network (XOM, from the Meteorological Service of Catalonia, SMC; Ripoll *et al*., 2016). Only confirmed cases, according to quality control from the original databases (i.e., QC1 and QC2 for the ESWD reports, Groenemeijer *et al*., 2017), were considered. These data were also complemented with other tornado and waterspout reports from the media and social networks, which have become increasingly important in recent years (Hyvärinen and Saltikoff, 2010). Thus, a sample of 1,102 individual cases was collected, after discarding 320 cases due to quality control.

It is well known that on some occasions, several tornadoes or waterspouts (here referred to simply as vortices) may form in a relatively short time window from the same convective storm or cloud system (Dowell and Bluestein, 2002; Bech *et al*., 2007; Sioutas *et al*., 2013). As mentioned above, the main goal of this study was to analyse environmental conditions from individual cases. However, to avoid the overrepresentation of specific meteorological situations, an event was considered unique when:

1. two or more vortices occurred within 50 km.
2. the time elapsed among them was less than 2 hours.

Moreover, in the case of multiple vortices that formed offshore and inland, they were considered as only one tornado event. As a result, 426 tornado and 481 waterspout events were analysed.

Tornadoes can be formed in different environments depending on the convective mode (e.g., supercells or mesoscale convective systems; see, for example, Agee and Jones (2009), Grams *et al.* (2012), Markowski and Richardson, (2009), Thompson *et al.* (2012, 2013)). For instance, mesocyclonic tornadoes require high-shear environments, whereas those spawned by multicells are usually associated with low-shear environments. Therefore, it would be ideal to classify the analysed events according to the parent-convective cell type to avoid compensations in the parameter values. However, there are several limitations to the radar data collected from the region of study (see Quirantes *et al.*, 2014 for further details), specifically with the data concerning the first half of the analysed period. The Spanish radar network was not completed until late 2007, with the radar on the Balearic Islands the last one to be put into operation. As these islands are where tornadoes occur the most frequently in the study region (together with Catalonia), it would not be possible to make the complete convective mode analysis for a substantial number of the tornado events studied here. Following similar previous studies (Craven and Brooks, 2004; Púčik *et al.*, 2015; Ingrosso *et al.*, 2020), the 426 tornadic events were clustered according to their intensity, which was estimated using the F-scale or the EF-scale, into the categories (E)F0, (E)F1, (E)F2+ (i.e., F2/EF2 or stronger) and UR (unrated). In these categories, (E) indicates the use of the EF-scale and F the F-scale. On the other hand, waterspout events were grouped into a single category (WAT) (Table 1).

When analysing the monthly distributions of the tornadoes and waterspouts, two different subregions became apparent (Figure 1): the north-east of the Iberian Peninsula and the Balearic Islands (NE), and the south-west of the Iberian Peninsula (SW). In the NE, events occur more frequently during the warm-season (72.9% from May to October), similar to other Mediterranean countries such as Italy (Miglietta and Matsangouras, 2018), while in the SW, the events are more common during the cool-season (73.3% from November to April). These differences in seasonal distribution are a consequence of synoptic configurations that favour deep moist convection and tornado formation in both areas. Tornadoes in the SW are mostly associated with cool-season Atlantic fronts, whereas the tornadic synoptic situations in the NE are usually associated with the inland diurnal heating cycle during the warm-season and the Mediterranean thermodynamic instability that is typical from late summer and autumn (Riesco *et al.*, 2015). Therefore, in this paper, these two different areas were studied separately.

The number of reported events is significantly higher in the NE than in the SW (Figure 1 and Table 1). Gayà (2018) and Antonescu *et al.* (2017) pointed out that the Mediterranean slope of the Iberian Peninsula and the Balearic Islands are the most frequently affected by tornadoes in the study region. The moister and relatively warm marine boundary layer of that area increases low-tropospheric instability and makes environmental conditions more favourable to deep convection (Miglietta *et al.*, 2017), which is also consistent with the spatial and temporal distribution of lightning events (Taszarek *et al.*, 2019). This has been highlighted by the exhaustive monitoring of tornadoes and waterspouts in Catalonia and the Balearic Islands during the last three decades by several studies (Gayà *et al.*, 2001; Gayà, 2011; Arús, 2018; Rodríguez *et al.*, 2020). This may explain the higher detection of non-damaging or weakly-damaging events such as waterspouts and (E)F0 tornadoes in this subarea, in contrast to the rest of the Iberian Peninsula where the ratio of these types of events is much lower.

2.2 | ERA5

Vertical temperature, dew point and wind profiles from each tornado and waterspout event contained in the database were retrieved from the ECMWF ERA5 reanalysis (C3S, 2017), whose spatial and temporal resolution are

TABLE 1 Number of individual vortices (tornadoes and waterspouts), number of atmospheric profiles and number of NE and SW profiles analysed for each category considering (Enhanced) Fujita scale intensities (E)F0, (E)F1, (E)F2+, unrated tornadoes (UR) and waterspouts (WAT)

Category	Number of individual vortices	Number of profiles	Number of NE profiles	Number of SW profiles
(E)F0	211	196	128	68
(E)F1	185	166	64	102
(E)F2+	47	44	30	14
UR	22	20	10	10
WAT	637	481	424	57

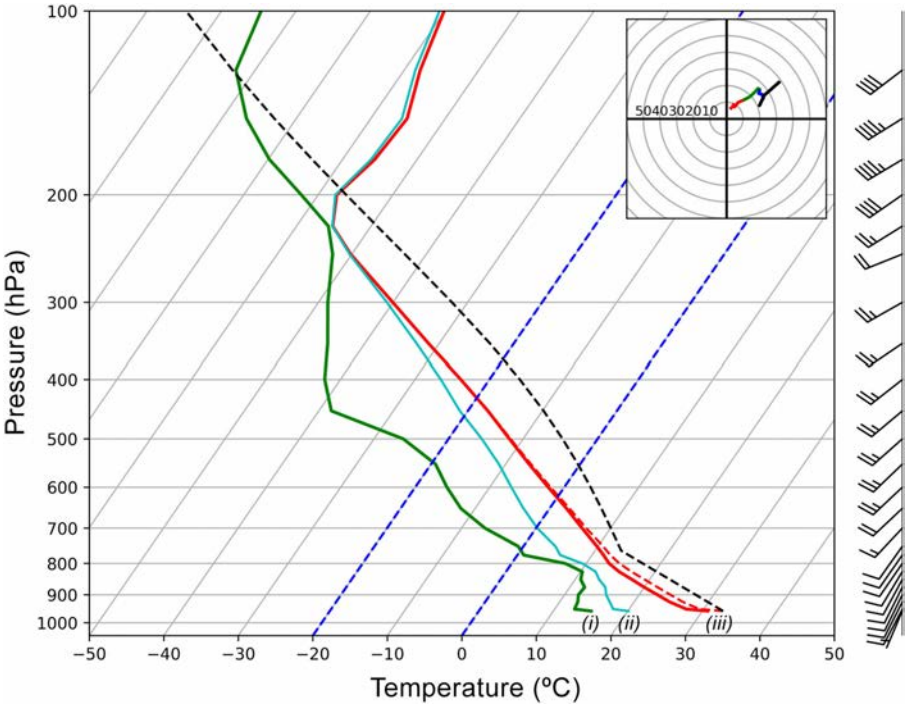

FIGURE 2 Skew T – logp diagram for l'Espluga de Francolí (Catalonia) tornado of 31st August 1994 at 1445 UTC (41.39°N, 1.11°E). ERA5 reanalysis data from 14 UTC August 31, 1994 and 41.50°N, 1.00°E grid point has been used to analyse this case and Sounding and Hodograph Analysis and Research Program in Python (SHARPpy), from Blumberg *et al.* (2017), has been used to plot the diagram. Profiles plotted include dew point (solid line (i)), wet-bulb temperature (solid line (ii)) and temperature (solid line (iii)) [Colour figure can be viewed at wileyonlinelibrary.com]

0.25° and 1 hr, respectively, with data available on 37 pressure levels and surface. The most representative sounding of an event was considered, that is, the vertical profile from the closest grid point and immediately prior to touchdown of the analysed case, with this point being offshore for waterspouts even if there was landfall. Figure 2 shows the sounding selected to describe the 1994 tornado in l'Espluga de Francolí in Catalonia (Ramis *et al*., 1997) as an example. Therefore, 907 soundings were analysed (Table 1).

2.3 | Parameters analysed

The selection of the thermodynamic and kinematic parameters to be analysed was based on similar previous studies (e.g., Craven and Brooks, 2004; Groenemeijer and van Delden, 2007; Kaltenböck *et al*., 2009). Therefore, convective available potential energy (CAPE), convective inhibition (CIN), storm-relative helicity (SRH) and windshear (WS) were studied to characterize severe storm environments (Table A1 in Appendix A). Moreover, composite parameters (i.e., a combination of the above-mentioned parameters) were also investigated to assess favourable environments for tornadic storms. Taszarek and Kolendowicz (2013) proposed the Universal Tornadic Index (UTI) to distinguish between tornadic and non-tornadic environments in Poland. As shown in Table A1, the UTI takes into account low-level humidity, instability and shear, which are required for tornadic storms, as discussed previously (Rasmussen and Blanchard, 1998; Grams *et al*., 2012). RB18 demonstrated that the UTI could distinguish non-tornadic thunderstorms from EF1 or stronger cases in Catalonia. Several studies have recently assessed the behaviour of the product of WS and the square root of two times CAPE (WMAXSHEAR) to identify significant tornado environments (Taszarek *et al*., 2017; Chernokulsky *et al*., 2019). Therefore, these two composite parameters were also analysed in this study, with the aim of testing them with data from the Iberian Peninsula and Balearic Islands.

Calculations of the thermodynamic and kinematic parameters were carried out using Sounding and Hodograph Analysis and Research Program in Python (SHARPpy; Blumberg *et al*., 2017). CAPE and CIN were calculated using the virtual temperature correction (Doswell and Rasmussen, 1994) and the most-unstable

air parcel. This parcel allows the assessment of convection when it does not develop from near-surface air, but from a higher level. This is common in nocturnal convection, where the surface-air is cooler than at higher altitudes (Groenemeijer *et al.*, 2019). Moreover, most-unstable CAPE has been used in other studies to investigate environments favourable to tornadic storms (Púčik *et al.*, 2015; Renko *et al.*, 2016; Ingrosso *et al.*, 2020).

SRH was calculated for the 0–3 km (SRH_{03}) and 0–1 km (SRH_{01}) layers. Storm-motion vector, which is required to calculate SRH (Table A1), was estimated with the Bunkers method (Bunkers *et al.*, 2000), which is used by SHARPpy. WS was calculated for the deep (0–6 km, WS_{06}), middle (0–3 km, WS_{03}) and low (0–1 km, WS_{01}) layers, and WMAXSHEAR for the 0–6 km ($WMAXSHEAR_{06}$) and 0–3 km ($WMAXSHEAR_{03}$) layers. All these layers are defined as above ground level (AGL).

The Kolmogorov–Smirnov (KS) test was carried out to assess significant differences among the categories for each parameter and to compare the distributions of each parameter between the NE and SW events. The results of this test are shown in Tables B1 and B2 (Appendix B).

Finally, the convective cloud depth (CCD) was calculated for waterspout events, that is, the difference between the equilibrium level (EL) and the lifting condensation level (LCL), also using the most-unstable air parcel. Data on the sea surface temperature (SST), and the 850 hPa temperature (T850) and wind speed (W850) for each waterspout event were directly provided by the ERA5 reanalysis. All these data were used to analyse waterspout distribution on the Szilagyi Waterspout Nomogram (Szilagyi, 2009).

3 | RESULTS AND DISCUSSION

In this section, results from the parameter analysis are presented and discussed in three subsections: thermodynamic parameters (CAPE and CIN), kinematic parameters (SRH and WS) and composite parameters (UTI, WMAXSHEAR, the relationship between CAPE and WS_{03}, and the Szilagyi Waterspout Nomogram).

3.1 | Thermodynamic parameters

3.1.1 | Convective available potential energy

CAPE presents substantial differences for each category between the NE and SW regions (Figure 3a,b). CAPE has

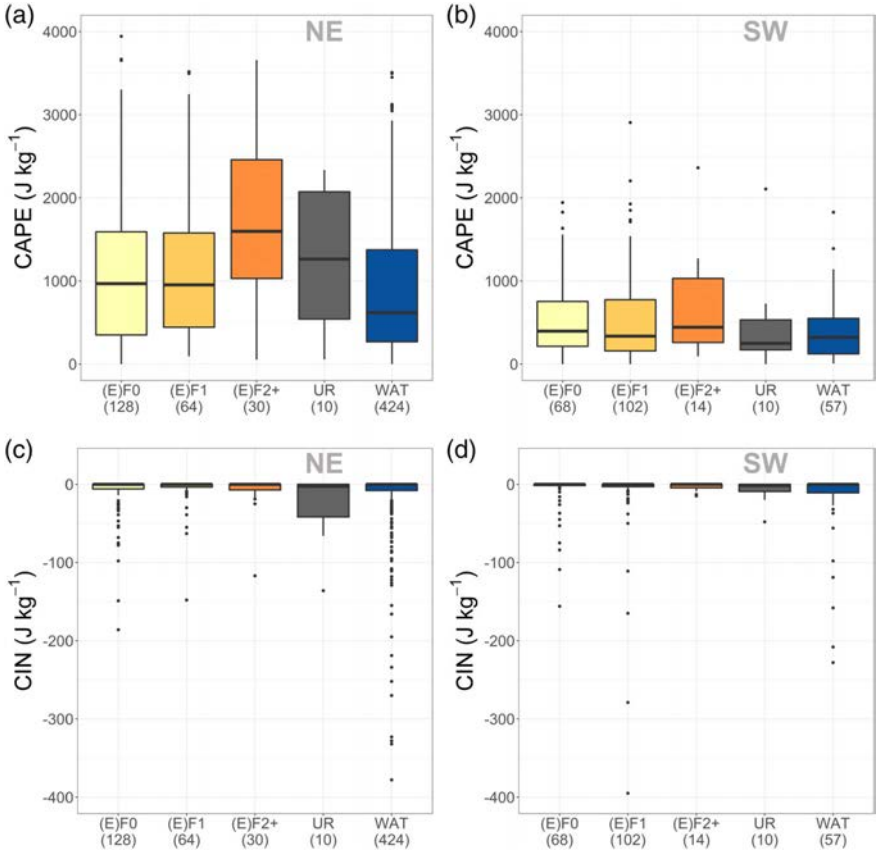

FIGURE 3 CAPE boxplots for NE events (a) and SW events (b), and for CIN for NE (c) and SW (d) events showing 25th, 50th and 75th percentiles. Whiskers extend from 25th and 75th percentiles to minimum and maximum values, respectively, unless these exceed 1.5 times the inter-quartile range. Then, outliers are presented as points above or below whiskers. The number of analysed vertical profiles of each sounding type is shown in brackets below the boxplot category name including rated tornadoes ((E)F0, (E)F1, (E)F2+), unrated tornadoes (UR) and waterspout (WAT) events [Colour figure can be viewed at wileyonlinelibrary.com]

a wide range of values for the NE events, usually being higher than those for the SW events. As explained in Section 2.1, most of the SW cases occur during the cool-season, when surface specific humidity is lower than in the warm-season, thereby favouring low CAPE (as discussed by Riemann-Campe *et al*., 2009). The small number of warm-season tornadic events in the SW favour low CAPE and a smaller CAPE range, which is consistent with the findings of previous studies (Matsangouras *et al*., 2017; Childs *et al*., 2018).

Weak tornadic events (i.e., (E)F0 and (E)F1) present similar CAPE, with a median of around 950 $J{\cdot}kg^{-1}$ for the NE events and 370 $J{\cdot}kg^{-1}$ for the SW events. On the other hand, significant tornadic events ((E)F2+) tend to present higher values than the rest of the sounding types, with statistically significant differences for the NE events (Table B1). By contrast, the differences are not statistically significant for the events in the SW subregion, although the median for the (E)F2+ events is slightly higher than that for the weak cases.

WAT are associated with similar or slightly lower CAPE compared to that for weak tornadoes in both regions, as reported previously (Gayà *et al*., 2001; Kahraman *et al*., 2017). However, the 50th percentile for the NE WAT is 618 $J{\cdot}kg^{-1}$, comparable to that reported by Renko *et al*. (2016), and 321 $J{\cdot}kg^{-1}$ for the SW, which is similar to the results from other colder seawaters (e.g., Groenemeijer and van Delden [2007], who studied tornadic upper-air conditions in the Netherlands).

Here, CAPE values are generally smaller than those presented in the studies on US tornadic events (Thompson *et al*., 2012), but similar to those reported in studies performed in Europe (Groenemeijer and van Delden, 2007; Púčik *et al*., 2015). The combination of steep lapse rates developing over the Rocky Mountains and very low-level moist-air from the Gulf of Mexico produces higher-CAPE environments in the United States than in Europe. Therefore, whereas tornadoes can be associated with a large range of CAPE in the United States, they are usually related to lower CAPE values in Europe (Grünwald and Brooks, 2011).

3.1.2 | Convective inhibition

WAT events in both the NE and SW regions present the largest CIN (more negative), despite the UR events in the NE, probably due to the small sample size (Figure 3c,d). The 25th percentile is −8 $J{\cdot}kg^{-1}$ for the NE WAT, surpassing −200 $J\ kg^{-1}$ in several cases, and −11 $J{\cdot}kg^{-1}$ for the SW WAT. These results are similar to those presented in Renko *et al*. (2016). It is remarkable that whereas only 1–4% of the (E)F0, (E)F1 and (E)F2+ tornado events are associated with CIN surpassing −100 $J{\cdot}kg^{-1}$, this percentage rises up to 6–7% for WAT. Nevertheless, there is a considerable overlap between the distributions. In summary, CIN does not exhibit statistically significant differences between the categories (Table B1) or between the NE and SW subregions (Table B2).

The greater CIN associated with WAT events might be related to the shallow stable layer that forms just over the sea surface when a warm air mass is advected. Thus, the dew point approaches the SST, resulting in high CAPE that is often highly capped with high CIN (Groenemeijer *et al*., 2019). A mechanism to force the lifting to initiate convection is required, particularly in these cases.

3.2 | Kinematic parameters

3.2.1 | Storm-relative helicity

SRH quantifies the potential for cyclonic updraft rotation in right-moving supercells (Davies-Jones *et al*., 1990). Thus, environments characterized by high SRH usually support the formation of mesocyclones and tornadoes (Rasmussen and Blanchard, 1998; Thompson *et al*., 2003). More specifically, SRH_{01} accounts for the possible existence of large low-level horizontal vorticity, which plays a very important role in tornadogenesis (Wade *et al*., 2018).

As shown in Figure 4, SRH presents higher values for all the SW tornado categories (Figure 4b,d) than for the NE ones (Figure 4a,c). This is consistent with the occurrence of SW tornadoes during the cool-season, which usually presents high-shear, low-CAPE (HSLC) environments (Sherburn and Parker, 2014), as shown in Table 2. This is also in accordance with the low CAPE mentioned above. In these situations, tornadoes are usually formed within low-topped mini-supercells or in quasi-linear convective system mesovortices (Thompson *et al*., 2012; Davis and Parker, 2014).

Tornado formation has been observed occasionally in environments with low helicity ($SRH_{01} < 75\ m^2{\cdot}s^{-2}$) and/or high LCL (>1,300 m), the so-called LHHLCL environments (Davies, 2006). These conditions, which are more usual inland during the warm-season and are therefore more common in the NE atmospheric profile samples (Table 2), may contribute to the decreased SRH percentiles for the NE events. As an example, the vertical profile shown in Figure 2, which corresponds to the l'Espluga de Francolí (Catalonia) tornado of 31st August 1994, presents similarities to the high-based tornadic environments reported in Davies (2006).

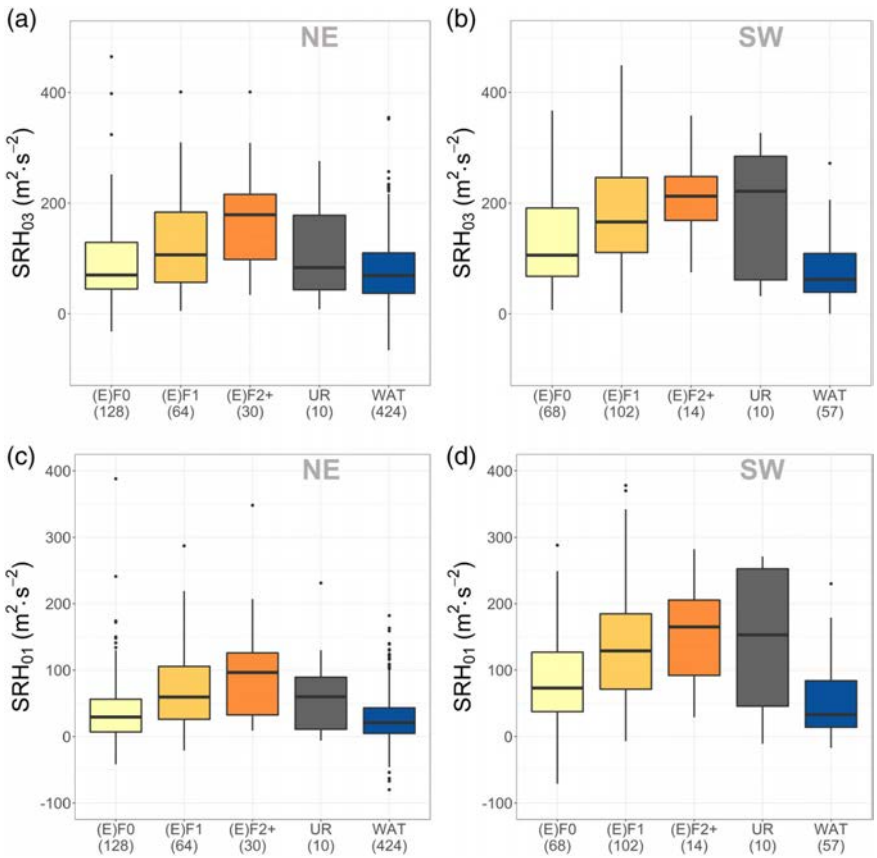

FIGURE 4 As Figure 3, but for SRH_{03} for NE (a) and SW (b), and for SRH_{01} for NE (c) and SW (d) [Colour figure can be viewed at wileyonlinelibrary.com]

TABLE 2 Number of warm-season, cool-season, high-shear, low-CAPE (HSLC) and low-helicity, high-LCL (LHHLCL) soundings for NE tornado (NE-TOR), NE waterspout (NE-WAT), SW tornado (SW-TOR) and SW waterspout (SW-WAT) sounding groups

Sounding group	Warm-season (over total)	Cool-season (over total)	HSLC (over total)	HSLC (over warm-season)	HSLC (over cool-season)	LHHLCL (over total)	LHHLCL (over warm-season)	LHHLCL (over cool-season)
NE-TOR	169 (73%)	63 (27%)	31 (13%)	14 (8%)	17 (27%)	31 (13%)	29 (17%)	2 (3%)
NE-WAT	309 (73%)	115 (27%)	75 (18%)	39 (13%)	36 (31%)	7 (2%)	4 (1%)	3 (3%)
SW-TOR	55 (28%)	139 (72%)	85 (44%)	9 (16%)	76 (55%)	11 (6%)	10 (18%)	1 (1%)
SW-WAT	12 (21%)	45 (79%)	15 (26%)	2 (17%)	13 (29%)	1 (2%)	1 (8%)	0 (0%)

Note: In brackets, the percentage over the sample data indicated is shown. Note that HSLC environment is defined by SBCAPE $\leq$500 J·kg^{-1}, MUCAPE $\leq$ 1,000 J·kg^{-1}, and $WS_{06} \geq 18$ m·s^{-1}, and LHHLCL is defined by $SRH_{01} < 75$ m^2·s^{-2} and LCL > 1,300 m.

In Figure 4, a clear positive correlation can be seen between helicity and tornado intensity: the higher the SRH, the stronger the tornado can be. This is consistent with previous studies such as Groenemeijer and van Delden (2007) and Taszarek and Kolendowicz (2013). However, the helicity values found here are smaller than those reported in the other two studies, especially for the NE cases. This could be due to a higher fraction of non-mesocyclonic tornadoes (Markowski and Richardson, 2009; Thompson *et al*., 2012), given that 34% of the tornadoes analysed in this study were formed offshore.

WAT events are commonly associated with weak environmental helicity, as explained in Sioutas and Keul (2007) and Renko *et al*. (2016). SRH_{03} is usually between 35 and 110 m^2·s^{-2}, and SRH_{01} between 10 and 85 m^2·s^{-2}.

It is remarkable that for the NE tornado events, the SRH values of the UR cases overlap with those of the (E)F0 and (E)F1 tornadoes, but are smaller than those of the (E)F2+ cases, which is consistent with the observations of Grünwald and Brooks (2011). By contrast, for the SW tornado events, the SRH_{03} and SRH_{01} of the UR events

are comparable to those of all the other categories, including the (E)F2+ cases. This suggests the possible presence of significant tornadoes in the SW UR class.

In RB18, the thresholds $SRH_{03} > 150\ m^2 \cdot s^{-2}$ and $SRH_{01} > 70\ m^2 \cdot s^{-2}$ were proposed to distinguish between (E)F1+ tornadoes and non-tornadic storms. Here, 40% of the NE (E)F1+ tornadoes and 58% of the SW (E)F1+ events surpass the SRH_{03} threshold, while 47% of the NE (E)F1+ tornadoes and 76% of the SW (E)F1+ events exceed the SRH_{01} threshold. These values were also surpassed by the majority of the tornadic events analysed in Thompson *et al.* (2003), which were supercell-related. Nevertheless, it should be noted that these SRH thresholds can generate a high number of false alarms when used to detect tornadic environments. Furthermore, most of the non-severe events studied in Groenemeijer and van Delden (2007) had an SRH_{01} between 11 and 97 $m^2 \cdot s^{-2}$.

3.2.2 | Wind-shear

WS presents similar trends as the SRH, showing a positive correlation with tornado intensity. This is consistent

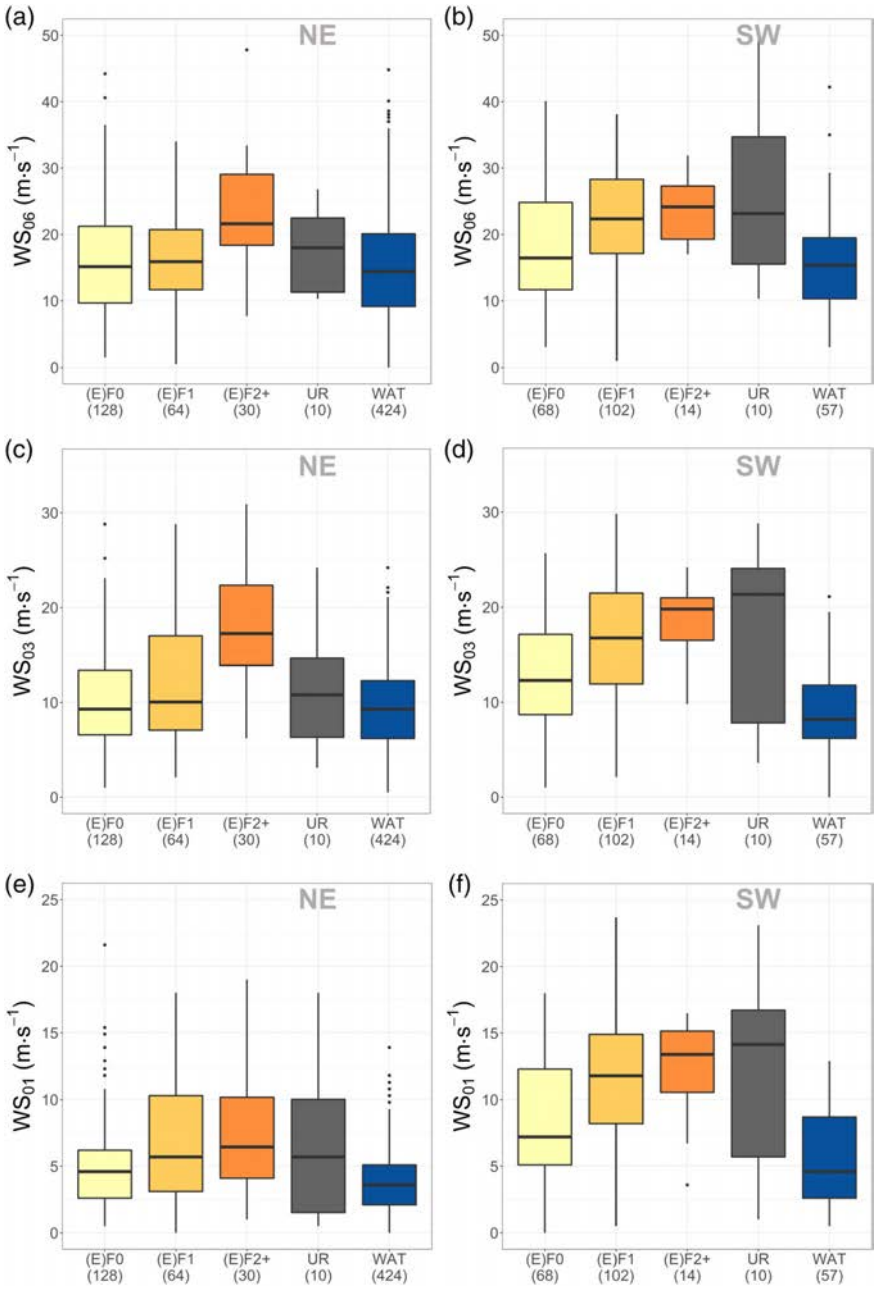

FIGURE 5 As Figure 3, but for WS_{06} for NE (a) and SW (b), for WS_{03} for NE (c) and SW (d), and for WS_{01} for NE (e) and SW (f) [Colour figure can be viewed at wileyonlinelibrary.com]

with the fact that WS and SRH are dependent on each other (see Weisman and Rotunno, 2000 for further discussion). Therefore, the significant tornadoes in our dataset are usually associated with stronger WS compared to weak tornadoes and WAT (Figure 5), which is consistent with previous studies (e.g., Monteverdi *et al*., 2003; Groenemeijer and van Delden, 2007). However, although the median WS of the (E)F2+ SW events is higher than that of the (E)F1 tornadoes (Figure 5b,d,f), there are no statistically significant differences between these two categories (Table B1). By contrast, the NE events (Figure 5a,c,e) show significant differences between the (E)F1 and (E)F2+ tornadoes for WS_{06} and WS_{03}, but not for WS_{01}. The WS for UR events follows a similar pattern as the helicity. Thus, whereas the UR and weak tornadoes have comparable WS in the NE, the WS for the UR events is also similar to that of the (E)F2+ tornadoes in the SW.

There are statistically significant differences in WS between the NE and SW subregions for all the analysed layers due to the monthly distribution of the tornado events. WS is higher for the SW events than the NE ones, which is consistent with the helicity and CAPE results. This shows the predominance of HSLC environments for the events occurring during the cool-season and, therefore, in the south-west of the Iberian Peninsula (Table 2).

Previous studies have indicated that environments with $WS_{06} > 20$ m·s^{-1} are associated with the occurrence of significant tornadoes (Weisman and Klemp, 1982; Thompson *et al*., 2003, 2012; Grams *et al*., 2012; Ingrosso *et al*., 2020). These tornadoes usually have a mesocyclonic origin (Markowski and Richardson, 2009). Almost 63% of the NE and 71% of the SW (E)F2+ events surpass the above-mentioned WS_{06} threshold (Figure 5a, b). The 50th percentile is 21.6 m·s^{-1} for the NE events and 24.2 m·s^{-1} for the SW cases, which are similar to those reported by Taszarek and Kolendowicz (2013) and Chernokulsky *et al*. (2019).

Taszarek *et al*. (2017) and RB18 pointed out that WS_{03} is a good discriminator between (E)F1+ tornadoes and non-tornadic storms (see Appendix C). WS_{03} greater than 15 m·s^{-1} is usually associated with environments that favour tornadoes, especially the significant ones. Here, 48% of the NE and 66% of the SW (E)F1+ events exceed this value, although the percentage is higher for the (E)F2+ cases from both subregions (more than 70% of all the significant events), as shown in Figure 5c,d.

WS_{01} presents the most significant differences between the NE and SW subregions (Figure 5e,f). In the NE, the median WS_{01} is 4.6 m·s^{-1} for weak events (considering the (E)F0 and (E)F1 categories together) and 6.4 m·s^{-1} for significant events. In the SW, the corresponding medians are 10.6 and 13.0 m·s^{-1}, respectively. The values for the SW tornado environments are similar to those of the other studies performed in Europe (Groenemeijer and van Delden, 2007; Taszarek and Kolendowicz, 2013). By contrast, the values for the NE tornado profiles are 30–50% smaller, probably due to the monthly distribution of the tornadic events. In fact, only 40% of the significant tornado environments in the NE exceed 8 m·s^{-1}, a threshold proposed in RB18, whereas 79% of the SW (E)F2+ events surpass this threshold. The seasonal dependence of WS observed for the significant events is also reported in Ingrosso *et al*. (2020), where the lowest values for (E)F2+ tornadoes in Italy occur during the spring and summer, and the highest in autumn.

Waterspouts are commonly associated with weak-shear environments (Keul *et al*., 2009; Sioutas *et al*., 2013). For all the atmospheric layers analysed, WAT category presents the lowest medians, with the differences between the NE and SW events not being statistically significant for the 0–6 km and the 0–3 km layers (Table B2). Similar results have been reported for other European regions (Groenemeijer and van Delden, 2007; Renko *et al*., 2016) and the Florida Keys in the USA (Devanas and Stefanova, 2018).

3.3 | Composite parameters

3.3.1 | Universal tornadic index

The UTI, originally proposed by Taszarek and Kolendowicz (2013), was used in Catalonia by RB18 to successfully distinguish between non-tornadic thunderstorms and (E)F1+ tornado-related environments, with the UTI exceeding 0.3 for the latter. In the present study, 21% of the (E)F0 events, 40% of the (E)F1 cases, 66% of the (E)F2+ tornadoes, 40% of the UR cases and 9% of the WAT events from the whole dataset surpass this threshold.

According to its definition (see Table A1), UTI = 0 when LCL > 1,500 m. Therefore, for LHHLCL environments (such as the example shown in Figure 2, where the LCL is 1,950 m), this parameter is not useful in detecting a potential tornado environment. Thus, as explained in detail in Davies (2006), other elements have to be examined to assess the potential of tornado formation in LHHLCL environments, such as high low-level lapse-rates, high CAPE in the 0–3 km layer, and small CIN (not shown).

Significant tornadoes are usually associated with a higher UTI than weak tornadic events (see Figure 6a,b). A positive correlation between the UTI and tornado intensity can be inferred from the percentiles of this

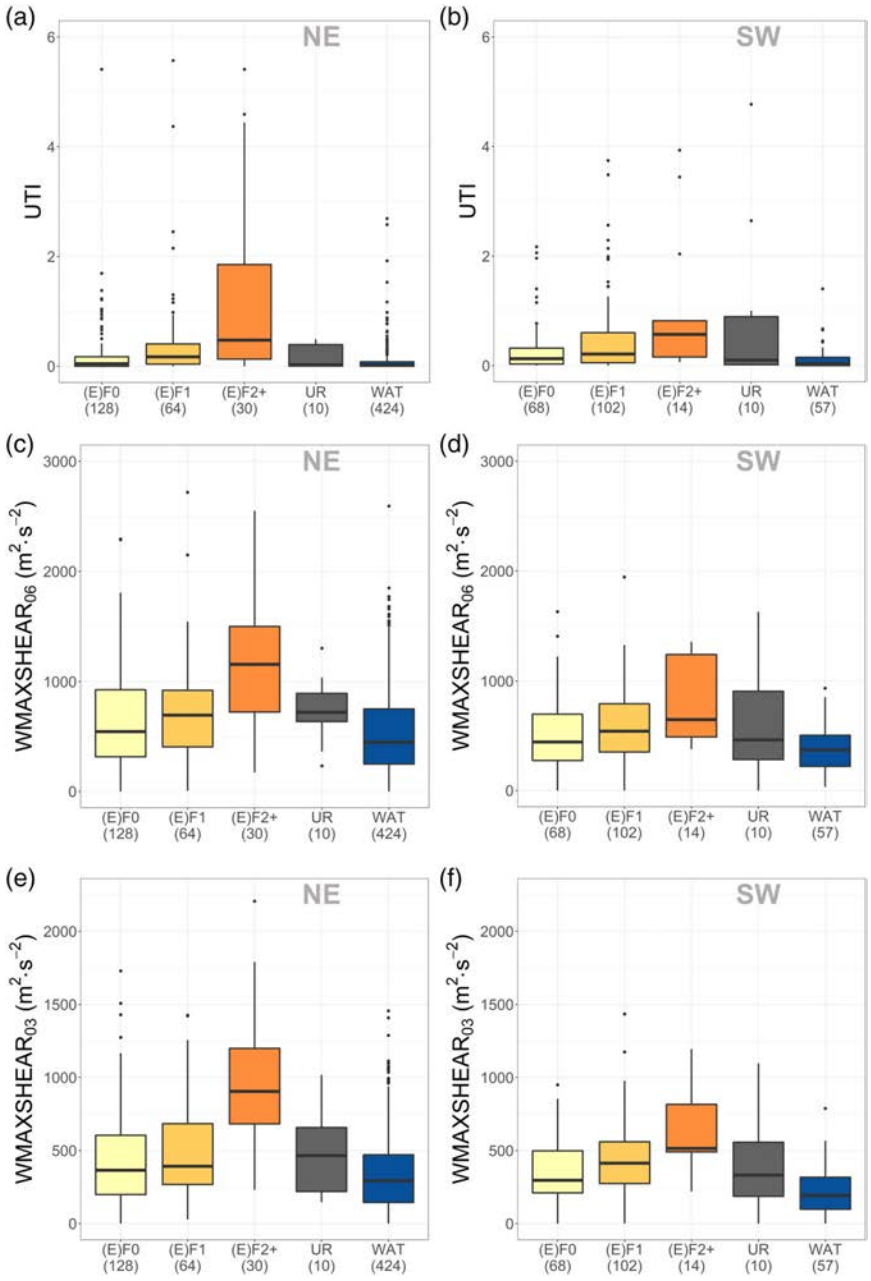

FIGURE 6 As Figure 3, but for UTI for NE (a) and SW (b), for $WMAXSHEAR_{06}$ for NE (c) and SW (d), and for $WMAXSHEAR_{03}$ for NE (e) and SW (f) [Colour figure can be viewed at wileyonlinelibrary.com]

parameter for each category. The median is around 0.05 for (E)F0 cases (in both the NE and SW subregions), 0.20 for (E)F1 tornadoes and 0.50 for (E)F2+ events. These values are smaller than those presented in Taszarek and Kolendowicz (2013), mainly because kinematic low-level parameters (i.e., WS_{01} and SRH_{01}) are also smaller in the study area. Nevertheless, our results are similar to the median UTI reported by RB18.

There are no significant differences in the UTI between the NE and SW events, except for the (E)F0 cases (Table B2). Therefore, this parameter can also detect warm-season and cool-season tornadic events, in contrast to the parameters analysed previously. Moreover, the UTI can distinguish between the (E)F0, (E)F1, (E)F2+ and WAT sounding types ($p < .080$), although the KS-test results show that the differences between the (E)F1 and (E)F2+ tornadoes for the SW are not statistically significant (Table B1). Furthermore, whereas the UR and weak events have a similar UTI in the NE cases, the UTI for the UR events is also comparable to that of the

significant events in the SW data, similar to that found for the kinematic parameters.

3.3.2 | WMAXSHEAR

$WMAXSHEAR_{06}$ was used in Taszarek *et al*. (2017) to assess thunderstorm severity and in Chernokulsky *et al*. (2019) to discriminate between significant tornadoes and weaker events. Both studies showed the efficiency of this composite parameter in discriminating between (E)F0/(E)F1 and (E)F2+ cases. As shown in Figure 6c,d, both the (E)F0 and (E)F1 categories exhibit similar $WMAXSHEAR_{06}$, presenting smaller values for the SW than for the NE as a consequence of the lower CAPE. Significant tornadic events are usually associated with higher $WMAXSHEAR_{06}$, which is significantly different to that of the weak cases ($p < .030$), except that between the (E)F1 and (E)F2+ cases for the SW.

Chernokulsky *et al*. (2019) proposed the threshold of 940 $m^2 \cdot s^{-2}$ to distinguish between significant and weak tornadic environments. This value is too high for the SW events in our study (only 36% surpass it) and for those analysed in Taszarek *et al*. (2017), where less than 25% surpassed this threshold. The strong dependence of this parameter on CAPE, which is generally lower in the SW than in the NE, and the weak differences in the WS_{06} between the SW and NE (E)F2+ events are the reasons for the lower $WMAXSHEAR_{06}$ among the SW events. In addition, the similar WS_{06} of the (E)F1 and (E)F2+ cases in the SW subregion makes $WMAXSHEAR_{06}$ less useful in discriminating between significant and weak tornadic events in high-shear, low-CAPE environments. By contrast, 63% of the NE (E)F2+ events surpass the above-mentioned threshold.

To increase the difference in the WMAXSHEAR between the weak and significant tornadic events in HSLC environments, WS_{03} instead of WS_{06} has been proposed for the calculation of this parameter. Whereas the WS_{03} presents significant differences between weak (grouping the (E)F0 and (E)F1 categories, not shown) and significant events for both the NE and SW subregions, the differences in the WS_{06} between these vertical profile types are not statistically significant for the SW events.

Using WS_{03}, the differences in the WMAXSHEAR between the (E)F0, (E)F1 and WAT events with respect to (E)F2+ tornadoes are statistically significant for both the NE and SW subregions (Figure 6e,f). Although the 50th percentile for significant events is greater for the NE than the SW events, the KS-test results show that the distributions are not different, even for the other tornado categories (Table B2). Therefore, $WMAXSHEAR_{03}$, like the UTI, is unaffected by seasonal variations, that is, the ability to distinguish between the tornado categories is invariant with seasonal changes.

TABLE 3 $WMAXSHEAR_{03}$ 25th, 50th and 75th percentiles (in $m^2 \cdot s^{-2}$) for weak ((E)F0 and (E)F1) and significant ((E)F2+) events, merging NE and SW subregions

Percentile	Weak	Significant
P25	231	531
P50	380	811
P75	575	1,117

Interestingly, the 25th percentile for $WMAXSHEAR_{03}$ of all the (E)F2+ soundings (500 $m^2 \cdot s^{-2}$) is comparable to the 75th percentile of the weak tornado environments (Table 3). Therefore, this value could act as a threshold to distinguish between significant and weak tornado environments. Whereas only 29% of the (E)F0 cases and 35% of the (E)F1 events surpass this threshold, 84% of the (E)F2+ events exceed it.

3.3.3 | CAPE versus WS_{03}

The results from the previous sections indicate that SW tornadic events (more frequent during the cool-season) are usually associated with lower CAPE and higher helicity and WS than the NE events. Sherburn and Parker (2014) defined the criteria for HSLC environments as surface-based parcel CAPE $\leq$500 $J \cdot kg^{-1}$, most-unstable parcel CAPE $\leq$ 1,000 $J \cdot kg^{-1}$, and $WS_{06} \geq 18$ $m \cdot s^{-1}$. In our study, 45% of the SW tornadoes meet these conditions compared to only 15% of the NE tornadoes (Table 2). This is consistent with the fact that cool-season severe weather events, including tornadoes, are usually associated with HSLC environments, as found in previous studies (Hanstrum *et al*., 2002; Childs *et al*., 2018; Gatzen *et al*., 2019; Celiński-Mysław *et al*., 2020).

Figure 7 shows the tornado and waterspout scatter plots of CAPE and WS_{03} values overlaid onto $WMAXSHEAR_{03}$ contour lines. It is apparent that significant tornadoes associated with low CAPE are usually related to high WS_{03}, typically well above 15 $m \cdot s^{-1}$. By contrast, when CAPE increases, significant tornadoes can occur even when $WS_{03} < 15$ $m \cdot s^{-1}$. (E)F2+ events in the NE exhibit a wide range of CAPE and WS_{03} values (Figure 7a), unlike the SW cases, which usually have CAPE <1,000 $J \cdot kg^{-1}$ and $WS_{03} > 15$ $m \cdot s^{-1}$ and only occasionally present high-CAPE and low-to-moderate WS_{03} conditions (Figure 7b). Despite this apparent inverse correlation between CAPE and WS_{03}, as stated in Section 3.2.2, more than 75% of significant events from both subregions exhibit $WMAXSHEAR_{03} > 500$ $m^2 \cdot s^{-2}$.

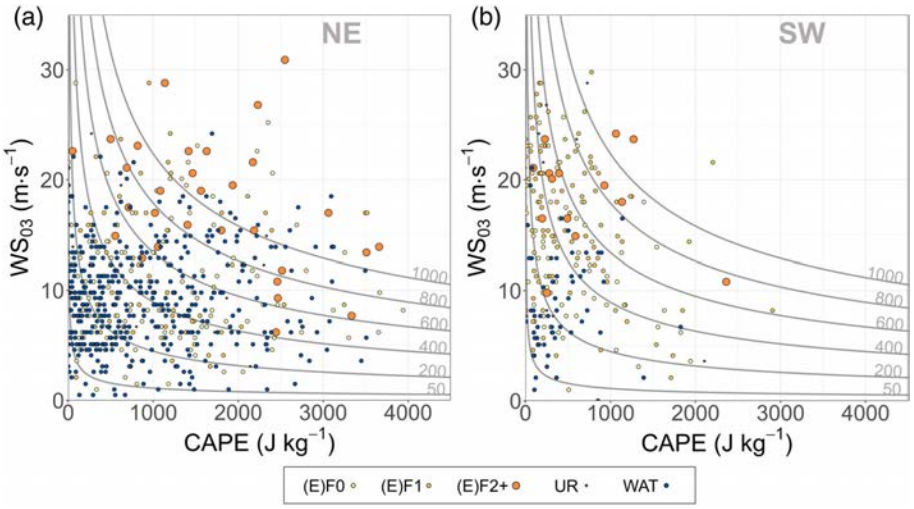

FIGURE 7 NE (a) and SW (b) tornado and waterspout CAPE versus WS_{03} scatter plots overlaid with $WMAXSHEAR_{03}$ contour lines (labels expressed in $m^2 \cdot s^{-2}$). [Colour figure can be viewed at wileyonlinelibrary.com]

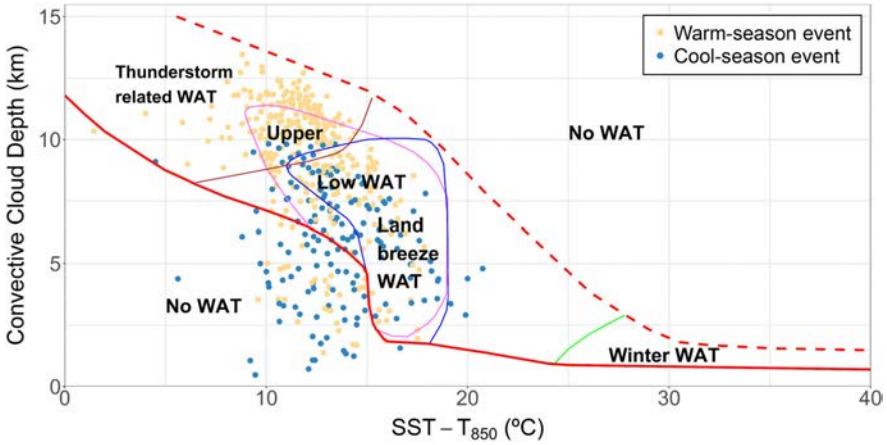

FIGURE 8 Szilagyi Waterspout Nomogram, where waterspout events are plotted according to the difference between the sea surface temperature (SST) and 850 hPa temperature (T_{850}), and the convective cloud depth (CCD), which is the difference between equilibrium level (EL) and lifting condensation level (LCL). [Colour figure can be viewed at wileyonlinelibrary.com]

WAT and (E)F0 events are less restrictive than EF1+ events and are therefore associated with a wide range of CAPE and WS. However, they are more common when CAPE <1,500 $J \cdot kg^{-1}$ and WS_{03} is around 10 $m \cdot s^{-1}$ or even less, presenting $WMAXSHEAR_{03}$ smaller than 500 $m^2 \cdot s^{-2}$.

3.3.4 | Szilagyi Waterspout Nomogram

The Szilagyi Waterspout Nomogram (Szilagyi, 2009) is an empirical graphical technique used to forecast waterspouts that was originally developed in the Great Lakes region of North America. It is based on two thermodynamic parameters: the difference between the SST and T850 (*x*-axis, ΔT) and the CCD (*y*-axis). Additionally, the 850 hPa wind speed must be lower than 40 kt (20.6 $m \cdot s^{-1}$). Depending on the ΔT and CCD, the nomogram classifies events into two broad areas: favourable conditions for waterspout formation (distinguishing four environments, that is, thunder-related, upper-low, land-breeze and winter waterspouts; Figure 8) and unfavourable conditions (labelled 'No WAT' in Figure 8). According to Szilagyi (2009), the area of favourable conditions is limited by two threshold lines (thick-solid and thick-dashed lines in Figure 8), which are the upper and lower boundaries of the two areas of unfavourable conditions for waterspout formation.

We found that 81% of WAT events from the analysed dataset fit in the area where waterspout conditions are favourable. Here, the vast majority of warm-season events are associated with thunderstorm-related waterspout environments, similar to that reported by Keul *et al.* (2009). They are characterized by deep convective clouds (CCD exceeding 8.5 km) and low-to-moderate ΔT (below 16°C).

Unsurprisingly, the so-called winter waterspout conditions in the Szilagyi nomogram (Winter WAT in Figure 8), characterized by a high ΔT and low CCD, are not met in the study region, which is consistent with the findings of previous studies using the nomogram in other

parts of the Mediterranean (Sioutas *et al*., 2013; Renko *et al*., 2016). In our dataset, there was no waterspout case where $\Delta T > 25°C$, with only two cases exceeding 20°C. It should be noted that this forecasting method was developed for the Great Lakes, where very cold low- and mid-level air advections in winter are common and, therefore, the difference between the surface temperature of the lake and T850 can reach large values. By contrast, in the Mediterranean basin and the south-western European Atlantic slope, cold air advections are weaker than at higher latitudes; thus, the ΔT in winter is not so extreme (Chandra *et al*., 1990; Reynolds and Smith, 1995). In this sense, Keul *et al*. (2009) proposed a modification of the nomogram, excluding winter events where $\Delta T > 20°C$ for the Mediterranean.

Most waterspout events that are not in the nomogram area of favourable conditions are characterized by a CCD between 1.5 and 6 km and a ΔT between 10 and 15°C. Of these, 63% are related to cool-season events, which are consistent with previous findings (Renko *et al*., 2018) that have detected some winter Mediterranean waterspouts in this area of the nomogram. Therefore, this region should also be considered a potential area that is prone to mid-latitude winter waterspouts. Hence, the original nomogram should be modified when used for studies in southern Europe.

Apart from cool-season cases, the nomogram is a reliable source to identify conditions that are favourable for waterspouts in the study region. However, as pointed out by Szilagyi (2009), the nomogram is a complementary tool that should be used alongside the identification of additional factors such as lateral boundaries, frontal surfaces or low-level convergence lines. All of these can produce horizontal WS and generate low-level vertical vorticity, which can be stretched by updrafts, favouring waterspout formation (Brady and Szoke, 1989; Markowski and Richardson, 2009; Miglietta, 2019).

4 | SUMMARY AND CONCLUSIONS

A dataset including 907 tornado and waterspout events recorded from 1980 to 2018 in the Iberian Peninsula and Balearic Islands was analysed. Events were grouped depending on their intensity and type, with five categories considered ((E)F0, (E)F1, (E)F2+, UR and WAT). Data on the vertical temperature, dew point and wind profile of each event were retrieved from the ERA5 reanalysis. Thermodynamic (CAPE and CIN), kinematic (SRH and WS) and composite (UTI, WMAXSHEAR and the relationship between CAPE and WS_{03}) sounding-derived parameters were determined to characterize convective environments. Moreover, the Szilagyi Waterspout Nomogram was tested for waterspout events in the dataset. We observed that there are substantial differences in the monthly distributions of tornadoes and waterspouts between the NE and SW parts of the study region. The events are more common during the warm-season (May to October) in the NE and during the cool-season (November to April) in the SW.

The NE tornado and waterspout environments are characterized by higher CAPE and lower WS and helicity (especially at low levels) compared to the SW events. In fact, 44% of the SW tornado atmospheric profiles are associated with high-shear, low-CAPE environments, in contrast to 13% for the NE events. Low-shear, high-LCL tornado environments occur in both areas, being more frequent inland during the warm-season. For this reason, they are more common in the NE (13% of the tornado events) than in the SW (6%).

There is a positive correlation between helicity and WS with respect to the intensity of the event. Generally, the higher the SRH and WS, the stronger the tornadoes can be. The majority of the (E)F2+ soundings in our dataset exceed the thresholds proposed by previous studies for significant tornadoes: $SRH_{03} > 180\ m^2 \cdot s^{-2}$ (57%); $SRH_{01} > 70\ m^2 \cdot s^{-2}$ (64%); $WS_{06} > 20\ m \cdot s^{-1}$ (66%); $WS_{03} > 15\ m \cdot s^{-1}$ (75%); and $WS_{01} > 8\ m \cdot s^{-1}$ (52%). Moreover, the ratio of threshold exceedance is higher for the SW events than for the NE cases due to differences in the monthly distribution.

There is a weak inverse correlation between CAPE and WS_{03}. Whereas significant tornado environments with low CAPE ($<1{,}000\ J \cdot kg^{-1}$) usually present $WS_{03} > 15\ m \cdot s^{-1}$, increasing CAPE makes it possible for EF2+ tornadoes to occur with smaller WS_{03}. This behaviour is similar for all the tornado and WAT categories.

Composite parameters such as the UTI (>0.3) and $WMAXSHEAR_{06}$ ($>940\ m^2 \cdot s^{-2}$) are also generally good discriminators between weak and significant tornadoes. However, the $WMAXSHEAR_{06}$ for SW (E)F2+ events is not as high as that for the NE ones due to the lower CAPE. Furthermore, the differences between the (E)F0/(E)F1 and (E)F2+ tornadoes are not statistically significant, making this parameter less useful in identifying significant tornado environments in HSLC conditions. This led us to apply a variant of WMAXSHEAR that uses WS_{03} instead of WS_{06}, and presents greater differences between the significant and weak tornadoes. Our results, which are also consistent with the inverse correlation between CAPE and WS_{03}, show that (E)F2+ environments are usually associated with $WMAXSHEAR_{03} > 500\ m^2 \cdot s^{-2}$. In this study, 80% of the significant tornado cases exceed this threshold, whereas only 29% of the weak tornadoes surpass it.

Neither the UTI nor $WMAXSHEAR_{03}$ presents significant differences between the NE and SW subregions for each category. This makes them useful in distinguishing between significant and weak tornado events, independently of their association with HSLC environments. However, there are some limitations in using the UTI for LHHLCL environments as, according to its definition, the UTI is zero when LCL > 1,500 m, which often occurs in LHHLCL cases.

It is remarkable that the UR and weak tornado events have similar values in the NE, while the UR and significant tornado events have comparable values for the kinematic parameters and UTI in the SW. This indicates that the UR events could be mostly weak in the NE, while some of the UR tornado cases might be significant in the SW.

By contrast, WAT are associated with low-to-moderate CAPE and low helicity and shear. Composite parameters also present low values for WAT compared to tornadoes, even the weak ones. Thus, the environmental conditions for waterspout formation are less restrictive than those for the formation of inland tornadoes.

The Szilagyi Waterspout Nomogram is a useful tool for forecasting waterspouts in our study area. The vast majority of the events (81%) fit into the nomogram area delimited by waterspout threshold lines, most of them being characterized by CCD > 8.5 km and $\Delta T < 16^{\circ}C$. However, the nomogram could be adapted to mid-latitudes by removing the $\Delta T > 25^{\circ}C$ winter waterspout area, as already discussed in previous studies, and defining a new cool-season waterspout area, with the CCD between 1.5 and 6 km and the ΔT between 10 and 15°C.

Our results might have been improved if the tornadic database used could distinguish between mesocyclonic and non-mesocyclonic cases. Therefore, future work should include an analysis of radar data to assess the convective mode (e.g., multicell, supercell, mesoscale convective system) of tornadic storms (Smith *et al*., 2012), preferably over a larger region (i.e., Europe). Our analysis should be replicated, but through classifying tornadic events according to the type of parent-convective system, similar to that of Grams *et al*. (2012) or Thompson *et al*. (2012, 2013) in the USA. Moreover, it would be useful to determine the ratio of mesocyclonic tornadoes in non-typical supercell environments (i.e., WS_{06} smaller than 20 $m \cdot s^{-1}$). Finally, the SRH for the 0–500 m layer could also be analysed, as this parameter has been reported to be good at distinguishing between tornadic and non-tornadic supercell environments (Coffer *et al*., 2019).

ACKNOWLEDGEMENTS

We would like to thank Delia Gutiérrez (Spanish Meteorological Agency) and Ricard Ripoll (Meteorological Service of Catalonia) for providing the tornado and waterspout data from the SINOBAS and XOM platforms, respectively. This study was carried out within the framework of the HYdrological cycle in the Mediterranean Experiment (HyMeX) programme and with partial support from the projects CGL 2015-65627-C3-2-R (MINECO/FEDER), CGL 2016-81828-REDT (AEI) and RTI 2018-098693-B643-C32 (AEI), and the Water Research Institute (IdRA) of the University of Barcelona.

ORCID

Oriol Rodríguez https://orcid.org/0000-0003-1893-9959
Joan Bech https://orcid.org/0000-0003-3597-7439

REFERENCES

Agee, A. and Jones, E. (2009) Proposed conceptual taxonomy for proper identification and classification of tornado events. *Weather and Forecasting*, 24, 609–6017. https://doi.org/10.1175/2008WAF2222163.1.

Allen, J.T., Karoly, D.J. and Walsh, K.J. (2014) Future Australian severe thunderstorm environments. Part II: the influence of a strongly warming climate on convective environments. *Journal of Climate*, 27, 3848–3868. https://doi.org/10.1175/JCLI-D-13-00426.1.

Antonescu, B., Schultz, D.M., Holzer, A. and Groenemeijer, P. (2017) Tornadoes in Europe: an underestimated threat. *Bulletin of the American Meteorological Society*, 98, 713–728. https://doi.org/10.1175/BAMS-D-16-0171.1.

Arús, J. (2018). *25 años de tornados en Cataluña (1992–2017). (25 years of tornadoes in Catalonia, in Spanish).* Simposio Nacional de Predicción "Memorial Antonio Mestre". pp. 563–574. DOI: https://doi.org/10.31978/639-19-010-0.563.

Bech, J., Pascual, R., Rigo, T., Pineda, N., López, J.M., Arús, J. and Gayà, M. (2007) An observational study of the 7 September 2005 Barcelona tornado outbreak. *Natural Hazards and Earth System Science*, 7, 129–139. https://doi.org/10.5194/nhess-7-129-2007.

Bech, J., Pineda, N., Rigo, T., Aran, M., Amaro, J., Gayà, M., Arús, J., Montanyà, J. and van der Velde, O. (2011) A Mediterranean nocturnal heavy rainfall and tornadic event. Part I: overview, damage survey and radar analysis. *Atmospheric Research*, 100(4), 621–637. https://doi.org/10.1016/j.atmosres.2010.12.024.

Belo-Pereira, M., Andrade, C. and Pinto, P. (2017) A long-lived tornado on 7 December 2010 in mainland Portugal. *Atmospheric Research*, 185, 202–215. https://doi.org/10.1016/j.atmosres.2016.11.002.

Blumberg, W.G., Halbert, K.T., Supinie, T.A., Marsh, P.T., Thompson, R.L. and Hart, J.A. (2017) SHARPpy: an open-source sounding analysis toolkit for the atmospheric sciences. *Bulletin of the American Meteorological Society*, 98, 1625–1636. https://doi.org/10.1175/BAMS-D-15-00309.1.

Brady, R.H. and Szoke, E.J. (1989) A case study of nonmesocyclone tornado development in Northeast Colorado: similarities to waterspout formation. *Monthly Weather Review*, 117(4), 843–856.

Bunkers, M.J., Klimowski, B.A., Zeitler, J.W., Thompson, R.L. and Weisman, M.L. (2000) Predicting supercell motion using anew

hodograph technique. *Weather and Forecasting*, 15, 61–79. https://doi.org/10.1175/1520-0434(2000)015,0061:PSMUAN.2.0.CO;2.

Celiński-Mysław, D., Palarz, A. and Taszarek, M. (2020) Climatology and atmospheric conditions associated with cool season bow echo storms in Poland. *Atmospheric Research*, 240, 104944. https://doi.org/10.1016/j.atmosres.2020.104944.

Chandra, S., Fleming, E.L., Schoeberl, M.R. and Barnett, J.J. (1990) Monthly mean global climatology of temperature, wind, geopotential height and pressure for 0–120 km. *Advances in Space Research*, 10(6), 3–12. https://doi.org/10.1016/0273-1177(90)90230-W.

Chernokulsky, A.V., Kurgansky, M.V. and Mokhov, I.I. (2019) On characteristic reanalysis-based values of convective instability indices for Northern Eurasia tornadoes. *IOP Conference Series: Earth and Environmental Science*, 231, 012012. https://doi.org/10.1088/1755-1315/231/1/012012.

Childs, S.J., Schumacher, R.S. and Allen, J.T. (2018) Cold-season tornadoes: climatological and meteorological insights. *Weather and Forecasting*, 33, 671–691. https://doi.org/10.1175/WAF-D-17-0120.1.

Coffer, B.E., Parker, M.D., Thompson, R.L., Smith, B.T. and Jewell, R.E. (2019) Using near-ground storm relative helicity in supercell tornado forecasting. *Weather and Forecasting*, 34(5), 1417–1435. https://doi.org/10.1175/WAF-D-19-0115.1.

Copernicus Climate Change Service (C3S) (2017). *ERA5: fifth generation of ECMWF atmospheric reanalyses of the global climate*. Copernicus Climate Change Service Climate Data Store (CDS). https://cds.climate.copernicus.eu/cdsapp#!/home. [17 April 2019]. DOI: 10.24381/cds.adbb2d47.

Craven, J.P. and Brooks, H.E. (2004) Baseline climatology of sounding derived parameters associated with deep, moist convection. *National Weather Digest*, 28(1), 13–24.

Davies, J.M. (2006) Tornadoes in environments with small helicity and/or high LCL Heights. *Weather and Forecasting*, 21, 579–594. https://doi.org/10.1175/WAF928.1.

Davies-Jones, R.P., Burgess, D., Foster, M. (1990). Test of Helicity as a Tornado Forecast Parameter. Preprints, *16th Conference on Severe Local Storms, Kananaskis Park, AB, Canada*. American Meteorological Society: 588–592.

Davis, J.M. and Parker, M.D. (2014) Radar climatology of tornadic and nontornadic vortices in high-shear, low-CAPE environments in the mid-Atlantic and southeastern United States. *Weather and Forecasting*, 29, 828–853. https://doi.org/10.1175/WAF-D-13-00127.1.

Devanas, A. and Stefanova, L. (2018) Statistical prediction of waterspout probability for the Florida keys. *Weather and Forecasting*, 33, 389–410. https://doi.org/10.1175/WAF-D-17-0100.1.

Doswell, C.A. and Schultz, D.M. (2006) On the use of indices and parameters in forecasting severe storms. *Electronic Journal of Severe Storms Meteorology*, 1(3), 1–22.

Doswell, C.A., III, Brooks, H.E. and Dotzek, N. (2009) On the implementation of the enhanced Fujita scale in the USA. *Atmospheric Research*, 93(1–3), 554–563. https://doi.org/10.1016/j.atmosres.2008.11.003.

Doswell, C.A., IIIand Rasmussen, E.N. (1994) The effect of neglecting the virtual temperature correction on CAPE calculations. *Weather and Forecasting*, 9, 625–629. https://doi.org/10.1175/1520-0434(1994)009<0625:TEONTV>2.0.CO;2.

Dotzek, N., Groenemeijer, P., Feuerstein, B. and Holzer, A.M. (2009) Overview of ESSL's severe convective storms research using the European severe weather database ESWD. *Atmospheric Research*, 93(1–3), 575–586. https://doi.org/10.1016/j.atmosres.2008.10.020.

Dowell, D.C. and Bluestein, H.B. (2002) The 8 June 1995 McLean, Texas, storm. Part I: observations of cyclic tornadogenesis. *Monthly Weather Review*, 130(11), 2626–2648. https://doi.org/10.1175/1520-0493(2002)130<2626:TJMTSP>2.0.CO;2.

Fujita, T.T. (1971). *Proposed characterization of tornadoes and hurricanes by area and intensity*. SMRP res. pap., University of Chicago, 91, 42 pp.

Gall, M., Borden, K.A. and Cutter, S.L. (2008) When do losses count? Six fallacies of natural hazards loss data. *Bulletin of the American Meteorological Society*, 90, 799–810. https://doi.org/10.1175/2008BAMS2721.1.

Gatzen, C.P., Fink, A.H., Schultz, D.M. and Pinto, J.G. (2019) An 18-year climatology of derechos in Germany. *Natural Hazards and Earth System Sciences*, 20(5), 1335–1351. https://doi.org/10.5194/nhess-20-1335-2020.

Gayà, M. (2011) Tornadoes and severe storms in Spain. *Atmospheric Research*, 100(4), 334–343. https://doi.org/10.1016/j.atmosres.2010.10.019.

Gayà, M. (2018) *Els Fiblons a Espanya: Climatologia i catàleg de Tornados i Trombes (Whirlwinds in Spain: Climatology and Catalogue of Tornadoes and Waterspouts, in Catalan)*, 2nd edition. Palma, Spain: Universitat de les Illes Balears 619 pp.

Gayà, M., Homar, V., Romero, R. and Ramis, C. (2001) Tornadoes and waterspouts in the Balearic Islands: phenomena and environment characterization. *Atmospheric Research*, 56(1–4), 253–267. https://doi.org/10.1016/S0169-8095(00)00076-4.

Glickman, T.S. and Zenk, W. (2000) *Glossary of Meteorology*, 2nd edition. Boston, MA: American Meteorological Society 855 pp.

Grams, J.S., Thompson, R.L., Snively, D.V., Prentice, J.A., Hodges, G.M. and Reames, L.J. (2012) A climatology and comparison of parameters for significant tornado events in the United States. *Weather and Forecasting*, 27, 106–123. https://doi.org/10.1175/WAF-D-11-00008.1.

Groenemeijer, P., Púčik, T., Holzer, A.M., Antonescu, B., Riemann-Campe, K., Schultz, D.M., Kühne, T., Feuerstein, B., Brooks, H.E., Doswell, C.A., Koppert, H.J. and Sausen, R. (2017) Severe convective storms in Europe. Ten years of research and education at the European severe storms laboratory. *Bulletin of the American Meteorological Society*, 98, 2641–2651. https://doi.org/10.1175/BAMS-D-16-0067.1.

Groenemeijer, P., Púcik, T., Tsonevsky, I., Bechtold, P. (2019). An overview of convective available potential energy and convective inhibition provided by NWP models for operational forecasting. *ECMWF Technical Memoranda, 852*. DOI: 10.21957/q392hofrl.

Groenemeijer, P.H. and van Delden, A. (2007) Sounding-derived parameters associated with large hail and tornadoes in The Netherlands. *Atmospheric Research*, 83(2–4), 473–487. https://doi.org/10.1016/j.atmosres.2005.08.006.

Grünwald, S. and Brooks, H.E. (2011) Relationship between sounding derived parameters and the strength of tornadoes in Europe and the USA from reanalysis data. *Atmospheric Research*, 100(4), 479–488. https://doi.org/10.1016/j.atmosres.2010.11.011.

Gutiérrez, D., Riesco, J. and Ponce, S. (2015) SINOBAS, a tool for collaborative mapping applied to observation of "singular" weather phenomena. In: *15th EMS Annual Meeting & 12th European Conference on Applications of Meteorology (ECAM)*. Sofia, Bulgaria: European Meteorological Society.

Hanstrum, B.N., Mills, G.A., Watson, A., Monteverdi, J.P. and Doswell, C.A. (2002) The cool-season tornadoes of California and southern Australia. *Weather and Forecasting*, 17, 705–722. https://doi.org/10.1175/1520-0434(2002)017<0705:TCSTOC>2.0.CO;2.

Hersbach, H., Bell, B., Berrisford, P., Hirahara, S., Horányi, A., Muñoz-Sabater, J., Nicolas, J., Peubey, C., Radu, R., Schepers, D., Simmons, A., Soci, C., Abdalla, S., Abellan, X., Balsamo, G., Bechtold, P., Biavati, G., Bidlot, J., Bonavita, M., Chiara, G., Dahlgren, P., Dee, D., Diamantakis, M., Dragani, R., Flemming, J., Forbes, R., Fuentes, M., Geer, A., Haimberger, L., Healy, S., Hogan, R.J., Hólm, E., Janisková, M., Keeley, S., Laloyaux, P., Lopez, P., Lupu, C., Radnoti, G., Rosnay, P., Rozum, I., Vamborg, F., Villaume, S. and Thépaut, J.N. (2020) The ERA5 global reanalysis. *Quarterly Journal of the Royal Meteorological Society*, 146, 1999–2049. https://doi.org/10.1002/qj.3803.

Homar, V., Gayà, M., Romero, R., Ramis, C. and Alonso, S. (2003) Tornadoes over complex terrain: an analysis of the 28th August 1999 tornadic event in eastern Spain. *Atmospheric Research*, 67–68, 301–317. https://doi.org/10.1016/S0169-8095(03)00064-4.

Hyvärinen, O. and Saltikoff, E. (2010) Social media as a source of meteorological observations. *Monthly Weather Review*, 138(8), 3175–3184. https://doi.org/10.1175/2010MWR3270.1.

Ingrosso, R., Lionello, P., Miglietta, M.M. and Salvadori, G. (2020) A statistical investigation of mesoscale precursors of significant tornadoes: the Italian case study. *Atmosphere*, 11(3), 301. https://doi.org/10.3390/atmos11030301.

Jahn, M. (2015) Economics of extreme weather events: terminology and regional impact models. *Weather and Climate Extremes*, 10 (B), 29–39. https://doi.org/10.1016/j.wace.2015.08.005.

Kahraman, A., Kadioglu, M. and Markowski, P.M. (2017) Severe convective storm environments in Turkey. *Monthly Weather Review*, 145, 4711–4725. https://doi.org/10.1175/MWR-D-16-0338.1.

Kaltenböck, R., Diendorfer, G. and Dotzek, N. (2009) Evaluation of thunderstorm indices from ECMWF analyses, lightning data and severe storm reports. *Atmospheric Research*, 93(1–3), 381–396. https://doi.org/10.1016/j.atmosres.2008.11.005.

Keul, A.G., Sioutas, M.V. and Szilagyi, W. (2009) Prognosis of central-eastern Mediterranean waterspouts. *Atmospheric Research*, 93(1–3), 426–436. https://doi.org/10.1016/j.atmosres.2008.10.028.

Leitão, P. (2003) Tornadoes in Portugal. *Atmospheric Research*, 67, 381–390. https://doi.org/10.1016/S0169-8095(03)00057-7.

Maddox, R.A. (1976) An evaluation of tornado proximity wind and stability data. *Monthly Weather Review*, 104, 133–142. https://doi.org/10.1175/1520-0493(1976)104<0133:AEOTPW>2.0.CO;2.

Markowski, P.M. and Richardson, Y.P. (2009) Tornadogenesis: our current understanding, forecasting considerations, and questions to guide future research. *Atmospheric Research*, 93(1–3), 3–10. https://doi.org/10.1016/j.atmosres.2008.09.015.

Matsangouras, I.T., Nastos, P.T., Bluestein, H.B., Pytharoulis, I., Papachristopoulou, K. and Miglietta, M.M. (2017) Analysis of waterspout environmental conditions and of parent-storm behaviour based on satellite data over the southern Aegean Sea of Greece. *International Journal of Climatology*, 37(2), 1022–1039. https://doi.org/10.1002/joc.4757.

Miglietta, M.M. (2019). Waterspouts: a review. *Reference Module in Earth Systems and Environmental Sciences*. DOI: 10.1016/B978-0-12-409548-9.12414-5.

Miglietta, M.M. and Matsangouras, I.T. (2018) An updated "climatology" of tornadoes and waterspouts in Italy. *International Journal of Climatology*, 38(9), 3667–3683. https://doi.org/10.1002/joc.5526.

Miglietta, M.M., Mazon, J. and Rotunno, R. (2017) Numerical simulations of a tornadic supercell over the Mediterranean. *Weather and Forecasting*, 32, 1209–1226. https://doi.org/10.1175/WAF-D-16-0223.1.

Moncrieff, M.W. and Miller, M.J. (1976) The dynamics and simulation of tropical cumulonimbus and squall lines. *Quarterly Journal Royal Meteorological Society*, 102, 373–394. https://doi.org/10.1002/qj.49710243208.

Monteverdi, J.P., Doswell, C.A. and Lipari, G.S. (2003) Shear parameter thresholds for forecasting tornadic thunderstorms in northern and Central California. *Weather and Forecasting*, 18, 357–370. https://doi.org/10.1175/1520-0434(2003)018<0357:SPTFFT>2.0.CO;2.

Orlanski, I. (1975) A rational subdivision of scales for atmospheric processes. *Bulletin of the American Meteorological Society*, 56(5), 527–530.

Potvin, C.K., Elmore, K.L. and Weiss, S.J. (2010) Assessing the impacts of proximity sounding criteria on the climatology of significant tornado environments. *Weather and Forecasting*, 25, 921–930. https://doi.org/10.1175/2010WAF2222368.1.

Púčik, T., Groenemeijer, P., Rädler, A.T., Tijssen, L., Nikulin, G., Prein, A.F., van Meijgaard, E., Fealy, R., Jacob, D. and Teichmann, C. (2017) Future changes in European severe convection environments in a regional climate model ensemble. *Journal of Climate*, 30, 6771–6794. https://doi.org/10.1175/JCLI-D-16-0777.1.

Púčik, T., Groenemeijer, P., Rýva, D. and Kolář, M. (2015) Proximity soundings of severe and nonsevere thunderstorms in Central Europe. *Monthly Weather Review*, 143, 4805–4821. https://doi.org/10.1175/MWR-D-15-0104.1.

Quirantes, J.A., Riesco, J., Núñez, J.A. (2014). *Características básicas de las supercélulas en España (Supercell basic characteristics in Spain, in Spanish)*. AEMET - Publicaciones en línea. http://hdl.handle.net/20.500.11765/709.

Ramis, C., Arús, J., López, J. and Mestres, A. (1997) Two cases of severe weather in Catalonia (Spain): an observational study. *Meteorological Applications*, 4(3), 207–217. https://doi.org/10.1017/S1350482797000510.

Ramis, C., Romero, R. and Homar, V. (2009) The severe thunderstorm of 4 October 2007 in Mallorca: an observational study. *Natural Hazards and Earth System Sciences*, 9(4), 1237–1245. https://doi.org/10.5194/nhess-9-1237-2009.

Rasmussen, E.N. (2003) Refined supercell and tornado forecast parameters. *Weather and Forecasting*, 18, 530–535. https://doi.org/10.1175/1520-0434(2003)18<530:RSATFP>2.0.CO;2.

Rasmussen, E.N. and Blanchard, D.O. (1998) A baseline climatology of sounding-derived supercell and tornado forecast parameters. *Weather and Forecasting*, 13, 1148–1164. https://doi.org/10.1175/1520-0434(1998)013<1148:ABCOSD>2.0.CO;2.

Renko, T., Ivušić, S., Prtenjak, M.T., Šoljan, V. and Horvat, I. (2018) Waterspout forecasting method over the eastern Adriatic using a high-resolution numerical weather model. *Pure and Applied Geophysics*, 175, 3759–3778. https://doi.org/10.1007/s00024-018-1833-x.

Renko, T., Kuzmić, J., Šoljan, V. and Mahović, N.S. (2016) Waterspouts in the eastern Adriatic from 2001 to 2013. *Natural Hazards*, 82, 441–470. https://doi.org/10.1007/s11069-016-2192-5.

Reynolds, R.W. and Smith, T.M. (1995) A high-resolution Global Sea surface temperature climatology. *Journal of Climate*, 8, 1571–1583. https://doi.org/10.1175/1520-0442(1995)008<1571:AHRGSS>2.0.CO;2.

Riemann-Campe, K., Fraedrich, K. and Lunkeit, F. (2009) Global climatology of convective available potential energy (CAPE) and convective inhibition (CIN) in ERA-40 reanalysis. *Atmospheric Research*, 93(1–3), 534–545. https://doi.org/10.1016/j.atmosres.2008.09.037.

Riesco, J., Polvorinos, F., Núñez, J.A., Soriano, J.D. and Jiménez, C. (2015) *Climatología de tornados en España Peninsular y Baleares (Tornado Climatology in the Peninsular Spain and Balearic Islands, in Spanish)*. Madrid, Spain: Spanish Meteorological Agency (AEMet), 83 pp. Available at: http://www.aemet.es/documentos/es/conocermas/publicaciones/Climatologia_tornados/Climatologia_tornados.pdf [Accessed 27th February 2020].

Ripoll, R., del Amo, X. and Vendrell, R. (2016) The weather observers network of the Meteorological Service of Catalonia. In: *In WMO Technical Conference on Meteorological and Environmental Instruments and Methods of Observation (CIMO TECO)*. Spain, Madrid: World Meteorological Organization.

Rodríguez, O. and Bech, J. (2018) Sounding-derived parameters associated with tornadic storms in Catalonia. *International Journal of Climatology*, 38, 2400–2414. https://doi.org/10.1002/joc.5343.

Rodríguez, O. and Bech, J. (2020) Reanalysing strong-convective wind damage paths using high-resolution aerial images. *Natural Hazards*, 104, 1021–1038. https://doi.org/10.1007/s11069-020-04202-6.

Rodríguez, O., Bech, J., Soriano, J.D., Gutiérrez, D. and Castán, S. (2020) A methodology to conduct wind damage field surveys for high-impact weather events of convective origin. *Natural Hazards and Earth System Science*, 20(5), 1513–1531. https://doi.org/10.5194/nhess-20-1513-2020.

Romero, R., Gayà, M. and Doswell, C.A. (2007) European climatology of severe convective storm environmental parameters: a test for significant tornado events. *Atmospheric Research*, 83 (2–4), 389–404. https://doi.org/10.1016/j.atmosres.2005.06.011.

Sánchez-Laulhé, J.M. (2009) El tornado de Málaga del 1 de Febrero de 2009 (the Málaga tornado from 1 February 2009, in Spanish). *AME Boletín*, 24, 34–36.

Seeley, J.T. and Romps, D.M. (2015) The effect of global warming on severe thunderstorms in the United States. *Journal of Climate*, 28, 2443–2458. https://doi.org/10.1175/JCLI-D-14-00382.1.

Sherburn, K.D. and Parker, M.D. (2014) Climatology and ingredients of significant severe convection in high-shear, low-CAPE environments. *Weather and Forecasting*, 29, 854–877. https://doi.org/10.1175/WAF-D-13-00041.1.

Sioutas, M., Szilagyi, W. and Keul, A. (2013) Waterspout outbreaks over areas of Europe and North America: environment and predictability. *Atmospheric Research*, 123, 167–179. https://doi.org/10.1016/j.atmosres.2012.09.013.

Sioutas, M.V. and Keul, A.G. (2007) Waterspouts of the Adriatic, Ionian and Aegean Sea and their meteorological environment. *Atmospheric Research*, 83(2–4), 542–557. https://doi.org/10.1016/j.atmosres.2005.08.009.

Smith, B.T., Thompson, R.L., Grams, J.S., Broyles, C. and Brooks, H.E. (2012) Convective modes for significant severe thunderstorms in the contiguous United States. Part I: storm classification and climatology. *Weather and Forecasting*, 27, 1114–1135. https://doi.org/10.1175/WAF-D-11-00115.1.

Szilagyi, W. (2009) A waterspout forecasting technique. In: *5h European Conference on Severe Storms (ECSS)*. Landshut, Germany: European Severe Weather Laboratory. Available at: https://www.essl.org/ECSS/2009/preprints/O05-14-sziladgyi.pdf. [Accessed 25th August 2020].

Taszarek, M., Allen, J., Púčik, T., Groenemeijer, P., Czernecki, B., Kolendowicz, L., Lagouvardos, K., Kotroni, V. and Schulz, W. (2019) A climatology of thunderstorms across Europe from a synthesis of multiple data sources. *Journal of Climate*, 32, 1813–1837. https://doi.org/10.1175/JCLI-D-18-0372.1.

Taszarek, M., Brooks, H.E. and Czernecki, B. (2017) Sounding-derived parameters associated with convective hazards in Europe. *Monthly Weather Review*, 145, 1511–1528. https://doi.org/10.1175/MWR-D-16-0384.1.

Taszarek, M., Brooks, H.E., Czernecki, B., Szuster, P. and Fortuniak, K. (2018) Climatological aspects of convective parameters over Europe: a comparison of ERA-interim and sounding data. *Journal of Climate*, 31, 4281–4308. https://doi.org/10.1175/JCLI-D-17-0596.1.

Taszarek, M. and Kolendowicz, L. (2013) Sounding-derived parameters associated with tornado occurrence in Poland and Universal Tornadic Index. *Atmospheric Research*, 134, 186–197. https://doi.org/10.1016/j.atmosres.2013.07.016.

Thompson, R.L., Edwards, R., Hart, J.A., Elmore, K.L. and Markowski, P. (2003) Close proximity soundings within supercell environments obtained from the rapid update cycle. *Weather and Forecasting*, 18, 1243–1261. https://doi.org/10.1175/1520-0434(2003)018<1243:CPSWSE>2.0.CO;2.

Thompson, R.L., Smith, B.T., Dean, A.R. and Marsh, P.T. (2013) Spatial distributions of tornadic near-storm environments by convective mode. *Electronic Journal of Severe Storms Meteorology*, 8(5), 1–22.

Thompson, R.L., Smith, B.T., Grams, J.S., Dean, A.R. and Broyles, C. (2012) Convective modes for significant severe thunderstorms in the contiguous United States. Part II: supercell and QLCS tornado environments. *Weather and Forecasting*, 27, 1136–1154. https://doi.org/10.1175/WAF-D-11-00116.1.

Viceto, C., Marta-Almeida, M. and Rocha, A. (2017) Future climate change of stability indices for the Iberian Peninsula. *International Journal of Climatology*, 37(12), 4390–4408. https://doi.org/10.1002/joc.5094.

Wade, A.R., Coniglio, M.C. and Ziegler, C.L. (2018) Comparison of near- and far-field supercell inflow environments using radiosonde observations. *Monthly Weather Review*, 146, 2403–2415. https://doi.org/10.1175/MWR-D-17-0276.1.

Wakimoto, R.M., Atkins, N.T., Butler, K.M., Bluestein, H.B., Thiem, K., Snyder, J. and Houser, J. (2015) Photogrammetric analysis of the 2013 El Reno tornado combined with Mobile X-band Polarimetric radar data. *Monthly Weather Review*, 143, 2657–2683. https://doi.org/10.1175/MWR-D-15-0034.1.

Weisman, M.L. and Klemp, J.B. (1982) The dependence of numerically simulated convective storms on vertical wind shear and buoyancy. *Monthly Weather Review*, 110, 504–520. https://doi.org/10.1175/1520-0493(1982)110<0504:TDONSC>2.0.CO;2.

Weisman, M.L. and Rotunno, R. (2000) The use of vertical wind shear versus helicity in interpreting supercell dynamics. *Journal of the Atmospheric Sciences*, 57, 1452–1472. https://doi.org/10.1175/1520-0469(2000)057<1452:TUOVWS>2.0.CO;2.

Weisman, M.L., Trapp, R.J., Romine, G.S., Davis, C., Torn, R., Baldwin, M., Bosart, L., Brown, J., Coniglio, M., Dowell, D., Evans, A.C., Galarneau, T.J., Haggerty, J., Hock, T., Manning, K., Roebber, P., Romashkin, P., Schumacher, R., Schwartz, C.S., Sobash, R., Stensrud, D. and Trier, S.B. (2015) The mesoscale predictability experiment (MPEX). *Bulletin of the American Meteorological Society*, 96, 2127–2149. https://doi.org/10.1175/BAMS-D-13-00281.1.

WSEC. (2006) *A Recommendation for an Enhanced Fujita Scale (EF-scale)*. Lubbock, TX: Wind Science and Engineering Center 111 pp. Available at: http://www.spc.noaa.gov/faq/tornado/EFScale.pdf. [Accessed 4th March 2020].

How to cite this article: Rodríguez O, Bech J. Tornadic environments in the Iberian Peninsula and the Balearic Islands based on ERA5 reanalysis. *Int J Climatol*. 2020;1–21. https://doi.org/10.1002/joc.6825

APPENDIX A.

In this Appendix, the equations for all the parameters analysed are shown (Table A1).

TABLE A1 Equation, units and reference for the parameters analysed. Variables used are g (acceleration of gravity), LFC (level of free convection), EL (equilibrium level), $T_{v_{LP}}$ (lifting parcel temperature), T_{v_e} (environmental temperature), h (height of the upper-limit of an air layer above ground level), $\mathbf{v}$ (horizontal wind vector), $\mathbf{k}$ (upward unit vector), $\mathbf{c}$ (storm motion vector), SBCAPE (surface-based CAPE), SBLCL (surface-based lifting condensation level), $SBCAPE_{03}$ (surface-based CAPE integrated up to 3 km) and AMR_{500} (mixing ratio average in the lowest 500 m). Note that UTI is a dimensionless (d.l.) magnitude and that it is imposed that UTI = 0 if SBCAPE = 0 J·kg-1 and/or LCL > 1,500 m, whereas if $SRH_{01} < 0$ $m^2 \cdot s^{-2}$, then it is considered that $SRH_{01} = 0$ $m^2 \cdot s^{-2}$

Parameter equation	Units	Reference
$CAPE = g\int_{LFC}^{EL} \frac{T_{v_{LP}}(z) - T_{v_e}(z)}{T_{v_e}(z)} dz$	$J \cdot kg^{-1}$	Moncrieff and Miller (1976)
$CIN = g\int_{0}^{LFC} \frac{T_{v_{LP}}(z) - T_{v_e}(z)}{T_{v_e}(z)} dz$	$J \cdot kg^{-1}$	Moncrieff and Miller (1976)
$SRH_{0h} = -\int_0^h \mathbf{k} \cdot \left[(\mathbf{v} - \mathbf{c}) \times \frac{\partial \mathbf{v}}{\partial z} \right] dz$	$m^2 \cdot s^{-2}$	Davies-Jones *et al*. (1990)
$WS_{0h} = \lvert \mathbf{v_h} - \mathbf{v_0} \rvert$	$m \cdot s^{-1}$	Weisman and Klemp (1982)
$UTI = \frac{\left\{ \left[\frac{SBCAPE \cdot SRH_{01}}{200} \cdot \frac{5(WS_{06} - 20) + \left(\frac{2000 - SBLCL}{10} \right)}{100} \right] + SBCAPE_{03} + \frac{SRH_{01}}{4} \right\}}{1000} \cdot \frac{WS_{01}}{12} \cdot \frac{AMR_{500}}{10}$	d. l.	Taszarek and Kolendowicz (2013)
$WMAXSHEAR_{0h} = \sqrt{2 \cdot CAPE} \cdot WS_{0h}$	$m^2 \cdot s^{-2}$	Taszarek *et al*. (2017), this study

APPENDIX B.

Table B1 presents the results of the Kolmogorov–Smirnov (KS) test assessing the statistical significance of differences between the values of the analysed parameters in relation to the event classes ((E)F0, (E)F1, (E)F2+, UR and WAT) for both subregions of the study (NE and SW). Table B2 shows the *p*-values of the KS-test performed to determine how different the distributions of each parameter are, comparing the NE and SW subregions.

TABLE B1 *p*-values of the Kolmogorov–Smirnov test for all the parameters analysed for both NE and SW subregions, comparing among the different event classes. *p*-values over .100 are not shown and *p*-values equal to or lower than .010 are in bold

Parameter	(E)F0 vs. (E)F1	(E)F0 vs. (E)F2+	(E)F0 vs. UR	(E)F0 vs. WAT	(E)F1 vs. (E)F2+	(E)F1 vs. UR	(E)F1 vs. WAT	(E)F2+ vs. UR	(E)F2+ vs. WAT	UR vs. WAT
CAPE (NE)	–	.024	–	.012	.030	–	.038	–	**.000**	–
CAPE (SW)	–	–	–	–	–	–	–	–	–	–
CIN (NE)	–	–	–	–	–	–	–	–	–	–
CIN (SW)	–	–	–	–	–	–	–	–	–	–
SRH_{03} (NE)	.045	**.000**	–	–	.027	–	**.000**	–	**.000**	–
SRH_{03} (SW)	**.001**	**.005**	.070	**.002**	–	–	**.000**	–	**.000**	**.006**
SRH_{01} (NE)	**.001**	**.001**	–	.055	–	–	**.000**	–	**.000**	.066
SRH_{01} (SW)	**.001**	**.003**	–	**.001**	–	–	**.000**	–	**.000**	.017
WS_{06} (NE)	–	**.001**	–	–	**.001**	–	–	–	**.000**	–
WS_{06} (SW)	**.001**	**.006**	–	.023	–	–	**.000**	–	**.000**	.086
WS_{03} (NE)	.059	**.000**	–	–	**.002**	–	**.001**	.076	**.000**	–
WS_{03} (SW)	**.003**	**.007**	.056	**.003**	–	–	**.000**	–	**.000**	**.006**
WS_{01} (NE)	.018	.021	–	.018	–	–	**.000**	–	**.000**	–
WS_{01} (SW)	**.000**	.026	.084	**.003**	–	–	**.000**	–	**.000**	**.006**
UTI (NE)	**.005**	**.000**	–	.016	.013	–	**.000**	.047	**.000**	–
UTI (SW)	.074	.010	–	**.006**	–	–	**.000**	–	**.000**	–
$WMAXSHEAR_{06}$ (NE)	–	**.000**	–	**.006**	**.000**	–	**.001**	.021	**.000**	.018
$WMAXSHEAR_{06}$ (SW)	.053	.029	–	.069	–	–	**.000**	.076	**.000**	–
$WMAXSHEAR_{03}$ (NE)	.100	**.000**	–	.018	**.000**	–	**.000**	.012	**.000**	–
$WMAXSHEAR_{03}$ (SW)	–	**.006**	–	**.002**	.030	–	**.000**	–	**.000**	–

Parameter	(E)F0	(E)F1	(E)F2+	UR	WAT
CAPE	**.000**	**.000**	**.002**	–	**.000**
CIN	–	–	–	–	–
SRH_{03}	**.002**	**.003**	–	–	–
SRH_{01}	**.000**	**.000**	**.007**	–	**.008**
WS_{06}	.047	**.000**	–	–	–
WS_{03}	.022	**.000**	–	–	–
WS_{01}	**.000**	**.000**	.012	–	**.002**
UTI	.035	–	–	–	–
$WMAXSHEAR_{06}$	.097	.055	.018	–	.025
$WMAXSHEAR_{03}$	–	–	–	–	.022

TABLE B2 As Table B1 but for *p*-values of the Kolmogorov–Smirnov test for each parameter analysed, comparing NE and SW values distribution

APPENDIX C.

Tornadic events recorded in Catalonia between 2000 and 2016, which are included in the dataset used in this study, are analysed in this Appendix. ERA5 reanalysis data and real sounding observations previously used in RB18 are compared. In RB18, pre-convective environments were analysed by selecting the most representative sounding for each event, using the proximity-inflow method (Rasmussen and Blanchard, 1998). Values of the thermodynamic (CAPE), kinematic (WS_{03}) and composite ($WMAXSHEAR_{03}$) parameters from both datasets are presented and compared

Table C1 shows some of the differences in the 25th, 50th and 75th percentiles. CAPE ERA5 values are generally higher than those derived from the sounding data, except for the upper bound. This is consistent with the findings of Potvin *et al.* (2010), who reported that increasing the spatio-temporal distance between the sounding data and the tornadic event analysed produced lower CAPE environments. By contrast, reanalysis-derived WS_{03} and $WMAXSHEAR_{03}$ percentiles are similar or slightly lower than those derived from soundings. These differences could be explained by the:

- *Data used*: Here, ERA5 reanalysis data are employed, whereas real sounding data were used in RB18 (see Taszarek *et al.*, 2018 for further details on this issue).
- *Profile selection method*: We selected the closest spatio-temporal grid point to analyse convective environments, whereas the proximity-inflow method was used in RB18 (profiles could be at ranges farther than 200 km and several hours earlier than the event).

In any case, all these differences are not statistically significant ($p > .200$, according to the KS test, not shown).

TABLE C1 25th, 50th and 75th percentiles for CAPE, WS_{03} and $WMAXSHEAR_{03}$ for ERA5 (in bold, left columns) and radiosounding (right columns) data for (E)F0, (E)F1+ and WAT Catalonia (2000–2016) events analysed in Rodríguez and Bech (2018)

	(E)F0		(E)F1+		WAT	
CAPE ($J \cdot kg^{-1}$)						
P25	429	266	492	478	330	224
P50	**766**	757	**1,018**	702	**669**	539
P75	**1,367**	1,609	**1,359**	1701	**1,350**	1,209
WS_{03} ($m \cdot s^{-1}$)						
P25	**6.6**	7.9	**9.4**	12.9	**6.7**	6.5
P50	**9.8**	11.8	**14.7**	16.0	**9.8**	9.0
P75	**13.4**	14.0	**21.2**	18.5	**12.9**	13.2
$WMAXSHEAR_{03}$ ($m^2 \cdot s^{-2}$)						
P25	**156**	255	**394**	437	**167**	147
P50	**354**	389	**483**	527	**331**	283
P75	**461**	744	**841**	830	**573**	517

Capítol 5

Conclusions

En aquest apartat es presenten les conclusions finals fruit de la investigació duta a terme durant el període predoctoral. Cal recordar que a la secció 1.3.1 s'havien formulat tres objectius generals, al voltant dels quals s'ha estructurat la tesi. Aquests són:

- OG1. Explorar noves eines per a generar una base de dades de tornados i mànegues marines homogènia i robusta.
- OG2. Caracteritzar els entorns favorables per a la formació de tornados i mànegues marines al conjunt de la Península Ibèrica i les Illes Balears.
- OG3. Identificar possibles factors relacionats amb els episodis més intensos.

A partir dels objectius generals s'havien detallat els objectius específics, entorn dels quals s'ha fet la vertebració dels resultats. Així, per tal d'exposar les conclusions de manera ordenada, es presenten com a resposta a cadascun dels sis objectius específics. Finalment, es descriuen les línies de treball futur per a millorar la detecció, la predicció i el seguiment d'aquest tipus d'episodis de temps violent.

5.1 Conclusions finals

- OE1. Proposar una metodologia per a dur a terme treballs de camp.

Es presenta una metodologia per a analitzar *in situ* els danys ocasionats per ventades fortes d'origen convectiu. Està basada en estudis anteriors i en l'experiència adquirida pels autors de l'article que conforma la secció 2.1.2 en dur a terme 136 estudis de camp a Espanya entre els anys 2004 i 2018. Es tracta d'un procediment fàcilment reproduïble i que optimitza el temps i els recursos destinats a l'anàlisi dels episodis, complint els requisits que ens havíem proposat.

La geolocalització dels elements afectats mitjançant l'ús de càmeres de fotografiar amb GPS i la recollida d'informació d'interès, com per exemple el testimoni d'observadors directes o les imatges de càmeres de seguretat, permeten representar l'escenari dels danys de manera fidedigna. Amb les dades obtingudes es generen tres lliurables per a facilitar la interpretació i l'ús de la informació: (i) una fitxa estandarditzada amb el resum del treball de camp, (ii) una taula en què hi consta la informació geolocalitzada i (iii) un mapa o un arxiu KML (Keyhole Markup Language) que conté la informació presentada a la taula.

Amb tota aquesta informació és possible caracteritzar la traça de danys (longitud i amplada) i estimar la intensitat del fenomen. Per altra banda, l'anàlisi del patró de danys sovint permet conèixer quin fenomen ha tingut lloc (p. ex. tornado o esclafit) encara que no hi hagi hagut cap observador directe o imatge d'aquest. Tot i això, en el cas d'episodis febles que afecten una

àrea petita o quan la velocitat de translació és comparable amb la velocitat tangencial d'un tornado o amb la velocitat radial d'un esclafit, les diferències que presenten el patró de danys d'ambdós fenòmens no són suficients per a poder arribar a un resultat concloent.

La metodologia presenta algunes limitacions que cal tenir en compte, si bé es proposen tècniques per a intentar minimitzar-les. Per una banda, l'error del GPS genera una incertesa en la localització dels elements afectats, fet que influeix en algunes dades derivades com l'amplada i la llargada de la traça de danys. Per altra banda, l'ús de l'escala EF presenta algunes dificultats fora dels Estats Units, especialment a l'hora d'estimar la velocitat del vent a partir dels danys en edificacions. Finalment, el fet que la metodologia es basi en l'anàlisi en superfície de l'àrea afectada fa que els episodis extensos o les zones d'orografia complexa siguin difícils d'estudiar. En qualsevol cas, la metodologia proposada pot contribuir a estandarditzar l'elaboració dels treballs de camp, els quals són essencials per a construir i mantenir bases de dades de fenòmens de temps violent que discriminin entre tornados i esclafits.

- OE2. Utilitzar ortofotografies per a analitzar episodis de ventades fortes d'origen convectiu.

Les imatges aèries d'alta resolució, com les ortofotografies de l'ICGC, permeten tenir una visió general de la zona afectada per un episodi de vent fort d'origen convectiu, independentment de la seva extensió i de l'orografia del terreny. En alguns casos es poden arribar a detectar traces de danys d'episodis dels quals no es tenia coneixement en haver afectat regions amb una densitat de població molt baixa.

La identificació dels arbres caiguts fa possible estudiar el patró de danys i, d'aquesta manera, conèixer si foren causats per un tornado o un esclafit. A més, també es pot caracteritzar la traça de danys amb la mesura de la seva amplada i llargada. Per tant, aquest tipus d'anàlisi esdevé un complement idoni dels treballs de camp.

Els casos més febles, que causen pocs danys i de manera dispersa, són difícilment detectables amb ortofotografies, ja que no hi ha canvis apreciables en la cobertura vegetal ni en les edificacions entre les imatges anterior i posterior al cas d'estudi. A banda, arran de la freqüència anual de les ortofotografies de l'ICGC, ocasionalment hi pot haver la superposició de diversos episodis en una mateixa zona, fet que pot complicar la identificació dels danys associats a l'esdeveniment d'interès.

Amb aquesta tècnica no és possible disposar d'una anàlisi individual per a cadascun dels elements malmesos tenint en compte els diversos factors que poden influir en la seva vulnerabilitat (p. ex. l'estat de conservació de les estructures afectades, la humitat del sòl), tal com es fa en un treball de camp. Nogensmenys, diversos articles han mostrat que existeix una relació entre l'amplada i la llargada de la traça de danys amb la intensitat d'un tornado, segons l'escala de Fujita. També es pot relacionar la intensitat del fenomen amb la ràtio d'arbres tombats o escapçats en un bosc, en aquest cas en funció de l'escala de Fujita millorada. Així, amb aquests dos mètodes és possible fer una estimació raonable de la intensitat del fibló.

- OE3. Desenvolupar una base de dades de tornados i trombes marines a Catalunya i analitzar les característiques dels episodis.

Es genera una base de dades d'episodis de tornados i trombes marines detectats a Catalunya entre els anys 2000 i 2019 mitjançant la combinació de diverses fonts d'informació, com els observadors meteorològics, els mitjans de comunicació, els estudis ja existents i les xarxes socials. La posterior verificació de cadascun dels casos i l'anàlisi de les traces de danys mitjançant l'elaboració de treballs de camp i amb l'ús d'ortofotografies permet desenvolupar un conjunt de dades robust i homogeni.

El recull d'episodis conté 105 tornados i 329 mànegues marines, fet que dona lloc a una de les majors densitats de fiblons per unitat d'àrea de la conca mediterrània. L'anàlisi de les

dades mostra que la distribució espacial dels tornados i les trombes marines a Catalunya no és homogènia, un fet que té relació amb la densitat de població, però també amb l'orografia complexa de la zona d'estudi i la interacció d'aquesta amb l'atmosfera. La zona més afectada és el litoral i prelitoral central, incloent-hi les dues àrees metropolitanes més importants, la de Barcelona i la de Tarragona. L'època de l'any en la qual són més freqüents és entre els mesos d'agost i novembre, i habitualment s'observen durant la tarda. Tot i això, en el cas de les mànegues marines es detecta un segon màxim al matí, que és coherent amb la climatologia de llamps del mar Balear.

Durant el període d'estudi hi ha hagut 17 *outbreaks* (el més remarcable fou el dels dies 7 i 8 de setembre de 2005) i 54 esdeveniments múltiples (essent els dos més importants l'associat a l'*outbreak* esmentat i el del 8 de març de 2018). La majoria dels tornados registrats són febles (d'intensitat EF0 o EF1) i la traça de danys sol tenir una longitud inferior als 5 km de llargada i una amplada de menys de 200 m. Tot i això, ocasionalment es registren episodis significatius, amb una traça de més de 10 km de llarg i de 500 m d'ample. A banda, l'orientació de les franges de danys sol oscil·lar entre SE-NW i SW-NE, essent la direcció SE-NW la predominant per a les trombes marines que toquen terra. Pel que fa a l'impacte socioeconòmic, fins a 26 persones han estat ferides per tornados, principalment per contusions, talls i fractures. A més, els danys provocats pels fiblons s'estimen en 30,8 M€.

- OE4. Estudiar paràmetres termodinàmics i cinemàtics per a diversos tipus de temps.

Els dies sense precipitació (DRY) solen presentar valors de CAPE, de WS i d'SRH menors que els dies de tempesta sense tornados (NTTD), els dies de mànega marina (WAT), els dies de tornado d'intensitat EF0 (EF0) i els d'intensitat EF1 o superior (EF1+). Per la seva banda, els entorns EF1+ són els que presenten unes condicions més extremes, amb valors més alts per al conjunt de paràmetres respecte a la resta de categories de sondatges.

No hi ha una relació clara entre la CAPE i la formació de tornados. És a dir, que el rang de valors de CAPE que presenten els NTTD és força semblant al d'EF0 i EF1+. Tot i això, habitualment els episodis de tornados significatius tendeixen a estar associats a una CAPE superior als 400 J kg^{-1}.

Els valors de WS i SRH per als radiosondatges de NTTD i de WAT tenen una distribució semblant. Això indica que els episodis de trombes marines tenen lloc en entorns poc restrictius, a diferència dels tornados i, especialment, dels casos més intensos. Aquests resultats poden tenir relació amb el fet que és possible que hi hagi una major proporció de mànegues marines d'origen no mesociclònic que no pas de tornados no lligats a un mesocicló. Això també explicaria que la formació de mànegues marines sigui més habitual que la de fiblons terra endins.

Es detecta que existeix una relació directa entre els paràmetres cinemàtics (WS i SRH) i la intensitat màxima dels episodis, essent especialment notable per a l'estrat 0-3 km. Així, els tornados significatius solen estar associats a entorns amb un cisallament vertical del vent i una helicitat més marcats que no pas els casos febles. A banda, les diferències que presenten el WS i l'SRH per als estrats 0-1 km i 0-3 km entre NTTD i EF1+ motiven la definició de nous llindars per a discriminar entre ambdós tipus de sondatges.

- OE5. Analitzar el comportament de paràmetres específics per a detectar entorns favorables per a la formació de tornados.

La distribució temporal dels episodis de tornado no és la mateixa al conjunt de la Península Ibèrica i de les Illes Balears. Mentre que al nord-est de la Península i a les Illes (NE) són més freqüents durant l'època càlida (de maig a octubre), al sud-oest de la Península (SW) ho són a l'època freda (de novembre a abril). Això dona lloc a uns entorns característics diferents. Al NE els episodis de tornado solen estar lligats a valors de CAPE elevats i a un cisallament

i helicitat a nivells baixos més modestos. En canvi, al SW acostumen a presentar una CAPE relativament baixa i valors de WS i d'SRH elevats per als estrats més propers a la superfície.

S'identifiquen dos casos particulars d'entorns favorables per a la tornadogènesi, descrits prèviament per altres autors. Per una banda, l'associat a una elevada helicitat i a una CAPE baixa (HSLC), més freqüents de l'època hivernal i, per tant, observats més habitualment al SW. Per l'altra, els entorns de poca helicitat i un nivell de condensació per elevació elevat (LHHLCL), més usual a l'època estival i, per consegüent, més freqüents al NE.

S'observa que hi ha una compensació entre la CAPE i el WS, és a dir, que mentre que en entorns molt inestables es poden formar tornados amb un cisallament vertical del vent més aviat moderat, en condicions de poca inestabilitat és necessari un WS més marcat. Precisament, el paràmetre WMAXSHEAR, originalment formulat per a l'estrat 0-6 km, reflecteix aquest fet: mostra unes diferències entre els episodis del NE i del SW més modestes que no pas la CAPE i el WS per separat. Tot i això, per a reduir encara més les diferències entre les dues subregions i alhora accentuar-les entre els episodis febles i els significatius, es proposa utilitzar el WS 0-3 km en comptes del WS 0-6 km per a calcular una nova versió del WMAXSHEAR. Com a resultat, s'obté que els tornados significatius solen estar lligats a valors de WMAXSHEAR 0-3 km superiors a 500 m^2 s^{-2}.

Es determina que l'STP és poc útil a l'hora d'identificar entorns favorables per a la tornadogènesi. Si bé és cert que aquest paràmetre fa referència especialment als tornados significatius, en general presenta valors força més baixos que no pas als Estats Units, on es va desenvolupar l'índex. El fet que els episodis més intensos no destaquin gaire respecte a la resta de casos en limita el seu ús. Per contra, l'UTI, que està basat en diversos paràmetres termodinàmics i cinemàtics normalitzats amb els valors típics de l'Europa central, sí que demostra ser un índex d'ajut per a distingir els entorns favorables per a la tornadogènesi, prenent els valors més elevats per als casos de fiblons intensos. De la mateixa manera, es comprova que l'EHI per a l'estrat 0-1 km, el VGP per a l'estrat 0-4 km i l'SCP també són d'utilitat per a identificar entorns típics de dies de tornado.

- OE6. Validar la detecció d'entorns favorables per a la formació de mànegues marines mitjançant el nomograma de Szilagyi.

Per primera vegada s'utilitza el nomograma de Szilagyi per a analitzar episodis de mànegues marines de la Mediterrània occidental, així com de la costa atlàntica i cantàbrica de la Península Ibèrica. Demostra ser una eina molt útil per a identificar els entorns propicis per a la formació de trombes marines. En aquest sentit, el 81% dels casos estudiats se situen dins la regió favorable del nomograma. La majoria d'aquests episodis, sobretot els de l'època càlida, estan caracteritzats per una diferència entre l'EL i l'LCL (CCD) superior a 8,5 km i una diferència entre la temperatura de la superfície del mar i 850 hPa (ΔT) inferior a 16 °C.

No s'observa cap cas que satisfaci les condicions per a ser classificat com a episodi hivernal. Tot i això, es detecta un conjunt d'entorns situats fora de la zona favorable, concretament amb un CCD entre 1,5 i 6 km i un ΔT entre 10 °C i 15 °C, dels quals més de la meitat corresponen a l'època freda. Es tracta d'un resultat consistent amb els d'estudis anteriors elaborats en altres àmbits mediterranis.

Aquest mètode de predicció fou desenvolupat a la regió dels Grans Llacs d'Amèrica del Nord, on les adveccions d'aire fred a l'hivern són més freqüents i més intenses que no pas al sud d'Europa. Això genera valors de ΔT elevats durant l'època freda, que a la Mediterrània són extremadament rars. És per aquest motiu que convindria adaptar el nomograma a la realitat de la nostra àrea d'estudi.

5.2 Perspectives de futur

Una de les tasques que convindria dur a terme en un futur és l'automatització de la identificació de canvis en la cobertura vegetal mitjançant la comparativa d'ortofotografies (Shikhov i Chernokulsky, 2018). Així, es podrien observar traces de danys en zones forestals, les quals poden tenir diversos orígens (p. ex. vent, esllavissades, incendis, tales). Amb una anàlisi visual d'aquestes zones seria factible detectar les que han estat afectades per vent i, mitjançant l'estudi del patró de danys, esclarir quin fenomen meteorològic n'ha estat el responsable. D'aquesta manera es resoldria, en part, la dependència de l'observació de ventades fortes d'origen convectiu amb la densitat de població. Malgrat tot, hi continuaria havent una manca d'informació en zones desforestades i de dades d'episodis febles, amb danys discontinus i poc importants.

Havent estudiat la distribució temporal i espacial dels tornados a Catalunya i les característiques de les traces de danys, el següent pas és analitzar les cèl·lules i els sistemes convectius que els formen mitjançant dades de teledetecció (Rigo i Llasat, 2007; Gallus et al., 2008; Agee i Jones, 2009). Això implica determinar el mode convectiu (cèl·lula individual, multicèl·lula, sistema convectiu), analitzar la presència o no d'un mesocicló, estudiar el cicle de vida de les cèl·lules i determinar en quin moment d'aquest es formen els tornados, i la freqüència amb què hi ha fiblons (sobretot mànegues marines) en condicions de bon temps. També es podrien validar productes de *nowcasting* com el *Lightning Jump*, el qual actualment es troba operatiu a l'SMC (Farnell et al., 2017). Tot plegat aportaria una millora en el seguiment i la vigilància d'aquest tipus de situacions.

Per tal d'augmentar la mostra de casos, seria positiu de dur a terme la caracterització de les cèl·lules convectives per al conjunt de la Península Ibèrica i les Illes Balears, o fins i tot per a un àmbit més extens. Això donaria peu a repetir l'anàlisi de la caracterització dels perfils verticals, però agrupant els casos en funció del mode convectiu (Thompson et al., 2012, 2013). Precisament, es podria determinar la proporció de tornados mesociclònics que es produeixen en entorns típicament desfavorables per a les supercèl·lules (i.e. WS 0-6 km inferior a 20 m s^{-1}), alhora que es podria estudiar el paràmetre SRH per a l'estrat 0-500 m, que segons alguns articles recents és útil per a discriminar entre els entorns de supercèl·lules tornàdiques i no tornàdiques (Coffer et al., 2019, 2020).

Un treball que seria molt interessant és el de caracteritzar els patrons sinòptics que donen lloc a tornados, tant a Catalunya com a la resta de la Península Ibèrica i les Illes Balears. Finalment, es podria testejar la posada en operatiu del nomograma de Szilagyi utilitzant dades de models de predicció per a diversos punts propers a la costa. Així, es podrien detectar entorns favorables per a la formació de trombes marines que, juntament amb la identificació de fronteres de masses d'aire o de zones de convergència en superfície, podrien millorar la predicció d'aquests episodis. Abans, però, caldria redefinir les regions del nomograma per a adaptar-lo a la Mediterrània.

En qualsevol cas, l'estudi dels fenòmens de temps violent, i més concretament els tornados, encara té molt de camp per recórrer. En aquesta secció tan sols s'ha volgut apuntar algunes de les línies que es podria seguir d'ara endavant i que, a més, aportarien una millora i tindrien una aplicació directa en la detecció d'episodis passats i en l'operativa de la predicció i vigilància meteorològica al sud-oest del continent europeu.

Bibliografia

Agee E. i Jones E. (2009): Proposed Conceptual Taxonomy for Proper Identification and Classification of Tornado Events. *Weather and Forecasting*, **24(2)**: 609–617. doi:10.1175/2008WAF2222163.1.

Allen J.T., Karoly D.J. i Walsh K.J. (2014): Future Australian Severe Thunderstorm Environments. Part II: The Influence of a Strongly Warming Climate on Convective Environments. *Journal of Climate*, **27(10)**: 3848–3868. doi:10.1175/JCLI-D-13-00426.1.

Altube P., Bech J., Argemí O. i Rigo T. (2015): Quality Control of Antenna Alignment and Receiver Calibration Using the Sun: Adaptation to Midrange Weather Radar Observations at Low Elevation Angles. *Journal of Atmospheric and Oceanic Technology*, **32(5)**: 927–942. doi:10.1175/JTECH-D-14-00116.1.

Altube P., Bech J., Argemí O., Rigo T., Pineda N., Collis S. i Helmus J. (2017): Correction of Dual-PRF Doppler Velocity Outliers in the Presence of Aliasing. *Journal of Atmospheric and Oceanic Technology*, **34(7)**: 1529–1543. doi:10.1175/JTECH-D-16-0065.1.

AMS (2020): Glossary of Meteorology. American Meteorological Society. `http://glossary.ametsoc.org`.

Antonescu B. i Bell A. (2015): Tornadoes in Romania. *Monthly Weather Review*, **143(3)**: 689–701. doi:10.1175/MWR-D-14-00181.1.

Antonescu B., Púçik T. i Schultz D.M. (2020): Hindcasting the First Tornado Forecast in Europe: 25 June 1967. *Weather and Forecasting*, **35(2)**: 417–436. doi:10.1175/WAF-D-19-0173.1.

Antonescu B., Ricketts H.M.A.M. i Schultz D.M. (2019): 100 Years Later: Reflecting on Alfred Wegener's Contributions to Tornado Research in Europe. *Bulletin of the American Meteorological Society*, **100(4)**: 567–578. doi:10.1175/BAMS-D-17-0316.1.

Antonescu B., Schultz D.M., Holzer A. i Groenemeijer P. (2017): Tornadoes in Europe: An Underestimated Threat. *Bulletin of the American Meteorological Society*, **98(4)**: 713–728. doi:10.1175/BAMS-D-16-0171.1.

Antonescu B., Schultz D.M., Lomas F. i Kühne T. (2016): Tornadoes in Europe: Synthesis of the Observational Datasets. *Monthly Weather Review*, **144(7)**: 2445–2480. doi:10.1175/MWR-D-15-0298.1.

Apsley M.L., Mulder K.J. i Schultz D.M. (2016): Reexamining the United Kingdom's Greatest Tornado Outbreak: Forecasting the Limited Extent of Tornadoes along a Cold Front. *Weather and Forecasting*, **31(3)**: 853–875. doi:10.1175/WAF-D-15-0131.1.

Aran M., Amaro J., Arús J., Bech J., Figuerola F., Gayà M. i Vilaclara E. (2009): Synoptic and mesoscale diagnosis of a tornado event in Castellcir, Catalonia, on 18th October 2006.

Atmospheric Research, **93(1)**: 147–160. doi:10.1016/j.atmosres.2008.09.031. 4th European Conference on Severe Storms.

Arús J. (2018): 25 años de tornados en Cataluña (1992–2017). *Simposio Nacional de Predicción "Memorial Antonio Mestre", Madrid, Spain*. Agencia Estatal de Meteorología.

Ashley W.S., Strader S., Rosencrants T. i Krmenec A.J. (2014): Spatiotemporal Changes in Tornado Hazard Exposure: The Case of the Expanding Bull's-Eye Effect in Chicago, Illinois. *Weather, Climate, and Society*, **6(2)**: 175–193. doi:10.1175/WCAS-D-13-00047.1.

Bai L., Meng Z., Huang L., Yan L., Li Z., Mai X., Huang Y., Yao D. i Wang X. (2017): An Integrated Damage, Visual, and Radar Analysis of the 2015 Foshan, Guangdong, EF3 Tornado in China Produced by the Landfalling Typhoon Mujigae (2015). *Bulletin of the American Meteorological Society*, **98(12)**: 2619–2640. doi:10.1175/BAMS-D-16-0015.1.

Barnolas M. i Llasat M.C. (2007): A flood geodatabase and its climatological applications: the case of Catalonia for the last century. *Natural Hazards and Earth System Sciences*, **7(2)**: 271–281. doi:10.5194/nhess-7-271-2007.

Barredo J.I., Saurí D. i Llasat M.C. (2012): Assessing trends in insured losses from floods in Spain 1971–2008. *Natural Hazards and Earth System Sciences*, **12(5)**: 1723–1729. doi: 10.5194/nhess-12-1723-2012.

Barrett B.S., Marin J.C. i Jacques-Coper M. (2020): A multiscale analysis of the tornadoes of 30–31 May 2019 in south-central Chile. *Atmospheric Research*, **236**: 104811. doi:10.1016/j.atmosres.2019.104811.

Bech J., Arús J., Castán S., Pineda N., Rigo T., Montanyà J. i van der Velde O. (2015): A study of the 21 March 2012 tornadic quasi linear convective system in Catalonia. *Atmospheric Research*, **158-159**: 192–209. doi:10.1016/j.atmosres.2014.08.009.

Bech J., Castán S., Arús J., Rodríguez O., Pascual R., Cuevas G., Pineda N., Rigo T., Montanyà J. i van der Velde O. (2016): Observational study of the 2014 Vilabella tornadic thunderstorm. *9th European Conference on Radar in Meteorology and Hydrology (ERAD2016)*.

Bech J., Codina B., Lorente J. i Bebbington D. (2003): The Sensitivity of Single Polarization Weather Radar Beam Blockage Correction to Variability in the Vertical Refractivity Gradient. *Journal of Atmospheric and Oceanic Technology*, **20(6)**: 845–855. doi: 10.1175/1520-0426(2003)020⟨0845:TSOSPW⟩2.0.CO;2.

Bech J., Gayà M., Aran M., Figuerola F., Amaro J. i Arús J. (2009): Tornado damage analysis of a forest area using site survey observations, radar data and a simple analytical vortex model. *Atmospheric Research*, **93(1)**: 118–130. doi:10.1016/j.atmosres.2008.10.016. 4th European Conference on Severe Storms.

Bech J., Pascual R., Rigo T., Pineda N., López J.M., Arús J. i Gayà M. (2007): An observational study of the 7 September 2005 Barcelona tornado outbreak. *Natural Hazards and Earth System Sciences*, **7(1)**: 129–139. doi:10.5194/nhess-7-129-2007.

Bech J., Pineda N., Rigo T. i Aran M. (2013): Remote sensing analysis of a Mediterranean thundersnow and low-altitude heavy snowfall event. *Atmospheric Research*, **123**: 305–322. doi:10.1016/j.atmosres.2012.06.021. 6th European Conference on Severe Storms 2011. Palma de Mallorca, Spain.

Bech J., Pineda N., Rigo T., Aran M., Amaro J., Gayà M., Arús J., Montanyà J. i van der Velde O. (2011): A Mediterranean nocturnal heavy rainfall and tornadic event. Part I: Overview, damage survey and radar analysis. *Atmospheric Research*, **100(4)**: 621–637. doi:10.1016/j.atmosres.2010.12.024. 5th European Conference on Severe Storms.

Bech J., Rodríguez O., Altube P., Rigo T., Pineda N., Castán S., Arús J. i Montanyà J. (2018): Doppler radar observations of two tornadic thunderstorm cases in the Western Mediterranean region. *10th European Conference on Radar in Meteorology and Hydrology (ERAD2018)*.

Beck V. i Dotzek N. (2010): Reconstruction of Near-Surface Tornado Wind Fields from Forest Damage. *Journal of Applied Meteorology and Climatology*, **49(7)**: 1517–1537. doi:10.1175/2010JAMC2254.1.

Belo-Pereira M., Andrade C. i Pinto P. (2017): A long-lived tornado on 7 December 2010 in mainland Portugal. *Atmospheric Research*, **185**: 202–215. doi:10.1016/j.atmosres.2016.11.002.

Bertotti L., Bidlot J.R., Bunney C., Cavaleri L., Delli Passeri L., Gomez M., Lefèvre J.M., Paccagnella T., Torrisi L., Valentini A. i Vocino A. (2012): Performance of different forecast systems in an exceptional storm in the Western Mediterranean Sea. *Quarterly Journal of the Royal Meteorological Society*, **138(662)**: 34–55. doi:10.1002/qj.892.

Beven K.J., Aspinall W.P., Bates P.D., Borgomeo E., Goda K., Hall J.W., Page T., Phillips J.C., Simpson M., Smith P.J., Wagener T. i Watson M. (2018): Epistemic uncertainties and natural hazard risk assessment – Part 2: What should constitute good practice? *Natural Hazards and Earth System Sciences*, **18(10)**: 2769–2783. doi:10.5194/nhess-18-2769-2018.

Bissolli P., Grieser J., Dotzek N. i Welsch M. (2007): Tornadoes in Germany 1950–2003 and their relation to particular weather conditions. *Global and Planetary Change*, **57(1)**: 124–138. doi:10.1016/j.gloplacha.2006.11.007. Extreme Climatic Events.

Blumberg W.G., Halbert K.T., Supinie T.A., Marsh P.T., Thompson R.L. i Hart J.A. (2017): SHARPpy: An Open-Source Sounding Analysis Toolkit for the Atmospheric Sciences. *Bulletin of the American Meteorological Society*, **98(8)**: 1625–1636. doi:10.1175/BAMS-D-15-00309.1.

Bolgiani P., Fernández-González S., Valero F., Merino A., García-Ortega E., Sánchez J.L. i Martín M.L. (2020): Simulation of Atmospheric Microbursts Using a Numerical Mesoscale Model at High Spatiotemporal Resolution. *Journal of Geophysical Research: Atmospheres*, **125(4)**: e2019JD031791. doi:10.1029/2019JD031791.

Brady R.H. i Szoke E.J. (1989): A Case Study of Nonmesocyclone Tornado Development in Northeast Colorado: Similarities to Waterspout Formation. *Monthly Weather Review*, **117(4)**: 843–856. doi:10.1175/1520-0493(1989)117⟨0843:ACSONT⟩2.0.CO;2.

Brooks H.E. (2004): On the Relationship of Tornado Path Length and Width to Intensity. *Weather and Forecasting*, **19(2)**: 310–319. doi:10.1175/1520-0434(2004)019⟨0310:OTROTP⟩2.0.CO;2.

Brooks H.E., Doswell Charles A. I. i Cooper J. (1994): On the Environments of Tornadic and Nontornadic Mesocyclones. *Weather and Forecasting*, **9(4)**: 606–618. doi:10.1175/1520-0434(1994)009⟨0606:OTEOTA⟩2.0.CO;2.

Brooks H.E., Lee J.W. i Craven J.P. (2003): The spatial distribution of severe thunderstorm and tornado environments from global reanalysis data. *Atmospheric Research*, **67-68**: 73–94. doi:10.1016/S0169-8095(03)00045-0. European Conference on Severe Storms 2002.

Brown S., Archer P., Kruger E. i Mallonee S. (2002): Tornado-Related Deaths and Injuries in Oklahoma due to the 3 May 1999 Tornadoes. *Weather and Forecasting*, **17(3)**: 343–353. doi:10.1175/1520-0434(2002)017⟨0343:TRDAII⟩2.0.CO;2.

Bunkers M.J., Klimowski B.A., Zeitler J.W., Thompson R.L. i Weisman M.L. (2000): Predicting Supercell Motion Using a New Hodograph Technique. *Weather and Forecasting*, **15(1)**: 61–79. doi:10.1175/1520-0434(2000)015⟨0061:PSMUAN⟩2.0.CO;2.

Bunting W.F. i Smith B.E. (1993): *A guide for conducting convective windstorm surveys*. NOAA, Fort Worth, Texas.

Burgess D., Ortega K., Stumpf G., Garfield G., Karstens C., Meyer T., Smith B., Speheger D., Ladue J., Smith R. i Marshall T. (2014): 20 May 2013 Moore, Oklahoma, Tornado: Damage Survey and Analysis. *Weather and Forecasting*, **29(5)**: 1229–1237. doi:10.1175/WAF-D-14-00039.1.

Burow D., Herrero H. i Ellis K. (2020): Damage Analysis of Three Long-Track Tornadoes Using High-Resolution Satellite Imagery. *Atmosphere*, **11**: 613. doi:10.3390/atmos11060613.

C3S (2017): ERA5: Fifth generation of ECMWF atmospheric reanalyses of the global climate. Copernicus Climate Change Service Climate Data Store (CDS). `https://cds.climate.copernicus.eu/cdsapp#!/home`. doi:10.24381/cds.adbb2d47.

Callado A. i Pascual R. (2005): Diagnosis and modelling of a summer convective storm over Mediterranean Pyrenees. *Advances in Geosciences*, **2**: 273–277. doi:10.5194/adgeo-2-273-2005.

Calvo-Sancho C. i Martín Y. (2020): The influence of synoptic weather patterns in supercell formation in Spain. *EGU Assembly Conference*. European Geosciences Union.

Cannon J.B., Hepinstall-Cymerman J., Godfrey C.M. i Peterson C.J. (2016): Landscape-scale characteristics of forest tornado damage in mountainous terrain. *Landscape Ecology*, **31**: 2097–2114. doi:10.1007/s10980-016-0384-8.

Celiński-Mysław D., Palarz A. i Taszarek M. (2020): Climatology and atmospheric conditions associated with cool season bow echo storms in Poland. *Atmospheric Research*, **240**: 104944. doi:10.1016/j.atmosres.2020.104944.

Chandra S., Fleming E.L., Schoeberl M.R. i Barnett J.J. (1990): Monthly mean global climatology of temperature, wind, geopotential height and pressure for 0–120 km. *Advances in Space Research*, **10(6)**: 3–12. doi:10.1016/0273-1177(90)90230-W.

Chen J., Cai X., Wang H., Kang L., Zhang H., Song Y., Zhu H., Zheng W. i Li F. (2018): Tornado climatology of China. *International Journal of Climatology*, **38(5)**: 2478–2489. doi:10.1002/joc.5369.

Chernokulsky A., Kurgansky M., Mokhov I., Shikhov A., Azhigov I., Selezneva E., Zakharchenko D., Antonescu B. i Kühne T. (2020): Tornadoes in Northern Eurasia: From the Middle Age to the Information Era. *Monthly Weather Review*, **148(8)**: 3081–3110. doi:10.1175/MWR-D-19-0251.1.

Chernokulsky A. i Shikhov A. (2018): 1984 Ivanovo tornado outbreak: Determination of actual tornado tracks with satellite data. *Atmospheric Research*, **207**: 111–121. doi:10.1016/j.atmosres.2018.02.011.

Chernokulsky A.V., Kurgansky M.V. i Mokhov I.I. (2019): On characteristic reanalysis-based values of convective instability indices for Northern Eurasia tornadoes. *IOP Conference Series: Earth and Environmental Science*, **231**: 012012. doi:10.1088/1755-1315/231/1/012012.

Childs S.J., Schumacher R.S. i Allen J.T. (2018): Cold-Season Tornadoes: Climatological and Meteorological Insights. *Weather and Forecasting*, **33(3)**: 671–691. doi:10.1175/WAF-D-17-0120.1.

Chmielewski T., Szer J. i Bobra P. (2020): Derecho wind storm in Poland on 11–12 August 2017: results of the post-disaster investigation. *Environmental Hazards*, **19(5)**: 508–528. doi:10.1080/17477891.2020.1730154.

Coffer B.E., Parker M.D., Thompson R.L., Smith B.T. i Jewell R.E. (2019): Using Near-Ground Storm Relative Helicity in Supercell Tornado Forecasting. *Weather and Forecasting*, **34(5)**: 1417–1435. doi:10.1175/WAF-D-19-0115.1.

Coffer B.E., Taszarek M. i Parker M.D. (2020): Near-ground wind profiles of tornadic and nontornadic environments in the United States and Europe from ERA5 reanalyses. *Weather and Forecasting*, 1–52. doi:10.1175/WAF-D-20-0153.1.

Cortès M., Turco M., Llasat-Botija M. i Llasat M.C. (2018): The relationship between precipitation and insurance data for floods in a Mediterranean region (northeast Spain). *Natural Hazards and Earth System Sciences*, **18(3)**: 857–868. doi:10.5194/nhess-18-857-2018.

Craven J.P. i Brooks H.E. (2004): Baseline climatology of sounding derived parameters associated with deep moist convection. *National Weather Digest*, **28**: 13–24.

Davies J.M. (1993): Hourly helicity, instability, and EHI in forecasting supercell tornadoes. *17th Conference on Severe Local Storms, St. Louis, Missouri, USA*. American Meteorological Society.

Davies J.M. (2006): Tornadoes in Environments with Small Helicity and/or High LCL Heights. *Weather and Forecasting*, **21(4)**: 579–594. doi:10.1175/WAF928.1.

Davies-Jones R.P., Burgess D. i Foster M. (1990): Test of helicity as a tornado forecast parameter. *17th Conference on Severe Local Storms, Kananaskis Park, Alberta, Canada*. American Meteorological Society.

Davis (2020): Wireless Vantage Pro2™ & Vantage Pro2™ Plus Stations. `https://www.davisinstruments.com/product_documents/weather/spec_sheets/6152_62_53_63_SS.pdf`.

Davis J.M. i Parker M.D. (2014): Radar Climatology of Tornadic and Nontornadic Vortices in High-Shear, Low-CAPE Environments in the Mid-Atlantic and Southeastern United States. *Weather and Forecasting*, **29(4)**: 828–853. doi:10.1175/WAF-D-13-00127.1.

De Groeve T., Poljansek K. i Ehrlich D. (2013): *Recording disasters losses: recommendation for a European approach*. Joint Research Centre (European Comission), Ispra, Italy.

De Groeve T., Poljansek K., Ehrlich D. i Corbane C. (2014): *Current status and best practices for disaster loss data recording in EU Member States*. Joint Research Centre (European Comission), Ispra, Italy.

Deijns A.A., Bevington A.R., van Zadelhoff F., de Jong S.M., Geertsema M. i McDougall S. (2020): Semi-automated detection of landslide timing using harmonic modelling of satellite imagery, Buckinghorse River, Canada. *International Journal of Applied Earth Observation and Geoinformation*, **84**: 101943. doi:10.1016/j.jag.2019.101943.

del Moral A., Llasat M.C. i Rigo T. (2017): Identification of anomalous motion of thunderstorms using daily rainfall fields. *Atmospheric Research*, **185**: 92–100. doi:10.1016/j.atmosres.2016.11.001.

del Moral A., Llasat M.C. i Rigo T. (2020): Connecting flash flood events with radar-derived convective storm characteristics on the northwestern Mediterranean coast: knowing the present for better future scenarios adaptation. *Atmospheric Research*, **238**: 104863. doi:10.1016/j.atmosres.2020.104863.

del Moral A., Weckwerth T.M., Rigo T., Bell M.M. i Llasat M.C. (2020): C-Band Dual-Doppler Retrievals in Complex Terrain: Improving the Knowledge of Severe Storm Dynamics in Catalonia. *Remote Sensing*, **12**: 2930. doi:10.3390/rs12182930.

Devanas A. i Stefanova L. (2018): Statistical Prediction of Waterspout Probability for the Florida Keys. *Weather and Forecasting*, **33(2)**: 389–410. doi:10.1175/WAF-D-17-0100.1.

Donner W.R. (2007): The political ecology of disaster: An analysis of factors influencing U.S. tornado fatalities and injuries, 1998–2000. *Demography*, **44**: 669–685. doi:110.1353/dem.2007.0024.

Doswell C.A. (2003): *A guide to F-scale damage assessment*. National Oceanic and Atmospheric Administration, Silver Spring, Maryland.

Doswell C.A., Brooks H.E. i Dotzek N. (2009): On the implementation of the enhanced Fujita scale in the USA. *Atmospheric Research*, **93(1)**: 554–563. doi:10.1016/j.atmosres.2008.11.003. 4th European Conference on Severe Storms.

Doswell C.A. i Evans J.S. (2003): Proximity sounding analysis for derechos and supercells: an assessment of similarities and differences. *Atmospheric Research*, **67-68**: 117–133. doi:10.1016/S0169-8095(03)00047-4. European Conference on Severe Storms 2002.

Doswell C.A. i Rasmussen E.N. (1994): The Effect of Neglecting the Virtual Temperature Correction on CAPE Calculations. *Weather and Forecasting*, **9(4)**: 625–629. doi:10.1175/1520-0434(1994)009⟨0625:TEONTV⟩2.0.CO;2.

Doswell C.A. i Schultz D.M. (2006): On the use of indices and parameters in forecasting severe storms. *E-Journal of Severe Storms Meteorology*, **1(3)**: 1–22.

Dotzek N. (2003): An updated estimate of tornado occurrence in Europe. *Atmospheric Research*, **67-68**: 153–161. doi:10.1016/S0169-8095(03)00049-8. European Conference on Severe Storms 2002.

Dotzek N., Groenemeijer P., Feuerstein B. i Holzer A.M. (2009): Overview of ESSL's severe convective storms research using the European Severe Weather Database ESWD. *Atmospheric Research*, **93(1)**: 575–586. doi:10.1016/j.atmosres.2008.10.020. 4th European Conference on Severe Storms.

Dowell D.C. i Bluestein H.B. (2002): The 8 June 1995 McLean, Texas, Storm. Part I: Observations of Cyclic Tornadogenesis. *Monthly Weather Review*, **130(11)**: 2626–2648. doi:10.1175/1520-0493(2002)130⟨2626:TJMTSP⟩2.0.CO;2.

Durage S.W., Wirasinghe S.C. i Ruwanpura J. (2013): Comparison of the Canadian and US tornado detection and warning systems. *Natural Hazards*, **66**: 117–137. doi:10.1007/s11069-012-0168-7.

Durst C.S. (1960): Wind speeds over short periods of time. *Meteorological Magazine*, **89(1056)**: 181–187.

Edwards R. (2020): Frequently Asked Questions about Tornadoes (NOAA). `https://www.spc.noaa.gov/faq/tornado/index.html`.

Edwards R., LaDue J.G., Ferree J.T., Scharfenberg K., Maier C. i Coulbourne W.L. (2013): Tornado Intensity Estimation: Past, Present, and Future. *Bulletin of the American Meteorological Society*, **94(5)**: 641–653. doi:10.1175/BAMS-D-11-00006.1.

Eidson M., Lybarger J.A., Parsons J.E., MacCormack J.N. i Freeman J.I. (1990): Risk Factors for Tornado Injuries. *International Journal of Epidemiology*, **19(4)**: 1051–1056. doi:10.1093/ije/19.4.1051.

Elizaga F., Conejo S. i Martín F. (2007): Automatic identification of mesocyclones and significant wind structures in Doppler radar images. *Atmospheric Research*, **83(2)**: 405–414. doi:10.1016/j.atmosres.2005.10.023. European Conference on Severe Storms 2004.

Environment Canada (2013): *Enhanced Fujita Scale Damage Indicators and Degrees Of Damage*. Environment Canada, Dartmouth, Canada.

Ermert J., Koch B., Dees M., Zhao W., Hetzenecker M., Scharrer K. i Amaro D. (2013): Mapping of forest damages caused by a tornado 2012 in Gera, Germany using TerraSAR-X change detection. `https://www.semanticscholar.org/paper/Mapping-of-forest-damages-caused-by-a-tornado-2012-Ermert-Koch/6e5b51eed62cafbc0a7cf21b65e11ef683cbb958?p2df`.

ESWD (2020): European Severe Weather Database. `https://eswd.eu/`.

Farnell C., Busto M., Aran M., Andrés A., Pineda N. i Torà M. (2009): Study of the hailstorm of 17 September 2007 at the Pla d'Urgell. Part one: fieldwork and analysis of hailpads. *Tethys*, **6**: 67–79. doi:10.3369/tethys.2009.6.05.

Farnell C. i Rigo T. (2020): The Lightning Jump, the 2018 "Picking up Hailstones" Campaign and a Climatological Analysis for Catalonia for the 2006-2018 Period. *Tethys*, **17**: 10–20. doi:10.3369/tethys.2020.17.02.

Farnell C., Rigo T. i Pineda N. (2017): Lightning jump as a nowcast predictor: Application to severe weather events in Catalonia. *Atmospheric Research*, **183**: 130–141. doi:10.1016/j.atmosres.2016.08.021.

Feuerstein B., Groenemeijer P., Dirksen E., Hubrig M., Holzer A.M. i Dotzek N. (2011): Towards an improved wind speed scale and damage description adapted for Central Europe. *Atmospheric Research*, **100(4)**: 547–564. doi:10.1016/j.atmosres.2010.12.026. 5th European Conference on Severe Storms.

Fontserè E. (1948): *Assaig d'un vocabulari meteorològic català*. Institut d'Estudis Catalans, Barcelona, Catalunya.

Forbes G.S. i Wakimoto R.M. (1983): A Concentrated Outbreak of Tornadoes, Downbursts and Microbursts, and Implications Regarding Vortex Classification. *Monthly Weather Review*, **111(1)**: 220–236. doi:10.1175/1520-0493(1983)111⟨0220:ACOOTD⟩2.0.CO;2.

Foster D.R. (1988): Species and Stand Response to Catastrophic Wind in Central New England, U.S.A. *Journal of Ecology*, **76(1)**: 135–151.

Fox-Hughes P., Barnes-Keoghan I. i Porter A. (2018): Observations of a tornado at an Automatic Weather Station in northern Tasmania. *Journal of Southern Hemisphere Earth Systems Science*, **68**: 215–230. doi:10.22499/3.6801.012.

Franzese G., Della Rocca V. i Esposito F. (2020): Resolution of the size/distance degeneracy of the dust devils signals observed with a stationary meteorological station. *Aeolian Research*, **44**: 100594. doi:10.1016/j.aeolia.2020.100594.

Frique J. (2012): Les tornades en Belgique. `https://dl.dropboxusercontent.com/u/1866013/Documents/Tornades/1779-2012-bilan-climatologiquedes-tornades-en-belgique.pdf`.

Fujita T.T. (1971): Proposed characterization of tornadoes and hurricanes by area and intensity. *SMRP Research Paper*, **91**: 48.

Fujita T.T. (1981): Tornadoes and Downbursts in the Context of Generalized Planetary Scales. *Journal of the Atmospheric Sciences*, **38(8)**: 1511–1534. doi:10.1175/1520-0469(1981)038⟨1511:TADITC⟩2.0.CO;2.

Fujita T.T. (1992): Mystery of severe storms. *WRL Research Paper*, **239**: 298.

Gall M., Borden K.A. i Cutter S.L. (2009): When Do Losses Count?: Six Fallacies of Natural Hazards Loss Data. *Bulletin of the American Meteorological Society*, **90(6)**: 799–810. doi:10.1175/2008BAMS2721.1.

Gallus William A. J., Snook N.A. i Johnson E.V. (2008): Spring and Summer Severe Weather Reports over the Midwest as a Function of Convective Mode: A Preliminary Study. *Weather and Forecasting*, **23(1)**: 101–113. doi:10.1175/2007WAF2006120.1.

Galway J.G. (1975): Relationship of Tornado Deaths to Severe Weather Watch Areas. *Monthly Weather Review*, **103(8)**: 737–741. doi:10.1175/1520-0493(1975)103⟨0737:ROTDTS⟩2.0.CO;2.

Galway J.G. (1977): Some Climatological Aspects of Tornado Outbreaks. *Monthly Weather Review*, **105(4)**: 477–484. doi:10.1175/1520-0493(1977)105⟨0477:SCAOTO⟩2.0.CO;2.

Gasull B. (2015): *Maleïda. L'aventura de Jacint Verdaguer a l'Aneto*. Verdaguer Edicions, Folgueroles, Catalunya.

Gatzen C.P., Fink A.H., Schultz D.M. i Pinto J.G. (2020): An 18-year climatology of derechos in Germany. *Natural Hazards and Earth System Sciences*, **20(5)**: 1335–1351. doi:10.5194/nhess-20-1335-2020.

Gayà M. (2007): The 1886 tornado of Madrid. *Atmospheric Research*, **83(2)**: 201–210. doi:10.1016/j.atmosres.2005.10.017. European Conference on Severe Storms 2004.

Gayà M. (2011): Tornadoes and severe storms in Spain. *Atmospheric Research*, **100(4)**: 334–343. doi:10.1016/j.atmosres.2010.10.019. 5th European Conference on Severe Storms.

Gayà M. (2018): *Els fiblons a Espanya. Climatologia i catàleg de tornados i trombes*. Edicions UIB, Palma, Illes Balears.

Gayà M., Homar V., Romero R. i Ramis C. (2001): Tornadoes and waterspouts in the Balearic Islands: phenomena and environment characterization. *Atmospheric Research*, **56(1)**: 253–267. doi:10.1016/S0169-8095(00)00076-4. Conference on European Tornadoes and Severe Storms.

Gayà M., Llasat M.C. i Arús J. (2011): Tornadoes and waterspouts in Catalonia (1950–2009). *Natural Hazards and Earth System Sciences*, **11(7)**: 1875–1883. doi:10.5194/nhess-11-1875-2011.

Gayà M. i Redaño A. (1999): El tornado de L'Espluga de Francolí. Medidas de campo y tratamiento de imágenes digitalizadas. *IV Simposio Nacional de Predicción del Instituto Nacional de Meteorología, Madrid, Espanya*. Instituto Nacional de Meteorología.

Giaiotti D.B., Giovannoni M., Pucillo A. i Stel F. (2007): The climatology of tornadoes and waterspouts in Italy. *Atmospheric Research*, **83(2)**: 534–541. doi:10.1016/j.atmosres.2005.10.020. European Conference on Severe Storms 2004.

Godfrey C.M. i Peterson C.J. (2017): Estimating Enhanced Fujita Scale Levels Based on Forest Damage Severity. *Weather and Forecasting*, **32(1)**: 243–252. doi:10.1175/WAF-D-16-0104.1.

Golden J.H. i Purcell D. (1977): Photogrammetric Velocities for the Great Bend, Kansas, Tornado of 30 August 1974: Accelerations and Asymmetries. *Monthly Weather Review*, **105(4)**: 485–492. doi:10.1175/1520-0493(1977)105⟨0485:PVFTGB⟩2.0.CO;2.

Goliger A.M. i Milford R.V. (1998): A review of worldwide occurrence of tornadoes. *Journal of Wind Engineering and Industrial Aerodynamics*, **74-76**: 111–121. doi:10.1016/S0167-6105(98)00009-9.

Gonzalez S., Callado A., Werner E., Escribà P. i Bech J. (2018): Coastally trapped disturbances caused by the tramontane wind on the northwestern Mediterranean: numerical study and sensitivity to short-wave radiation. *Quarterly Journal of the Royal Meteorological Society*, **144(714)**: 1321–1336. doi:10.1002/qj.3320.

Gorelick N., Hancher M., Dixon M., Ilyushchenko S., Thau D. i Moore R. (2017): Google Earth Engine: Planetary-scale geospatial analysis for everyone. *Remote Sensing of Environment*, **202**: 18–27. doi:10.1016/j.rse.2017.06.031. Big Remotely Sensed Data: tools, applications and experiences.

Grams J.S., Thompson R.L., Snively D.V., Prentice J.A., Hodges G.M. i Reames L.J. (2012): A Climatology and Comparison of Parameters for Significant Tornado Events in the United States. *Weather and Forecasting*, **27(1)**: 106–123. doi:10.1175/WAF-D-11-00008.1.

Grasso V., Zaza I., Zabini F., Pantaleo G., Nesi P. i Crisci A. (2017): Weather events identification in social media streams: tools to detect their evidence in Twitter. *PeerJ Preprints*, **5**: e2241v2. doi:10.7287/peerj.preprints.2241v2.

Grieser J. i Haines P. (2020): Tornado Risk Climatology in Europe. *Atmosphere*, **11(7)**: 768. doi:10.3390/atmos11070768.

Groenemeijer P., Holzer A.M., Hubrig M., Kühne T., Kaltenberger R., Soriano J.D., Bock L., Guitiérrez D., van de Ploeg B., Strommer G. i Schreiner T. (2019a): The International Fujita Scale: A Globally Applicable Scale for Tornado and Wind Damage Classification. *10th European Conference on Severe Storms, Kraków, Poland*. European Severe Storm Laboratory.

Groenemeijer P. i Kühne T. (2014): A Climatology of Tornadoes in Europe: Results from the European Severe Weather Database. *Monthly Weather Review*, **142(12)**: 4775–4790. doi:10.1175/MWR-D-14-00107.1.

Groenemeijer P., Púčik T., Holzer A.M., Antonescu B., Riemann-Campe K., Schultz D.M., Kühne T., Feuerstein B., Brooks H.E., Doswell Charles A. I., Koppert H.J. i Sausen R. (2017): Severe Convective Storms in Europe: Ten Years of Research and Education at the European Severe Storms Laboratory. *Bulletin of the American Meteorological Society*, **98(12)**: 2641–2651. doi:10.1175/BAMS-D-16-0067.1.

Groenemeijer P., Púčik T., Tsonevsky I. i Bechtold P. (2019b): An overview of convective available potential energy and convective inhibition provided by NWP models for operational forecasting. *ECMWF Technical Memoranda*, **852**. doi:10.21957/q392hofrl.

Groenemeijer P. i van Delden A. (2007): Sounding-derived parameters associated with large hail and tornadoes in the Netherlands. *Atmospheric Research*, **83(2)**: 473–487. doi:10.1016/j.atmosres.2005.08.006. European Conference on Severe Storms 2004.

Grünwald S. i Brooks H. (2011): Relationship between sounding derived parameters and the strength of tornadoes in Europe and the USA from reanalysis data. *Atmospheric Research*, **100(4)**: 479–488. doi:10.1016/j.atmosres.2010.11.011. 5th European Conference on Severe Storms.

Gutierrez-Corea F.V., Manso-Callejo M.A. i Vázquez-Hoehne A. (2013): Assessment of the availability of near-real time open weather data provided by networks of surface stations in Spain. *Earth Science Informatics*, **6**: 145–163. doi:10.1007/s12145-013-0120-8.

Gutiérrez D., Riesco J. i Ponce S. (2015): SINOBAS, a tool for collaborative mapping applied to observation of "singular" weather phenomena. *15th EMS Annual Meeting & 12th European Conference on Applications of Meteorology (ECAM), Sofia, Bulgaria*. European Meteorological Society.

Hagemeyer B.C. (1997): Peninsular Florida Tornado Outbreaks. *Weather and Forecasting*, **12(3)**: 399–427. doi:10.1175/1520-0434(1997)012⟨0399:PFTO⟩2.0.CO;2.

Hall F. i Brewer R.D. (1959): A sequence of tornado damage patterns. *Monthly Weather Review*, **87**: 207–216.

Hanstrum B.N., Mills G.A., Watson A., Monteverdi J.P. i Doswell Charles A. I. (2002): The Cool-Season Tornadoes of California and Southern Australia. *Weather and Forecasting*, **17(4)**: 705–722. doi:10.1175/1520-0434(2002)017⟨0705:TCSTOC⟩2.0.CO;2.

Hersbach H., Bell B., Berrisford P., Hirahara S., Horányi A., Muñoz-Sabater J., Nicolas J., Peubey C., Radu R., Schepers D., Simmons A., Soci C., Abdalla S., Abellan X., Balsamo G., Bechtold P., Biavati G., Bidlot J., Bonavita M., De Chiara G., Dahlgren P., Dee D., Diamantakis M., Dragani R., Flemming J., Forbes R., Fuentes M., Geer A., Haimberger L., Healy S., Hogan R.J., Hólm E., Janisková M., Keeley S., Laloyaux P., Lopez P., Lupu C., Radnoti G., de Rosnay P., Rozum I., Vamborg F., Villaume S. i Thépaut J.N. (2020): The ERA5 global reanalysis. *Quarterly Journal of the Royal Meteorological Society*, **146(730)**: 1999–2049. doi:10.1002/qj.3803.

Hoinka K.P. i de Castro M. (2005): A Renaissance Depiction of a Tornado. *Bulletin of the American Meteorological Society*, **86(4)**: 543–552. doi:10.1175/BAMS-86-4-543.

Holland A.P., Riordan A.J. i Franklin E.C. (2006): A Simple Model for Simulating Tornado Damage in Forests. *Journal of Applied Meteorology and Climatology*, **45(12)**: 1597–1611. doi:10.1175/JAM2413.1.

Holzer A.M., Schreiner T.M.E. i Púčik T. (2018): A forensic re-analysis of one of the deadliest European tornadoes. *Natural Hazards and Earth System Sciences*, **18(6)**: 1555–1565. doi:10.5194/nhess-18-1555-2018.

Homar V., Gayà M. i Ramis C. (2001): A synoptic and mesoscale diagnosis of a tornado outbreak in the Balearic Islands. *Atmospheric Research*, **56(1)**: 31–55. doi:10.1016/S0169-8095(00)00087-9. Conference on European Tornadoes and Severe Storms.

Homar V., Gayà M., Romero R., Ramis C. i Alonso S. (2003): Tornadoes over complex terrain: an analysis of the 28th August 1999 tornadic event in eastern Spain. *Atmospheric Research*, **67-68**: 301–317. doi:10.1016/S0169-8095(03)00064-4. European Conference on Severe Storms 2002.

Homar V., Romero R., Ramis C. i Alonso S. (2002): Numerical study of the October 2000 torrential precipitation event over eastern Spain: analysis of the synoptic-scale stationarity. *Annales Geophysicae*, **20**: 2047–2066.

Honerkamp R., Yan G. i Snyder J.C. (2020): A review of the characteristics of tornadic wind fields through observations and simulations. *Journal of Wind Engineering and Industrial Aerodynamics*, **202**: 104195. doi:10.1016/j.jweia.2020.104195.

Hyvärinen O. i Saltikoff E. (2010): Social Media as a Source of Meteorological Observations. *Monthly Weather Review*, **138(8)**: 3175–3184. doi:10.1175/2010MWR3270.1.

ICGC (2019): Institut Cartogràfic i Geològic de Catalunya. `https://www.icgc.cat/`.

IDESCAT (2019): Institut d'Estadística de Catalunya. `https://www.idescat.cat`.

Ingrosso R., Lionello P., Miglietta M. i Salvadori G. (2020): A Statistical Investigation of Mesoscale Precursors of Significant Tornadoes: The Italian Case Study. *Atmosphere*, **11**: 301. doi:10.3390/atmos11030301.

IRDR (2014): *Peril Classification and Hazard Glossary*. Integrated Research on Disaster Risk, Beijing, China.

Irons J.R., Dwyer J.L. i Barsi J.A. (2012): The next Landsat satellite: The Landsat Data Continuity Mission. *Remote Sensing of Environment*, **122**: 11–21. doi:10.1016/j.rse.2011.08.026. Landsat Legacy Special Issue.

Jahn M. (2015): Economics of extreme weather events: Terminology and regional impact models. *Weather and Climate Extremes*, **10**: 29–39. doi:10.1016/j.wace.2015.08.005.

JMA (2015): *Guidelines for the Japanese Enhanced Fujita Scale*. Japan Meteorological Agency, Tokyo, Japan.

Johns R.H. i Doswell C.A. (1992): Severe Local Storms Forecasting. *Weather and Forecasting*, **7(4)**: 588–612. doi:10.1175/1520-0434(1992)007⟨0588:SLSF⟩2.0.CO;2.

Kahraman A., Kadioglu M. i Markowski P.M. (2017): Severe Convective Storm Environments in Turkey. *Monthly Weather Review*, **145(12)**: 4711–4725. doi:10.1175/MWR-D-16-0338.1.

Kahraman A. i Markowski P.M. (2014): Tornado Climatology of Turkey. *Monthly Weather Review*, **142(6)**: 2345–2352. doi:10.1175/MWR-D-13-00364.1.

Kaltenböck R., Diendorfer G. i Dotzek N. (2009): Evaluation of thunderstorm indices from ECMWF analyses, lightning data and severe storm reports. *Atmospheric Research*, **93(1)**: 381–396. doi:10.1016/j.atmosres.2008.11.005. 4th European Conference on Severe Storms.

Karstens C.D., Gallus W.A., Lee B.D. i Finley C.A. (2013): Analysis of Tornado-Induced Tree Fall Using Aerial Photography from the Joplin, Missouri, and Tuscaloosa–Birmingham, Alabama, Tornadoes of 2011. *Journal of Applied Meteorology and Climatology*, **52(5)**: 1049–1068. doi:10.1175/JAMC-D-12-0206.1.

Karstens C.D., Samaras T.M., Gallus W.A. i Lee B.D. (2010a): Analysis of near-surface wind flow in close proximity to tornadoes. *25th Conference on Severe Local Storms, Denver, Colorado, USA*. American Meteorological Society.

Karstens C.D., Samaras T.M., Lee B.D., Gallus W.A. i Finley C.A. (2010b): Near-Ground Pressure and Wind Measurements in Tornadoes. *Monthly Weather Review*, **138(7)**: 2570–2588. doi:10.1175/2010MWR3201.1.

KERAUNOS (2020): Les tornades en France. `http://www.keraunos.org/climatologie/les-tornades-en-france.html`.

Kerr B.W. i Darkow G.L. (1996): Storm-Relative Winds and Helicity in the Tornadic Thunderstorm Environment. *Weather and Forecasting*, **11(4)**: 489–505. doi:10.1175/1520-0434(1996)011⟨0489:SRWAHI⟩2.0.CO;2.

Keul A.G., Sioutas M.V. i Szilagyi W. (2009): Prognosis of Central-Eastern Mediterranean waterspouts. *Atmospheric Research*, **93(1)**: 426–436. doi:10.1016/j.atmosres.2008.10.028. 4th European Conference on Severe Storms.

Kühne T., Kollmohr A., Hubrig M., Sävert T., Schlenczek O., Simon W. i Wichmann H. (2017): Statistical analysis of the spatial and temporal distribution of tornadoes in Germany. *9th European Conference on Severe Storms (ECSS), Pula, Croatia*. European Severe Storm Laboratory.

Kirk P.J. (2014): An updated tornado climatology for the UK: 1981–2010. *Weather*, **69(7)**: 171–175. doi:10.1002/wea.2247.

Knox J.A., Rackley J.A., Black A.W., Gensini V.A., Butler M., Dunn C., Gallo T., Hunter M.R., Lindsey L., Phan M., Scroggs R. i Brustad S. (2013): Tornado Debris Characteristics And Trajectories During The 27 April 2011 Super Outbreak As Determined Using Social Media Data. *Bulletin of the American Meteorological Society*, **94(9)**: 1371–1380. doi:10.1175/BAMS-D-12-00036.1.

Koch P., Wernli H. i Davies H.C. (2006): An event-based jet-stream climatology and typology. *International Journal of Climatology*, **26(3)**: 283–301. doi:10.1002/joc.1255.

Kosiba K., Wurman J., Richardson Y., Markowski P., Robinson P. i Marquis J. (2013): Genesis of the Goshen County, Wyoming, Tornado on 5 June 2009 during VORTEX2. *Monthly Weather Review*, **141(4)**: 1157–1181. doi:10.1175/MWR-D-12-00056.1.

Kryvasheyeu Y., Chen H., Obradovich N., Moro E., Van Hentenryck P., Fowler J. i M. C. (2016): Rapid assessment of disaster damage using social media activity. *Science Advances*, **3(2)**: e1500779. doi:10.1126/sciadv.1500779.

Lee B.D., Finley C.A., Karstens C.D. i Samaras T.M. (2010): Surface observations of the rear-flank downdraft evolution associated with the Aurora, NE tornado of 17 June 2009. *25th conference on severe local storms, Denver, CO*. American Meteorological Society.

Leitão P. (2003): Tornadoes in Portugal. *Atmospheric Research*, **67-68**: 381–390. doi:10.1016/S0169-8095(03)00057-7. European Conference on Severe Storms 2002.

Leitão P. i Pinto P. (2020): Tornadoes in Portugal: An Overview. *Atmosphere*, **11(7)**: 679. doi:10.3390/atmos11070679.

Lemon L.R., Stan-Sion A., Soci C. i Cordoneanu E. (2003): A strong, long-track, Romanian tornado. *Atmospheric Research*, **67-68**: 391–416. doi:10.1016/S0169-8095(03)00063-2. European Conference on Severe Storms 2002.

León-Cruz J.F., Carbajal N. i Pineda-Martínez L.F. (2019): The role of complex terrain in the generation of tornadoes in the west of Mexico. *Natural Hazards*, **97**: 335–353. doi:10.1007/s11069-019-03647-8.

Letchford C. i Chay M. (2002): Pressure distributions on a cube in a simulated thunderstorm downburst. Part B: moving downburst observations. *Journal of Wind Engineering and Industrial Aerodynamics*, **90(7)**: 733–753. doi:10.1016/S0167-6105(02)00163-0.

Li L., Yang J., Lin C.Y., Chua C.T., Wang Y., Zhao K., Wu Y.T., Liu P.L.F., Switzer A.D., Mok K.M., Wang P. i Peng D. (2018): Field survey of Typhoon Hato (2017) and a comparison with storm surge modeling in Macau. *Natural Hazards and Earth System Sciences*, **18(12)**: 3167–3178. doi:10.5194/nhess-18-3167-2018.

Liberato M.L.R., Pinto J.G., Trigo I.F. i Trigo R.M. (2011): Klaus – an exceptional winter storm over northern Iberia and southern France. *Weather*, **66(12)**: 330–334. doi:10.1002/wea.755.

Lin W.E., Orf L.G., Savory E. i Novacco C. (2007): Proposed large-scale modelling of the transient features of a downburst outflow. *Wind and Structures*, **10(4)**: 315–346. doi:10.12989/was.2007.10.4.315.

Llasat M.C., Turco M., Quintana-Seguí P. i Llasat-Botija M. (2014): The snow storm of 8 March 2010 in Catalonia (Spain): a paradigmatic wet-snow event with a high societal impact. *Natural Hazards and Earth System Sciences*, **14(2)**: 427–441. doi:10.5194/nhess-14-427-2014.

Lorenz R.D. (2016): Heuristic estimation of dust devil vortex parameters and trajectories from single-station meteorological observations: Application to InSight at Mars. *Icarus*, **271**: 326–337. doi:10.1016/j.icarus.2016.02.001.

López J.M. (2007): A Mediterranean derecho: Catalonia (Spain), 17th August 2003. *Atmospheric Research*, **83(2)**: 272 – 283. doi:10.1016/j.atmosres.2005.08.008. European Conference on Severe Storms 2004.

Lucía A., Comiti F., Borga M., Cavalli M. i Marchi L. (2015): Dynamics of large wood during a flash flood in two mountain catchments. *Natural Hazards and Earth System Sciences*, **15(8)**: 1741–1755. doi:10.5194/nhess-15-1741-2015.

Maddox R.A. (1976): An Evaluation of Tornado Proximity Wind and Stability Data. *Monthly Weather Review*, **104(2)**: 133–142. doi:10.1175/1520-0493(1976)104⟨0133:AEOTPW⟩2.0.CO;2.

Mahieu P. i Wesolek E. (2016): *Tornado Rating in Europe with the EF-scale*. KERAUNOS, Wattignies, France.

Markowski P.M. i Richardson Y.P. (2009): Tornadogenesis: Our current understanding, forecasting considerations, and questions to guide future research. *Atmospheric Research*, **93(1)**: 3–10. doi:10.1016/j.atmosres.2008.09.015. 4th European Conference on Severe Storms.

Markowski P.M. i Richardson Y.P. (2010): *Mesoscale Meteorology in Midlatitudes*. Wiley-Blackwell, Chichester, UK.

Markowski P.M. i Straka J.M. (2000): Some Observations of Rotating Updrafts in a Low-Buoyancy, Highly Sheared Environment. *Monthly Weather Review*, **128(2)**: 449–461. doi:10.1175/1520-0493(2000)128⟨0449:SOORUI⟩2.0.CO;2.

Marshall T.P. (2002): Tornado Damage Survey at Moore, Oklahoma. *Weather and Forecasting*, **17(3)**: 582–598. doi:10.1175/1520-0434(2002)017⟨0582:TDSAMO⟩2.0.CO;2.

Marshall T.P., Davis W. i Runnels S. (2012): Damage survey of the Joplin tornado. *26th Conference on Severe Local Storm, Nashville, Tennessee, USA*. American Meteorological Society.

Martins J., Rocha A., Viceto C., Pereira S.C. i Santos J.A. (2020): Future Projections for Wind, Wind Shear and Helicity in the Iberian Peninsula. *Atmosphere*, **11(9)**: 1001. doi:10.3390/atmos11091001. Climate Events and Extreme Weather.

Martín Y., Cívica M. i Pham E. (2020): Constructing a Supercell Database in Spain Using Publicly Available Two-Dimensional Radar Images and Citizen Science. *Annals of the American Association of Geographers*, **0(0)**: 1–21. doi:10.1080/24694452.2020.1812371.

Martínez-Gomariz E., Forero-Ortiz E., Guerrero-Hidalga M., Castán S. i Gómez M. (2020): Flood Depth–Damage Curves for Spanish Urban Areas. *Sustainability*, **12(7)**: 2666. doi:10.3390/su12072666.

Martínez-Gomariz E., Guerrero-Hidalga M., Russo B., Yubero D., Gómez M. i Castán S. (2019): Desarrollo y aplicación de curvas de daño y estanqueidad para la estimación del impacto económico de las inundaciones en zonas urbanas españolas. *Ingeniería del agua*, **23(4)**: 229–245. doi:10.4995/ia.2019.12137.

Mateo J., Ballart D., Brucet C., Aran M. i Bech J. (2009): A study of a heavy rainfall event and a tornado outbreak during the passage of a squall line over Catalonia. *Atmospheric Research*, **93(1)**: 131–146. doi:10.1016/j.atmosres.2008.09.030. 4th European Conference on Severe Storms.

Matsangouras I., Nastos P. i Pytharoulis I. (2016): Study of the tornado event in Greece on March 25, 2009: Synoptic analysis and numerical modeling using modified topography. *Atmospheric Research*, **169**: 566 – 583. doi:10.1016/j.atmosres.2015.08.010.

Matsangouras I.T., Nastos P.T., Bluestein H.B., Pytharoulis I., Papachristopoulou K. i Miglietta M.M. (2017): Analysis of waterspout environmental conditions and of parent-storm behaviour based on satellite data over the southern Aegean Sea of Greece. *International Journal of Climatology*, **37(2)**: 1022–1039. doi:10.1002/joc.4757.

Matsangouras I.T., Nastos P.T., Bluestein H.B. i Sioutas M.V. (2014a): A climatology of tornadic activity over Greece based on historical records. *International Journal of Climatology*, **34(8)**: 2538–2555. doi:10.1002/joc.3857.

Matsangouras I.T., Pytharoulis I. i Nastos P.T. (2014b): Numerical modeling and analysis of the effect of complex Greek topography on tornadogenesis. *Natural Hazards and Earth System Sciences*, **14(7)**: 1905–1919. doi:10.5194/nhess-14-1905-2014.

McDonald J.R. i Marshall T.P. (1984): *Tornado Damage Documentation*. Institute for Disaster Research (Texas Tech University), Lubbock, Texas, USA.

Meaden G.T. (1976): Tornadoes in Britain: Their intensities and distribu-tion in space and time. *Journal of Meteorology*, **1(8)**: 242–251.

Meaden G.T., Kochev S., Kolendowicz L., Kosa-Kiss A., Marcinoniene I., Sioutas M., Tooming H. i Tyrrell J. (2007): Comparing the theoretical versions of the Beaufort scale, the T-Scale and the Fujita scale. *Atmospheric Research*, **83(2)**: 446–449. doi:10.1016/j.atmosres.2005.11.014. European Conference on Severe Storms 2004.

Meng Z. i Yao D. (2014): Damage Survey, Radar, and Environment Analyses on the First-Ever Documented Tornado in Beijing during the Heavy Rainfall Event of 21 July 2012. *Weather and Forecasting*, **29(3)**: 702–724. doi:10.1175/WAF-D-13-00052.1.

Miglietta M. (2019): Waterspouts: A Review. *Reference Module in Earth Systems and Environmental Sciences*. Elsevier. doi:10.1016/B978-0-12-409548-9.12414-5.

Miglietta M.M., Arai K., Kusunoki K., Inoue H., Adachi T. i Niino H. (2020): Observational analysis of two waterspouts in northwestern Italy using an OPERA Doppler radar. *Atmospheric Research*, **234**: 104692. doi:10.1016/j.atmosres.2019.104692.

Miglietta M.M. i Matsangouras I.T. (2018): An updated "climatology" of tornadoes and waterspouts in Italy. *International Journal of Climatology*, **38(9)**: 3667–3683. doi:10.1002/joc.5526.

Miglietta M.M., Mazon J. i Rotunno R. (2017): Numerical Simulations of a Tornadic Supercell over the Mediterranean. *Weather and Forecasting*, **32(3)**: 1209–1226. doi:10.1175/WAF-D-16-0223.1.

Miglietta M.M. i Rotunno R. (2016): An EF3 multi-vortex tornado over the Ionian region: is it time for a dedicated warning system over Italy? *Bulletin of the American Meteorological Society*, **97(3)**: 337–344. doi:10.1175/BAMS-D-14-00227.1.

Miller P.W. i Mote T.L. (2018): Characterizing severe weather potential in synoptically weakly forced thunderstorm environments. *Natural Hazards and Earth System Sciences*, **18(4)**: 1261–1277. doi:10.5194/nhess-18-1261-2018.

Molinari D., Menoni S., Aronica G.T., Ballio F., Berni N., Pandolfo C., Stelluti M. i Minucci G. (2014): Ex post damage assessment: an Italian experience. *Natural Hazards and Earth System Sciences*, **14(4)**: 901–916. doi:10.5194/nhess-14-901-2014.

Molthan A., Jedlovec G. i Carcione B. (2011): NASA satellite data assist in tornado damage assessments. *Eos, Transactions American Geophysical Union*, **92(40)**: 337–339. doi:10.1029/2011EO400002.

Molthan A.L., Bell J.R., Cole T.A. i Burks J.E. (2014): Satellite-based identification of tornado damage tracks from the 27 April 2011 severe weather outbreak. *Journal of Operational Meteorology*, **2(16)**: 191–208. doi:10.15191/nwajom.

Molthan A.L., Schultz L.A., McGrath K.M., Burks J.E., Camp J.P., Angle K., Bell J.R. i Jedlovec G.J. (2020): Incorporation and Use of Earth Remote Sensing Imagery within the NOAA/NWS Damage Assessment Toolkit. *Bulletin of the American Meteorological Society*, **101(3)**: E323–E340. doi:10.1175/BAMS-D-19-0097.1.

Moncrieff M.W. i Miller M.J. (1976): The dynamics and simulation of tropical cumulonimbus and squall lines. *Quarterly Journal of the Royal Meteorological Society*, **102(432)**: 373–394. doi:10.1002/qj.49710243208.

Monteverdi J.P., Doswell C.A. i Lipari G.S. (2003): Shear Parameter Thresholds for Forecasting Tornadic Thunderstorms in Northern and Central California. *Weather and Forecasting*, **18(2)**: 357–370. doi:10.1175/1520-0434(2003)018⟨0357:SPTFFT⟩2.0.CO;2.

Morales M.E., Arús J., Llasat M.C., Gayà M. i Castán S. (2009): A database about the tornadic activity in Catalonia (NE Spain) since 1994. *11th Plinius Conference on Mediterranean Storms, Barcelona*. European Geoscience Union.

Mulder K.J. i Schultz D.M. (2015): Climatology, Storm Morphologies, and Environments of Tornadoes in the British Isles: 1980–2012. *Monthly Weather Review*, **143(6)**: 2224–2240. doi:10.1175/MWR-D-14-00299.1.

Mulholland J.P., Nesbitt S.W. i Trapp R.J. (2019): A Case Study of Terrain Influences on Upscale Convective Growth of a Supercell. *Monthly Weather Review*, **147(12)**: 4305–4324. doi:10.1175/MWR-D-19-0099.1.

NCDC (2020): U.S. Tornado Climatology. `https://www.ncdc.noaa.gov/climate-information/extreme-events/us-tornado-climatology`.

NOAA/SPC (2019): U.S. tornadoes (1950–2018). `https://www.spc.noaa.gov/wcm`.

Novlan D.J. i Gray W.M. (1974): Hurricane-Spawned Tornadoes. *Monthly Weather Review*, **102(7)**: 476–488. doi:10.1175/1520-0493(1974)102⟨0476:HST⟩2.0.CO;2.

NSSL/NOAA (2020): VORTEX Southeast. `https://www.nssl.noaa.gov/projects/vortexse`.

NWS (2020): Weather related fatality and injury statistics. `https://www.weather.gov/hazstat/`.

Orf L., Kantor E. i Savory E. (2012): Simulation of a downburst-producing thunderstorm using a very high-resolution three-dimensional cloud model. *Journal of Wind Engineering and Industrial Aerodynamics*, **104-106**: 547–557. doi:10.1016/j.jweia.2012.02.020. 13th International Conference on Wind Engineering.

Orlanski I. (1975): A Rational Subdivision of Scales for Atmospheric Processes. *Bulletin of the American Meteorological Society*, **56(5)**: 527–530.

Pastor F., Valiente J.A. i Palau J.L. (2018): Sea Surface Temperature in the Mediterranean: Trends and Spatial Patterns (1982–2016). *Pure and Applied Geophysics*, **175(11)**: 4017–4029. doi:10.1007/978-3-030-11958-4_18.

Paulikas M.J., Schmidlin T.W. i Marshall T.P. (2016): The Stability of Passenger Vehicles at Tornado Wind Intensities of the (Enhanced) Fujita Scale. *Weather, Climate, and Society*, **8(1)**: 85–91. doi:10.1175/WCAS-D-15-0051.1.

Pautz M.E. (1969): *Severe local storms occurrences, 1955–1967*. Weather Bureau, Washington, DC, USA.

Peña J.C., Aran M., Cunillera J. i Amaro J. (2011): Atmospheric circulation patterns associated with strong wind events in Catalonia. *Natural Hazards and Earth System Sciences*, **11(1)**: 145–155. doi:10.5194/nhess-11-145-2011.

Peterson C.J. (2019): Damage Diversity as a Metric of Structural Complexity after Forest Wind Disturbance. *Forests*, **10(2)**: 85. doi:10.3390/f10020085.

Peterson R.E. (1992): Johannes Letzmann: A Pioneer in the Study of Tornadoes. *Weather and Forecasting*, **7(1)**: 166–184. doi:10.1175/1520-0434(1992)007⟨0166:JLAPIT⟩2.0.CO;2.

Pineda N., Bech J., Rigo T. i Montanyà J. (2011): A Mediterranean nocturnal heavy rainfall and tornadic event. Part II: Total lightning analysis. *Atmospheric Research*, **100(4)**: 638–648. doi:10.1016/j.atmosres.2010.10.027. 5th European Conference on Severe Storms.

Pineda N. i Montanyà J. (2009): *Lightning Detection in Spain: The Particular Case of Catalonia*, 161–185. Springer Netherlands, Dordrecht. doi:10.1007/978-1-4020-9079-0_7.

Pineda N., Rigo T., Bech J. i Soler X. (2007): Lightning and precipitation relationship in summer thunderstorms: Case studies in the North Western Mediterranean region. *Atmospheric Research*, **85(2)**: 159–170. doi:10.1016/j.atmosres.2006.12.004.

Pineda N. i Soler X. (2015): The influence of the Mediterranean sea on the annual lightning distribution in Catalonia. *5th International Conference on Meteorology and Climatology of the Mediterranean, Istanbul, Turkey*. Catalan Association of Meteorology (ACAM), Network of Meteorology of the Mediterranean, Istanbul Technical University.

Pipinato A. (2018): Recent northeast Italian tornado events: lesson learned for improving structures. *Natural Hazards*. doi:10.1007/s11069-018-3380-2.

Pla J. (1966): *El quadern gris*. Destino, Barcelona, Catalunya.

Potvin C.K., Broyles C., Skinner P.S., Brooks H.E. i Rasmussen E. (2019): A Bayesian Hierarchical Modeling Framework for Correcting Reporting Bias in the U.S. Tornado Database. *Weather and Forecasting*, **34(1)**: 15–30. doi:10.1175/WAF-D-18-0137.1.

Potvin C.K., Elmore K.L. i Weiss S.J. (2010): Assessing the Impacts of Proximity Sounding Criteria on the Climatology of Significant Tornado Environments. *Weather and Forecasting*, **25(3)**: 921–930. doi:10.1175/2010WAF2222368.1.

Púčik T., Groenemeijer P., Rädler A.T., Tijssen L., Nikulin G., Prein A.F., van Meijgaard E., Fealy R., Jacob D. i Teichmann C. (2017): Future Changes in European Severe Convection Environments in a Regional Climate Model Ensemble. *Journal of Climate*, **30(17)**: 6771–6794. doi:10.1175/JCLI-D-16-0777.1.

Púčik T., Groenemeijer P., Rýva D. i Kolář M. (2015): Proximity Soundings of Severe and Nonsevere Thunderstorms in Central Europe. *Monthly Weather Review*, **143(12)**: 4805–4821. doi:10.1175/MWR-D-15-0104.1.

Quirantes J.A., Riesco J. i Núñez J.A. (2014): Características básicas de las supercélulas en España. *AEMET-Publicaciones en línea*.

Ramis C., Arús J., López J.M. i Mestres A.M. (1997): Two cases of severe weather in Catalonia (Spain): an observational study. *Meteorological Applications*, **4(3)**: 207–217. doi:10.1017/S1350482797000510.

Ramis C., López J.M. i Arús J. (1999): Two cases of severe weather in Catalonia (Spain). A diagnostic study. *Meteorological Applications*, **6(1)**: 11–27. doi:10.1017/S1350482799000869.

Ramis C., Romero R. i Homar V. (2009): The severe thunderstorm of 4 October 2007 in Mallorca: an observational study. *Natural Hazards and Earth System Sciences*, **9(4)**: 1237–1245. doi:10.5194/nhess-9-1237-2009.

Rasmussen E.N. (2003): Refined Supercell and Tornado Forecast Parameters. *Weather and Forecasting*, **18(3)**: 530–535. doi:10.1175/1520-0434(2003)18⟨530:RSATFP⟩2.0.CO;2.

Rasmussen E.N. i Blanchard D.O. (1998): A Baseline Climatology of Sounding-Derived Supercell and Tornado Forecast Parameters. *Weather and Forecasting*, **13(4)**: 1148–1164. doi:10.1175/1520-0434(1998)013⟨1148:ABCOSD⟩2.0.CO;2.

Rasmussen E.N., Davies-Jones R. i Holle R.L. (2003): Terrestrial Photogrammetry of Weather Images Acquired in Uncontrolled Circumstances. *Journal of Atmospheric and Oceanic Technology*, **20(12)**: 1790–1803. doi:10.1175/1520-0426(2003)020⟨1790:TPOWIA⟩2.0.CO;2.

Rasmussen E.N., Straka J.M., Davies-Jones R., Doswell Charles A. I., Carr F.H., Eilts M.D. i MacGorman D.R. (1994): Verification of the Origins of Rotation in Tornadoes Experiment: VORTEX. *Bulletin of the American Meteorological Society*, **75(6)**: 995–1006. doi:10.1175/1520-0477(1994)075⟨0995:VOTOOR⟩2.0.CO;2.

Rauhala J., Brooks H.E. i Schultz D.M. (2012): Tornado Climatology of Finland. *Monthly Weather Review*, **140(5)**: 1446–1456. doi:10.1175/MWR-D-11-00196.1.

Rauhala J. i Schultz D.M. (2009): Severe thunderstorm and tornado warnings in Europe. *Atmospheric Research*, **93(1)**: 369–380. doi:10.1016/j.atmosres.2008.09.026. 4th European Conference on Severe Storms.

Renko T., Ivušić S., Telišman Prtenjak M., Šoljan V. i Horvat I. (2018): Waterspout Forecasting Method Over the Eastern Adriatic Using a High-Resolution Numerical Weather Model. *Pure and Applied Geophysics*, **175**: 3759–3778. doi:10.1007/s00024-018-1833-x.

Renko T., Kuzmić J., Šoljan V. i Mahović N.S. (2016): Waterspouts in the eastern Adriatic from 2001 to 2013. *Natural Hazards*, **82**: 441–470. doi:10.1007/s11069-016-2192-5.

Reynolds R.W. i Smith T.M. (1995): A High-Resolution Global Sea Surface Temperature Climatology. *Journal of Climate*, **8(6)**: 1571–1583. doi:10.1175/1520-0442(1995)008⟨1571:AHRGSS⟩2.0.CO;2.

Rhee D.M. i Lombardo F.T. (2018): Improved near-surface wind speed characterization using damage patterns. *Journal of Wind Engineering and Industrial Aerodynamics*, **180**: 288–297. doi:10.1016/j.jweia.2018.07.017.

Riemann-Campe K., Fraedrich K. i Lunkeit F. (2009): Global climatology of Convective Available Potential Energy (CAPE) and Convective Inhibition (CIN) in ERA-40 reanalysis. *Atmospheric Research*, **93(1)**: 534–545. doi:10.1016/j.atmosres.2008.09.037. 4th European Conference on Severe Storms.

Riesco J., Polvorinos F., Núñez J.A., Soriano J.D. i Jiménez C. (2015): Climatología de tornados en España Peninsular y Baleares. http://www.aemet.es/documentos/es/conocermas/publicaciones/Climatologia_tornados/Climatologia_tornados.pdf.

Rigo T. i Farnell C. (2019): Using maximum Vertical Integrated Liquid (VIL) maps for identifying hail-affected areas: an operative application for agricultural purposes. *Tethys*, **16**: 15–24. doi:10.3369/tethys.2019.16.02.

Rigo T. i Llasat M.C. (2007): Analysis of mesoscale convective systems in Catalonia using meteorological radar for the period 1996–2000. *Atmospheric Research*, **83(2)**: 458–472. doi:10.1016/j.atmosres.2005.10.016. European Conference on Severe Storms 2004.

Ripoll R., del Amo X. i Vendrell R. (2016): The weather observers network of the Meteorological Service of Catalonia. *WMO Technical Conference on Meteorological and Environmental Instruments and Methods of Observation (CIMO TECO 2016), Madrid, Spain*. World Meteorological Organization.

Rodríguez O. i Bech J. (2018): Sounding-derived parameters associated with tornadic storms in Catalonia. *International Journal of Climatology*, **38(5)**: 2400–2414. doi:10.1002/joc.5343.

Rodríguez O. i Bech J. (2020a): Reanalysing strong-convective wind damage paths using high-resolution aerial images. *Natural Hazards*, **104(1)**: 1021–1038. doi:10.1007/s11069-020-04202-6.

Rodríguez O. i Bech J. (2020b): Tornadic environments in the Iberian Peninsula and the Balearic Islands based on ERA5 reanalysis. *International Journal of Climatology*, 1–21. doi:10.1002/joc.6825.

Rodríguez O., Bech J., Castán S. i Arús J. (2018): El tornado del 7 de gener de 2018: de l'Alt Empordà al Rosselló. Treball de camp i anàlisi de les destrosses (The 7 January 2018 tornado: from Alt Empordà to Rosselló. Fieldwork and damage analysis). *XXIV Jornades de Meteorologia Eduard Fontserè*. Associació Catalana de Meteorologia.

Rodríguez O., Bech J., Soriano J.D., Gutiérrez D. i Castán S. (2020): A methodology to conduct wind damage field surveys for high-impact weather events of convective origin. *Natural Hazards and Earth System Sciences*, **20(5)**: 1513–1531. doi:10.5194/nhess-20-1513-2020.

Romanic D., Refan M., Wu C.H. i Michel G. (2016): Oklahoma tornado risk and variability: A statistical model. *International Journal of Disaster Risk Reduction*, **16**: 19 – 32. doi:10.1016/j.ijdrr.2016.01.011.

Romero R., Doswell C. A. I. i Ramis C. (2000): Mesoscale Numerical Study of Two Cases of Long-Lived Quasi-Stationary Convective Systems over Eastern Spain. *Monthly Weather Review*, **128(11)**: 3731–3751. doi:10.1175/1520-0493(2001)129⟨3731:MNSOTC⟩2.0.CO;2.

Romero R., Gayà M. i Doswell C.A. (2007): European climatology of severe convective storm environmental parameters: A test for significant tornado events. *Atmospheric Research*, **83(2)**: 389–404. doi:10.1016/j.atmosres.2005.06.011. European Conference on Severe Storms 2004.

Rosencrants T.D. i Ashley W.S. (2015): Spatiotemporal analysis of tornado exposure in five US metropolitan areas. *Natural Hazards*, **78**: 121–140. doi:10.1007/s11069-015-1704-z.

Roueche D.B. i Prevatt D.O. (2013): Residential Damage Patterns Following the 2011 Tuscaloosa, AL and Joplin, MO Tornadoes. *Journal of Disaster Research*, **8(6)**: 1061–1067. doi:10.1007/s11069-015-1704-z.

Ruyra J. (1920): *Pinya de Rosa*. Edicions 62, Barcelona, Catalunya.

Saltikoff E., Tuovinen J.P., Kotro J., Kuitunen T. i Hohti H. (2010): A Climatological Comparison of Radar and Ground Observations of Hail in Finland. *Journal of Applied Meteorology and Climatology*, **49(1)**: 101–114. doi:10.1175/2009JAMC2116.1.

Sánchez-Laulhé J.M. (2009): El tornado de Málaga del 1 de Febrero de 2009. *Tiempo y Clima*, **24**: 34–36.

Sánchez-Laulhé J.M., Pérez-Rubín J. i Arús J. (2017): Las trombas marinas de Sant Feliu de Guíxols (2/IX/1965) y Málaga (8/III/1971): entre las más mediáticas del siglo XX (Parte I). *Tiempo y Clima*, **56**: 28–32.

Schuster S.S., Blong R.J. i Speer M.S. (2005): A hail climatology of the greater Sydney area and New South Wales, Australia. *International Journal of Climatology*, **25(12)**: 1633–1650. doi:10.1002/joc.1199.

Seeley J.T. i Romps D.M. (2015): The Effect of Global Warming on Severe Thunderstorms in the United States. *Journal of Climate*, **28(6)**: 2443–2458. doi:10.1175/JCLI-D-14-00382.1.

Seneviratne S.I., Nicholls N., Easterling D., Goodess C.M., Kanae S., James Kossin Y.L., Marengo J., McInnes K., Rahimi M., Reichstein M., Sorteberg A., Vera C. i Zhang X. (2012): *Managing the Risks of Extreme Events and Disasters to Advance Climate Change Adaptation*, Cap. Changes in Climate Extremes and their Impacts on the Natural Physical Environment, 109–230. Cambridge University Press, Cambridge, UK, and New York, NY, US.

Sherburn K.D. i Parker M.D. (2014): Climatology and Ingredients of Significant Severe Convection in High-Shear, Low-CAPE Environments. *Weather and Forecasting*, **29(4)**: 854–877. doi:10.1175/WAF-D-13-00041.1.

Shikhov A. i Chernokulsky A. (2018): A satellite-derived climatology of unreported tornadoes in forested regions of northeast Europe. *Remote Sensing of Environment*, **204**: 553–567. doi:10.1016/j.rse.2017.10.002.

Shikhov A.N., Perminova E.S. i Perminov S.I. (2019): Satellite-based analysis of the spatial patterns of fire-and storm-related forest disturbances in the Ural region, Russia. *Natural Hazards*, 1–26. doi:10.1007/s11069-019-03642-z.

Sioutas i Doe (2019): Significant tornado and strong waterspout climatology of Greece. *10th European Conference on Severe Storms (ECSS), Krakow, Poland*. European Severe Storm Laboratory.

Sioutas M., Szilagyi W. i Keul A. (2013): Waterspout outbreaks over areas of Europe and North America: Environment and predictability. *Atmospheric Research*, **123**: 167–179. doi: 10.1016/j.atmosres.2012.09.013. 6th European Conference on Severe Storms 2011. Palma de Mallorca, Spain.

Sioutas M.V. (2011): A tornado and waterspout climatology for Greece. *Atmospheric Research*, **100(4)**: 344 – 356. doi:10.1016/j.atmosres.2010.08.011. 5th European Conference on Severe Storms.

Sioutas M.V. i Keul A.G. (2007): Waterspouts of the Adriatic, Ionian and Aegean Sea and their meteorological environment. *Atmospheric Research*, **83(2)**: 542–557. doi:10.1016/j.atmosres.2005.08.009. European Conference on Severe Storms 2004.

SMC (2018a): Informe sobre el tornado de Cardona (el Bages) i Navès (el Solsonès). Servei Meteorològic de Catalunya. `https://static-m.meteo.cat/content/files/Informe_Tornado_Cardona_Naves.pdf`.

SMC (2018b): Informe sobre el tornado de Navata, Cistella, Terrades i Darnius (l'Alt Empordà). Servei Meteorològic de Catalunya. `https://static-m.meteo.cat/content/files/Informe_Tornado_Emporda.pdf`.

Smith B.T., Thompson R.L., Grams J.S., Broyles C. i Brooks H.E. (2012): Convective Modes for Significant Severe Thunderstorms in the Contiguous United States. Part I: Storm Classification and Climatology. *Weather and Forecasting*, **27(5)**: 1114–1135. doi:10.1175/WAF-D-11-00115.1.

SPC (2020): Prototype interactive local storm reports display. `https://www.spc.noaa.gov/climo/reports/today.html`.

Stensrud D.J., Cortinas J.V. i Brooks H.E. (1997): Discriminating between Tornadic and Non-tornadic Thunderstorms Using Mesoscale Model Output. *Weather and Forecasting*, **12(3)**: 613–632. doi:10.1175/1520-0434(1997)012⟨0613:DBTANT⟩2.0.CO;2.

Stensrud D.J., Xue M., Wicker L.J., Kelleher K.E., Foster M.P., Schaefer J.T., Schneider R.S., Benjamin S.G., Weygandt S.S., Ferree J.T. i Tuell J.P. (2009): Convective-Scale Warn-on-Forecast System: A Vision for 2020. *Bulletin of the American Meteorological Society*, **90(10)**: 1487–1500. doi:10.1175/2009BAMS2795.1.

Strader S.M., Ashley W., Irizarry A. i Hall S. (2015): A climatology of tornado intensity assessments. *Meteorological Applications*, **22(3)**: 513–524. doi:10.1002/met.1482.

Szilagyi W. (2009): A waterspout forecasting technique. *5h European Conference on Severe Storms, Landshut, Germany*. European Severe Weather Laboratory.

Tanamachi R.L., Bluestein H.B., Lee W.C., Bell M. i Pazmany A. (2007): Ground-Based Velocity Track Display (GBVTD) Analysis of W-Band Doppler Radar Data in a Tornado near Stockton, Kansas, on 15 May 1999. *Monthly Weather Review*, **135(3)**: 783–800. doi:10.1175/MWR3325.1.

Taszarek M., Allen J., Púčik T., Groenemeijer P., Czernecki B., Kolendowicz L., Lagouvardos K., Kotroni V. i Schulz W. (2019): A Climatology of Thunderstorms across Europe from a Synthesis of Multiple Data Sources. *Journal of Climate*, **32(6)**: 1813–1837. doi:10.1175/JCLI-D-18-0372.1.

Taszarek M., Allen J.T., Brooks H.E., Pilguj N. i Czernecki B. (2020a): Differing trends in United States and European severe thunderstorm environments in a warming climate. *Bulletin of the American Meteorological Society*, 1–51. doi:10.1175/BAMS-D-20-0004.1.

Taszarek M., Allen J.T., Púčik T., Hoogewind K.A. i Brooks H.E. (2020b): Severe convective storms across Europe and the United States. Part 2: ERA5 environments associated with lightning, large hail, severe wind and tornadoes. *Journal of Climate*, 1–53. doi:10.1175/JCLI-D-20-0346.1.

Taszarek M. i Brooks H.E. (2015): Tornado Climatology of Poland. *Monthly Weather Review*, **143(3)**: 702–717. doi:10.1175/MWR-D-14-00185.1.

Taszarek M., Brooks H.E. i Czernecki B. (2017): Sounding-Derived Parameters Associated with Convective Hazards in Europe. *Monthly Weather Review*, **145(4)**: 1511–1528. doi: 10.1175/MWR-D-16-0384.1.

Taszarek M., Brooks H.E., Czernecki B., Szuster P. i Fortuniak K. (2018): Climatological Aspects of Convective Parameters over Europe: A Comparison of ERA-Interim and Sounding Data. *Journal of Climate*, **31(11)**: 4281–4308. doi:10.1175/JCLI-D-17-0596.1.

Taszarek M. i Kolendowicz L. (2013): Sounding-derived parameters associated with tornado occurrence in Poland and Universal Tornadic Index. *Atmospheric Research*, **134**: 186–197. doi:10.1016/j.atmosres.2013.07.016.

Thompson R.L., Edwards R., Hart J.A., Elmore K.L. i Markowski P. (2003): Close Proximity Soundings within Supercell Environments Obtained from the Rapid Update Cycle. *Weather and Forecasting*, **18(6)**: 1243–1261. doi:10.1175/1520-0434(2003)018⟨1243: CPSWSE⟩2.0.CO;2.

Thompson R.L., Smith B.T., Dean A.R. i Marsh P.T. (2013): Spatial Distributions of Tornadic Near-Storm Environments by Convective Mode. *Electronic Journal of Severe Storms Meteorology*, **8(5)**: 1–22.

Thompson R.L., Smith B.T., Grams J.S., Dean A.R. i Broyles C. (2012): Convective Modes for Significant Severe Thunderstorms in the Contiguous United States. Part II: Supercell and QLCS Tornado Environments. *Weather and Forecasting*, **27(5)**: 1136–1154. doi:10.1175/ WAF-D-11-00116.1.

Toth M., Trapp R.J., Wurman J. i Kosiba K.A. (2013): Comparison of Mobile-Radar Measurements of Tornado Intensity with Corresponding WSR-88D Measurements. *Weather and Forecasting*, **28(2)**: 418–426. doi:10.1175/WAF-D-12-00019.1.

Trapero L., Bech J. i Lorente J. (2013): Numerical modelling of heavy precipitation events over Eastern Pyrenees: Analysis of orographic effects. *Atmospheric Research*, **123**: 368–383. doi:10.1016/j.atmosres.2012.09.014. 6th European Conference on Severe Storms 2011. Palma de Mallorca, Spain.

Trapero L., Bech J., Rigo T., Pineda N. i Forcadell D. (2009): Uncertainty of precipitation estimates in convective events by the Meteorological Service of Catalonia radar network. *Atmospheric Research*, **93(1)**: 408–418. doi:10.1016/j.atmosres.2009.01.021. 4th European Conference on Severe Storms.

Tucker C.J. (1978): Red and photographic infrared linear combinations for monitoring vegetation. *Remote Sensing of Environment*, **8**: 127–150.

Verbout S.M., Brooks H.E., Leslie L.M. i Schultz D.M. (2006): Evolution of the U.S. Tornado Database: 1954–2003. *Weather and Forecasting*, **21(1)**: 86–93. doi:10.1175/WAF910.1.

Verdaguer J. (1887): *Excursions i viatges*. Editorial Barcino, Barcelona, Catalunya.

Viceto C., Marta-Almeida M. i Rocha A. (2017): Future climate change of stability indices for the Iberian Peninsula. *International Journal of Climatology*, **37(12)**: 4390–4408. doi: 10.1002/joc.5094.

Wade A.R., Coniglio M.C. i Ziegler C.L. (2018): Comparison of Near- and Far-Field Supercell Inflow Environments Using Radiosonde Observations. *Monthly Weather Review*, **146(8)**: 2403–2415. doi:10.1175/MWR-D-17-0276.1.

Wagner M., Doe R.K., Johnson A., Chen Z., Das J. i Cerveny R.S. (2019): Unpiloted Aerial Systems (UASs) Application for Tornado Damage Surveys: Benefits and Procedures. *Bulletin of the American Meteorological Society*, **100(12)**: 2405–2409. doi:10.1175/BAMS-D-19-0124.1.

Wakimoto R.M., Atkins N.T., Butler K.M., Bluestein H.B., Thiem K., Snyder J. i Houser J. (2015): Photogrammetric Analysis of the 2013 El Reno Tornado Combined with Mobile X-Band Polarimetric Radar Data. *Monthly Weather Review*, **143(7)**: 2657–2683. doi:10.1175/MWR-D-15-0034.1.

Wakimoto R.M. i Lew J.K. (1993): Observations of a Florida Waterspout during CaPE. *Weather and Forecasting*, **8(4)**: 412–423. doi:10.1175/1520-0434(1993)008⟨0412:OOAFWD⟩2.0.CO;2.

Wakimoto R.M. i Liu C. (1998): The Garden City, Kansas, Storm during VORTEX 95. Part II: The Wall Cloud and Tornado. *Monthly Weather Review*, **126(2)**: 393–408. doi:10.1175/1520-0493(1998)126⟨0393:TGCKSD⟩2.0.CO;2.

Wakimoto R.M., Wienhoff Z., Bluestein H.B., Bodine D.J. i Kurdzo J.M. (2020): Mobile Radar Observations of the Evolving Debris Field Compared with a Damage Survey of the Shawnee, Oklahoma, Tornado of 19 May 2013. *Monthly Weather Review*, **148(5)**: 1779–1803. doi:10.1175/MWR-D-19-0215.1.

Wakimoto R.M., Wienhoff Z., Bluestein H.B. i Reif D. (2018): The Dodge City Tornadoes on 24 May 2016: Damage Survey, Photogrammetric Analysis Combined with Mobile Polarimetric Radar Data. *Monthly Weather Review*, **146(11)**: 3735–3771. doi:10.1175/MWR-D-18-0125.1.

Wakimoto R.M. i Wilson J.W. (1989): Non-supercell Tornadoes. *Monthly Weather Review*, **117(6)**: 1113–1140. doi:10.1175/1520-0493(1989)117⟨1113:NST⟩2.0.CO;2.

Wang W., Qu J.J., Hao X., Liu Y. i Stanturf J.A. (2010): Post-hurricane forest damage assessment using satellite remote sensing. *Agricultural and Forest Meteorology*, **150(1)**: 122–132. doi:10.1016/j.agrformet.2009.09.009.

Wegener A. (1917): *Wind-und Wasserhosen in Europa (tornadoes and waterspouts in Europe)*. Friedrich Vieweg and Sohn, Braunschweig, Germany.

Weisman M.L. i Klemp J.B. (1982): The Dependence of Numerically Simulated Convective Storms on Vertical Wind Shear and Buoyancy. *Monthly Weather Review*, **110(6)**: 504–520. doi:10.1175/1520-0493(1982)110⟨0504:TDONSC⟩2.0.CO;2.

Weisman M.L. i Rotunno R. (2000): The Use of Vertical Wind Shear versus Helicity in Interpreting Supercell Dynamics. *Journal of the Atmospheric Sciences*, **57(9)**: 1452–1472. doi:10.1175/1520-0469(2000)057⟨1452:TUOVWS⟩2.0.CO;2.

Weisman M.L., Trapp R.J., Romine G.S., Davis C., Torn R., Baldwin M., Bosart L., Brown J., Coniglio M., Dowell D., Evans A.C., Galarneau Thomas J. J., Haggerty J., Hock T., Manning K., Roebber P., Romashkin P., Schumacher R., Schwartz C.S., Sobash R., Stensrud D. i Trier S.B. (2015): The Mesoscale Predictability Experiment (MPEX). *Bulletin of the American Meteorological Society*, **96(12)**: 2127–2149. doi:10.1175/BAMS-D-13-00281.1.

Wesolek E. i Mahieu P. (2011): The F4 tornado of August 3, 2008, in Northern France: Case study of a tornadic storm in a low CAPE environment. *Atmospheric Research*, **100(4)**: 649–656. doi:10.1016/j.atmosres.2010.09.003. 5th European Conference on Severe Storms.

Wilks D.S. (2011): *Statistical Methods in the Atmospheric Sciences*. Academic Press, Oxford, UK.

Wilson J., Carbone R., Baynton H. i Serafin R. (1980): Operational Application of Meteorological Doppler Radar. *Bulletin of the American Meteorological Society*, **61(10)**: 1154–1168. doi:10.1175/1520-0477(1980)061⟨1154:OAOMDR⟩2.0.CO;2.

Womble J.A., Wood R.L. i Mohammadi M.E. (2018): Multi-Scale Remote Sensing of Tornado Effects. *Frontiers in Built Environment*, **4**: 66. doi:10.3389/fbuil.2018.00066.

WSEC (2006): *A Recommendation for an Enhanced Fujita Scale (EF-scale)*. Wind Science and Engineering Center (Texas Tech University), Lubbock, Texas, USA.

Wurman J., Dowell D., Richardson Y., Markowski P., Rasmussen E., Burgess D., Wicker L. i Bluestein H.B. (2012): The Second Verification of the Origins of Rotation in Tornadoes Experiment: VORTEX2. *Bulletin of the American Meteorological Society*, **93(8)**: 1147–1170. doi:10.1175/BAMS-D-11-00010.1.

Wurman J., Kosiba K. i Robinson P. (2013): In Situ, Doppler Radar, and Video Observations of the Interior Structure of a Tornado and the Wind–Damage Relationship. *Bulletin of the American Meteorological Society*, **94(6)**: 835–846. doi:10.1175/BAMS-D-12-00114.1.

Wurman J., Kosiba K., Robinson P. i Marshall T. (2014): The Role of Multiple-Vortex Tornado Structure in Causing Storm Researcher Fatalities. *Bulletin of the American Meteorological Society*, **95(1)**: 31–45. doi:10.1175/BAMS-D-13-00221.1.

Zanini M.A., Hofer L., Faleschini F. i Pellegrino C. (2017): Building damage assessment after the Riviera del Brenta tornado, northeast Italy. *Natural Hazards*, **86**: 1247–1273. doi:10.1007/s11069-019-03642-z.

Zehnder J.A., Hu J. i Razdan A. (2007): A Stereo Photogrammetric Technique Applied to Orographic Convection. *Monthly Weather Review*, **135(6)**: 2265–2277. doi:10.1175/MWR3401.1.

Zrnić D.S., Burgess D.W. i Hennington L.D. (1985): Automatic Detection of Mesocyclonic Shear with Doppler Radar. *Journal of Atmospheric and Oceanic Technology*, **2(4)**: 425–438. doi:10.1175/1520-0426(1985)002⟨0425:ADOMSW⟩2.0.CO;2.

Apèndix A

Equacions dels paràmetres estudiats

A.1 Paràmetres termodinàmics

- Energia potencial convectiva disponible (CAPE, en J kg^{-1}), fent ús de la correcció de la temperatura virtual:

$$CAPE = g \int_{LFC}^{EL} \frac{T_{v_{LP}}(z) - T_{v_e}(z)}{T_{v_e}(z)} dz \tag{A.1}$$

  essent g l'acceleració de la gravetat, $T_{v_{LP}}$ la temperatura virtual de la parcel·la d'aire en ascens i T_{v_e} la temperatura virtual de l'entorn.

- Inhibició convectiva (CIN, en J kg^{-1}), fent ús de la correcció de la temperatura virtual:

$$CIN = g \int_{0}^{LFC} \frac{T_{v_{LP}}(z) - T_{v_e}(z)}{T_{v_e}(z)} dz \tag{A.2}$$

  essent g l'acceleració de la gravetat, $T_{v_{LP}}$ la temperatura virtual de la parcel·la d'aire en ascens i T_{v_e} la temperatura virtual de l'entorn.

A.2 Paràmetres cinemàtics

- Cisallament vertical del vent per a l'estrat delimitat per z_1 i z_2 ($WS_{z_1 z_2}$, en m s^{-1}):

$$WS_{z_1 z_2} = \mid \mathbf{v}_{z_2} - \mathbf{v}_{z_1} \mid \tag{A.3}$$

  essent $\mathbf{v}_{z_1}$ el vector vent horitzontal del nivell z_1 i $\mathbf{v}_{z_2}$ el vector vent horitzontal del nivell z_2.

- Helicitat relativa a la cèl·lula convectiva per a l'estrat delimitat per z_1 i z_2 ($SRH_{z_1 z_2}$, en m^2 s^{-2}):

$$SRH_{z_1 z_2} = -\int_{z_1}^{z_2} \mathbf{k} \cdot \left[(\mathbf{v} - \mathbf{c}) \times \frac{\partial \mathbf{v}}{\partial z} \right] dz \tag{A.4}$$

  essent $\mathbf{k}$ el vector unitari de l'eix vertical, $\mathbf{v}$ el vector vent horitzontal i $\mathbf{c}$ el vector moviment de la cèl·lula convectiva.

- *Bulk Richardson number shear* (BRNSHR, en $m^2\ s^{-2}$):

$$BRNSHR = \frac{1}{2}(U - U_0)^2 \tag{A.5}$$

essent U el mòdul del vent mitjà ponderat per densitat per a l'estrat 0-6 km i U_0 el mòdul del vent mitjà ponderat per densitat per a l'estrat 0-500 m.

A.3 Paràmetres compostos

- *Energy helicity index* per a l'estrat delimitat per z_1 i z_2 ($EHI_{z_1 z_2}$, adimensional):

$$EHI_{z_1 z_2} = \frac{CAPE \cdot SRH_{z_1 z_2}}{160000} \tag{A.6}$$

- *Vorticity generation parameter* per a l'estrat delimitat per z_1 i z_2 ($VGP_{z_1 z_2}$, en $m\ s^{-2}$):

$$VGP_{z_1 z_2} = S \cdot \sqrt{CAPE} = \left(\int_{z_1}^{z_2} \frac{\partial v}{\partial z} dz / \int_{z_1}^{z_2} dz \right) \sqrt{CAPE} \tag{A.7}$$

essent S el cisallament vertical mitjà del vent (la longitud de l'hodògrafa dividida pel gruix de l'estrat delimitat per z_1 i z_2).

- *Supercell composite parameter* (SCP, adimensional):

$$SCP = \left(\frac{MUCAPE}{1000} \right) \left(\frac{SRH_{03}}{100} \right) \left(\frac{BRNSHR}{40} \right) \tag{A.8}$$

essent MUCAPE la CAPE calculada mitjançant la parcel·la d'aire més inestable i SRH_{03} l'SRH per a l'estrat 0-3 km.

- *Significat tornado parameter* (STP, adimensional):

$$STP = \left(\frac{MLCAPE}{1000} \right) \left(\frac{WS_{06}}{20} \right) \left(\frac{SRH_{01}}{100} \right) \left(\frac{2000 - MLLCL}{1500} \right) \tag{A.9}$$

essent MLCAPE la CAPE calculada mitjançant la parcel·la d'aire de la capa de mescla, WS_{06} el cisallament vertical del vent per a l'estrat 0-6 km, SRH_{01} l'SRH per a l'estrat 0-1 km i MLLCL el nivell de condensació per elevació calculat amb la parcel·la d'aire de la capa de mescla.

- *Universal tornadic index* (UTI, adimensional):

$$UTI = \frac{\left\{ \left[\frac{SBCAPE \cdot SRH_{01}}{200} \cdot \frac{5(WS_{06} - 20) + \frac{(2000 - SBLCL)}{10}}{100} \right] + SBCAPE_{03} + \frac{SRH_{01}}{4} \right\}}{1000} \cdot \frac{WS_{01}}{12} \cdot \frac{AMR_{500}}{10} \tag{A.10}$$

essent SBCAPE la CAPE calculada amb la parcel·la d'aire de superfície, SRH_{01} l'SRH per a l'estrat 0-1 km, WS_{06} el cisallament vertical del vent per a l'estrat 0-6 km, WS_{01} el cisallament vertical del vent per a l'estrat 0-1 km, SBLCL el nivell de condensació per elevació calculat mitjançant la parcel·la d'aire de superfície, $SBCAPE_{03}$ la CAPE

calculada amb la parcel·la d'aire de superfície per a l'estrat 0-3 km i AMR_{500} la raó de mescla mitjana de l'estrat 0-500 m.

Per definició, es considera que UTI = 0 si SBCAPE = 0 J kg^{-1} i/o SBLCL > 1500 m, mentre que si $SRH_{01} < 0$ m^2 s^{-2}, aleshores es considera que $SRH_{01} = 0$ m^2 s^{-2} per a calcular el paràmetre.

- Producte de la velocitat vertical màxima calculada a partir de la CAPE i el cisallament vertical del vent per a l'estrat delimitat per z_1 i z_2 ($WMAXSHEAR_{z_1 z_2}$, en m^2 s^{-2}):

$$WMAXSHEAR_{z_1 z_2} = \sqrt{2CAPE} \cdot WS_{z_1 z_2} \tag{A.11}$$

Apèndix B

Contribucions

En aquesta secció es llisten, ordenades cronològicament, les contribucions fetes durant el període predoctoral en format d'article, de presentació oral i de pòster en congressos i seminaris i d'informe.

B.1 Articles

- Rodríguez O. i Bech J. (2018): Sounding-derived parameters associated with tornadic storms in Catalonia. *International Journal of Climatology*, **38**: 2400–2414. doi:10.1002/joc.5343.

- Rodríguez O., Bech J., Soriano J.D., Gutiérrez D. i Castán S. (2020): A methodology to conduct wind damage field surveys for high-impact weather events of convective origin. *Natural Hazards and Earth System Sciences*, **20(5)**: 1513–1531. doi:10.5194/nhess-20-1513-2020.

- Rodríguez O. i Bech J. (2020): Reanalysing strong-convective wind damage paths using high-resolution aerial images. *Natural Hazards*, **104(1)**: 1021–1038. doi:10.1007/s11069-020-04202-6.

- Rodríguez O. i Bech J. (2020): Tornadic environments in the Iberian Peninsula and the Balearic Islands based on ERA5 reanalysis. *International Journal of Climatology*: 1–21. doi:10.1002/joc.6825.

- Rodríguez O., Bech J., Arús J., Castán S., Figuerola F. i Rigo T. (2021): An overview of tornado and waterspout events in Catalonia (2000-2019). *Atmospheric Research*, **250**: 105415. doi:10.1016/j.atmosres.2020.105415.

B.2 Presentacions orals

- Rodríguez O. i Bech J. (2017): A climatology of sounding parameters associated to tornadic storms in Catalonia. *6th International Conference on Meteorology and Climatology of the Mediterranean, Zagreb, Croàcia.* Associació Catalana de Meteorologia i Croatian Meteorological Society.

- Rigo T., Farnell C., Pineda N., Aran M., Castillo S., Gallego S., Mateo J. i Rodríguez O. (2017): First results of the 2016 Operational Campaign using the Lightning Jump algorithm as a nowcaster of Severe Weather in Catalonia. *2nd European Hail Workshop,*

Berna, Suïssa. Mobiliar Lab, Karlsruhe Institute of Technology, MeteoSwiss, i Oeschger Centre for Climate Change Research.

- Rodríguez O. i Bech J. (2017): Condicions meteorològiques en alçada favorables per a les tempestes tornàdiques a Catalunya. *II Jornada de Joves Investigadors de l'IdRA, Barcelona*. Institut de Recerca de l'Aigua.

- Rodríguez O. i Bech J. (2017): Tornadoes in the Iberian Mediterranean area and Balearic Islands: study of sounding-derived parameters. *9th European Conference on Severe Storms, Pula, Croàcia*. European Severe Storms Laboratory.

- Rodríguez O., Bech J. i García S. (2018): Tornadic storms in the Iberian Mediterranean area and Balearic Islands: study of upper air conditions. *XXXV Jornadas Científicas de la AME, León, Espanya*. Asociación Meteorológica Española.

- Bech J., Rodríguez O., Altube P., Rigo T., Pineda N., Castán S., Arús J. i Montanyà J. (2018): Doppler radar observations of two tornadic thunderstorm cases in the western Mediterranean region. *10th European Conference on Radar in Meteorology and Hydrology, Ede-Wageningen, Països Baixos*. Wageningen University & Research.

- Rodríguez O., Bech J., Soriano J.D., Gutiérrez D. i Castán S. (2019): A field work methodology for wind damage from strong-convective winds events. *7th International Conference on Meteorology and Climatology of the Mediterranean, Palma*. Tethys, Centre d'Estudis Ambientals del Mediterrani i Universitat de les Illes Balears.

- Bech J., Rodríguez O., Altube P., Rigo T. i Pineda N. (2019): Observational analysis of the 18 October 2017 Valls severe weather thunderstorm. *7th International Conference on Meteorology and Climatology of the Mediterranean, Palma*. Tethys, Centre d'Estudis Ambientals del Mediterrani i Universitat de les Illes Balears.

- Rodríguez O. i Bech J. (2019): Características de sondeos y reanálisis en episodios de tornados. *Seminario Final de la Red Temática Winter Precipitation and Strong Winds: Observational Studies (WiPSWis) (CGL2016-81828-REDT/AEI), Madrid, Espanya*. Red Temática CGL2016-81828-REDT/AEI.

- Pineda N., Altube P., Rigo T., Farnell C., Montanyà J., van der Velde O., Salvador A., Bech J. i Rodríguez O. (2019): Severe weather patterns of a tornadic event associated to a squall line in the western Mediterranean region. *10th European Conference on Severe Storms, Cracòvia, Polònia*. European Severe Storms Laboratory.

B.3 Pòsters

- Bech J., Castán S., Arús J., Rodríguez O., Pascual R., Cuevas G., Pineda N., Rigo T., Montanyà J. i van der Velde O. (2016): Observational study of the 2014 Vilabella tornadic thunderstorm. *9th European Conference on Radar in Meteorology, Antalya, Turquia*. Turkish State Meteorological Service.

- Rodríguez O. i Bech J. (2016): Aplicació de l'índex UTI als casos tornàdics recents a Catalunya. *XXII Jornades de Meteorologia Eduard Fontserè, Barcelona*. Associació Catalana de Meteorologia.

- Rodríguez O., Bech J. i García S. (2017): Upper air conditions for tornadic storms in the Iberian Mediterranean area and Balearic Islands. *10th HyMeX Workshop, Barcelona*. Hydrological Cycle in the Mediterranean Experiment.

- Rodríguez O. i Bech J. (2017): Metodologies per a l'elaboració d'una base de dades de tornados a Catalunya. *XXIII Jornades de Meteorologia Eduard Fontserè, Barcelona*. Associació Catalana de Meteorologia.
- Rodríguez O., Bech J., Soriano J.D. i Castán S. (2018): Metodología para la realización de trabajos de campo en episodios de vientos fuertes de origen convectivo. *XXXV Jornadas Científicas de la AME, León, Espanya*. Asociación Meteorológica Española.
- Rodríguez O., Bech J., Soriano J.D., Gutiérrez D. i Castán S. (2018): A field work methodology for wind damage from strong-convective winds events. *XXIV Jornades de Meteorologia Eduard Fontserè, Barcelona*. Associació Catalana de Meteorologia.
- Rodríguez O., Bech J., Castán S. i Arús J. (2018): El tornado del 7 de gener de 2018: de l'Alt Empordà al Rosselló. Treball de camp i anàlisi de les destrosses. *XXIV Jornades de Meteorologia Eduard Fontserè, Barcelona*. Associació Catalana de Meteorologia.
- Rodríguez O. i Bech J. (2019): Ortophotos: a source of information in tornado track and intensity studies. *7th International Conference on Meteorology and Climatology of the Mediterranean, Palma*. Tethys, Centre d'Estudis Ambientals del Mediterrani i Universitat de les Illes Balears.
- Llasat M.C., Cortès M., del Moral A., Llasat-Botija M., Rigo T. i Rodríguez O. (2019): A holistic approach to the analysis of the catastrophic flash flood event of 12 October 2016 in the Central Coast of Catalonia. *7th International Conference on Meteorology and Climatology of the Mediterranean, Palma*. Tethys, Centre d'Estudis Ambientals del Mediterrani i Universitat de les Illes Balears.
- Rodríguez O. i Bech J. (2019): Study of upper air conditions in tornadic and waterspout events in the Iberian Peninsula and Balearic Islands using ERA5 reanalysis data. *10th European Conference on Severe Storms, Cracòvia, Polònia*. European Severe Storms Laboratory.
- Gutiérrez D., Soriano J.D., Bech J., Rodríguez O. i Castán S. (2019): Forensic meteorology. A field survey methodology proposal for wind assessment. *10th European Conference on Severe Storms, Cracòvia, Polònia*. European Severe Storms Laboratory.
- Rodríguez O., Bech J., Rigo T., Arús J. i Castán S. (2019): Anàlisi de l'episodi de tornados del 8 de setembre de 2019 al Baix Llobregat i al Barcelonès. *XXV Jornades de Meteorologia Eduard Fontserè, Barcelona*. Associació Catalana de Meteorologia.
- Rodríguez O., Bech J., Arús J., Castán S., Figuerola F. i Rigo T. (2020): Caracterització dels episodis de tornados i de mànegues marines a Catalunya. *XXVI Jornades de Meteorologia Eduard Fontserè, Barcelona*. Associació Catalana de Meteorologia.

B.4 Informes

- SMC (2018): Informe sobre el tornado de Cardona (el Bages) i Navès (el Solsonès). Servei Meteorològic de Catalunya. `https://static-m.meteo.cat/content/files/Informe_Tornado_Cardona_Naves.pdf`.
- SMC (2018): Informe sobre el tornado de Navata, Cistella, Terrades i Darnius (l'Alt Empordà). Servei Meteorològic de Catalunya. `https://static-m.meteo.cat/content/files/Informe_Tornado_Emporda.pdf`.

Apèndix C

Treballs de camp realitzats

A la Taula C.1 es llisten els treballs de camp realitzats durant el període predoctoral. Des del març de 2016 fins al desembre de 2020 s'han analitzat *in situ* 38 episodis en 50 jornades. Alguns dels casos estudiats han requerit diverses visites a causa de l'extensió de la zona afectada, com per exemple el tornado de Navata - Terrats del 7 de gener de 2018 (6 dies), el de Cardona - Navès del 7 de gener de 2018 (4 dies), el de Malgrat de Mar - Massanes del 15 d'octubre de 2018 (4 dies) i el de Sant Celoni - Vilanova de Sau del 22 d'octubre de 2019 (4 dies).

Taula C.1: Data i població dels treballs de camp duts a terme entre el març de 2016 i el desembre de 2020 i origen dels danys de cadascun dels episodis analitzats.

Data	**Municipi**	**Comarca**	**Fenomen**
22/03/2016	St. Llorenç d'Hortons	l'Alt Penedès	Tornado
23/05/2016	Montblanc	la Conca de Barberà	Esclafit
08/06/2016	Alcalá de Guadaíra	*Sevilla*	Sense danys
14/09/2016	Badalona	el Barcelonès	Esclafit
14/10/2016 i 21/10/2016	Llinars del Vallès	el Vallès Oriental	Tornado
16/10/2016	Sabadell	el Vallès Occidental	Sense danys
19/10/2016	el Mas-roig	el Priorat	Sense danys
25/11/2016	Mataró	el Maresme	Tornado
29/11/2016	Olivella	el Garraf	Esclafit
19/10/2017	Bonastre	el Baix Penedès	Indeterminat
20/10/2017 i 21/10/2017	Valls	l'Alt Camp	Tornado
21/10/2017	Salou	el Tarragonès	Esclafit
02/12/2017	Juneda	les Garrigues	Tornado
07/01/2018, 08/01/2018, 09/01/2018, 14/01/2018, 28/03/2018 i 30/04/2018	Navata, Vilanant, Cistella, Terrades, Darnius, la Vajol, Agullana i Morellàs i les Illes	l'Alt Empordà i el Vallespir	Tornado
08/01/2018, 10/01/2018, 11/03/2018 i 20/01/2018	Cardona i Navès	el Bages i el Solsonès	Tornado
20/01/2018	Parets del Vallès i Lliçà d'Amunt	el Vallès Oriental	Tornado

Continua a la pàgina següent.

Data	**Municipi**	**Comarca**	**Fenomen**
05/02/2018	Mont-roig del Camp	el Baix Camp	Tornado
13/04/2018	Vila-seca	el Tarragonès	Tornado
06/08/2018	Sta. Eulàlia de Puig-oriol	Osona	Esclafit
02/09/2018	el Vendrell	el Baix Penedès	Sense danys
15/10/2018, 19/10/2018 i 24/10/2018 20/02/2019	Malgrat de Mar, Palafolls, Tordera, Forgars de la Selva i Massanes	el Maresme i la Selva	Tornado
16/10/2018 i 20/10/2018	els Pallaresos i Perafort	el Tarragonès	Tornado
16/10/2018 i 20/10/2018	Perafort	el Tarragonès	Tornado
19/10/2018	Sta. Coloma de Farners	la Selva	Tornado
13/11/2018	Alaior i Maó	*Menorca*	Tornado & Esclafit
15/11/2018 24/11/2018	Viladecavalls i Terrassa	el Vallès Occidental	Tornado
05/04/2019	Sta. Maria de Merlès i Lluçà	el Berguedà i Osona	Tornado
12/08/2019	Vilanova i la Geltrú	el Garraf	Esclafit
16/08/2019	Barcelona	el Barcelonès	Tornado
08/09/2019	el Prat de Llobregat	el Baix Llobregat	Tornado
09/09/2019	el Prat de Llobregat i St. Boi de Llobregat	el Baix Llobregat	Tornado
13/09/2019	Móra la Nova	la Ribera d'Ebre	Tornado
20/10/2019	Montgat	el Maresme	Tornado
23/10/2019, 25/10/2019, 30/10/2019 i 20/11/2019	St. Celoni, Gualba, Riells i Viabrea, Breda, St. Feliu de Buixalleu, Arbúcies, St. Hilari Sacalm i Vilanova de Sau	el Vallès Oriental, la Selva i Osona	Tornado
20/11/2019	St. Cebrià de Vallalta	el Maresme	Altres
17/06/2020	la Bisbal d'Empordà	el Baix Empordà	Tornado
30/07/2020	St. Miquel de Campmajor	el Pla de l'Estany	Esclafit
14/12/2020	Arenys de Lledó, Horta de St. Joan i Lledó d'Algars	el Matarranya i la Terra Alta	Tornado

Apèndix D

Geolocalització de fotografies de tornados

Quan es produeix un tornado en una zona poblada, si les condicions de visibilitat ho permeten, s'acostumen a publicar fotografies i vídeos a les xarxes socials i als mitjans de comunicació. Més enllà de mostrar l'espectacularitat del fenomen, les imatges poden aportar informació rellevant a l'hora d'estudiar l'episodi.

En cas de disposar de diverses fotografies i de conèixer la localització del punt des d'on s'han pres i l'orientació, és possible estimar la localització del vòrtex en superfície mitjançant la triangulació de les imatges. Per tal que l'error de la localització del tornado sigui mínim, s'ha de tenir en compte que s'han de complir tres condicions:

- Cal disposar d'un mínim de dues imatges preses des d'ubicacions diferents
- L'angle que forma la línia de visió d'ambdues fotografies ha de ser el més proper a 90° possible
- Les imatges han de correspondre al mateix instant de temps o a un de molt proper

Els autors de les fotografies i dels vídeos sovint poden proporcionar la informació necessària per a desenvolupar aquesta tasca, si bé hi ha altres eines que poden ser d'ajut, com per exemple *Google Street View* i *Google Earth*. La distinció d'elements singulars que apareixen a les imatges (edificis, arbres aïllats, l'orografia, la morfologia dels núvols i de les àrees amb precipitació) sol afavorir una correcta identificació de la localització del punt des d'on s'ha pres una imatge (Figura D.1).

Amb aquest procediment es pot estudiar el cicle de vida d'un fibló i delimitar la zona on podria haver-hi danys a fi de dur a terme un treball de camp. Per tal d'il·lustrar el segon dels supòsits descrits, a continuació es descriu el cas del tornado de Sant Llorenç d'Hortons (l'Alt Penedès) de l'any 2016.

El 21 de març de 2016 a les 15:45 UTC es va observar una tuba força ampla, però poc desenvolupada verticalment, al nord-est de la comarca de l'Alt Penedès. En aquest cas es van poder aconseguir cinc fotografies a través de les xarxes socials fetes des de tres punts diferents de la zona, als municipis de Piera, Sant Sadurní d'Anoia i Avinyonet del Penedès. En cap d'elles s'observava que el vòrtex estigués en contacte amb el terra.

A partir de l'anàlisi de les imatges i amb l'ajut de les aplicacions *Google Street View* i *Google Earth*, es van poder identificar els punts des d'on es varen prendre i la seva orientació (Figura D.2). Tot i desconèixer si les fotografies corresponien al mateix instant de temps, es va fer la triangulació i es va poder estimar l'àrea on, en cas que s'hagués produït el tornado, hi hauria d'haver les afectacions. Aquesta àrea correspon a la zona on se superposen els cons de projecció

Figura D.1: a) Fotografia del tornado de Vilabella (l'Alt Camp) del 30 de maig de 2014 feta des de la carretera TV-2035 (autor: Carles Puig). (b) Imatge del punt des d'on es va fer la fotografia (extreta de *Google Street View*). Les línies discontínues de color carabassa mostren alguns elements fàcilment identificables presents a les dues imatges.

de les tres imatges, obtinguts a partir de la direcció amb què es va fer la fotografia i tenint en compte un marge d'error de $\pm$ 5°.

L'endemà de l'episodi es va dur a terme un treball de camp a on se suposava que hi podia haver danys. Un veí de la zona ens van comentar que en una finca de Sant Llorenç d'Hortons (Can Prats) hi havia hagut alguns desperfectes fruit d'una forta ventada molt localitzada la tarda anterior. Aquest indret se situava dins l'àrea possiblement afectada. En arribar-hi, es va poder parlar amb una persona que havia estat testimoni del fenomen. Confirmà que s'havia pogut observar un remolí, i que aquest havia estat el responsable dels danys lleus (Figura D.3).

El vent va arrancar 15 m^2 d'una coberta de fibrociment molt vulnerable (la subjecció de les plaques a les bigues de fusta, que es trobaven en mal estat, era feble; Figura D.3b). Dos tubs de plàstic de 20 cm de diàmetre i 2 m de llargada que es trobaven a terra a tocar d'un dels edificis de la finca van ser desplaçats uns 30 m, segons un altre testimoni (Figura D.3c). També es van observar algunes branques de diàmetre inferior als 2 cm trencades. Amb tota aquesta informació es va poder confirmar que s'havia produït un tornado d'intensitat EF0 i que havia recorregut, pel cap baix, 0,3 km.

Figura D.2: Al mapa hi ha indicats els punts des d'on es van prendre les fotografies 1 (Piera, autor desconegut), 2 (Sant Sadurní d'Anoia, @illa_98) i 3 (Avinyonet del Penedès, Carles Roca). Les zones ombrejades de color blanc mostren la direcció amb què es van prendre les imatges amb un marge d'error de ± 5°. En color vermell hi ha delimitada l'àrea possiblement afectada.

Figura D.3: (a) Mapa amb la trajectòria de les restes localitzades a la finca afectada pel tornado, on s'indiquen els elements malmesos presentats a les fotografies (b) cobert d'uralita afectat i (c) tubs desplaçats per la força del vent. La línia vermella puntejada mostra la trajectòria del tornado.